INFORMATION TO USERS

This manuscript has been reproduced from the microfilm master. UMI films the text directly from the original or copy submitted. Thus, some thesis and dissertation copies are in typewriter face, while others may be from any type of computer printer.

The quality of this reproduction is dependent upon the quality of the copy submitted. Broken or indistinct print, colored or poor quality illustrations and photographs, print bleedthrough, substandard margins, and improper alignment can adversely affect reproduction.

In the unlikely event that the author did not send UMI a complete manuscript and there are missing pages, these will be noted. Also, if unauthorized copyright material had to be removed, a note will indicate the deletion.

Oversize materials (e.g., maps, drawings, charts) are reproduced by sectioning the original, beginning at the upper left-hand corner and continuing from left to right in equal sections with small overlaps.

Photographs included in the original manuscript have been reproduced xerographically in this copy. Higher quality 6" x 9" black and white photographic prints are available for any photographs or illustrations appearing in this copy for an additional charge. Contact UMI directly to order.

Bell & Howell Information and Learning
300 North Zeeb Road, Ann Arbor, MI 48106-1346 USA
800-521-0600

Dynamic Recurrent Neural Networks for Stable Adaptive Control of Wing Rock Motion

Steven Boon-Lam Kooi

A Thesis

in

The Department

of

Mechanical Engineering

Presented in Partial Fulfillment of the Requirements
for the Degree of Doctor of Philosophy at
Concordia University
Montréal, Québec, Canada

October 1999

Abstract

Dynamic Recurrent Neural Networks for Stable Adaptive Control of Wing Rock Motion

Steven B. L. Kooi, Ph.D.
Concordia University, 1999

Wing rock is a self-sustaining limit cycle oscillation (LCO) which occurs as the result of nonlinear coupling between the dynamic response of the aircraft and the unsteady aerodynamic forces. In this thesis, dynamic recurrent RBF (Radial Basis Function) network control methodology is proposed to control the wing rock motion. The concept based on the properties of the Presiach hysteresis model is used in the design of dynamic neural networks. The structure and memory mechanism in the Preisach model is analogous to the parallel connectivity and memory formation in the RBF neural networks. The proposed dynamic recurrent neural network has a feature for adding or pruning the neurons in the hidden layer according to the growth criteria based on the properties of ensemble average memory formation of the Preisach model. The recurrent feature of the RBF network deals with the dynamic nonlinearities and endowed temporal memories of the hysteresis model.

The control of wing rock is a tracking problem, the trajectory starts from non-zero initial conditions and it tends to zero as time goes to infinity. In the proposed neural control structure, the recurrent dynamic RBF network performs identification process in order to approximate the unknown non-linearities of the physical system based on the input-output data obtained from the wing rock phenomenon. The design of the RBF networks together with the network controllers are carried out in discrete time domain. The recurrent RBF networks employ two separate adaptation schemes where the RBF's centre and width are adjusted by the Extended Kalman Filter in order to

give a minimum networks size. while the outer networks layer weights are updated using the algorithm derived from Lyapunov stability analysis for the stable closed loop control. The issue of the robustness of the recurrent RBF networks is also addressed. The effectiveness of the proposed dynamic recurrent neural control methodology is demonstrated through simulations to suppress the wing rock motion in AFTI/F-16 testbed aircraft having the delta wing configuration. The potential implementation as well as the practicality of the control methodology are also discussed.

Dedication

To My Parents, My Family, My Aunt

and

My Father-in-Law, Prof. Dr. Na Chi

Acknowledgments

I would like to express my gratitude to Canadair, Bombardier Inc for providing financial support thereby allowing me to carry out my initial research in aircraft dynamics. I like to thank Mr. Clinton E. Tanner, Manager Flight Science, who introduces me the subject of wing rock and Dr. Sergio Cavalcanti for his technical assistance during my stay at Canadair.

I am greatly indebted to Dr. K. Khorasani, for his technical advice, valuable suggestions and comments in reviewing my thesis. I gained a lot of knowledge in my field through the control courses he had given and from our numerous technical discussions. I have the most respect for his academic integrity and fairness.

Dr. Noriyuki Hori, my external examiner from McGill University, had reviewed very thoroughly my thesis. I like to thank him for his time and the valuable critique.

I like to thank Prof. Edward C. Lan of the University of Kansas for his comments on wing rock model.

I would like to thank Dr.Neemeh, my administrative supervisor for his support and assistance and to Dr. James Jans, Ms. Suzanne Belson, Ms. Mary Appezato and the committe members in assisting me to have my defense completed. I especially express my thanks to the late Mr. Reginald K Groome for his concern and support during the difficult phase of my study.

I had received numerous helps from my friends, I would like to thank them in particular, Dr. Chen Tzu-Fang, Mr. Hank Wang, Prof F. D. Hamblin, Dr. Michel Perrier and Ms. Caryn Isenberg.

Finally, I wish to express my thanks to my family, particularly my wife Julia for her understanding, sacrifices and solid support in times of difficulty, and also to my children Donna and Sarah without whom my study and completion of this work would not have been possible.

List of Symbols

Symbols

a_o : effectiveness estimate relating to control input signal or angular acceleration, $1/\sec^2 \deg$

$a_f(k)$, $a_g(k)$: gradient vectors defined in equations (5.26) and (5.27)

A : matrix in plant model

A_m : matrix in reference model

b : wing span, ft

$C_l(t)$: aerodynamic roll moment coefficient defined in equation (2.28)

C_{lo} : rolling moment coefficient at zero sideslip

C_{lpt} : coefficient function defined in equation (2.29)

$C_{l\delta A}$: aerodynamic roll derivative due to aileron deflection

C_{lpo} : roll damping coefficient at zero sideslip

$C_{l\beta}$: the diherdal effect assuming negative (stable) and positive (unstable) values depending on configurations

$C_{lp\beta}$: dimensionless variation of roll damping derivative with sideslip, $\partial C_{lp}/\partial\beta$

C_{lpp} : dimensionless variation of roll damping derivative with roll rate, $\partial C_{lp}/\partial\,\bar{p}$

d : relative degree

e : error between the plant output and reference model output

$e_{\min}$: threshold value defined in equation (5.9)

e_{rms} : root mean square error defined in equation (5.34)

er : error between networks computed output and system output

$\hat{f}$, $\hat{g}$: estimated unknown nonlinear functions

$f_o(z)$, $g_o(z)$: prior knowledge of functions f and g given in equations (5.4) & (5.5)

$f_o(.)$, $g_o(.)$: differentiable unknown nonlinear functions defined in equations (6.21) or (7.32)

I : Identity matrix

I_{xx} : moment of inertia about X axis, $slug - ft^2$

$J(k)$: Jacobian matrix of $\frac{\partial \hat{f}}{\partial w_f}$ and $\frac{\partial \hat{g}}{\partial w_g}$

k : discrete time index

k_m : gain for the reference model

K_f, K_g : optimal number of hidden neurons in f and g nets

L_o : $qSbC_{lo}/I_{xx}$, s^{-2}

L_β : $qSbC_{l\beta}/I_{xx}$, s^{-2}

L_{po} : $qSb^2C_{lpo}/(2I_{xx}V)$, s^{-1}

$L_{p\beta}$: $qSb^2C_{lp\beta}(2I_{xx}V)$, s^{-1}

L_{pp} : $qSb^3C_{lpp}/(4I_{xx}V^2)$

L : rolling moment in X axis

M : number of observations for calculating root mean square error, defined in equation (5.34)

n : number of samples or observations

P : error covariance matrix

$\bar{p}$: dimensionless reduced rolling velocity

q : dynamic pressure, lb/ft^2

Q : the scalar used in the EKF algorithm

r : reference signal

s : Laplace variable

S : wing reference area, ft^2

$\check{S}$: Sensitivity measure defined in equation (7.41)

t : time in continuous domain

T_s : sampling period, sec

T : transpose of the matrix

u : control input, deflecting aerodynamic surface or velocity component of aircraft in X axis

u, v, w : velocity components along X, Y, and Z axes respectively, $ft/\sec$

V : magnitude of forward flight velocity, $ft/\sec$

V_∞ : free stream air speed, ft/sec

V_T : trim velocity, $ft/\sec$

$V(e, \phi)$: Lyapunov function in continuous time domain

$V(k)$: Lyapunov function in discrete time domain

w_f , w_g : linear weight vectors for f and g RBF networks

$\mathbf{w}$: weight vector defined in equation (3.1)

w : output function given in Figures 4.1 and 4.2

W : aircraft weight, lb

$\dot{W}$: work or energy in the system

X, Y, Z : rectangular coordinates of body-fixed axis system, ft

x : state variable vector in continuous time domain

$\mathbf{x}$: input space denoted by $\mathbf{x} \in \Re^K$ to the neurons in the networks

x_m : state variable vector of reference model

y : output vector

y_d : desired output function

$\hat{y}$: neural networks computed output

$\mathbf{y}$: output space denoted by $\mathbf{y} \in \Re^L$

$\dot{y}$: adaptive linear combiner's output defined in equation (3.1)

z : state variable vector in discrete time domain

Z^{-1} : unit delay

$|\ \ |$: absolute notation

$\|.\|$: Euclidean norm

$\oint$: contour integral

Greek Symbols

α : angle of attack (AOA), *rad* or deg, or switching value in the Preisach operator, or tuning constant for adaptive controller

α_s : steady-state angle of attack, rad

β : sideslip angle, *rad* or deg, or switching value in the Preisach operator

ϵ_{max}, ϵ_{min} : parameters defined in equation (5.10)

ϵ_n : threshold value defined in equations (5.7) & (5.8)

γ : relative degree, or decay constant defined in equation (5.10)

$\hat{\gamma}_{\alpha\beta}$: Preisach hysteresis operator

δ_A : aileron deflection, deg or rad

ζ : damping ratio or element of stochastic sample set given in equation (5.11) and (5.12)

η : networks learning rate

θ : parameter vector defined in equation (2.50)

$\dot{\theta}$: parameter vector defined in equation (6.53)

κ : overlapping factor

μ_f , μ_g : centres of radial basis function in f and g nets respectively

μ_a : ensemble average of the distance in centre of the hidden neurons to the input vector

μ_{nr} : nearest centre of the hidden neurons to input vector

$\mu(\alpha, \beta)$: weight function of the Preisach hysteresis model defined in equation (4.1)

$\mu_f(k, \zeta_i)$, $\mu_g(k, \zeta_i)$: samples of centres in f and g nets, where ζ_i represents the element of the sample set

ν : external disturbance

ρ_f, ρ_g : widths of the radial basis function in f and g nets respectively

σ : sigma modification used in the adaptive law given in equation (2.65)

$\phi(k)$: input vector to the recurrent RBF networks

ϕ : roll angle, rad or deg or parameter error vector

$\dot{\phi}$: roll rate, $rad/\sec$ or deg/sec or derivative of parameter error vector given in equation (2.65)

ω_n : natural frequency

τ : time constant . sec

Γ : weighting matrix

Θ : Gaussian radial basis function

$\sum$: summation notation

Ω : $(-\sin\alpha_s L_\beta)^{1/2}$, angular velocity in rotary test in wind tunnel experiment, $rad/\sec$

$\frac{\Omega b}{2V}$: rotation rate for test conducted in spin tunnel

$\triangle_f$, $\triangle_g$: approximation error defined in equations (6.45) and (6.46)

Abbreviations

AFTI : Advanced Fighter Technology Integration

DR-RBF : Dynamic Recurrent- Radial Basis Function

EKF : Extended Kalman Filter

GRBF : Growing Radial Basis Function

LCO : Limit Cycle Oscillation

LMS : Least Mean Square

MLP : Multilayer Perceptron

NARMA : Nonlinear Auto Regressive Moving Average

NARX : Nonlinear Auto Regressive with eXogenous input

RBF : Radial Basis Function

RLS : Recursive Least Square

RAN : Resource Allocating Networks

RANEKF : Resource Allocating Networks-Extended Kalman Filter

RBFNN : Radial Basis Function Neural Networks

Contents

List of Figures

Chapter 1

Introduction

1.1 Wing Rock Phenomenon

Wing rock is a self-sustaining limit cycle oscillation (LCO) which occurs as the result of nonlinear coupling between the dynamic response of the aircraft and the unsteady aerodynamic forces. Many aircrafts having slender planform may experience self-induced oscillatory rolling motion when operating at high angles of attack. This oscillatory motion is commonly known as *wing rock*. The wing rock motion also arises from nonlinear aerodynamic mechanisms which present at high angles of attack.

Wing rock can also be caused by inherent mechanical hysteresis in the aircraft for example, in certain commercial aircraft the occurrence of wing rock is due to backlash in power transmission system. The phenomenon of wing rock occurs only under certain flight conditions e.g. altitude of 3000 ft and Mach number of 0.6 for the aircraft under study. The precise knowledge and shape of the waveform of wing rock is difficult to obtain from the aircraft. The limit cycle is characterized by low amplitude in the range of 0.1 to 0.5 degree yaw oscillation and a period of 1.5 to 3.0 seconds. The study also shows that by reducing the magnitude of backlash in these sources, the problem of wing rock or limit cycle oscillation was significantly reduced.

A wide range of studies has also been conducted by researchers on aircraft exhibiting wing rock due to aerodynamic hysteresis, some of the aircrafts that have been documented to experience wing rock include, for example, F-4 Phantom, F-18 Hornet, F-14 Tomcat, F-16 Fighting Falcon, Gnat Trainer, Torando and A-4 Skyhawk. Owing to the different types of aircraft and different sources of primary physical mechanism responsible for the non-linearities, the scope and problem of wing rock are also not very well understood. In general, it is believed that wing rock motion is triggered by flow asymmetries, developed by negative roll damping and sustained by nonlinear aerodynamic roll damping. Wing rock motion may also be initiated either with a sideslip or during a zero sideslip flight with flow asymmetries over the aircraft flying at high angle of attack. For a study conducted on F-4 Phantom, it was observed that when operated at high angle of attack the aircraft could undergo divergence behavior in pitch and yaw known as " nose slice ". Preceding the nose slice, the aircraft would experience wing rock motion.

Wing rock in advanced aircraft can result from different sources. Figure 1.1 shows the schematic of the subsonic flow field over the top of the delta wing. Ericsson [1] describes three different fluid dynamic processes generating the wing rock namely *asymmetry of leading-edge vortices, asymmetry of forebody vortices and dynamic stall.*

At zero sideslip, the flow vortex pattern is essentially symmetric. However, under rotating conditions an asymmetric pattern is established in which the leading edge vortex appears to become more diffused and moves inwards whereas the trailing vortex remains strong and locate near the outer portion of the wing. Thus the *asymmetry of the leading edge vortex* shown in Figure 1.2 has the characteristic required for the increase of rolling moment resulting in the generation of wing rock motion.

The slender delta wing is preceded by a slender forebody as is mostly the case, the vortex asymmetry is generated by the forebody. The interaction of asymmetric

vortex with the downstream wing and or tail surfaces produces the wing rock. The source of the wing rock is mainly due to the *asymmetry of forebody vortex* (Figure 1.3).

Dynamic stall is a flow mechanism which causes wing rock of straight or moderately swept wings. If the aircraft is perturbed when flying close to stall, the down rolling wing will promote flow separation resulting in positive lift on one side and negative lift on the other. This generates a rolling moment which drives the wing rock motion.

Wing rock depends on the details of the configuration geometry of the aircraft. To suppress the wing rock on all types of aircraft, the primary mechanism responsible for the wing rock must be identified. Due to the complexity of flow fields for different aircraft, the identification of the exact causes and the source of primary mechanism could be difficult. To eliminate the aircraft configuration dependent effects, research has been devoted to slender delta wing model.

1.2 Problem Definition

Owing to the highly nonlinear nature of the flight dynamics, the problem of the wing rock is not very well understood. No satisfactory method has been developed to solve the problem. In general, the source of wing rock in the aircraft could be caused by aerodynamic conditions during flight or mechanical hysteresis due to backlash, cable stretching, dry friction and hydraulic oil compressibility. Wing rock motion is not acceptable from the operational and safety point of view. The problem is a concern to a pilot because it may have an adverse effect on aircraft maneuverability during landing approach or during a dogfight in a combat situation. The severity of wing rock may degrade the performance of weapon aiming control and accuracy.

During the aerodynamic design stage of the aircraft, consideration can be taken

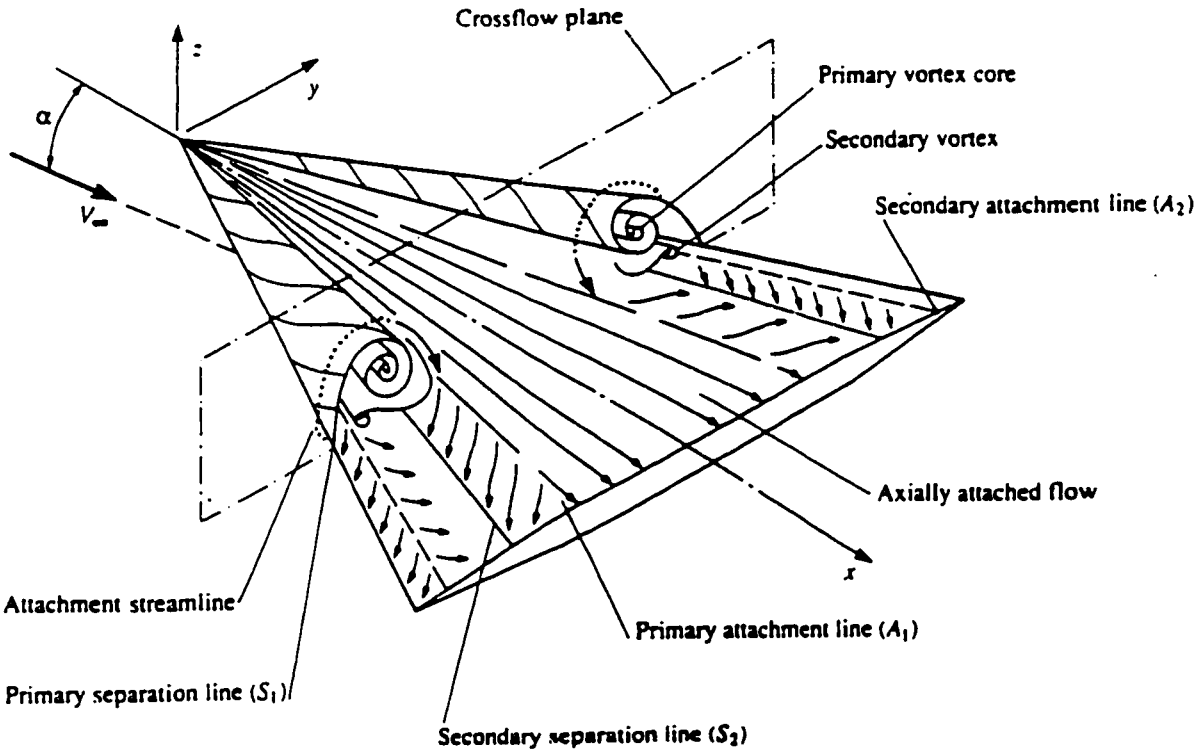

Figure 1.1: Flow field over Delta Wing , Anderson [36]

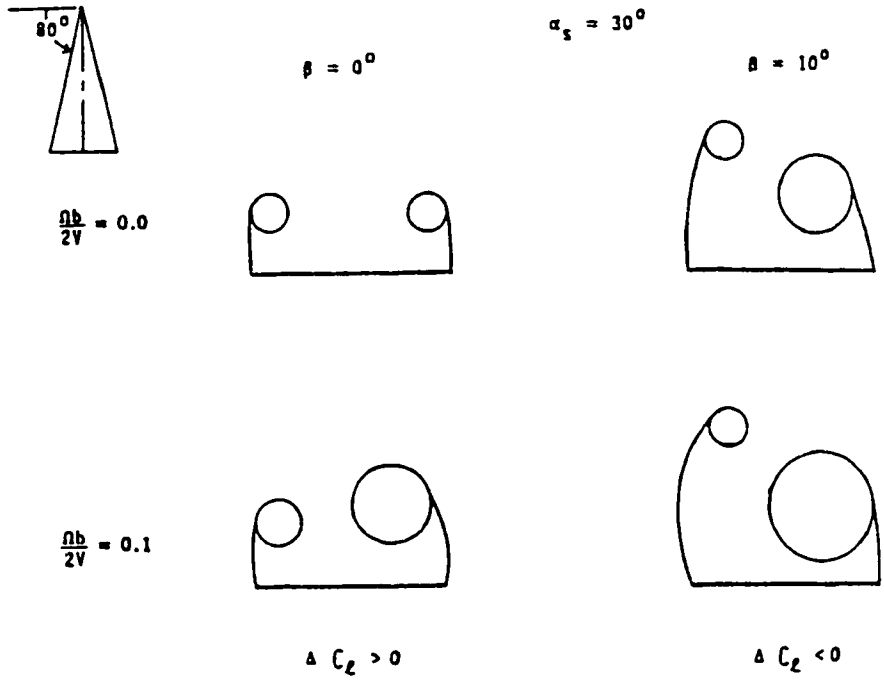

Figure 1.2: Asymmetric Leading Edge Vortices (80° delta wing) [34]

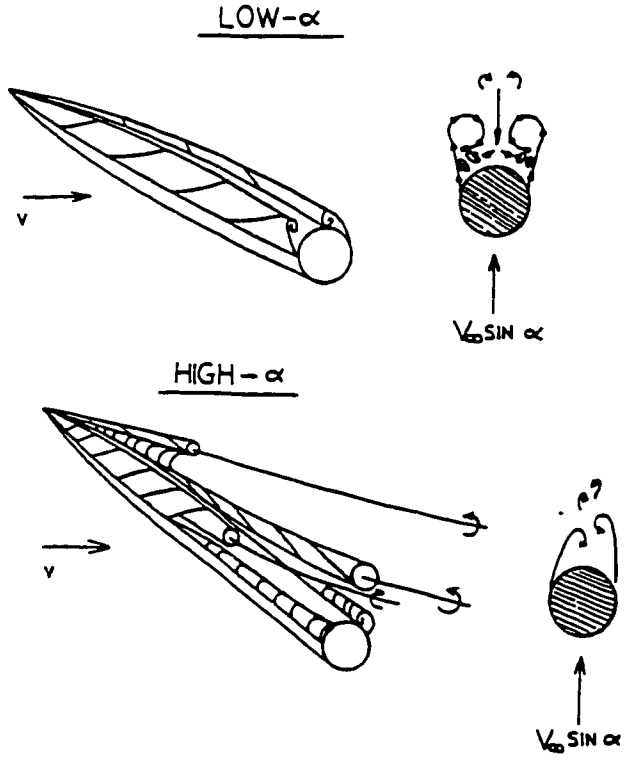

Figure 1.3: Asymmetric Forcebody Vortices [34]

to minimize the occurrence of the wing rock, such as the design with a slender body and highly swept wings, use of the roll damper, forebody jet blowing etc. These conventional control methods may not be effective to control wing rock occurring at high angle of attack.

Advanced control method such as adaptive control and neural control have been demonstrated to control the wing rock. The neural control method overcomes the limitation of adaptive control in which the structure of the nonlinearity of the unknown system does not have to be known as a " *priori* ". However, the standard neural control method uses fixed network architecture where huge number of neurons are employed.

The objective of this thesis is to develop a dynamic recurrent RBF (Radial Basis Function) control methodology for controlling the wing rock motion of aircraft having delta wings configuration. The identification of the unknown nonlinear system generating the wing rock is modelled by dynamic recurrent RBF networks. By applying the properties of the Preisach model, the concept of ensemble memory formation is used as a criteria for training the RBF networks. Adaptive hybrid control is then used to provide a closed loop control.

1.3 Review of Previous Research

The presence of wing rock motion or limit cycle oscillation (LCO) had been observed in flight and sometimes it is difficult to distinguish whether the cause is due to lightly damped Dutch Roll mode, aerodynamic hysteresis or mechanical hysteresis. The evidence suggests that in wing rock motion wherein the amplitude and period of the motion is solely the results of aerodynamic non-linearities [2]. This is in contrast to the limit cycle oscillation responded from lightly damped Dutch Roll wherein the amplitude is determined by initial conditions. Dutch Roll can be adequately described

by linear mathematical model. In the state transition matrix of the lateral directional equation of motion, the Dutch Roll roots can be identified.

Liebst and Nolan [3] conducted a research to examine the limit cycle due to Dutch Roll motion, they had concluded that Dutch Roll motion may consists of considerable roll, yaw and sideslip at low angle of attack, however the motion can become pure rolling motion as angle of attack is increased. The trigger parameters with the simple procedures were developed to predict the onset of wing rock.

Ananthkkrishnan and Sudhakar [4] constructed a model that will reveal one mechanism for large amplitude wing rock as a result of lateral longitudinal coupling and will also distinguish the Dutch Roll mode which is excited by the short period mode.

A nonlinear mathematical model of wing rock for slender delta wing has been developed experimentally by Hsu and Lan [5] where the wing rock motion was studied for one and three degree of freedom. The developed model has served as a benchmark for studying the phenomena of wing rock motion and controller design. Theoretical and experimental investigation of the wing rock for aircraft with slender delta wings have also been reported in [6]-[11]. Based on the delta wing model developed by Hsu and Lan [5] many modified analytical wing rock models have been developed by researchers to study the wing rock phenomenon.

In the paper given by Luo and Lan [12], theoretical analysis was conducted to determine the optimal input for suppressing the wing rock. The optimal equation was solved using the averaging technique of Beecham Tichener. In the control design, it is assumed that the aerodynamics parameters are known " a priori " which in practice is not always valid.

Wong et al. [13] employ leading edge blowing to control the wing rock. The method showed that for wing rock which is caused by the unsteadiness of the flow over the wing, the symmetric blowing has a damping effect to stop the limit cycle. To demonstrate experimentally the control method, a free to roll wind tunnel model

and a fast acting blowing control servo valves were developed. Control algorithm was developed and implemented in digital controller.

Optimal feedback control of wing rock was proposed by Shue et al. [14]. In the paper, a procedure is presented to optimize the state feedback control law. The closed loop Lyapunov function is assumed to have the same matrix form of state variables as the performance index. The optimal equation is derived using Hamilton Bellman equation and the control method requires the full state feedback.

The study of limit cycle oscillation in the context of providing adaptive excitation had been reported in the literature. In the study carried out in early sixties by A.Gelb [15], the limit cycle oscillation was thoroughly examined and analyzed. The limit cycle oscillation was used to provide sufficiency of excitation in the design of adaptive controllers. Along the similar line, the papers written by Horowitz et al. [16] and [17] detail the design of self oscillating adaptive system.

Adaptive control methods have been reported for backlash inverse control in the unknown nonlinear system. Kokotovic and Tao [18]-[20] proposed adaptive control of physical systems with backlash and hysteresis. In the control method, a mathematical model of the backlash was developed and an adaptive inverse controller was designed for unknown plant with backlash.

Control of the wing rock motion using adaptive feedback linearization was proposed by Monahemi and Kristic [21]. An adaptive controller design based on the backstepping method was developed to control wing rock of an aircraft having delta wings configuration.

R.M. Roger [22] presented an algorithm for determining the optimal constant coefficients that minimize the performance index for the control of nonlinear systems and applied to the optimal control of wing rock.

In the paper by Araujo et al. [23], a variable structure, model reference adaptive controller was proposed for controlling wing rock of a slender delta wing. Simula-

tion results show that the closed loop system is designed using bounds on uncertain function, the roll angle tracks the given reference trajectory and wing rock motion is suppressed.

In recent years, research has been reported of using neural networks for estimating aerodynamic coefficients and controlling the nonlinear dynamics in flight [24]-[27]. S.N Singh et al. [28] proposes neural networks for controlling wing rock motion of slender delta wings. In the paper, the wing rock model of roll dynamics based on aerodynamic hysteresis given in Hsu and Lan [5] is used. Radial Basis Function (RBF) neural networks are used in the design of an adaptive controller. The RBF network uses 441 neurons in hidden layer in the design, and an oscillatory closed loop response is observed during the learning phase of identifying nonlinear structure of the model. The control design does not take into considerations the model uncertainty and disturbances. In practice, the sources of wing rock in aircraft could be due to aerodynamic hysteresis, mechanical hysteresis or Dutch Roll dynamics, and normally the structure of nonlinearity is unknown. To employ the fixed structure of RBF to approximate high order nonlinearity coupled with model uncertainty and disturbance, the number of hidden units in RBF could be prohibitively large and computationally intensive.

Joshi et al. [29] in the most recent paper proposes the use of a single neuron controller to suppress the wing rock motion. The control method is based on a rule based fuzzy logic and a single neuron controller to suppress wing rock in delta wings. An experiment was carried out to demonstrate the effectiveness of the control method using a wing tunnel on a 80^o swept back wing. The proposed control method requires a priori knowledge of a physical system to specify a rule based control input based on past operating information as well as off-line training. A neural network is used to tune the rule-based controller. The method is demonstrated only to suppress wing rock in delta wings with some predetermined range of control inputs namely deflecting

aerodynamic control surfaces or different types of aerodynamic blowing mechanism in wind- tunnel experiments

1.4 Motivation

The current adaptive nonlinear control method for suppressing the wing rock is based on the assumption that the knowledge and structure of the nonlinearity in wing rock is known as "*a priori* ". Recently, neural networks have been proposed by researchers to model the nonlinear function of the wing rock for controller design purposes. However, the neural networks structure is fixed and the number of neurons required is arbitrarily determined and often resulting in over selecting an enormously large number of neurons than necessary. In this method the size of neurons is not optimal, and is pre-selected based on some heuristics.

The motivation for proposing the dynamic recurrent neural networks is to overcome the above limitations by minimizing the size of the neurons required in the network design. The identification of the unknown nonlinear system is carried out by dynamic recurrent RBF network. The interpretation of the properties of Preisach hysteresis model given in Mayergoyz [30] provides the criteria for neurons adding/pruning strategy during the training of the networks. The designed networks have robustness features by including a recurrent signal to take care of noise disturbances coming from sensor reading, wind gust etc. occurring in aircraft. The control methodology is carried out using adaptive hybrid control strategy.

1.5 Contributions of the thesis

The main contribution of this thesis is the design of an on-line, dynamic, self-adjusting, RBF network control methodology that will allow the neuron to add/prune to an op-

timum size during the identification of an unknown nonlinear physical system, while simultaneously the identified model is used in the design of an adaptive control law to suppress the wing rock. Prior research in the same application area uses RBF networks with a fixed and predetermined-size for the design of controllers. The size of networks is enormously large and computationally intensive. The specific contributions of this thesis are as follows:

(1) The application of the Preisach model by interpreting its properties in the design of dynamic recurrent RBF networks for modelling the uncertain nonlinear system that generates the wing rock motion. The RBF networks obtained from this design approach is minimal in their size.

(2) By interpreting the property of the Preisach model namely ensembles of the cells participating in the information storage, the concept of computing the ensemble average of the centres of the hidden units is introduced in training the networks. The ensemble average concept would lead to a finer approximation of the networks.

(3) By interpreting the properties of the memory formation mechanism described in the Preisach model, a criteria for adding/pruning of neurons during the training of the networks is developed. Using the strategy developed, the networks become dynamic in nature where the number of neurons will increase when the criteria is met and is decreased when it becomes superfluous.

(4) The use of the recurrent signal in the RBF networks will provide the robustness feature in dealing with the dynamic characteristics of a non-linear uncertain system that generates the wing rock motion.

(5) The use of sampled data hybrid control strategy by sampling the system's input and output allows the continuous time control of the system and discrete time identification and training of the networks. The training of the networks involves the adjustment of RBF's centre and width by using the Extended Kalman Filter (EKF) during the process of approximations for the unknown $\hat{f}$ and $\hat{g}$ functions. An in-

put term is included in the EKF for estimation of the weights associated with the $\hat{g}$ network.

1.6 Outline of the thesis

Chapter 2 provides the background material for the development of adaptive control methodology for controlling wing rock. Wing rock model obtained from a slender delta wing is used as a benchmark for the study. A review of the development of wing rock model and the analysis of the physical significance of the nonlinear terms are given. The rolling moment diagram is used to examine the hysteresis loop during the wing rocking conditions. The chapter discusses the current adaptive control methodology for controlling wing rock. A robustness feature of the adaptive control method is considered by modifying the adaptive update law and the results are verified by simulations.

Chapter 3 reviews different types of neural networks and provides the framework for the development of a neural control methodology. In particular, a radial basis function network is described which will be used in the neural control design. The concepts of learning and memory storage are discussed.

In chapter 4, the overview of the Preisach hysteresis model is given. The concept of hysteresis and the interpretation of the Preisach model are discussed. The similarity between the Preisach model and the radial basis function are compared and discussed. The interpretation and application of the Preisach hysteresis model as a radial basis function networks are detailed. The plausible reasonings of using its properties and memory formation mechanism in the design of radial basis function are given.

In chapter 5, the design architecture of the dynamic recurrent neural network for modelling the wing rock phenomenon is given. The criteria based on properties of the Preisach hysteresis model for the neuron growth are given. The training of

the networks is carried out as resource allocation network in which the neurons are allowed to grow to an optimal size. The design of the RBF networks together with the network controller is carried out in discrete time domain. The proposed recurrent RBF networks employ two separate adaptation schemes, where the RBF's centre and width are adjusted by the Extended Kalman Filter for the determination of an optimal network size, while the outer network layer weights are updated using the Lyapunov stability analysis for the closed loop control. Benchmarking of the proposed recurrent RBF network was carried out to evaluate the various features included in the design of the networks.

In chapter 6, the concept of geometric nonlinear control theory is presented and theory of feedback linearization is reviewed. The procedure for transforming a continuous non-linear system to a sampled data system is given. The design of the recurrent neural controller and the proof of the boundness of all the signals and stability of the controller are given.

In chapter 7, the developed neural control methodology is applied in controlling wing rock in delta wing. Using the wing rock model of a slender delta wing, the performance comparison on dynamic neural networks and the networks using a fixed structure is given. The wing rock in aircraft is examined using AFTI/F-16 testbed aircraft having a delta wings configuration. The effectiveness of the proposed dynamic recurrent RBF control methodology is demonstrated by simulations in the suppression of the wing rock. The robustness analysis of for the proposed recurrent RBF networks is also given and through simulations are also performed.

Finally in chapter 8, conclusions derived from this work are discussed and suggestions for future research are outlined.

Chapter 2

Adaptive Control Approach of Wing Rock

In this chapter a concept of *adaptive control methodology* is reviewed. A wing rock model obtained from a slender delta wing is used as a benchmark for illustrating the adaptive control design approach. The wing rock model used in the simulation study is discussed and the physical significance of the nonlinear damping terms are explained with examples. Control of wing rock is considered as a tracking problem, given a reference trajectory starting from non-zero initial conditions and it tends to zero as time goes to infinity. In the design for the adaptive nonlinear control, robustness feature in the presence of external disturbances is included

2.1 Review of Adaptive Control Methodology

A general notions of stability and preliminaries to be used later in this section are summarized as below. They are essential to the understanding of the adaptive control method used in the study of the thesis.

2.1.1 Lyapunov Stability

Consider an adaptive system represented by the following nonlinear vector differential equation of the form,

$$\dot{x} = f(x,t)\,, \qquad f(0,t) = 0, \qquad \forall\, t \geq t_o \tag{2.1}$$

where $x(t_o) = x_o$ and $f : \Re^+ \rightarrow \Re^n$ is such that a solution $x(t;\, x_o, t_o)$ exists for all $t \geq t_o$. It implies that $f(0,t) = 0$ is an origin. an equilibrium state. The concept of Lyapunov stability given by the following definitions and the theorems can be found in [31] and [32].

Definition 1 *The equilibrium state $x = 0$ of equation (2.1) is said to be stable if for every $\epsilon > 0$, and $t_o > 0$, there exists a $\delta(\epsilon, t_o) > 0$ such that $\|x_o\| < \delta$ implies $\|x(t; x_o, t_o)\| < \epsilon$, $\forall\, t \geq t_o$. On the contrary if the system is not stable, it is said to be unstable.*

Stability means that the system trajectory can be kept arbitrary close to the origin by starting sufficiently close to it. If the origin is stable, the state trajectory $x(t)$ will remain in the ball of arbitrarily specified radius B_R, and $r(R)$ can be found such that starting the state from within the ball B_R at $t = t_o$ will guarantee that the state will remain within the ball. Conversely, the equilibrium is unstable if there exists at least one ball B_R such that for $r > 0$ it is possible that for the system trajectory $x(t)$ starting within the ball eventually leaves the ball B_R.

Definition 2 *The equilibrium state $x = 0$ of equation (2.1) is said to be uniformly stable if $\delta(\epsilon, t_o)$ is independent of the initial time t_o*

Definition 3 *The equilibrium state $x = 0$ of equation (2.1) is said to be uniformly asymptotically stable if it is uniformly stable and for some $\epsilon_1 > 0$ and every $\epsilon_2 > 0$*

there exists $T(\epsilon_1,\epsilon_2) > 0$ *such that if* $\|x_o\| < \epsilon_1$, *then* $\|x(t;x_o,t_o)\| < \epsilon_2$ *for all* $t \geq t_o + T$.

Definition 4 *The equilibrium state* $x = 0$ *of the system given in equation (2.1) is said to be exponentially stable if there exists constants* $k > 0$ *and* $r > 0$ *such* $t\|x(t;x_o,t_o)\| \leq k\exp\{-r(t-t_o)\}\|x_o\|$, $\forall t \geq t_o$, *for all* t_o *and in a certain neighborhood of the origin.*

Definition 5 *If, in the ball* B_R, *the function* $V(x)$ *is positive definite and has continuous partial derivatives, and if its time derivative along any state trajectory of system (2.1) is negative semi-definite, i.e.* $\dot{V}(x) \leq 0$ *then* $V(x)$ *is said to be a Lyapunov function for the system (2.1).*

Theorem 1 *(Local Stability) If, in the ball* B_R, *there exists a scalar function* $V(x)$ *with continuous first partial derivatives such that*

.$V(x)$ *is positive definite*

.$\dot{V}(x)$ *is negative semi-definite*

then the equilibrium at the origin is stable.

Theorem 2 *(Global Stability) If there exists a scalar function* V *of the state* x,*with continuous first order derivatives such that*

.$V(x)$ *is positive definite*

.$\dot{V}(x)$ *is negative definite*

.$V(x) \to \infty$ *as* $\|x\| \to \infty$

then the equilibrium at the origin is globally asymptotically stable.

2.1.2 Strictly Positive Real (SPR) Functions

A rational function $H(s)$ is SPR if and only if the following conditions are satisfied.(refer to Narendra [31]).

(i) $H(s)$ is analytic in $\mathrm{Re}[s] \geq 0$

(ii) $\mathrm{Re}[H(j\omega)] > 0 \quad \forall\omega \in (-\infty, \infty)$

(iii) $(a)\ \lim_{\omega^2 \to \infty} \omega^2\, \mathrm{Re}[H(j\omega)] > 0$ when $n^* = 1$, and

$(b)\ \lim_{|\omega| \to \infty} \frac{H(j\omega)}{j\omega} > 0$ where $n^* = -1$

where n^* is the relative degree of $H(s)$ and is defined as number of poles of $H(s)$ - the number of finite zeros of $H(s)$.

2.1.3 Model Reference Adaptive Control

Generally, a model reference adaptive control system consists of a *plant* containing unknown parameters, a *reference model* for specifying the desired output of the control system, a *feedback control law* containing adjustable parameters and an *adaptation mechanism* for updating the adjustable parameters. The general control scheme is shown in Figure 2.1.

The simple example given below is served to illustrate the general concept of the adaptive control methodology. The comprehensive treatment of the subject can be found in [31].

Error Dynamics

Let the dynamic system or the plant to be controlled, be given by the following function :

$$K_p W(s) = K_p \frac{Z_p(s)}{R_p(s)} \tag{2.2}$$

where K_p is unknown nonzero constant with a known sign, and $Z_p(s)$, $R_p(s)$ are monic Hurwitz polynomials of degree $n-1$ and n respectively.

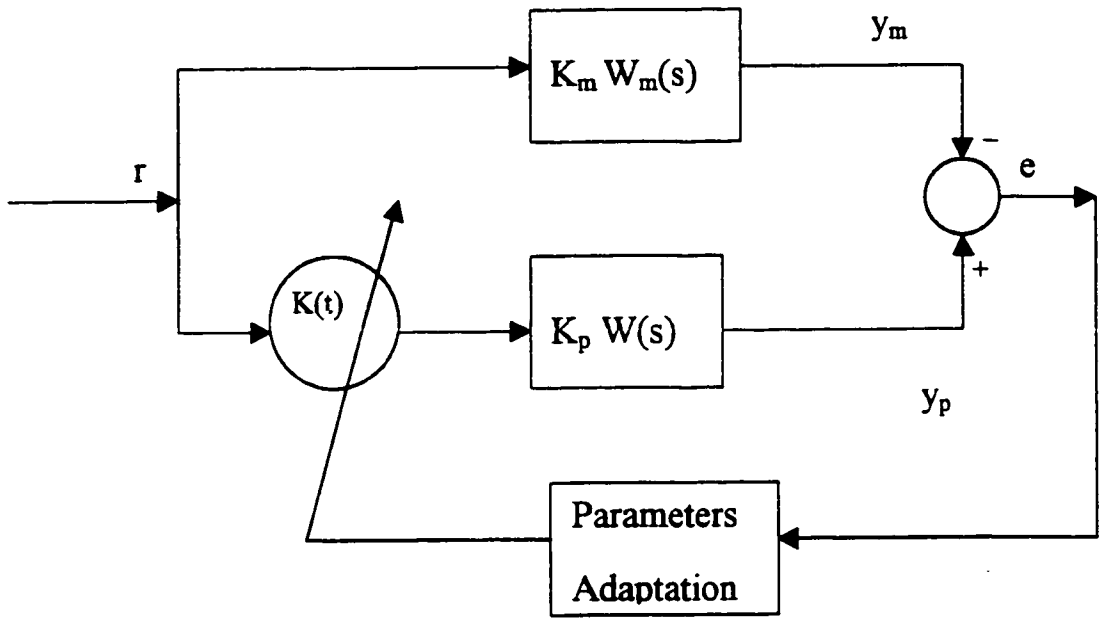

Figure 2.1: Control Scheme of Model Reference Adaptive Control

Let the model reference be given as

$$K_m W_m(s) = K_m \frac{Z_m(s)}{R_m(s)} \tag{2.3}$$

where $Z_m(s)$, $R_m(s)$ are monic Hurwitz polynomials of degree $n-1$ and n respectively.

For the purpose of illustrating the adaptive control concept, the following simple case is given.

(i) The transfer function of the plant is known except the high frequency gain K_p.

(ii) $Z_p(s) = Z_m(s)$, $R_p(s) = R_m(s)$, hence $W(s) = W_m(s)$

Choose the following control input to the plant

$$u(t) = K(t)r(t) \tag{2.4}$$

where $K(t)$ is an adjustable parameter and $r(t)$ is a reference signal. The plant output

$y_p(t)$ and model output, $y_m(t)$ are given as.

$$\begin{aligned} y_p(t) &= K_p W(s)u(t) \\ &= K_p W(s)K(t)r(t) \end{aligned} \tag{2.5}$$

$$y_m(t) = K_m W(s)r(t) \tag{2.6}$$

Define the error between the plant and model outputs as e and the parameter error, ψ as given below.

$$\begin{aligned} & e(t) \triangleq y_p(t) - y_m(t) \\ = \; & K_p W(s)r(t)K(t) - K_m W(s)r(t) \\ = \; & W(s)r(t)K_p[K(t) - \frac{K_m}{K_p}] \\ = \; & W(s)K_p\psi(t)r(t) \end{aligned} \tag{2.7}$$

$$\psi(t) \triangleq K(t) - \frac{K_m}{K_p} \tag{2.8}$$

Adaptive Law Derivation

The aim of the adaptive model reference control is to determine the bounded control input $u(t)$ so that all signals in the system remain bounded and the error satisfies $\lim_{t\to\infty} \|y_p(t) - y_m(t)\| = 0$. To derive the adaptive law, consider the following lemma.

Lemma 1 [31]

Consider the following general dynamical system :

$$\dot{x}\,(t) = Ax(t) + b\phi^T(t)w(t) \tag{2.9}$$

$$y = h^T x(t) \tag{2.10}$$

$$z_1(t) = ky(t) \tag{2.11}$$

where (A, b) is stabilizable, (h^T, A) is detectable and $h^T(sI - A)^{-1}b \triangleq H(s)$ is SPR (strictly positive real)

Let $\phi : R^+ \rightarrow R^m$ be a vector of adjustable parameters, k be unknown with a known sign, and $w : R^+ \rightarrow R^m$ be an input vector and $z_1 : R^+ \rightarrow R$, be time varying measurable functions. If ϕ is adjustable, then

$$\dot{\phi}(t) = -sgn(k)\, z_1(t)\, w(t) \tag{2.12}$$

then the equilibrium state $(x = 0, \phi = 0)$ of system in equations (2.9), (2.10) and (2.11) is uniformly stable at large.

Based on **Lemma 1,** the adaptive control law for the given system (2.1) can be obtained as below. If

$$\dot{K}(t) = -sgn(K_p)\, e(t)\, r(t) \tag{2.13}$$

$e(t)$ and $\phi(t)$ are bounded for $t \geq t_o$, since $r(t)$ is uniformly bounded $\dot{e}(t)$ is bounded. From the following Barbalat's lemma, it follows that $\lim_{t\rightarrow\infty} \|y_p(t) - y_m(t)\| = 0$, so that the plant output approaches the reference model *output* asymptotically.

Barbalat's Lemma

If $f(t)$ is a uniformly continuous function s.t. $\lim_{t\rightarrow\infty} \int_o^t f(\tau)d\tau$ *exists and finite, then* $\lim_{t\rightarrow\infty} f(t) \rightarrow 0$.

Adaptive Control using Lyapunov Redesign

Let the plant and reference models be described by the following :

$$\dot{y_p} = -a_p y_p + K_p u(t) \tag{2.14}$$

$$\dot{y_m} = -a_m y_m + K_m r(t) \tag{2.15}$$

Defining $e = \dot{y}_p - \dot{y}_m$

$$\dot{e} = -(a_p - a_m)e + r(t)K_p(K(t) - \frac{K_m}{K_p}) \tag{2.16}$$

If $K(t)$ is forced to converge to the constant value $\frac{K_m^*}{K_p^*} = K^*$, the error equation becomes

$$\dot{e} = -(a_p - a_m)e + r(t)K_p(K(t) - K^*) \tag{2.17}$$

Letting $\phi = K(t) - K^*$ and since K_p^* is fixed, although K_p is unknown, it follows that $\dot{\phi} = \dot{K}(t)$.

The Lyapunov redesign approach implies finding the adaptive update law such that the following Lyapunov function

$$V(e, \phi) = e^2 + K_p\phi^2 \tag{2.18}$$

is decreasing along the trajectory of the error system

$$\dot{e} = -(a_p - a_m)e + r(t)K_p\phi \tag{2.19}$$

where ϕ is the update law and assuming $(a_p - a_m) > 0$. For stability, the Lyapunov function should be positive definite which implies the sign of K_p should be known and positive $K_p > 0$ in equation (2.19). Taking the derivative of Lyapunov function $V(e, \phi)$ along the trajectory of the error system in equation (2.19) the following is obtained.

$$\dot{V}(e, \phi) = -2(a_p - a_m)e^2 + 2K_pe\phi r(t) + 2K_p\phi\dot{\phi} \tag{2.20}$$

Choosing $\dot{K} = \dot{\phi} = -er(t)$ gives $\dot{V}(e, \phi) = -2(a_p - a_m)e^2 \leq 0$, implying $e \to 0$ as $t \to \infty$. Since $\dot{V}(e, \phi)$ is negative semidefinite, asymptotic stability of the origin in the (e, ϕ) space is not conclusive. The convergence of $K(t)$ to K^* depends on the

persistent excitation of the reference signal $r(t)$.

2.2 Wing Rock Model

Wing rock is a self-induced oscillatory rolling motion, a dynamic phenomena experienced by slender wing aircraft flying at high angle of attack. Wing rock motion is attributed to nonlinear aerodynamic mechanism prevails at high angle of attack and is characterized by a buildup of limit cycle oscillation. It has been reported that wing rock exhibited by actual aircraft is chaotic in the amplitude of limit cycle.

There are several theoretical models proposed by researchers to describe the wing rock motion. However, each model is verified for a particular configuration and none of these models can be applied to predict the wing rocking for all different configurations.

Ross [9] carried out combined experimental and theoretical study of the nonlinear lateral oscillation experienced by slender wing H.P 115 research aircraft. A three-degree-of-freedom lateral directional equations of motion with fourth order differential equation in sideslip, β are obtained. The wing rock motion is analyzed using the approximation method to obtain the solution. The study shows that wing rock develops with the bank angle of about 30 deg.

Schmidt [2] assumes aerodynamic hysteresis of the rolling moment with sideslip in the development of a two-degree-of-freedom model including rolling and yawing moments. It is concluded that the wing rock motion due to aerodynamic hysteresis corresponding to a roll moment relay action is dependent upon the sign of the sideslip angle.

An analysis of slender wing rock phenomenon caused by asymmetric leading edge vortices was studied by by Ericsson [7]. A one-degree-of-freedom model for delta wing with leading-edge sweep larger than 74 deg was developed to predict the wing rock motion. The study concludes that the vortex breakdown has a damping effect on the

roll oscillation and is not contributing to the wing rock. Wing rock will only occur for a delta wings with more than 74 deg leading edge sweep for the asymmetric vortex before it bursts as the angle of attack is increased.

Konstadinopoulos et al [11] carried out the experimental studies of the self -excited motion of the flat delta wing about an axis parallel to the midspan chord. An unsteady vortex-lattice method is used to provide the aerodynamic loads. The solution of the equation of motion provides the wing rock motion and the flowfield simultaneously. For a small angle of attack, the wing rock does not develop. When the angle of attack exceeds certain critical value, the asymmetric vortex becomes unstable. The studies conclude that for a small disturbance, the limit cycle is stable, however, for a large disturbance the motion does not achieve limit cycle. The studies and modelling of wing rock using slender delta wings have been carried out using different approaches such as experimentally, computationally and analytically. A through review of wing rock in slender delta wing is given by Arena [33].

2.2.1 One-Degree-of-Freedom Model

Based on experimental data and rigid body equations, Hsu and Lan [5] and Hsu [34] developed a one-degree-of-freedom model for wing rock in slender delta wing. The following appropriate assumptions are made regarding the development of the model.

(1)The wind tunnel is constrained so that it can perform in a rolling motion. The principal motion variable is Euler roll angle, ϕ.

(2)The pitching and yawing effect are ignored.

(3)The flight path properties such as flight velocity, Mach number, altitude, Reynolds number, mass distribution are constants through the motion.

(4)The effect of gravitational force, elastic force, and propulsion force are excluded.

(5)The rigid aircraft with the observer is fixed at body axis system, the origin is the centre of mass of the aircraft.

(6)There is no roll divergence occurring in the motion

(7)Wind tunnel model is a free-to-roll delta wing with 80 deg sweep (Figure 2.2).

The equation governing the pure rolling motion is obtained from Newton's second law [35].

$$\sum L = I_{xx} \ddot{\phi} \tag{2.21}$$

where I_{xx} is the rolling moments of inertia in body fixed X axis (Figure 2.3), $\ddot{\phi}$ is roll angle acceleration. The rolling moment, L and the roll angle, ϕ can be expressed in terms of an initial reference and small pertubations from the nominal values by the following expressions

$$L = L_o + \Delta L \tag{2.22}$$

$$\phi = \phi_o + \Delta\phi \tag{2.23}$$

where respectively L_o and ϕ_o are initial references of rolling moment and roll angle, ΔL and $\Delta\phi$ are perturbed rolling moment and roll angle. Equation (2.21) then reduces to the following

$$\Delta L = I_{xx} \Delta \ddot{\phi} \tag{2.24}$$

For ease of analysis the notation Δ is dropped with the notion that the variables are understood to be perturbation variables. The rolling moment L is given by the following equation.

$$L = C_l(t)\, q\, S\, b \tag{2.25}$$

Substituting equation (2.25) into equation (2.21) yields the following.

$$(\frac{I_{xx}}{qSb})\,\dot{p} = C_l(t) \tag{2.26}$$

where I_{xx} is a moment of inertia about X axis, q the dynamic pressure, S the reference wing area, b the wing span, $\dot{p} = \ddot{\varphi}$, the roll angular acceleration, and $C_l(t)$ the total aerodynamic rolling moment coefficient. Equation (2.26) is interpreted as that the inertial rolling moment is balanced by the time dependent aerodynamic rolling moment. The aerodynamic rolling moment coefficient at steady state is expressed as a function below, the detailed analysis are given in reference [34].

$$C_l(t) = C_l(\alpha_s,\, \beta(t),\, \bar{p}\,(t),\, \delta_A(t)) \tag{2.27}$$

where α_s is a steady state angle of attack (AOA), $\bar{p}$ is a reduced rolling velocity with respect to roll axis and δ_A is aileron deflection.

$C_l(t)$ is expressed as component functions as below:

$$C_l(t) = C_{lo} + C_{l\beta}\beta + C_{lpt}\ \bar{p} + C_{l\delta A}\ \delta_A \tag{2.28}$$

where

$$C_{lpt} = C_{lpo} + C_{lp\beta}\,|\beta| + C_{lpp}\ |\bar{p}| \tag{2.29}$$

In equation (2.28), C_{lo} is a rolling moment coefficient at zero sideslip. $C_{l\beta}$ is dihedral effect assuming negative (stable) and positive (unstable) values depending on configurations, $C_{l\delta A}$ is a aerodynamic roll derivative due to aileron deflection, C_{lpo} is a roll damping coefficient at zero sideslip. $C_{lp\beta}$, dimensionless variation of roll damping derivative with sideslip, $\partial C_{lp}/\partial\beta$, and C_{lpp}, a dimensionless variation of roll damping derivative with roll rate, $\partial C_{lp}/\partial\bar{p}$.

Equation (2.28) describes the aerodynamic nonlinearities of the model. The ab-

solute sign on β and $\bar{p}$ is important and they cause the values of C_{lpl} to be the same if $|\beta|$ or $|\bar{p}|$ have the same values at the corresponding instants in the limit cycle oscillation. At fixed β, $C_l(t)$ may have two values if the sign of $\bar{p}$ is different, and for fixed $\bar{p}$, $C_l(t)$ may have two values if the sign of β is different. Thus β and $\bar{p}$ dependent roll damping will produce hysteresis loop with respect to β and $\bar{p}$.

Using the kinematic relationships below,

$$p = \dot{\phi} \tag{2.30}$$

$$\beta \approx \phi \sin \alpha_s \tag{2.31}$$

Substituting equations (2.28), (2.29) (2.30) and (2.31) into equation (2.26), the following wing rock model expressed in dimensionless derivatives is obtained

$$\ddot{\phi} = L_o + L_{\delta A}\ \delta_A + \sin\ \alpha_s L_\beta \phi + L_{po}\,\dot{\phi} + \sin\alpha_s\ L_{p\beta}\ |\phi|\ \dot{\phi} + L_{pp}\left|\dot{\phi}\right|\dot{\phi} \tag{2.32}$$

Dropping the dimensionless derivative due to aileron deflection $L_{\delta A}\ \delta_A$ and including the control input u, the following is the common model reported in most literature and it will be used in this research.

$$\ddot{\phi} = L_o + \sin\ \alpha_s L_\beta \phi + L_{po}\,\dot{\phi} + \sin\alpha_s\ L_{p\beta}\ |\phi|\ \dot{\phi} + L_{pp}\left|\dot{\phi}\right|\dot{\phi} + a_o\ u \tag{2.33}$$

where $c_o = L_o$, $c_1 = \sin\alpha_s\ L_\beta$, $c_2 = L_{po}$, $c_3 = \sin\alpha\ L_{p\beta}$, $c_4 = L_{pp}$, and the parameters $c_i\ s$ are expressed in terms of dimensional derivatives L_o, L_β, L_{po}, $L_{p\beta}$, and L_{pp} defined as below.

$L_o = qSbC_{lo}/I_{xx},\ \ s^{-2}$

$L_\beta = qSbC_{l\beta}/I_{xx},\ \ s^{-2}$

$L_{po} = qSb^2 C_{lpo}/(2I_{xx}V),\ \ s^{-1}$

$L_{p\beta} = qSb^2 C_{lp\beta}(2I_{xx}V),\ \ s^{-1}$

$L_{pp} = qSb^3 C_{lpp}/(4I_{xx}V^2)$

$L_{\delta A} = qSbC_{l\delta A}/I_{xx},\ s^{-2}$

where

I_{xx} is moment of inertia about X axis, q is a dynamic pressure, S is a wing reference area, b is a wing span, u is a control input and a_o is a estimate of the control effectiveness relating to control input signal and angular acceleration.

X, Y, Z is a rectangular coordinates of body-fixed axis system as shown in Figure 2.3. The angle of attack (AOA) is defined as $\alpha = \tan^{-1}\frac{w}{u}$ and the sideslip angle as $\beta = \sin^{-1}\frac{v}{V}$ where u, v, w are the velocity components along X, Y, Z axes respectively and V is a magnitude of forward flight velocity.

Letting $\phi = x_1$ and $\dot{\phi} = x_2$, equation (2.33) can be written in state equations as

$$\begin{aligned} \dot{x}_1 &= \dot{\phi} \\ \dot{x}_2 &= \ddot{\phi} = f(x) + a_o u \\ where\ f(x) &= c_o + c_1 x_1 + c_2 x_2 + c_3 |x_1| x_2 + c_4 |x_2| x_2 \end{aligned} \tag{2.34}$$

and $c_o = L_o$, $c_1 = \sin\alpha_s\, L_\beta$, $c_2 = L_{po}$, $c_3 = \sin\alpha\, L_{p\beta}$, $c_4 = L_{pp}$

For the three-degree-of-freedom model, in addition to rolling moment coefficient, more extra nonlinearity terms of side force and yawing moments coefficients are considered. These coefficients can be expressed as functional relationship similar to equation (2.27) with extra terms such as yaw rate and rudder deflection. The complete derivation is given in [34]. In general, an aircraft in the air should be six-degree-of-freedom motion and rolling may be the primary mode in the wing rock motion. In most of the research reported, the researchers deal with the model in wind tunnel test

stand for a single-degree-of-freedom rolling motion. The use of one-degree-of-freedom model in this thesis work is served to illustrate a concept of the proposed control methodology and the equations used were those necessary for achieving that goal.

Based on the formulation of the wing rock given equation (2.32), many modified wing rock models have been proposed by other researchers. Nayfeh et al. [6] proposed an analytical expression for the aerodynamic roll moment characteristic of wing rock. The expression for dimensionless roll moment was assumed to be

$$C_l(t) = a_1\varphi + a_2\,\dot{\varphi} + a_3\,|\varphi|\,\dot{\varphi} + a_4\,\left|\dot{\phi}\right|\,\dot{\phi} \tag{2.35}$$

where coefficients a_i s are obtained numerically from the least-squares fitting from roll moments. In the model estimation process, the model developed by Hsu in equation (2.32) is used to generate the test data for fitting the estimated moment given in equation (2.35) to obtain the unknown coefficients a_i s. The estimated model is then compared with Hsu's model for convergence analysis. Nayfeh added a cubic term to the roll moment expression to allow for roll divergence so that different equilibrium states could be obtained, yielding

$$C_l = a_1\phi + a_2\,\dot{\phi} + a_3\,|\phi|\,\dot{\phi} + a_4\,\left|\dot{\phi}\right|\,\dot{\phi} + a_5\phi^3 \tag{2.36}$$

Due to the cubic term, roll divergence could be obtained for certain initial conditions outside the narrow band near limit cycle attractor. As shown in Figure 2.4 that some initial conditions lead to a stable limit cycle, an equilibrium states, while other initial conditions lead to roll divergence indicated in the boundary labeled A. It was suggested by Nayfeh that if the non analytical term, a nonlinear damping term used in Hsu and Lan's formulation, $|\phi|\,\dot{\phi}$, be replaced by analytical term, $\phi^2\,\dot{\phi}$ a better agreement with experiments could be obtained. There are infinite possible combinations of nonlinear terms in order to generate a limit cycle. However, to fully

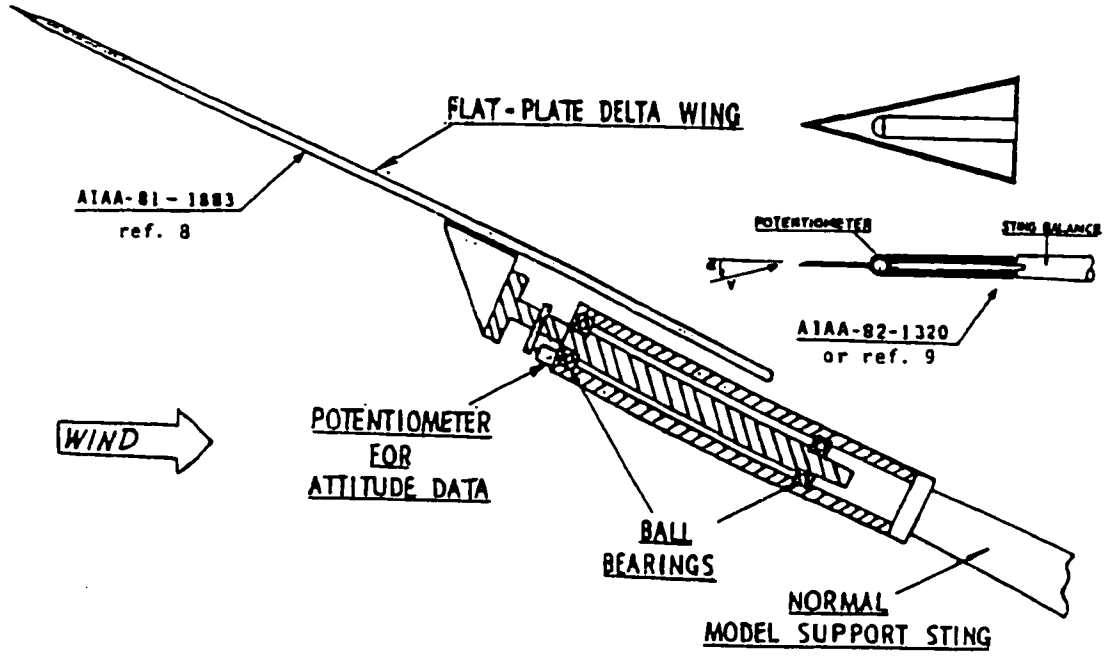

Figure 2.2: Free-to-Roll Rig (Wind Tunnel Experiment) [34]

understand the wing rock, the physical insights or mechanisms which are responsible for these non-linearities such as vortical flow field characteristics, planform geometry, slender forcebodies, leading edge extension etc. have to be identified.

2.2.2 Nonlinear Damping and Hysteresis Loop in Wing Rock

Analytical Model 1

For selecting the model to fit the estimated rolling moment, the following model equation is assumed by Tan [37].

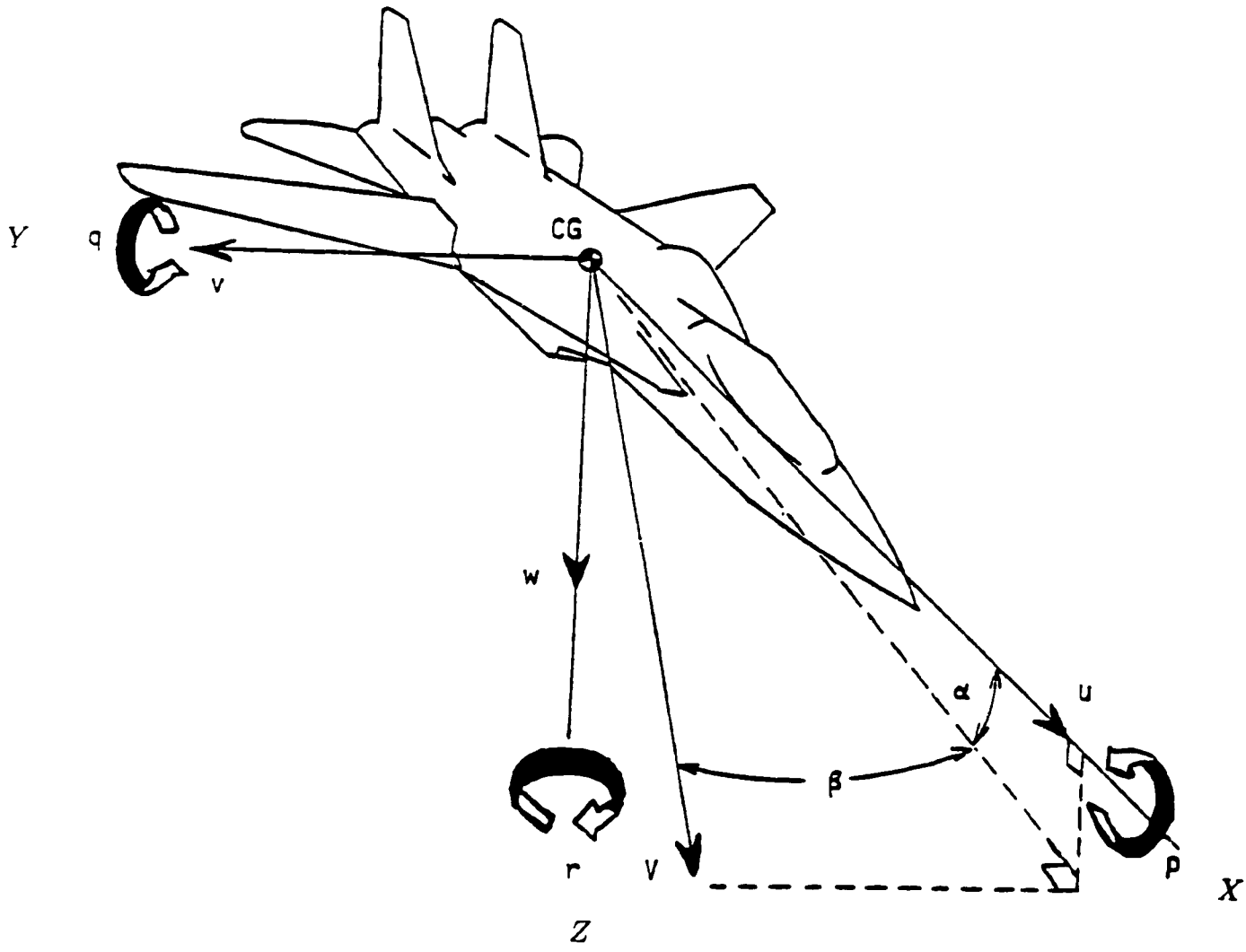

Figure 2.3: Body System of axes [34]

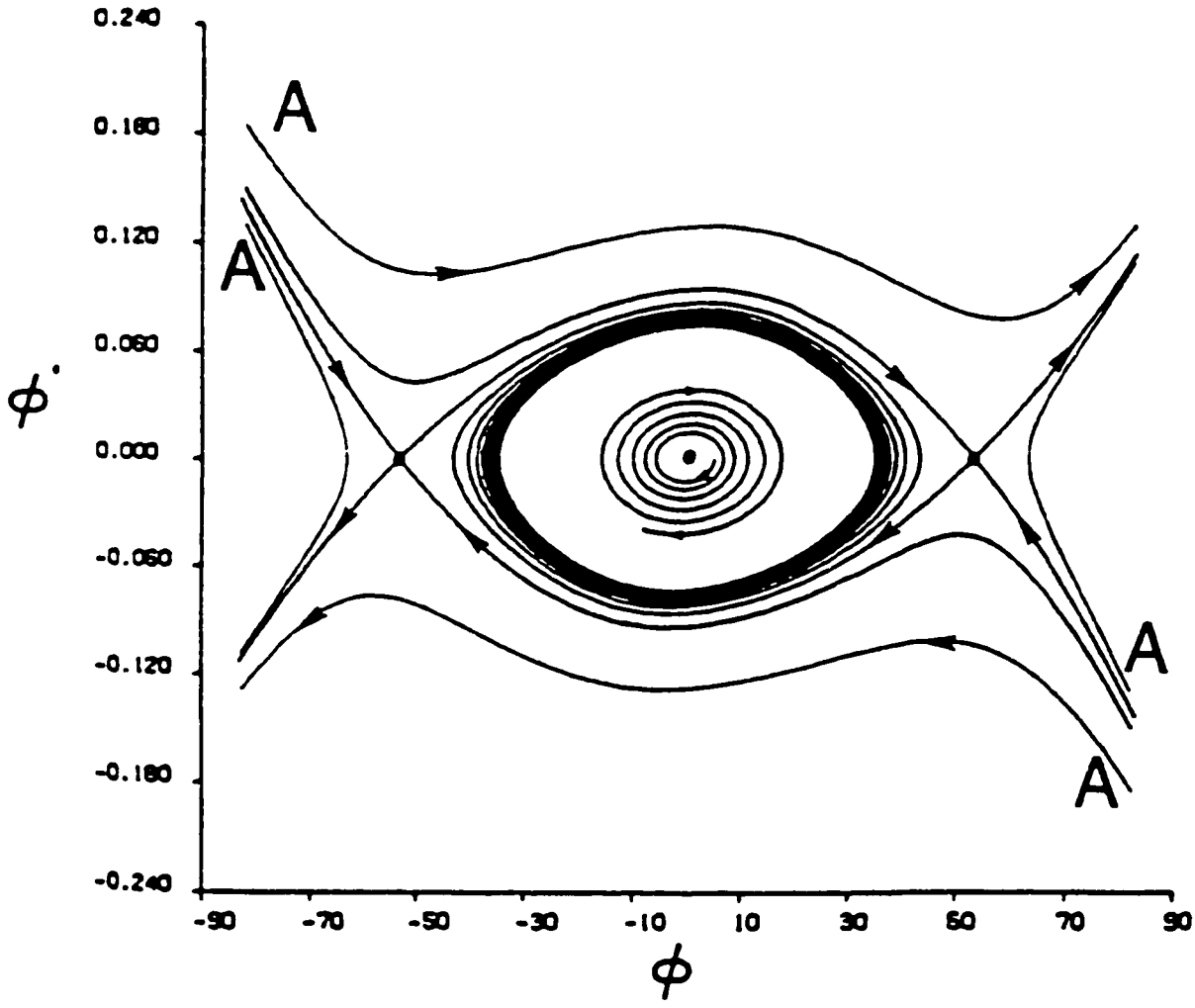

Figure 2.4: Phase Diagram, Nayfeh [6]

$$Cl(t) = a_1\phi + a_2\dot{\phi} + a_3|\phi|\dot{\phi} + a_4\phi^2 + a_5\phi\dot{\phi} + a_6\dot{\phi}^2 + a_7\phi^3 + a_8\phi^2\dot{\phi} + a_9\phi\dot{\phi}^2 + a_{10}\dot{\phi}^3 + \ldots a_m\phi^n + \ldots + a_{m+n}\dot{\phi}^n \quad (2.37)$$

where $m = n(n+2)/n$, m is the number of terms and n is the degree in the polynomial.

Tan had carried out the analytical fitting using the least square method for Hsu's model [5] based on 80 degree delta wing and considering only the three terms in the model. The estimated model is given as below.

$$\ddot{\phi} = -26.592\,\phi + 0.739\,\dot{\phi} - 2.822\,\dot{\phi}\,|\phi| \quad (2.38)$$

In the model, $\dot{\phi}$ is a linear damping term and $|\phi|\,\dot{\phi}$ is a nonlinear damping term. Using the initial conditions of $\phi_o = 0.1\ rad$ and $\dot{\phi}_o = 0.032\ rad/\sec$ the roll angle response is given in Figure 2.5 and the phase plane is given in Figure 2.6 which shows that the limit cycle is stable. The change of the nonlinear term, $\dot{\phi}\,|\phi|$ with roll angle is given in Figure 2.7.

As wing rock is developed by negative roll damping and sustained by nonlinear aerodynamic roll damping, Figures 2.6 and 2.7 will provide the information regarding the sustaining mechanism of the oscillation. According to [37], comparing these two figures it shows that for the small roll angle ϕ, the linear negative damping $\dot{\phi}$, is larger than the nonlinear damping $|\phi|\,\dot{\phi}$. as the result, the net damping is negative and the roll amplitude grows. As the roll amplitude becomes larger, the nonlinear damping is increased and the roll rate is decreased. When roll angle increases to certain value ($\phi \approx \pm$ 0.6 rad in Figure 2.6), the net damping changes from negative to positive, and the restoring rolling moment then drives the roll angle back to the original point $\phi = 0$.

Hysteresis Loop

In the wind tunnel experiment, the free-to-roll tests of the physical model allow the measurement of roll angle, ϕ for estimating the angle of attack α, sideslip β, roll rate, $\dot{\phi}$ and the total rolling moment coefficient, $C_l(t)$ given in equation (2.26). The plot of $C_l(t)$ versus roll angle ϕ is a rolling moment histogram and it will provide a lot of information during actual wing rock conditions.

Katz et [38] uses the rolling moment histogram to examine wing rock by observing the hysteresis loops in the diagram. The rolling moment diagram hysteresis loop given in Figure 2.8 shows that the undamped loop, corresponding to negative damping near the level point of wing rock (zero roll angle) is balanced by the two damped loops, corresponding to positive damping at two ends of limit cycle. From the viewpoint of energy exchange, the existence of hysteresis loops indicate there is a gain and loss of energy during the limit cycle oscillation.

The energy integral for the rolling moment is given below [37].

$$\dot{W} = qSb/2 \oint C_l \, d\phi \tag{2.39}$$

where $\dot{W}$ is the work done to the system, q is a dynamic pressure, S is a wing reference area, b is a wing span and $\oint$ is a contour integral, C_l is a rolling moment coefficient. If $\dot{W} > 0$, the system is unstable, the direction of hysteresis is clockwise as shown in the centre loop in Figure 2.8. At the other two outer loops, energy is dissipated, $\dot{W} < 0$, through positive net damping, the system is then stable and the direction of hysteresis moves counterclockwise. The balance of the energy exchange sustains the limit cycle oscillation

Figure 2.9 shows the rolling moment histogram of the model given in equation (2.38), it is observed that the system has three hysteresis loops, the unstable loop in the centre, and two outer stable loops. The net energy in the system is balanced and

the limit cycle is stable.

Analytical Model 2

The second example is least square fitted analytical model consisting of six terms given as below.

$$\begin{aligned} \ddot{\phi} &= -130.414\phi + 1.081\,\dot{\phi} - 111.553\,\dot{\phi}\,|\phi| \\ &\quad +43.390\phi^2 - 0.711\,\dot{\phi}\,\phi - 0.248\,\dot{\phi}^2 \end{aligned} \tag{2.40}$$

The estimated model [37] is for first mode oscillation using the experimental free-to-roll sting fuselage-vertical tail in the low speed wind tunnel of AIDC, Taiwan. The test data are collected at : angle of attack $\alpha = 10^o \sim 42^o$, sideslip $\beta = 0$, dynamic pressure $q = 31.1\ lb/ft^2$.

The limit cycle oscillation is triggered by asymmetric vortex shedding from the forebody. The roll angle response of the model given in equation (2.40) is shown in Figure 2.10. The response is quite different from Figure 2.5 that the limit cycle builds up rapidly to the full amplitude. Using the different initial conditions as reported in [37] $\phi_o = -0.2\ rad$ and $\dot{\phi}_o = 0.01\ rad/sec$, the phase plot shown in Figure 2.11 is stable. The nonlinear damping diagram shown in Figure 2.12 is quite different from Figure 2.7. The trajectory arrives at and leaves the critical point (roll angle $\phi = 0$) but never go through this point. The rolling moment diagram given in Figure 2.13 shows there is a clockwise stable loop balanced by two counterclockwise unstable loops.

The analytical studies of wing rock concern only with modelling the non-linearities in the rolling moment. The problem with this approach is that the model lacks physical insights of the flow field characteristics which are responsible for these non-linearities.

These models also do not help in determining the fluid mechanism associated with wing rock. A viewpoint held by the author, Edward Lan [39] who developed the wing rock model states that "the continuous wing rock model given in equation (2.32) involving non-analytical function is an efficient way to model the aerodynamics. To develop wing rock, the rolling moment coefficient versus the roll angle curve must show clockwise hysteresis. The mechanism is aerodynamic and not dynamic in nature. Hysteresis is not regarded as discontinuous function or phenomena, it just indicates being rate dependent".

2.3 Adaptive Nonlinear Control of Wing Rock

Limit cycle oscillation in wing rock of slender delta wing is a non linear control problem. There are number of methods available for the design of nonlinear controller namely feedback linearization, adaptive control, sliding mode control, neural control etc. The application of feedback linearization for controlling the nonlinear system are numerous and some application examples can be found in [40]-[42].

The adaptive control methodology has been developed in earlier seventies, although mostly to linear systems. There are two earlier papers published by I.D. Landau et al. [43], and K. S. Narendra et al. [44] on adaptive control methods as applied to aircraft. In these papers, the adaptive control method was used to adjust the time-varying parameters of the aircraft flight controller. In most physical systems there exist some nonlinearities, but with limitation, the adaptive control developed for linear system can be applied for nonlinear systems. Adaptive inferential control developed in [45] has been proposed to control a nonlinear chip refiner.

Based on the analysis given in [28] and [31] the adaptive control method will be illustrated for controlling wing rock motion. Adaptive model reference control will be used in the design of non linear control system. In applying the control method,

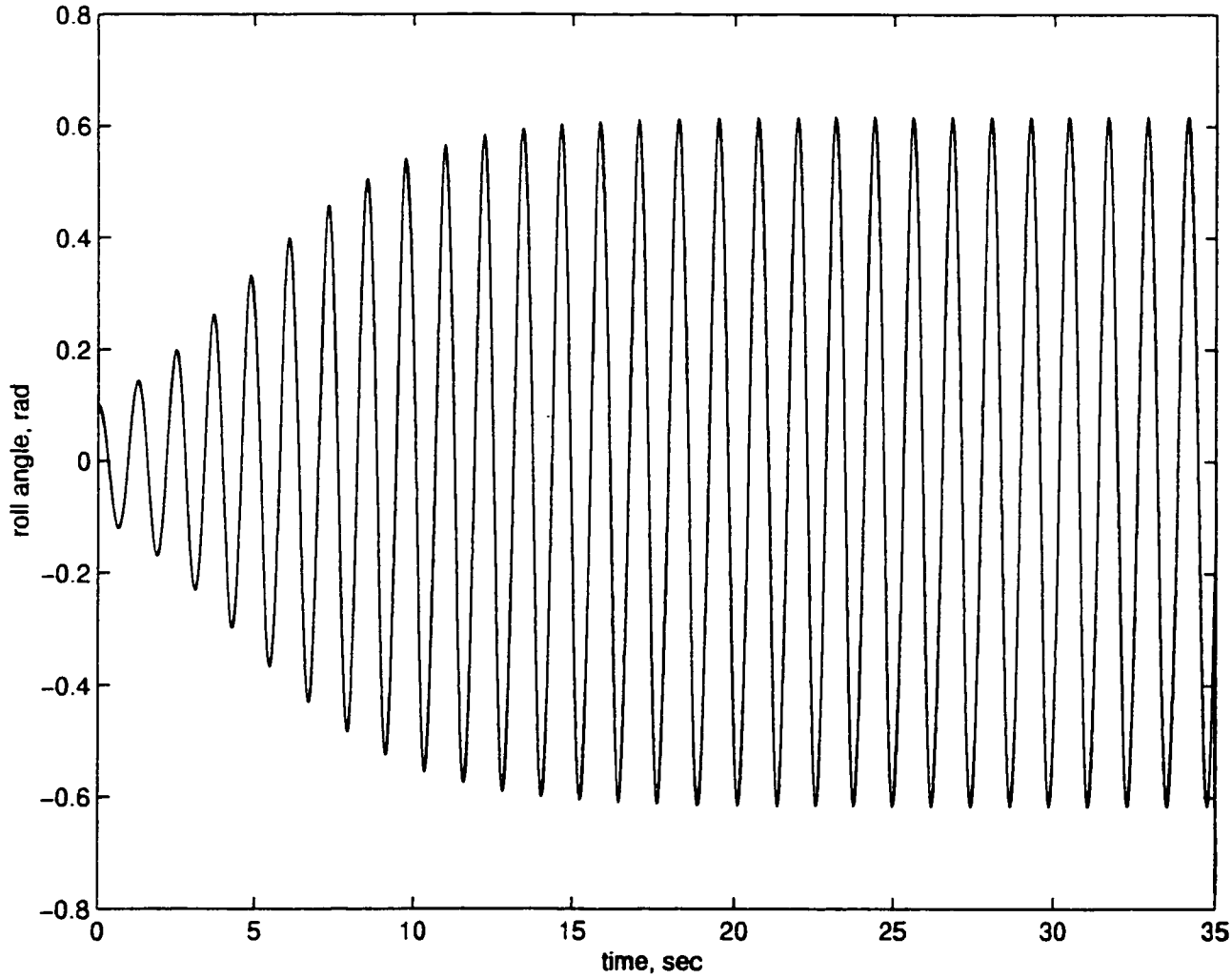

Figure 2.5: Roll angle response

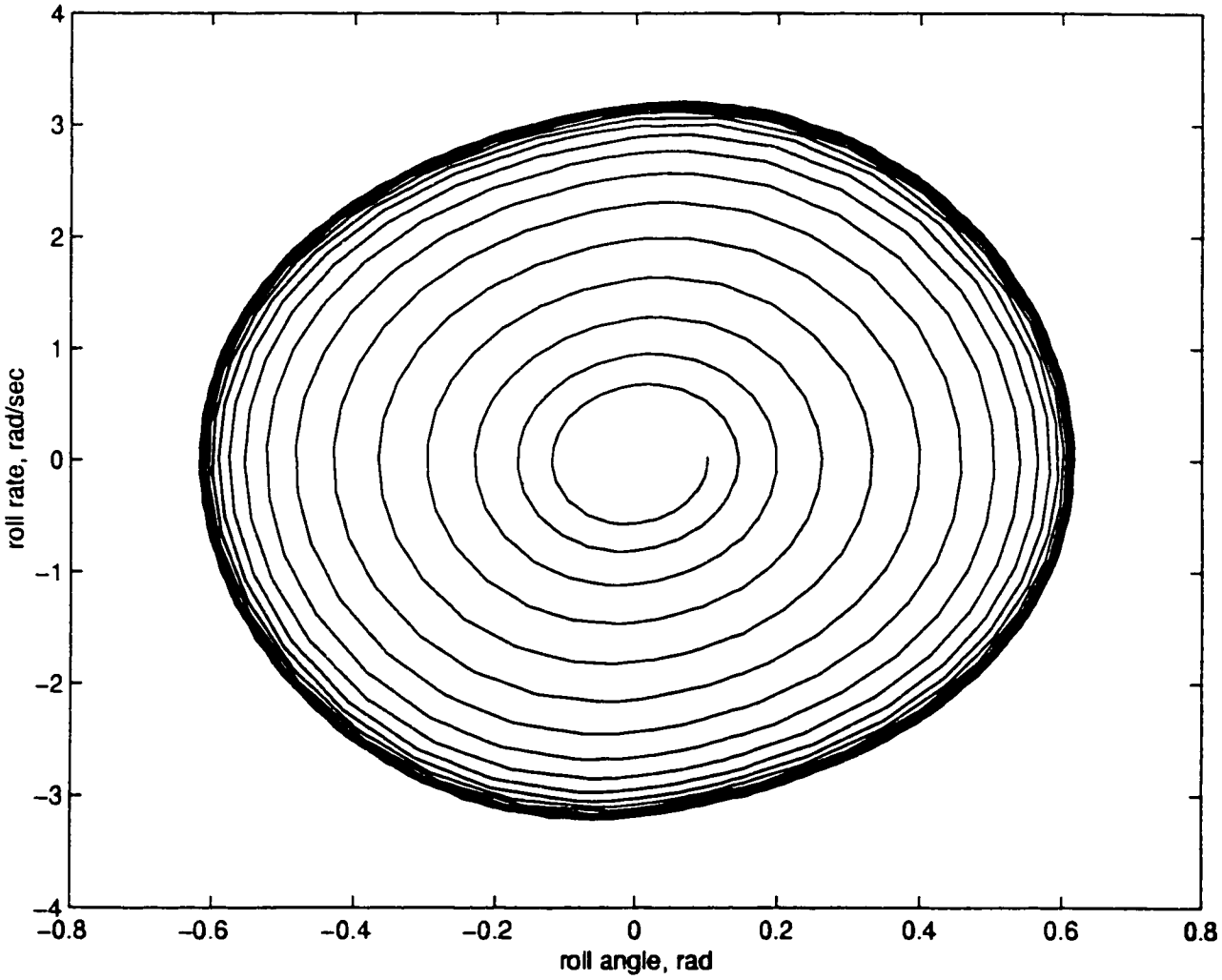

Figure 2.6: Phase diagram for Tan's fitted model

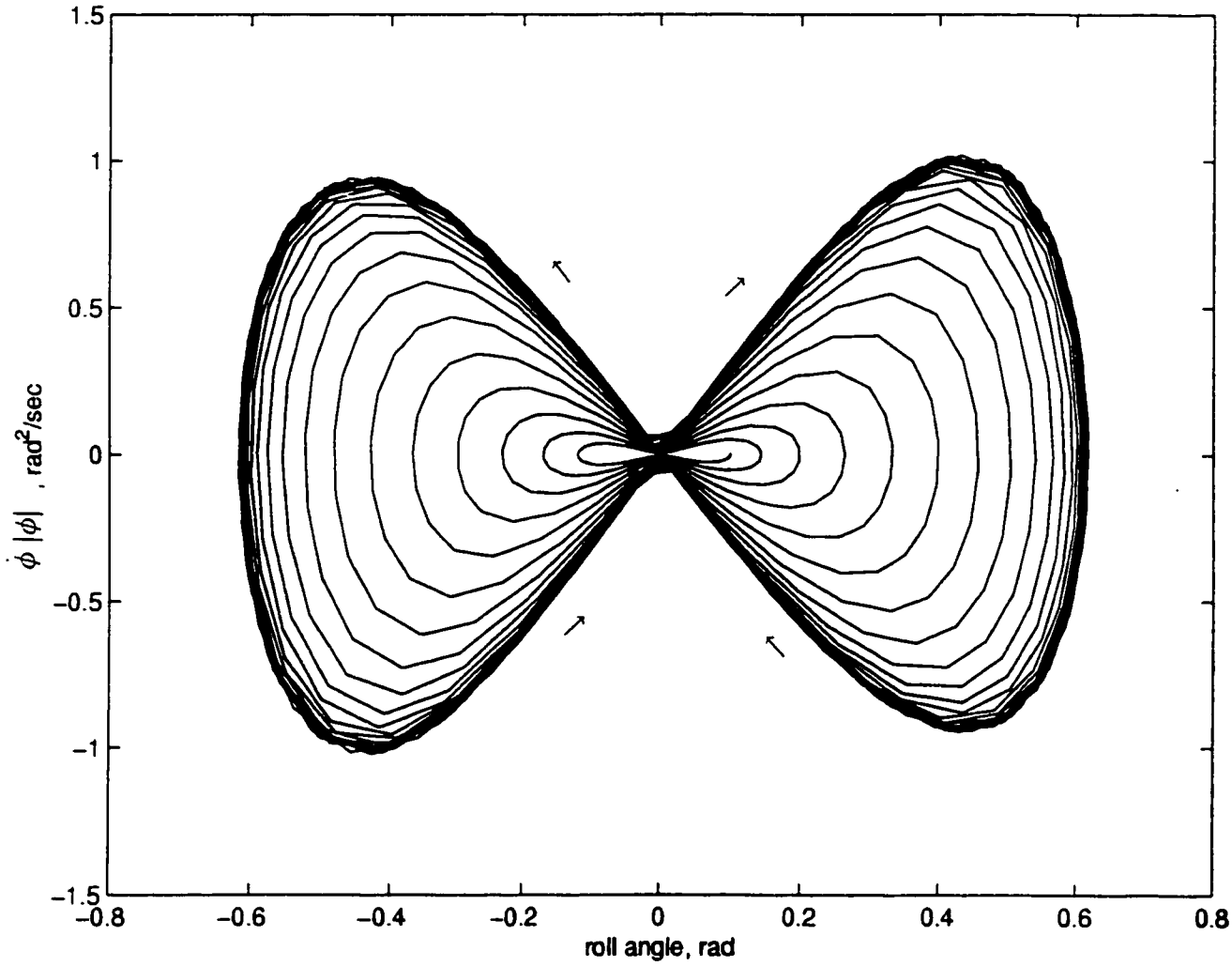

Figure 2.7: Nonlinear damping vs roll angle (Fitted model)

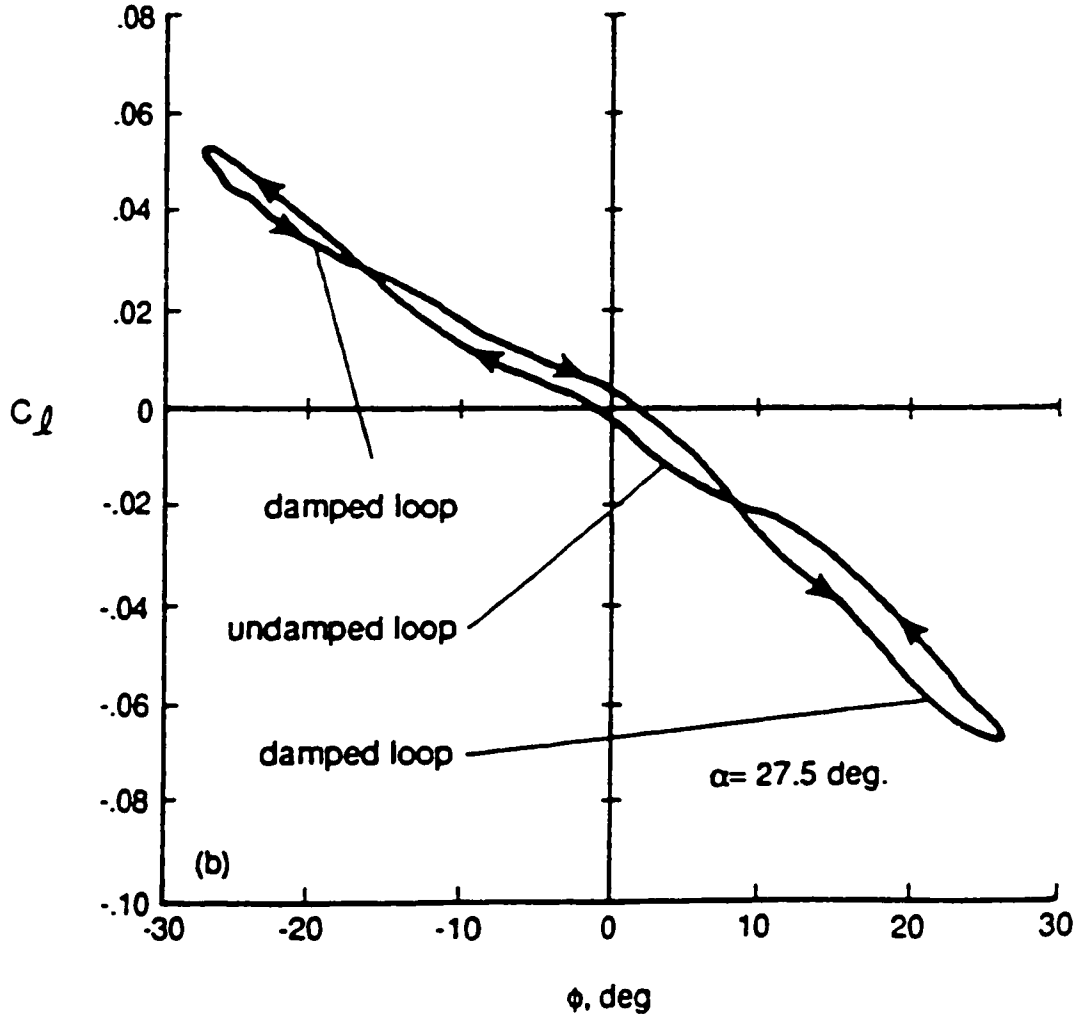

Figure 2.8: Rolling Moment Histogram [38]

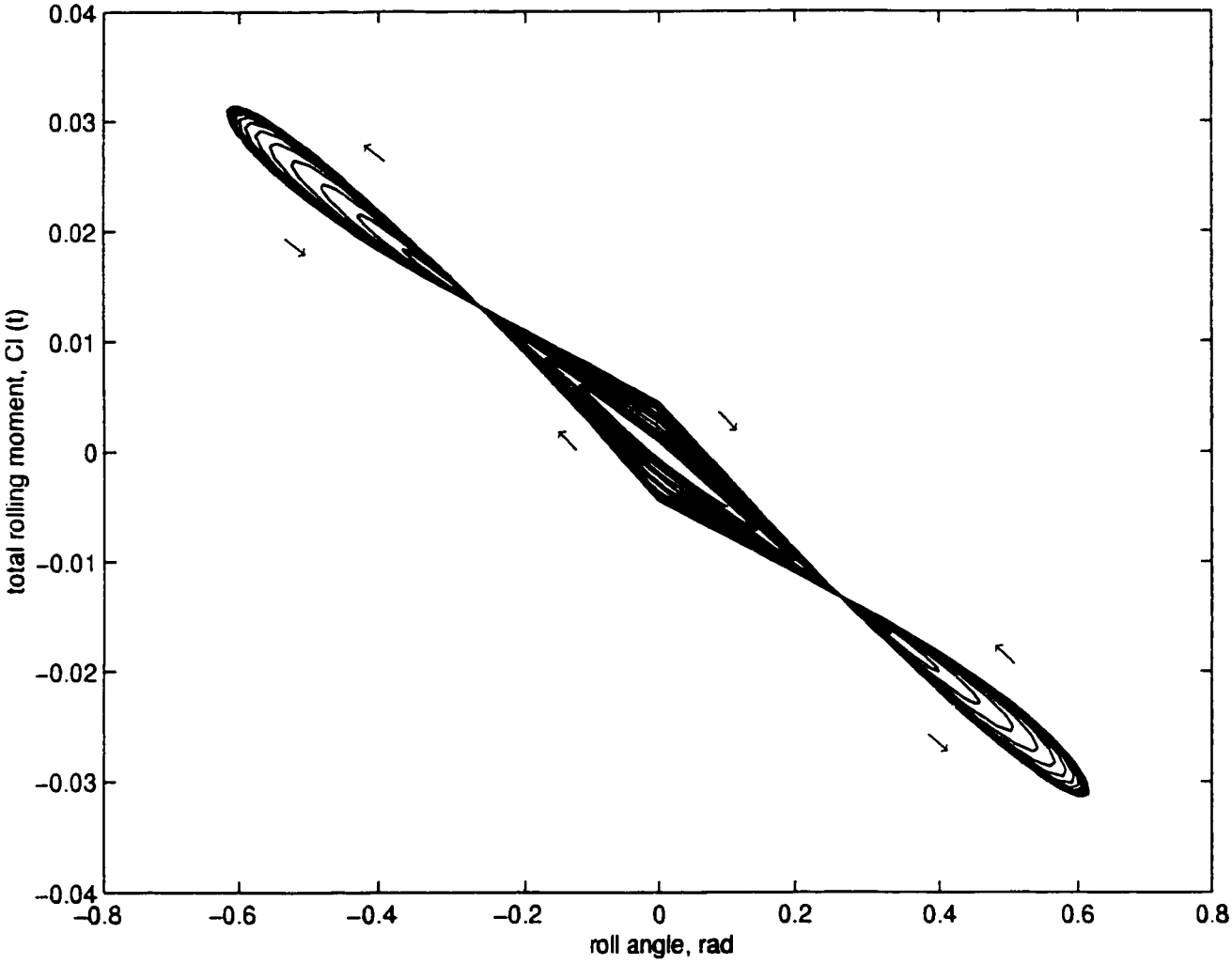

Figure 2.9: Hysteresis loop of wing rock (Fitted model)

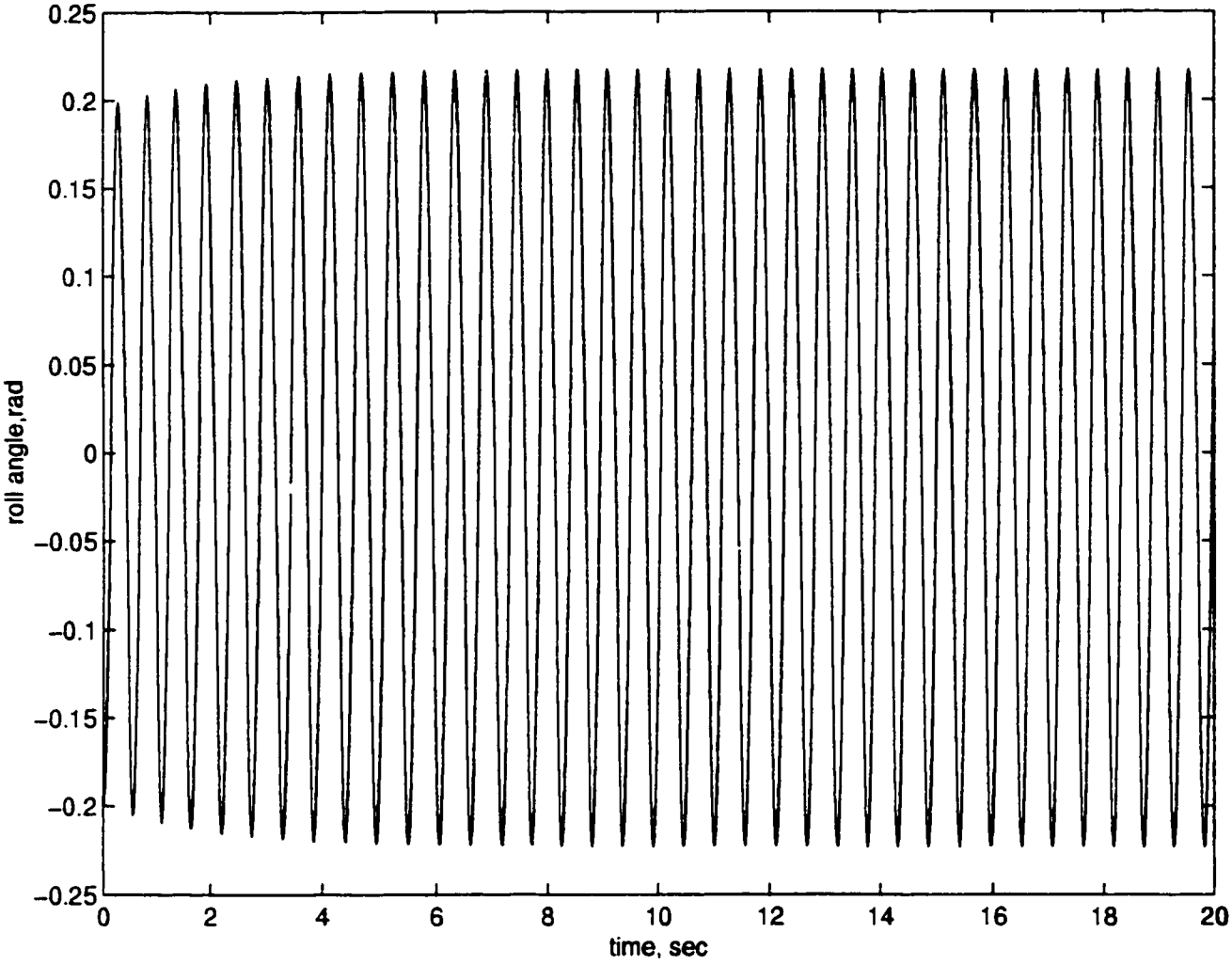

Figure 2.10: Roll angle response for analytical model 2

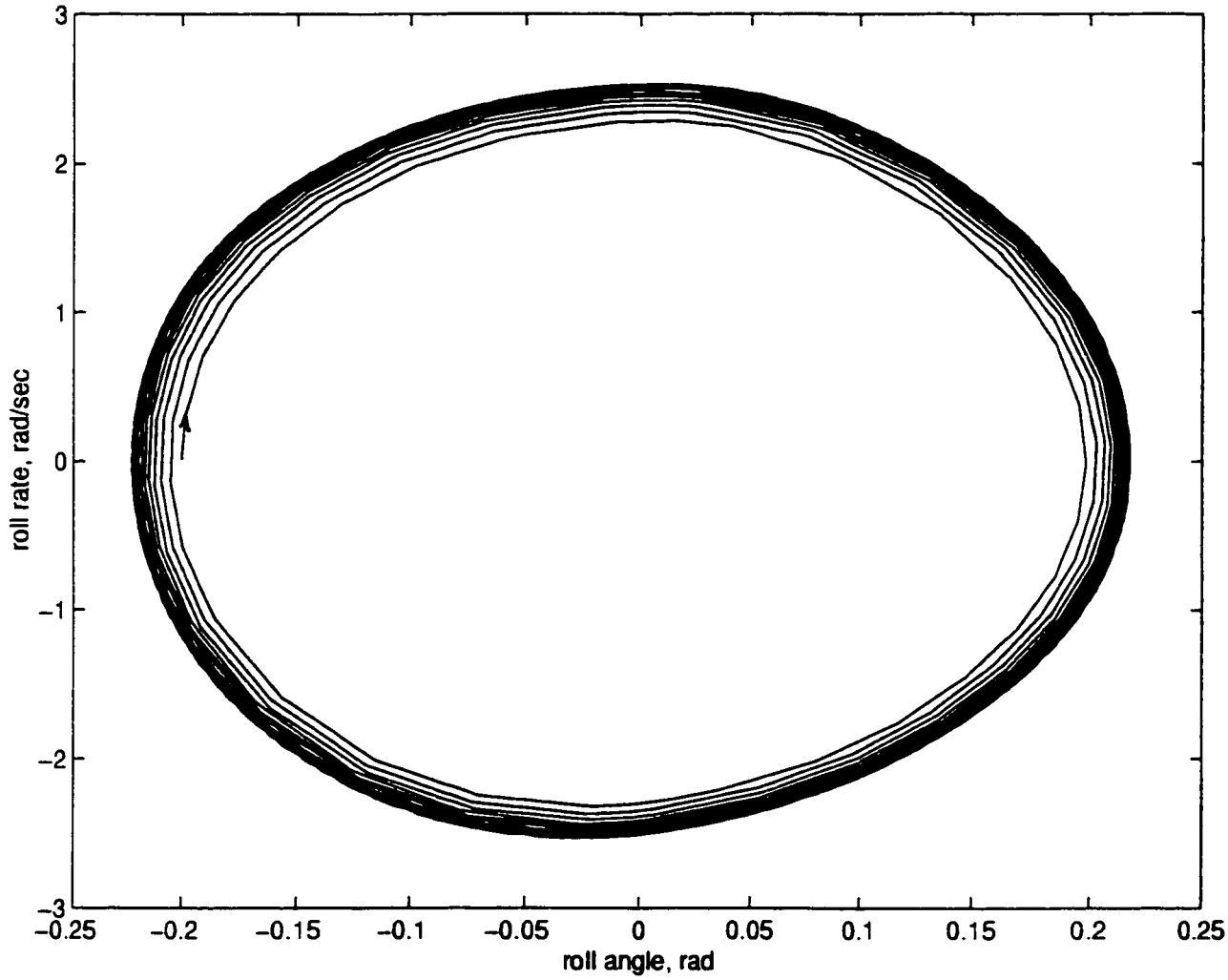

Figure 2.11: Phase plot for analytical model 2

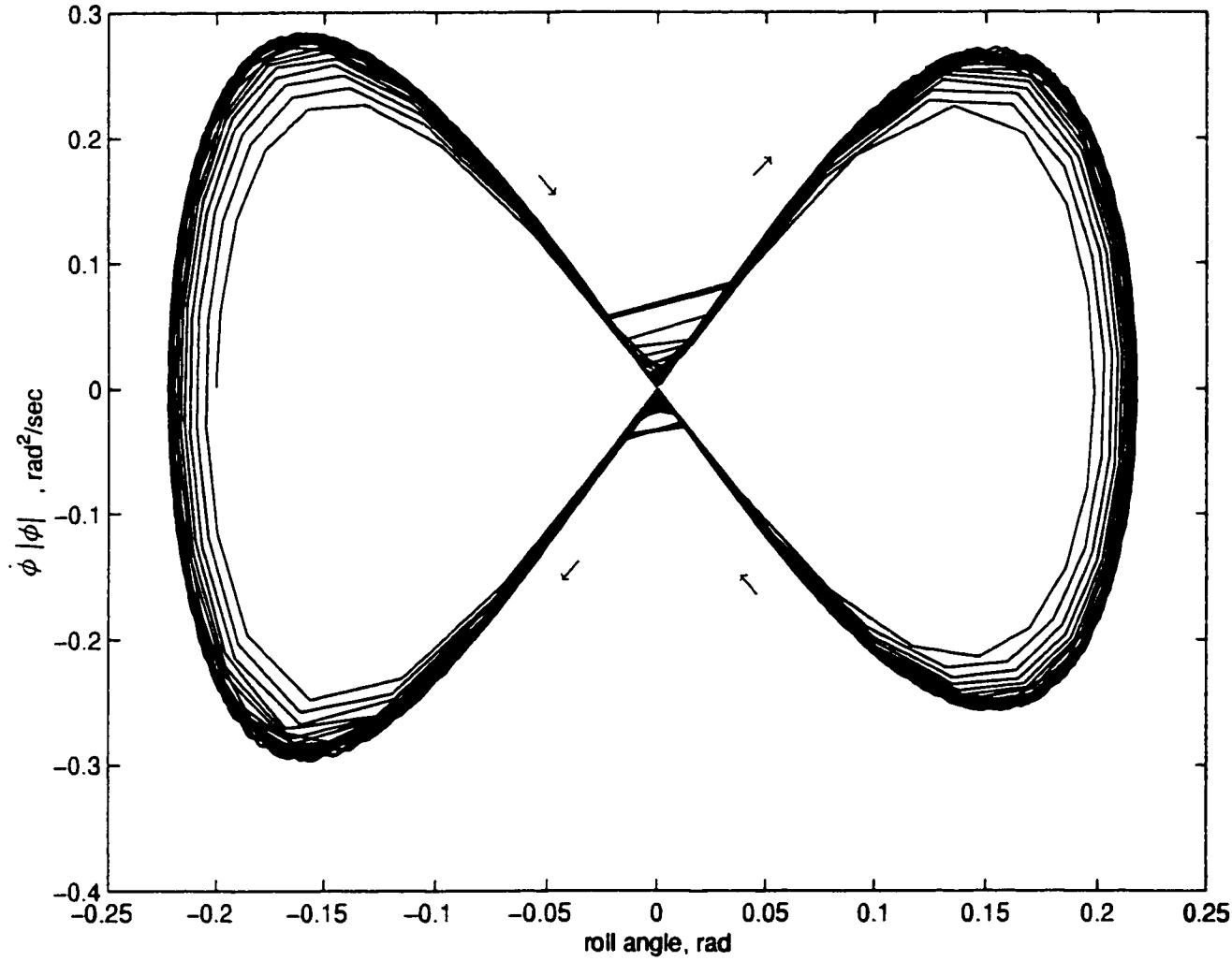

Figure 2.12: Nonlinear damping vs roll angle for analytical model 2

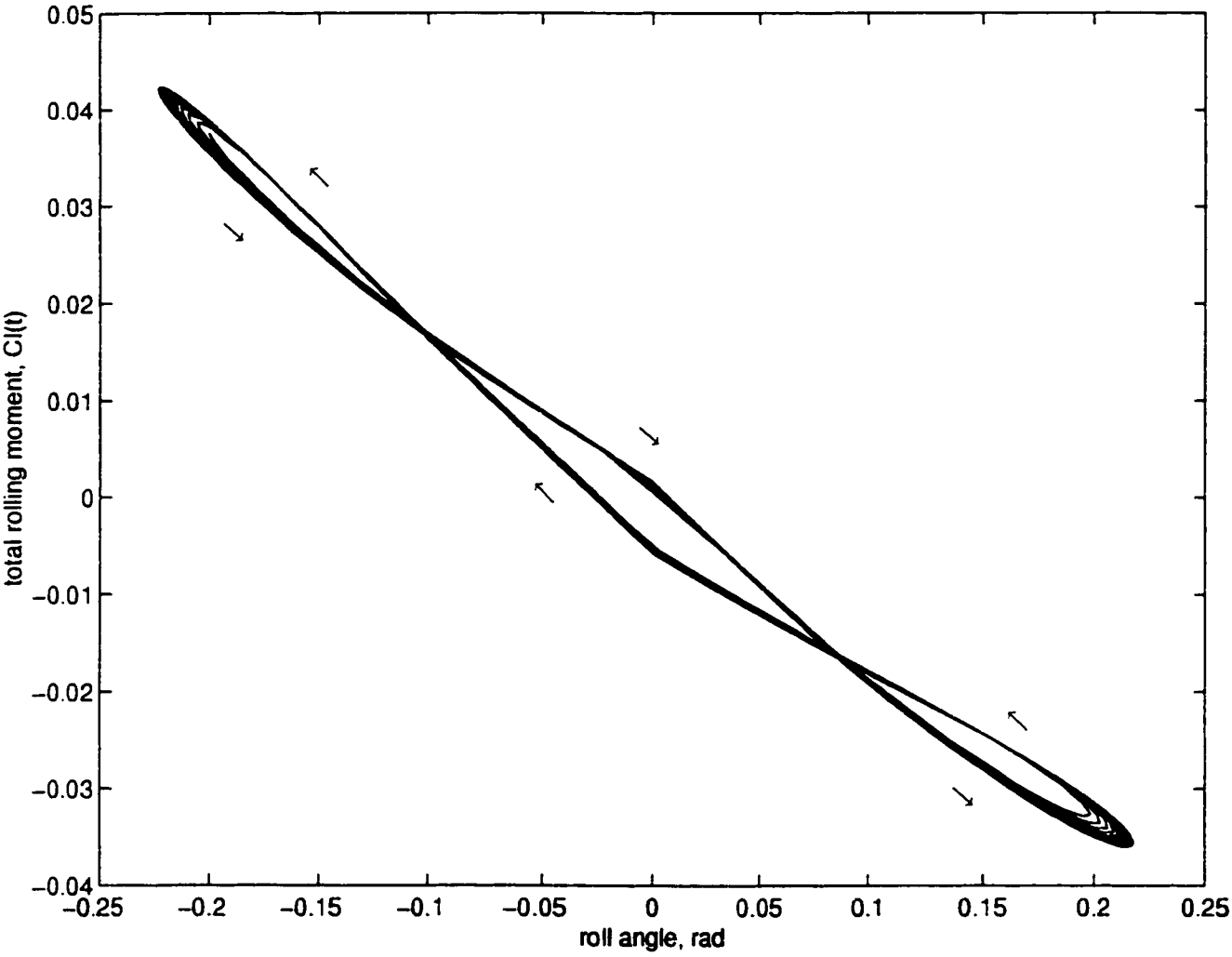

Figure 2.13: Rolling moment diagram for analytical model 2

the knowledge of the structure of the plant is assumed. The derivation of the control law is based on the Lyapunov stability analysis. The robustness feature has been included in the adaptive law by using the σ *modification* [31] and [46].

From Hsu's model in equation (2.34) given as below

$$\begin{aligned} \dot{x_1} &= \dot{\phi} \\ \dot{x_2} &= \ddot{\phi} = f(x) + a_o u \\ where\ f(x) &= c_o + c_1 x_1 + c_2 x_2 + c_3 |x_1| x_2 + c_4 |x_2| x_2 \end{aligned} \tag{2.41}$$

where $x_1 = \phi$, roll angle and $x_2 = \dot{\phi}$, roll rate. The following reference model is selected as

$$\dot{x_m} = A_m x_m + K_m r \tag{2.42}$$

where $A_m = \begin{bmatrix} 0 & 1 \\ -\omega_n^2 & -2\zeta\omega_n \end{bmatrix}$, $x_m = (x_{m1}, x_{m2})^T$, $\zeta > 0$, $\omega_n > 0$, $K_m = \begin{bmatrix} 0 \\ k_m \end{bmatrix}$ where $k_m < 0$, x_{m1}, x_{m2} are state variables of reference model, ζ is a damping ratio and ω_n is a natural frequency. Define the error signal as

$$\begin{aligned} \dot{e} &= \dot{x} - \dot{x_m} \\ (e_1, e_2) &= [(x_1 - x_{m1}), (x_2 - x_{m2})]^T \end{aligned} \tag{2.43}$$

which gives the error equation as

$$\dot{e} = A_m(x - x_m) + (\dot{x} - A_m x) - K_m r \tag{2.44}$$

$$\dot{e}= A_m e + \begin{bmatrix} x_2 \\ f(x) + a_o u \end{bmatrix} - \begin{bmatrix} 0 & 1 \\ -\omega_n^2 & -2\zeta\omega_n \end{bmatrix} \begin{bmatrix} x_1 \\ x_2 \end{bmatrix} - \begin{bmatrix} 0 \\ k_m \end{bmatrix} r \qquad (2.45)$$

$$\dot{e}= A_m e + \begin{bmatrix} x_2 \\ f(x) + a_o u \end{bmatrix} - \begin{bmatrix} x_2 \\ -\omega_n^2 x_1 - 2\zeta\omega_n x_2 \end{bmatrix} - \begin{bmatrix} 0 \\ k_m \end{bmatrix} r \qquad (2.46)$$

Choosing u equal to r, the error equation (2.46) can be expressed as

$$\dot{e} = A_m e + b_m[d(x) + (a_o - k_m)u] \qquad (2.47)$$

where

$$d(x) = c_o + (c_1 + \omega_n^2)x_1 + (c_2 + 2\zeta\omega_n)x_2 + c_3 |x_1| x_2 + c_4 |x_2| x_2 \qquad (2.48)$$

and $b_m = [0,\ 1]^T$, $(a_o - k_m) \neq 0$ is unknown but its sign assumed known. Assume the reference signal input, r is piecewise-continuous and bounded for all $t \geq 0$. The objective of adaptive control is to derive a control law such that $\lim_{t\to\infty} (x - x_m) = 0$ and all the signals remain bounded. Let us define the following control law for u where the parameters are to be estimated from the adaptive scheme:

$$u = -[\theta_o(t) + \theta_1(t)x_1 + \theta_2(t)x_2 + \theta_3(t) |x_1| x_2 + \theta_4(t) |x_2| x_2] \qquad (2.49)$$

Defining

$$\theta = [\theta_o,\ \ \theta_1,\ \ \theta_2,\ \ \theta_3,\ \ \theta_4]^T, \qquad (2.50)$$

Substituting equations (2.48), (2.49) into equation (2.47) and rearranging the terms,

the following is obtained.

$$\begin{aligned}\dot{e} &= A_m e + b_m(a_o - k_m)(\{\frac{c_o}{(a_o - k_m)} - \theta_o\} + \{\frac{c_1 + \omega_n^2}{(a_o - k_m)} - \theta_1\}x_1 \\ &+\{\frac{c_2 + 2\zeta\omega_n}{(a_o - k_m)} - \theta_2\}x_2 + \{\frac{c_3}{(a_o - k_m)} - \theta_3\}\,|x_1|\,x_2 \\ &+\{\frac{c_4}{(a_o - k_m)} - \theta_4\}\,|x_2|\,x_2) \end{aligned} \tag{2.51}$$

Express equation (2.51) in compact form as below

$$\dot{e} = A_m e + (a_o - k_m) b_m \phi^T g(x) \tag{2.52}$$

where the parameter error vector is defined as

$$\begin{aligned}\phi &= \theta^* - \theta \\ &= [(\theta_o^* - \theta_o), (\theta_1^* - \theta_1), ...(\theta_4^* - \theta_4)]^T \end{aligned} \tag{2.53}$$

and $\theta_i^* s$ are known values given as follows :

$$\theta_1^* = (c_1 + \omega_n^2)/(a_o - k_m) \tag{2.54}$$

$$\theta_2^* = (c_2 + 2\zeta\omega_n)/(a_o - k_m) \tag{2.55}$$

$$\theta_i^* = c_i/(a_o - k_m), \quad i = 0, 3, 4 \tag{2.56}$$

and the vector function $g(x)$ is defined as

$$g(x) = [1, \;\; x_1, \;\; x_2, \;\; |x_1|\,x_2, \;\; |x_2|\,x_2]^T \tag{2.57}$$

In the parameter error vector $\phi = \theta^* - \theta(t)$ *where* $\theta(t)$ are the adjustable gain parameters of adaptive controller.

2.3.1 Stability Analysis

The Lypaunov's approach of stability analysis for closed loop systems is used below. For A_m in the reference model, given a positive definite matrix $Q, (Q > 0)$, there exists a matrix $P > 0$ such that the following Lyapunov equation is satisfied :

$$A_m^T P + P A_m = -Q \tag{2.58}$$

The following Lyapunov function is selected

$$V(e, \phi) = e^T P e + \phi^T \Gamma \phi \, |a_o - k_m| \tag{2.59}$$

Taking the derivative of $V(e, \phi)$ along the trajectory of $\dot{e}$ given in equation (2.47) yields

$$\dot{V}(e, \phi) = \dot{e}^T P e + e^T P \dot{e} + |a_o - k_m| (\dot{\phi} \Gamma \phi + \phi^T \Gamma \dot{\phi}) \tag{2.60}$$

$$\begin{aligned} \dot{V}(e, \phi) &= (A_m^T e^T + (a_o - k_m) b_m \phi^T g(x) P e + \\ &\quad e^T P (A_m e + (a_o - k_m) b_m \phi^T g(x)) + 2 |a_o - k_m| \phi^T \Gamma \dot{\phi} \end{aligned} \tag{2.61}$$

$$\dot{V}(e, \phi) = e^T (P A_m + A_m^T P) e + 2 e^T P (a_o - k_m) b_m \phi^T g(x) + 2 |a_o - k_m| \phi^T \Gamma \dot{\phi} \tag{2.62}$$

The adaptive law is chosen from the above equation as

$$\dot{\theta} = sgn\ (a_o - k_m) \Gamma^{-1} e^T P b_m g(x) \tag{2.63}$$

where Γ is a non-singular weighting matrix. $\Gamma > 0$. From equation (2.53), $\dot{\phi} = -\dot{\theta}$ and substituting equation (2.63) into (2.62) shows that

$$\begin{aligned} \dot{V}(e,\phi) &= -e^T Q e + 2e^T P(a_o - k_m) b_m \phi^T g(x) \\ &\quad -2e^T P(a_o - k_m) b_m \phi^T g(x) \\ \dot{V}(e,\phi) &\leq 0 \end{aligned} \tag{2.64}$$

implying $e(t) \rightarrow 0$ as $t \rightarrow 0$.

2.3.2 Simulations

An application of the derived adaptive law to control the wing rock motion is illustrated. Based on the model developed by Hsu [5] and the aerodynamic parameters reported in Lan [12] and [21] are used in equation (2.41) for the simulation.

$c_o = 5$

$c_1 = -26.66675\ s^{-2}$

$c_2 = 0.764855\ s^{-2}$

$c_3 = -2.92173\ rad\ s^{-1}$

$c_4 = -2.5$

$\dot{x_2} = 5 - 26.66675x_1 + 0.764855x_2 - 2.92173\,|x_1|\,x_2 - 2.5\,|x_2|\,x_2 + u$

$a_o = 1$

Without adaptive control, using the model given in equation (2.33) and step input, the wing rock in roll-angle and roll-rate responses are shown in Figs 2.14 and 2.15. The phase plane is given in Figure 2.16 which shows that the limit cycle is stable.

For the simplicity purpose the reference trajectory is chosen as $x_m = 0$. Assuming the parameters in the reference model be $\zeta = 0.707$ and $\omega = 0.5$, and the matrix Q in Lypaunov equation be identity matrix I, solving the Lypaunov equation $A_m P + P A_m$

the following is obtained

$$\begin{bmatrix} p_{11} & p_{12} \\ p_{21} & p_{22} \end{bmatrix} = \begin{bmatrix} 2\zeta\omega_n p_{12} + \omega_n^2 p_{22} & 1/(2\omega_n^2) \\ 0 & (0.5 + p_{12})/2\zeta\omega_n \end{bmatrix} = \begin{bmatrix} 2.298 & 2.0 \\ 0 & 3.536 \end{bmatrix}$$

Using the given parameters and known constants, the adaptive law in equation (2.63) is derived as below.

$$\dot{\theta}_o = 2x_1 + 3.56x_2$$

$$\dot{\theta}_1 = (2x_1 + 3.56x_2)x_1$$

$$\dot{\theta}_2 = (2x_1 + 3.56x_2)x_2$$

$$\dot{\theta}_3 = (2x_1 + 3.56x_2)\,|x_1|\,x_2$$

$$\dot{\theta}_4 = (2x_1 + 3.56x_2)\,|x_2|\,x_2$$

Figures 2.17 and 2.18 show that the limit cycle in the roll rate and roll angle is suppressed while Figure 2.19 shows the convergence of roll angle to zero in the phase portrait. The phenomenon of the intersection in the phase plot is because wing rock is still developed from the initial conditions. In a fully developed wing rock, the phase plane is a circle. The initial condition of roll angle and roll rate are ($\phi_o = 0.25\ rad$, $\dot{\phi}_o = 0.25\ rad/\sec$) and it takes $t = 30$ secs to converge to zero. The gain parameters θ_1, θ_2, θ_3, and θ_4 of the adaptive controller converge to constant values as shown in Figures 2.20, 2.21, 2.22 and 2.23.

In the above simulation the weighting matrix Γ is set to $\Gamma = 5I$ where I is identity matrix. The deflection surface is assumed as the control device and the control input u reflects an oscillatory action shown in Figure 2.24

2.4 Modified σ Adaptive Law

In modifying the adaptive law for robustness in the presence of external disturbances, several schemes are available such dead zone, bounds on θ and e_1 modification. In

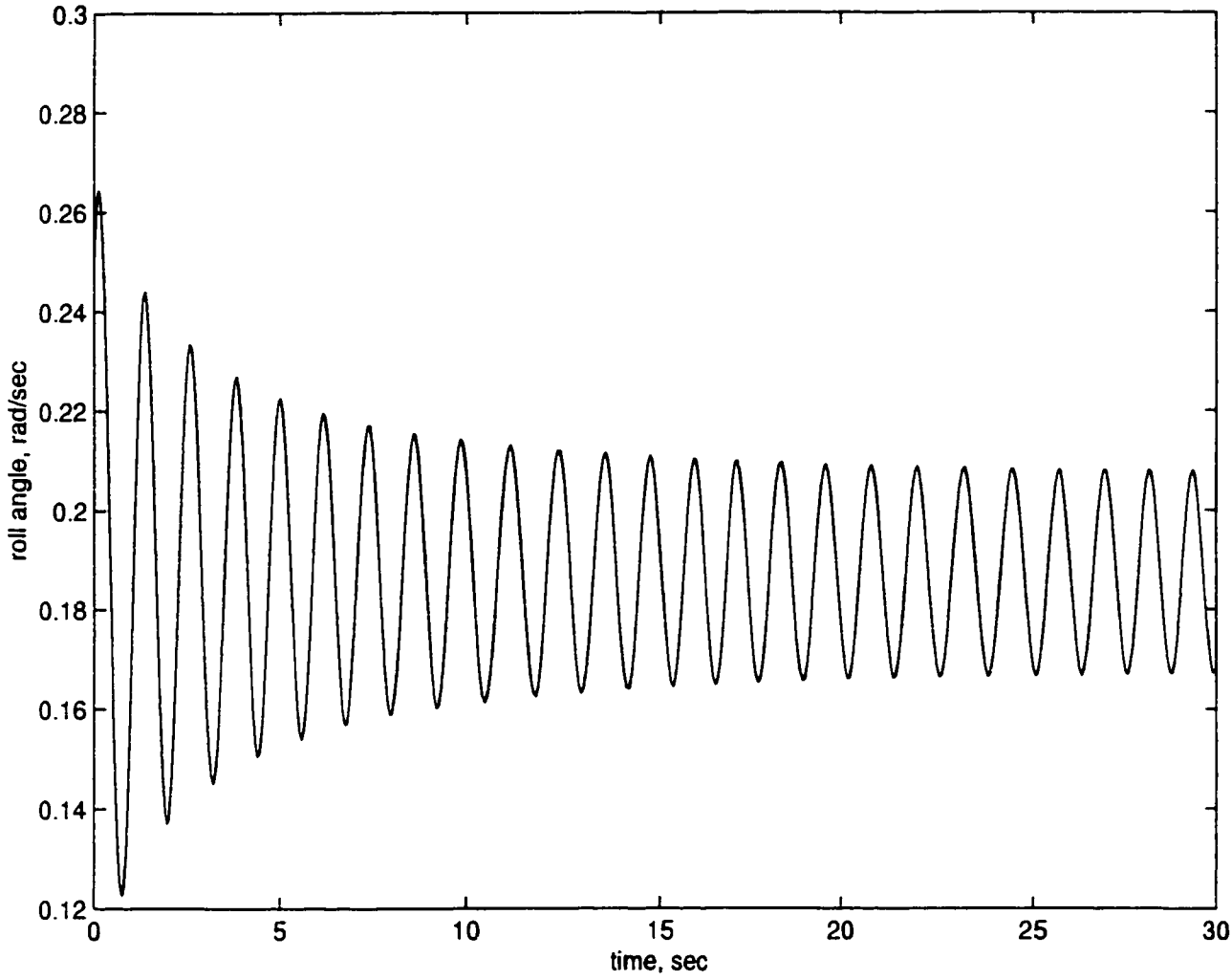

Figure 2.14: Wing rock in roll angle

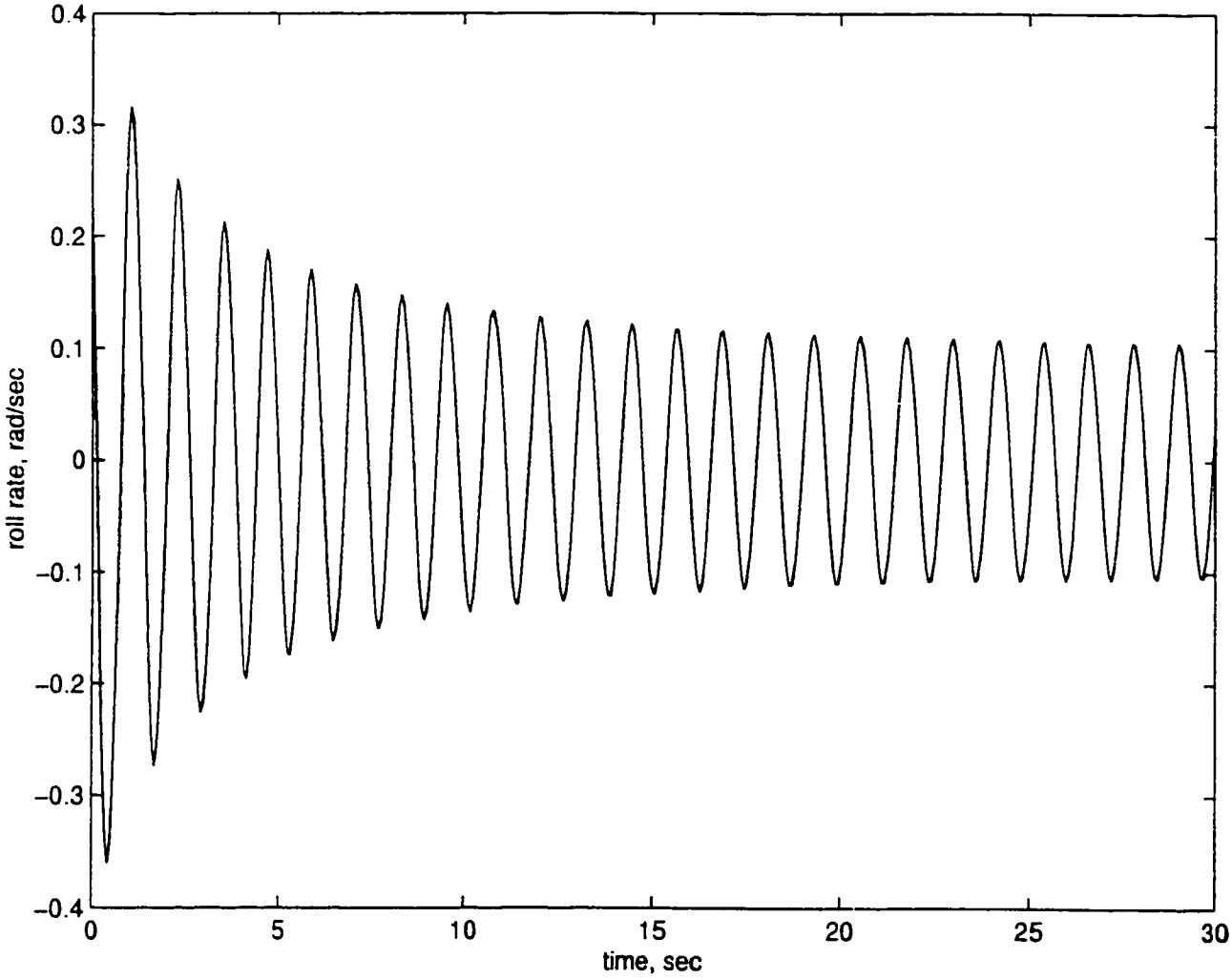

Figure 2.15: Wing rock in roll rate

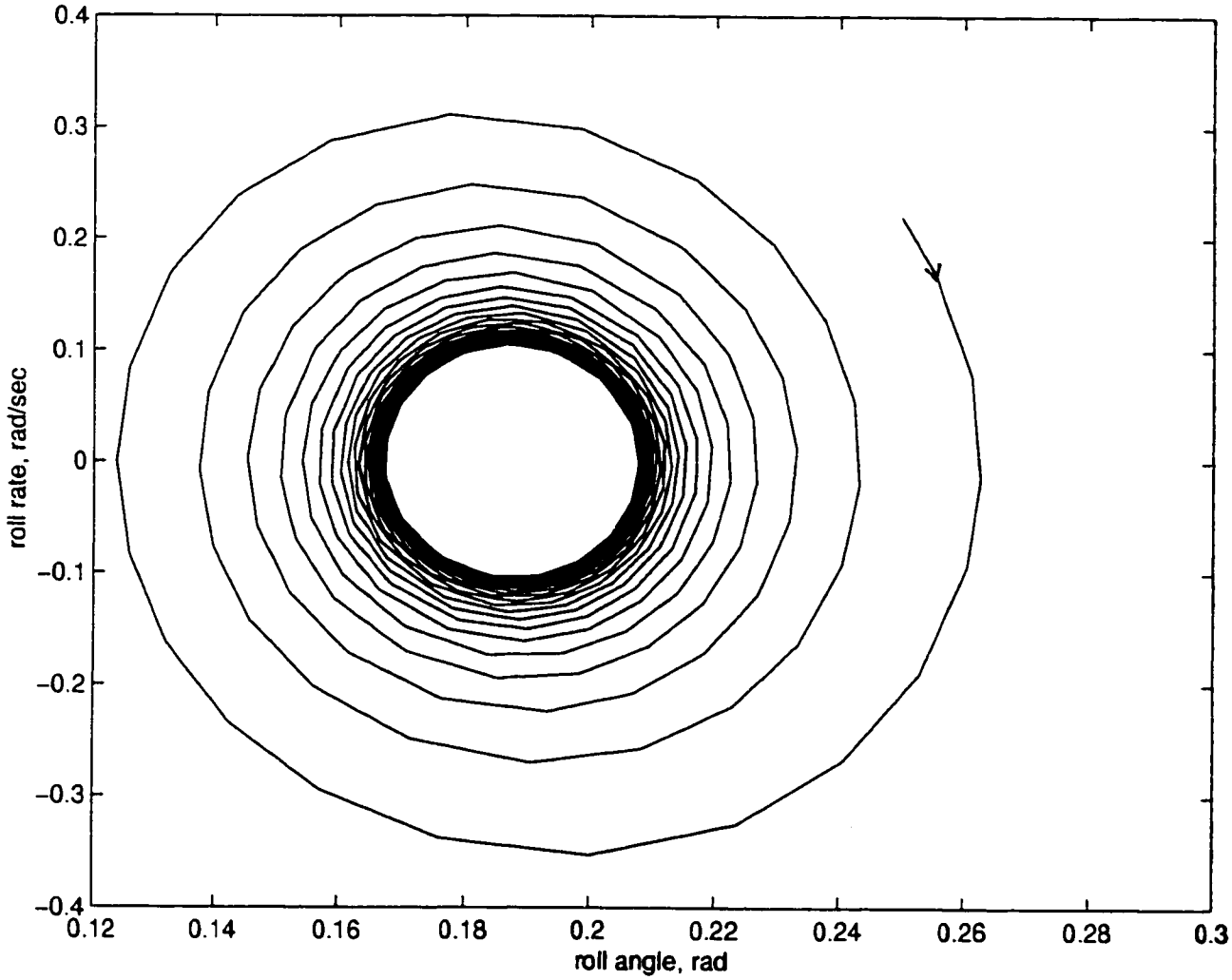

Figure 2.16: Phase plot (roll angle vs roll rate)

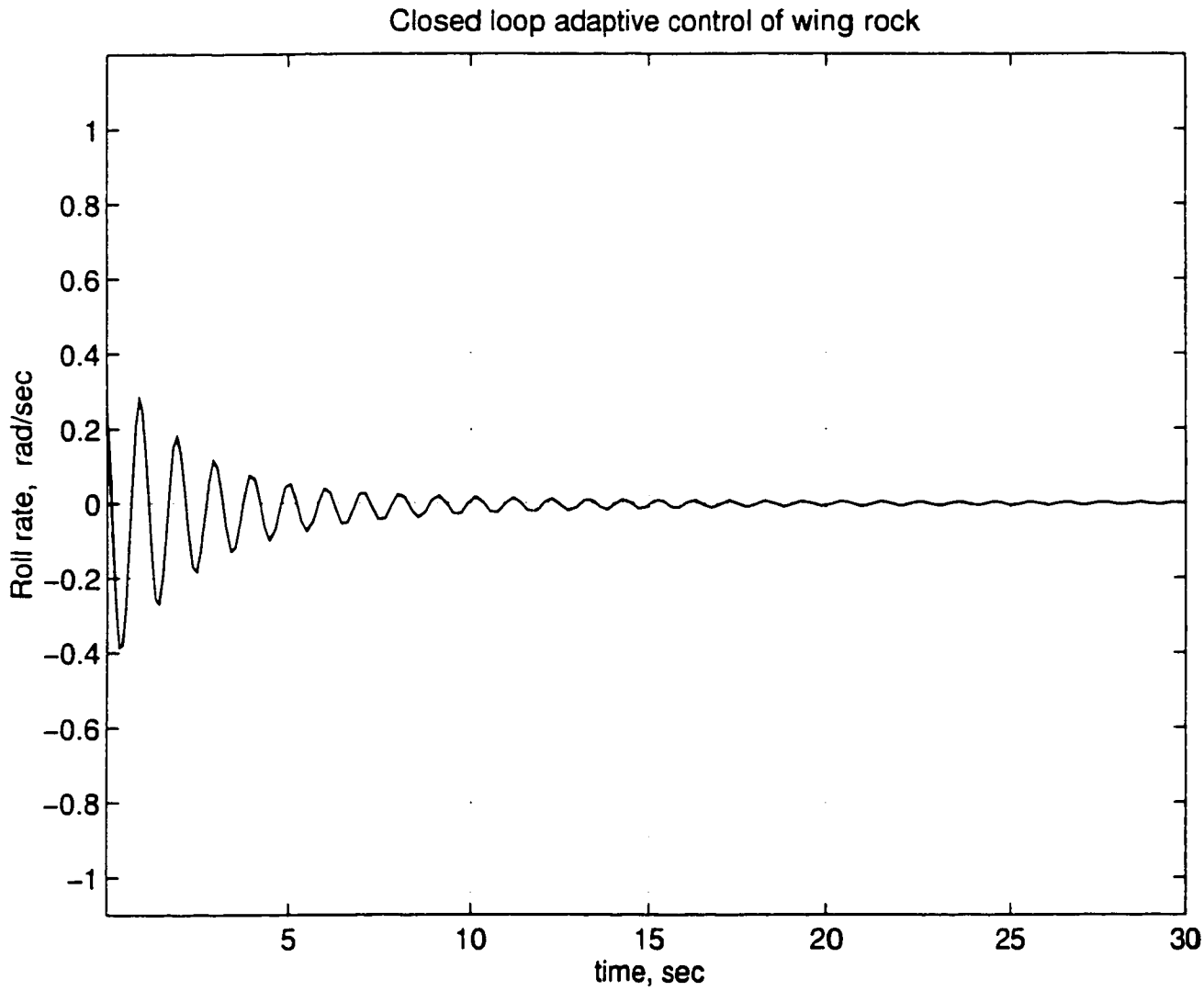

Figure 2.17: Suppression of wing rock in roll rate

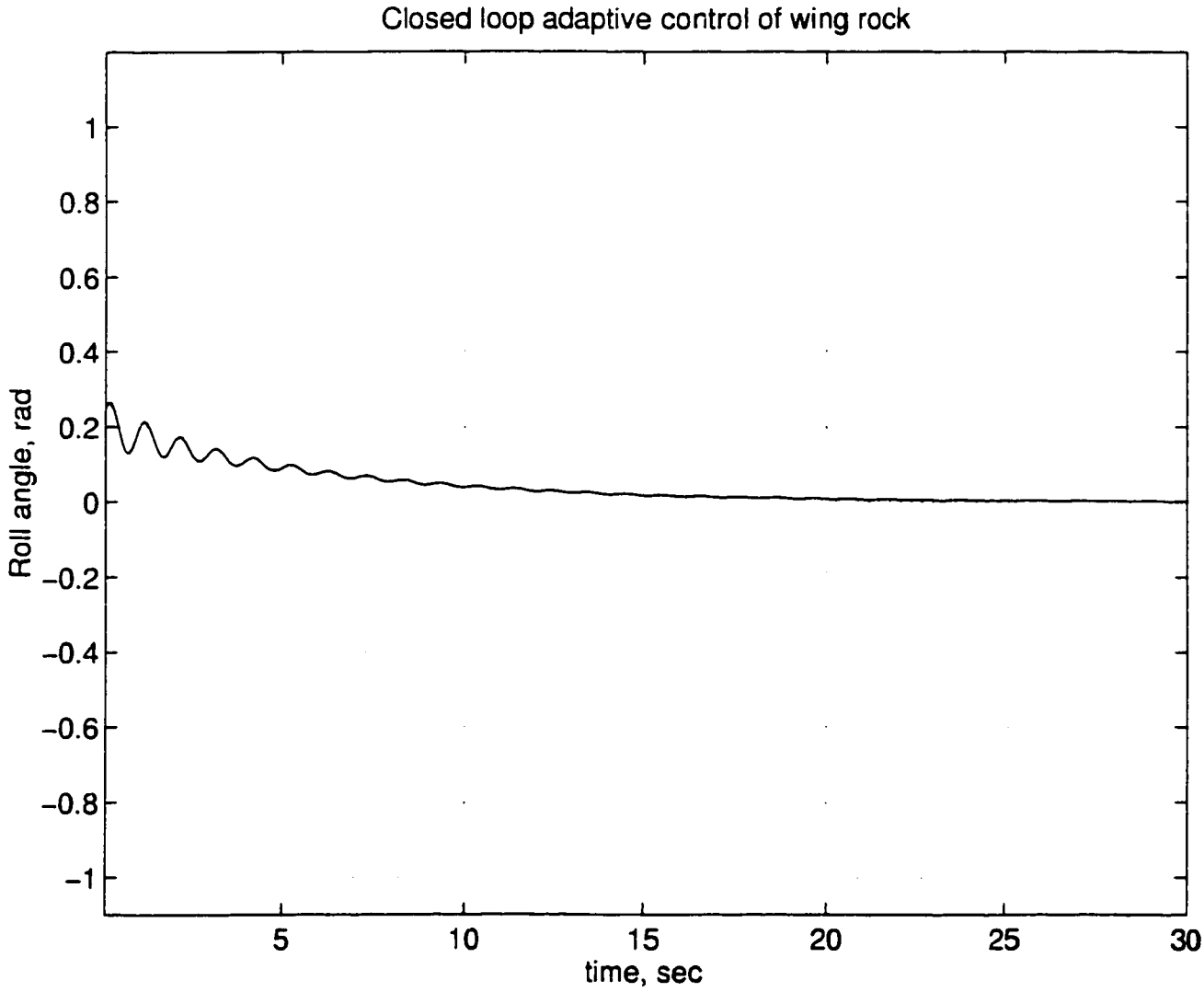

Figure 2.18: Suppression of wing rock in roll angle

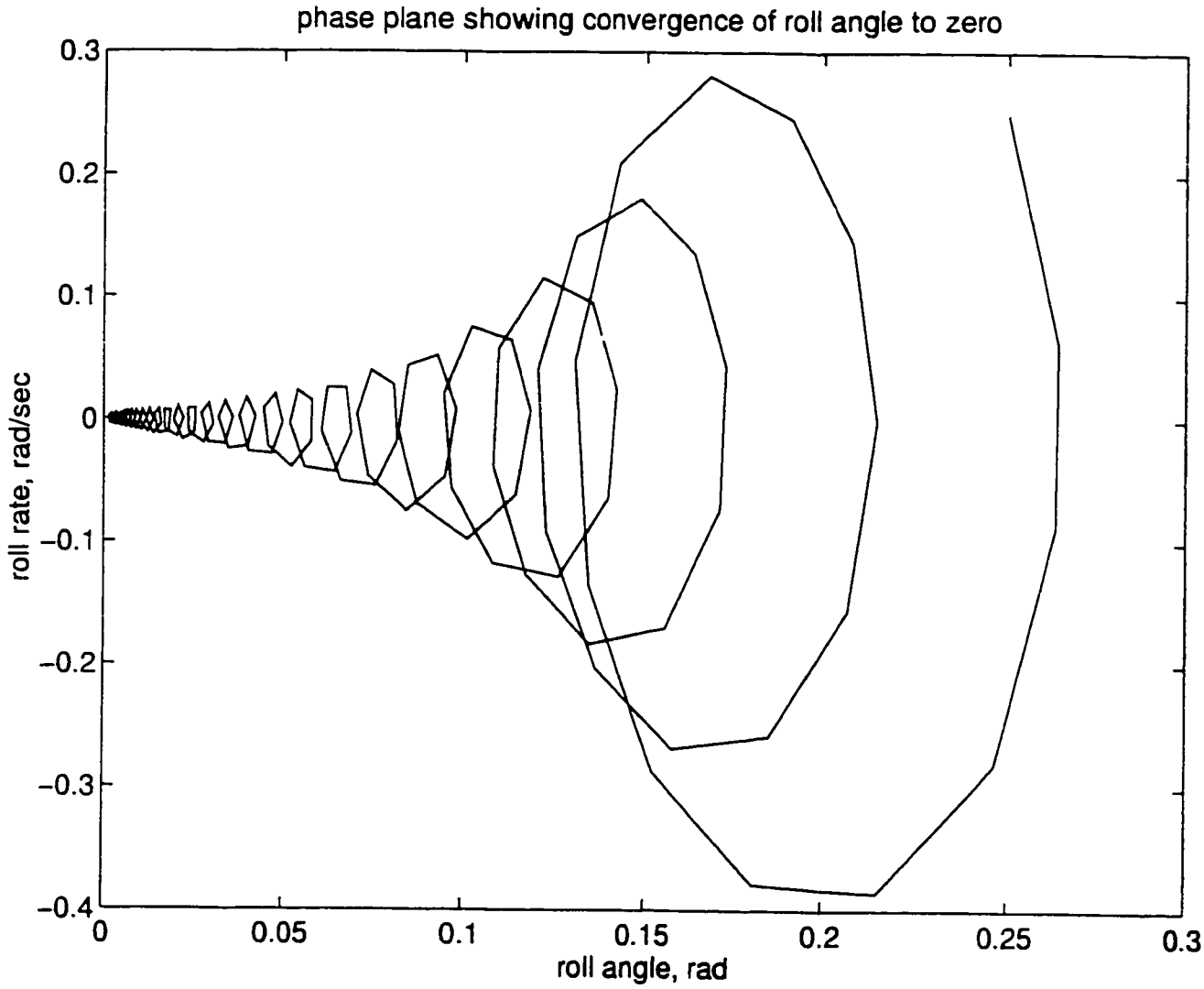

Figure 2.19: Convergence of roll angle to zero

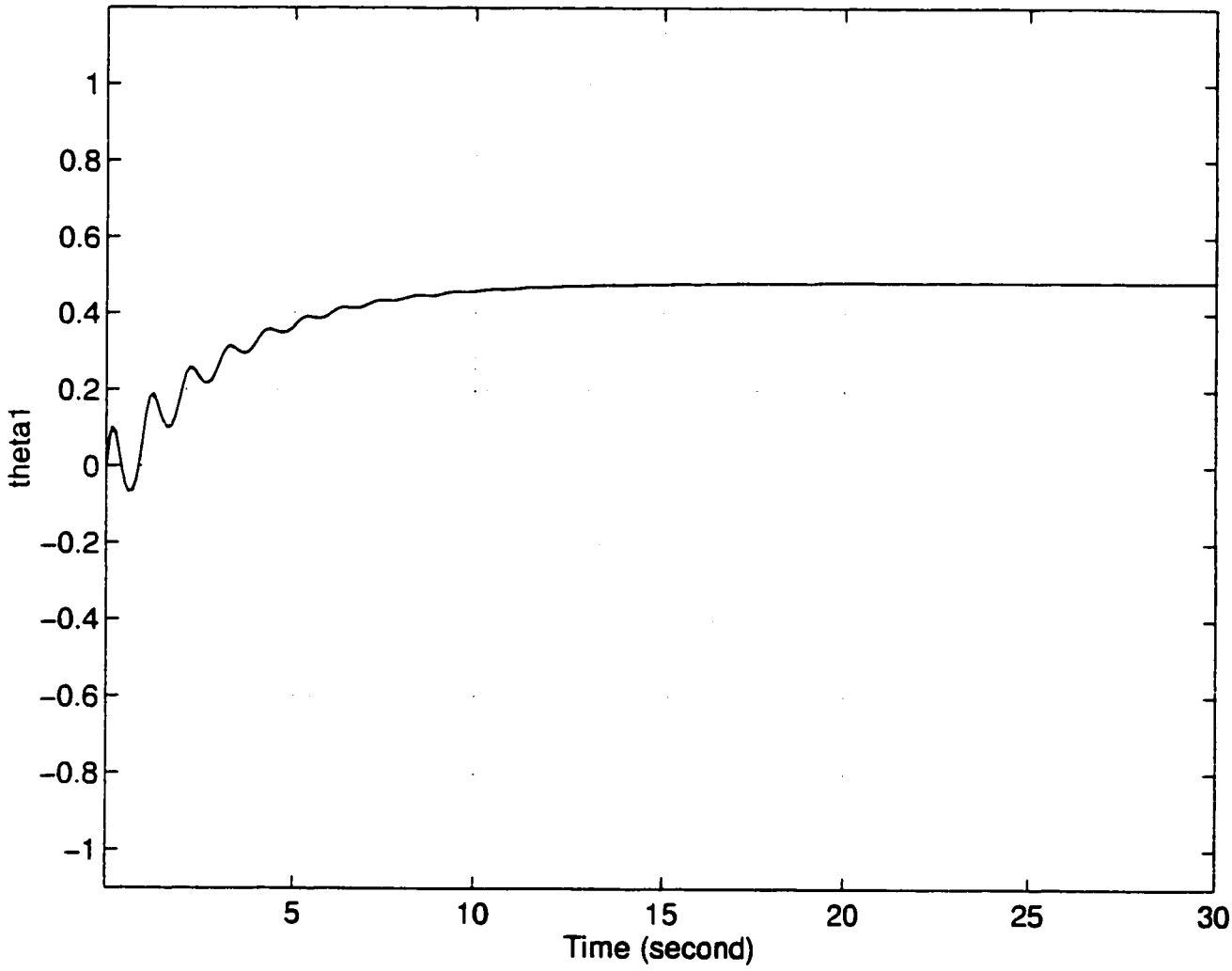

Figure 2.20: Convergence of parameter θ_1

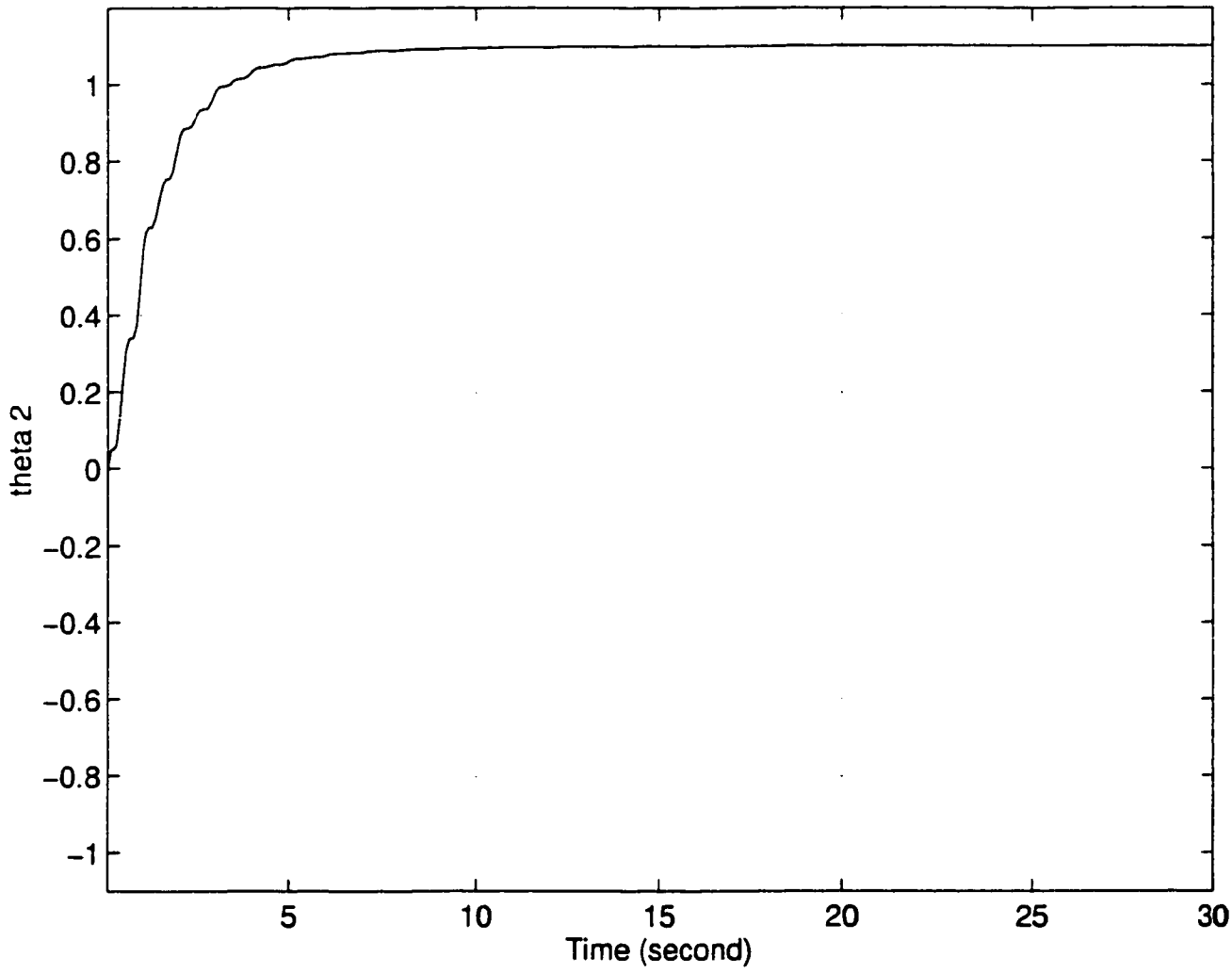

Figure 2.21: Convergence of parameter θ_2

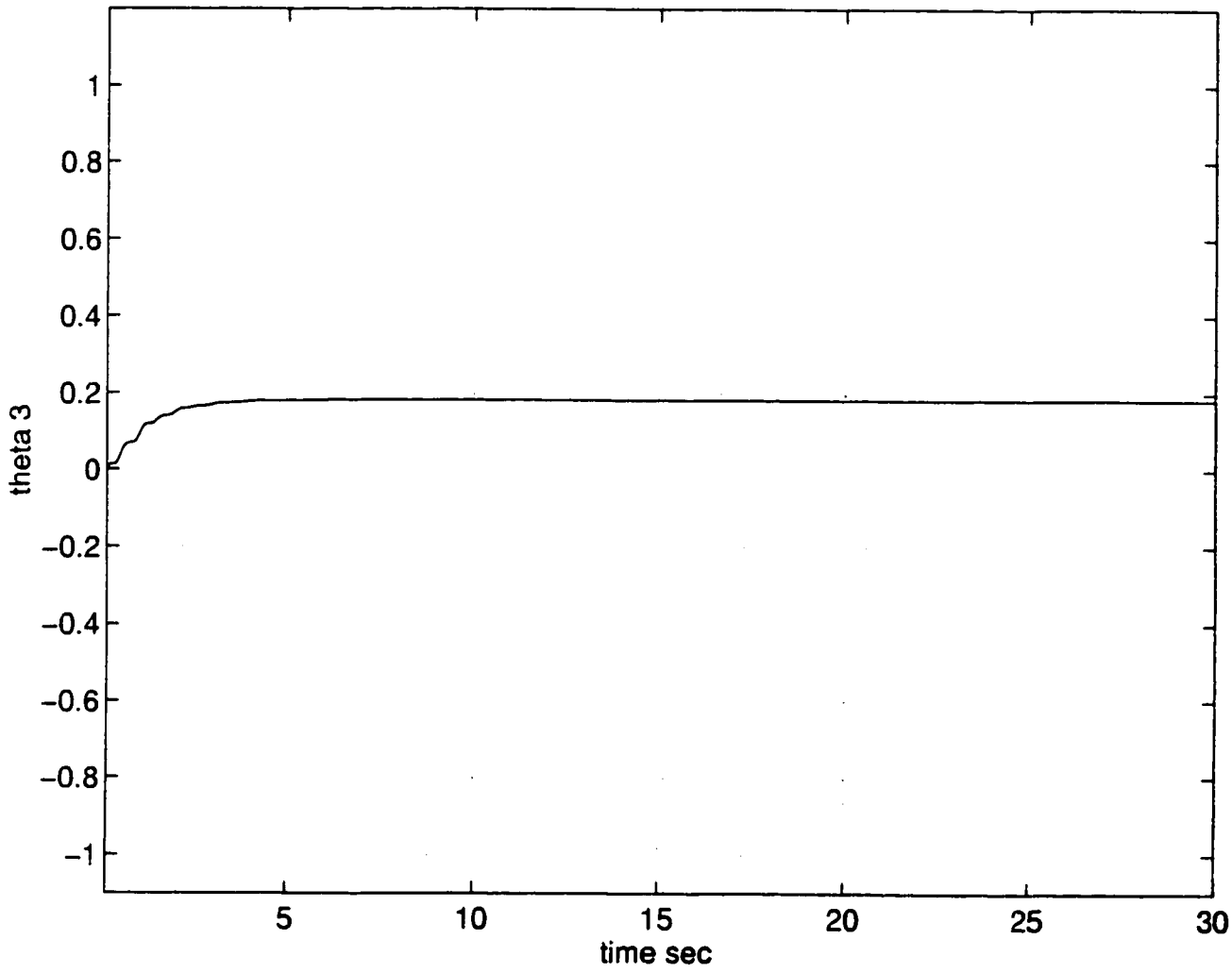

Figure 2.22: Convergence of parameter θ_3

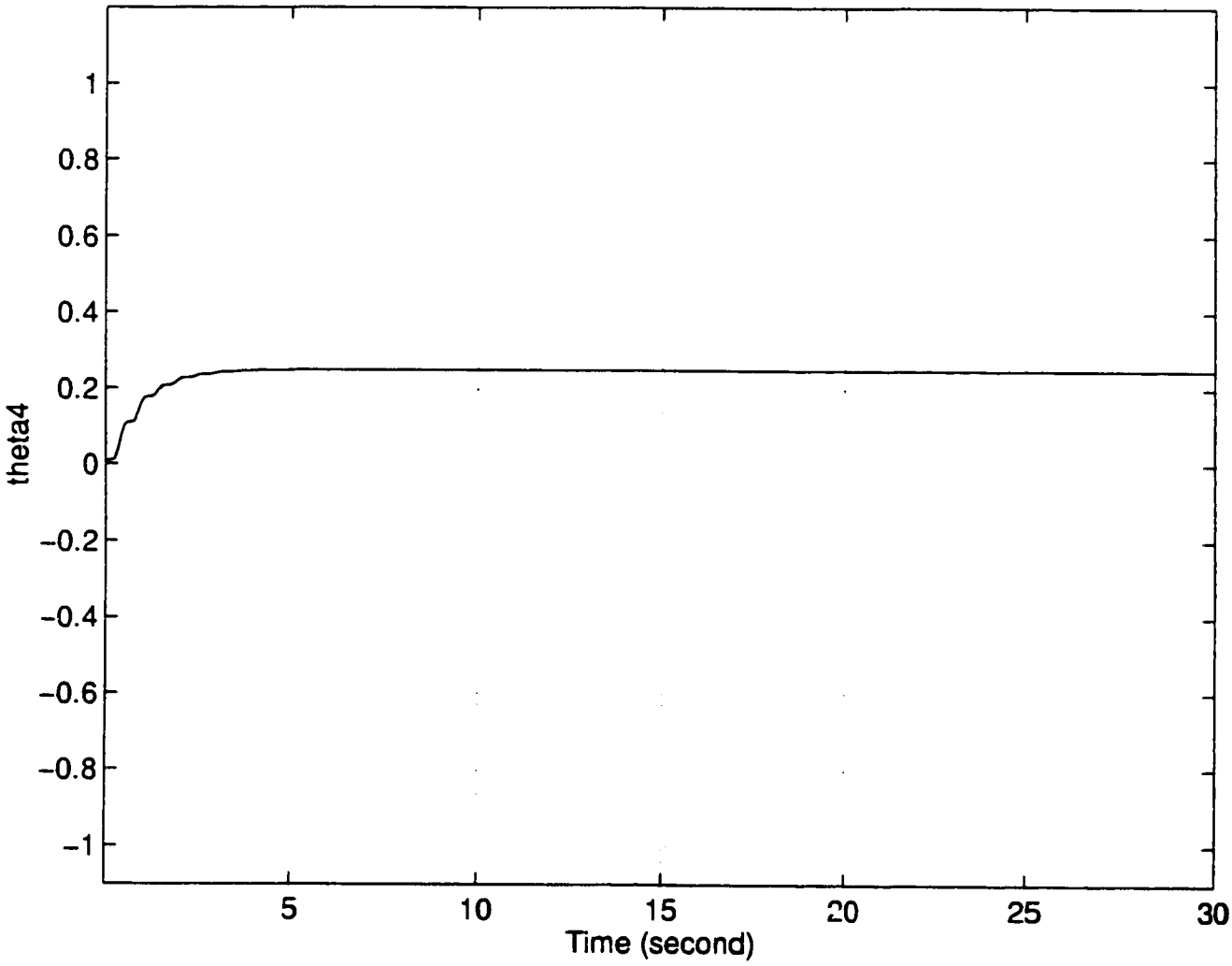

Figure 2.23: Convergence of parameter θ_4

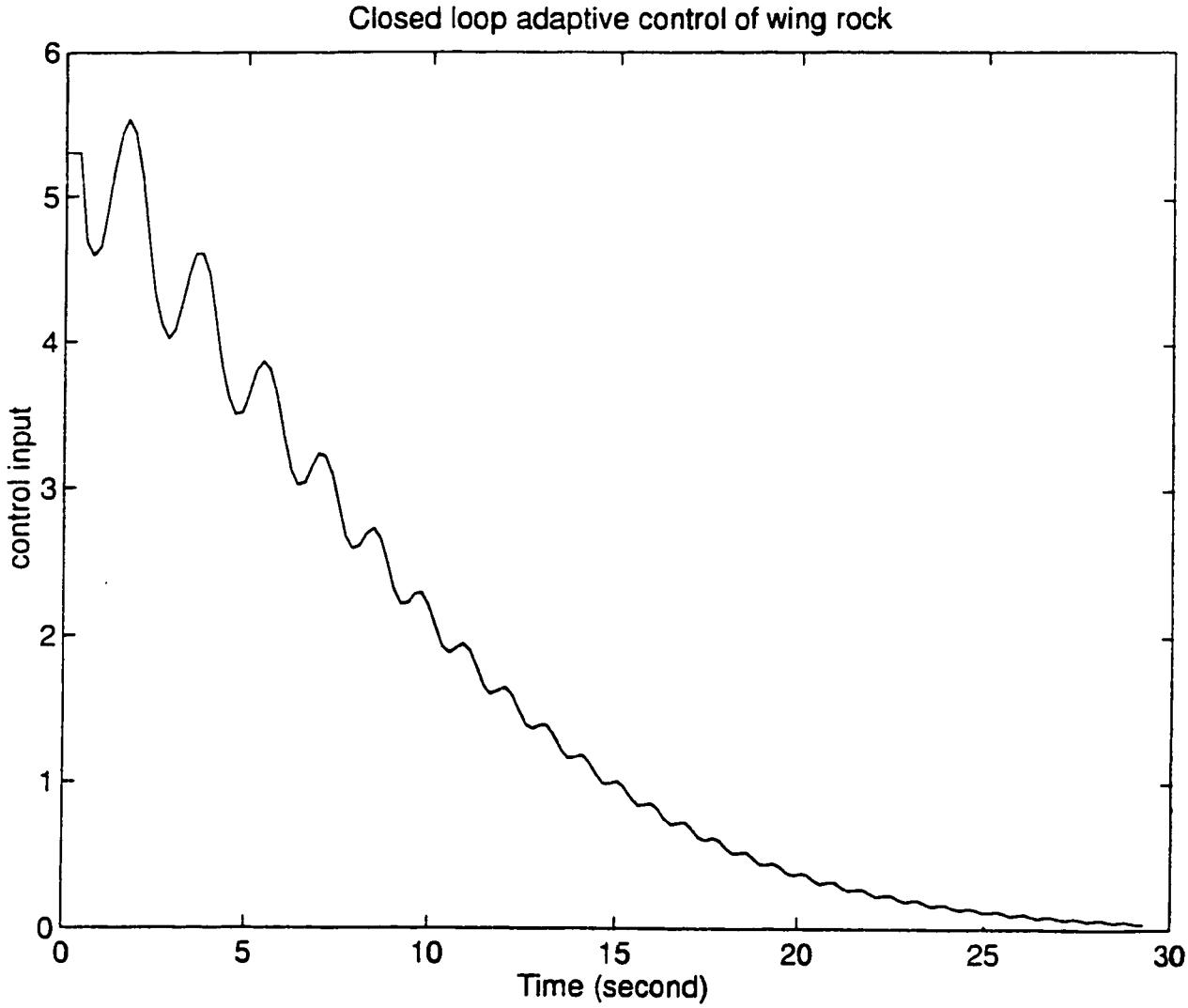

Figure 2.24: Closed loop control input

this section an adaptive control law will be modified by adding the term $-\sigma\theta$ as proposed in [31] & [46] to study the robust adaptive control in the presence of external disturbances. A robust adaptive control system for nonlinear systems reported in [47] will be applied to control the wing rock motion.

In order to improve and stabilize the system as well as to take care of the external disturbance the following σ modified adaptive law is proposed.

$$\dot{\phi} = -\frac{1}{\alpha} \{ sgn(a_o - k_m)\Gamma^{-1}e^T P b_m g(x) \} - \sigma\theta \tag{2.65}$$

Let the Lyapunov function be chosen as follow

$$V(e,\phi) = e^T Pe + \alpha\,\phi^T\Gamma\phi\,|a_o - k_m| \tag{2.66}$$

where α and σ are small positive constants given as $0 < \alpha < 1$ and $0 < \sigma < 1$. The wing rock model with disturbance ν and the corresponding error equation are given below.

$$\begin{aligned} \dot{x_1} &= \dot{\phi} \\ \dot{x_2} &= \ddot{\phi} = f(x) + a_o u + \nu \end{aligned} \tag{2.67}$$

where $f(x)$ is given by equation (2.41), and

$$\dot{e} = A_m e(a_o - k_m)b_m\phi^T g(x) + \nu \tag{2.68}$$

Taking the derivative of $V(e,\phi)$ in equation (2.66) along the trajectories in equations (2.65) and (2.68) yields

$$\dot{V}\,(e,\phi) = \dot{e}^T\,Pe + e^T P\,\dot{e} + \alpha\,|a_o - k_m|\,(\dot{\phi}^T\,\Gamma\phi + \phi^T\Gamma\,\dot{\phi}) \tag{2.69}$$

$$\begin{aligned}\dot{V}(e,\phi) &= e^T(PA_m + A_m^T P)e + 2e^T P(a_o - k_m)b_m\phi^T g(x) \\ &\quad +2e^T P\nu + 2\alpha\,|a_o - k_m|\,\phi^T\Gamma\,\dot{\phi} \end{aligned} \tag{2.70}$$

Substituting σ modified adaptive law, $\dot{\phi}$ from equations (2.65) into equation (2.70) the following is obtained.

$$\begin{aligned}\dot{V}(e,\phi) &= -e^T Qe + 2e^T P\nu \\ &\quad -2\alpha(a_o - k_m)\Gamma\sigma\phi\theta^* - 2\alpha(a_o - k_m)\Gamma\sigma\phi^2 \end{aligned} \tag{2.71}$$

Hence, $\dot{V}(e,\phi) < 0$ is outside the compact region of $D = \{\,(e,\phi)\ \ |e| \leq k_1,\ |\phi| \leq k_2\ \}$ where $k_1 > 0$and $k_2 > 0$ are positive constants, $\alpha > 0$, $\sigma > 0$ and $(a_o - k_m) > 0$. The tracking error $x - x_m$ can be minimized by adjusting the parameters α and σ, the magnitude of σ will influence the magnitude of the error. The use of the term $-\sigma\theta$ in the right hand side of equation (2.65) makes the adaptive system robust under external disturbance.

2.4.1 Simulations

Using the modified adaptive law, the suppression of roll rate and roll angle in the wing rock motion are shown in Figures 2.25 and 2.26. It was observed that the wing rock is suppressed within 10 seconds. In the simulation example the values of α and σ are tuned to the values of 0.08 and 0.01 respectively. With σ modified law, the roll rate given in Figure 2.25 shows a faster convergence to zero in 10 secs as compared to the case given in Figure 2.17 where roll rate converges to zero in 30 secs. The phase plot between roll angle and roll rate is shown in Figure 2.27. It is observed that during the transient stage, the closed loop response given in Figure 2.28 indicates that for σ modified control, the control signal is less oscillatory as compared to Figure 2.24 for

the case of control without σ modification.

2.5 Concluding Remarks

The adaptive control concept and notion of Lyapunov stability are reviewed. A model reference adaptive control methodology was outlined and the application is shown to suppress the wing rock based on delta wing model. The wing rock model used in the simulation study is reviewed and the physical significance of the nonlinear terms are discussed with examples. The adaptive control law is later modified to include the robustness feature for external disturbance. Simulations were carried out to illustrate the control methodology. The adaptive control method is based on the assumption that the knowledge of the system is known as " a priori " with respect to structure of nonlinearity present in the wing rock model.

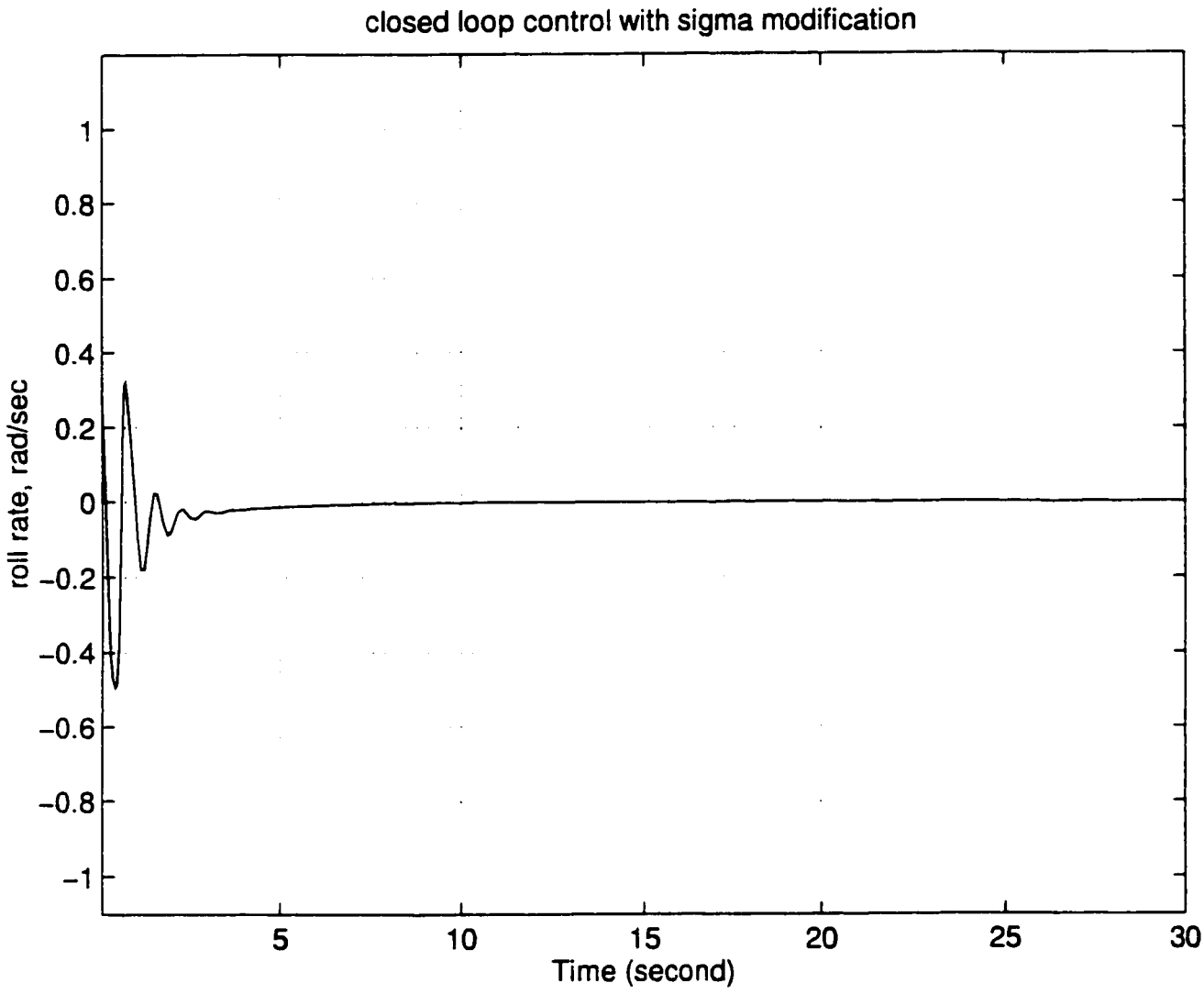

Figure 2.25: Suppression in roll rate (σ modification)

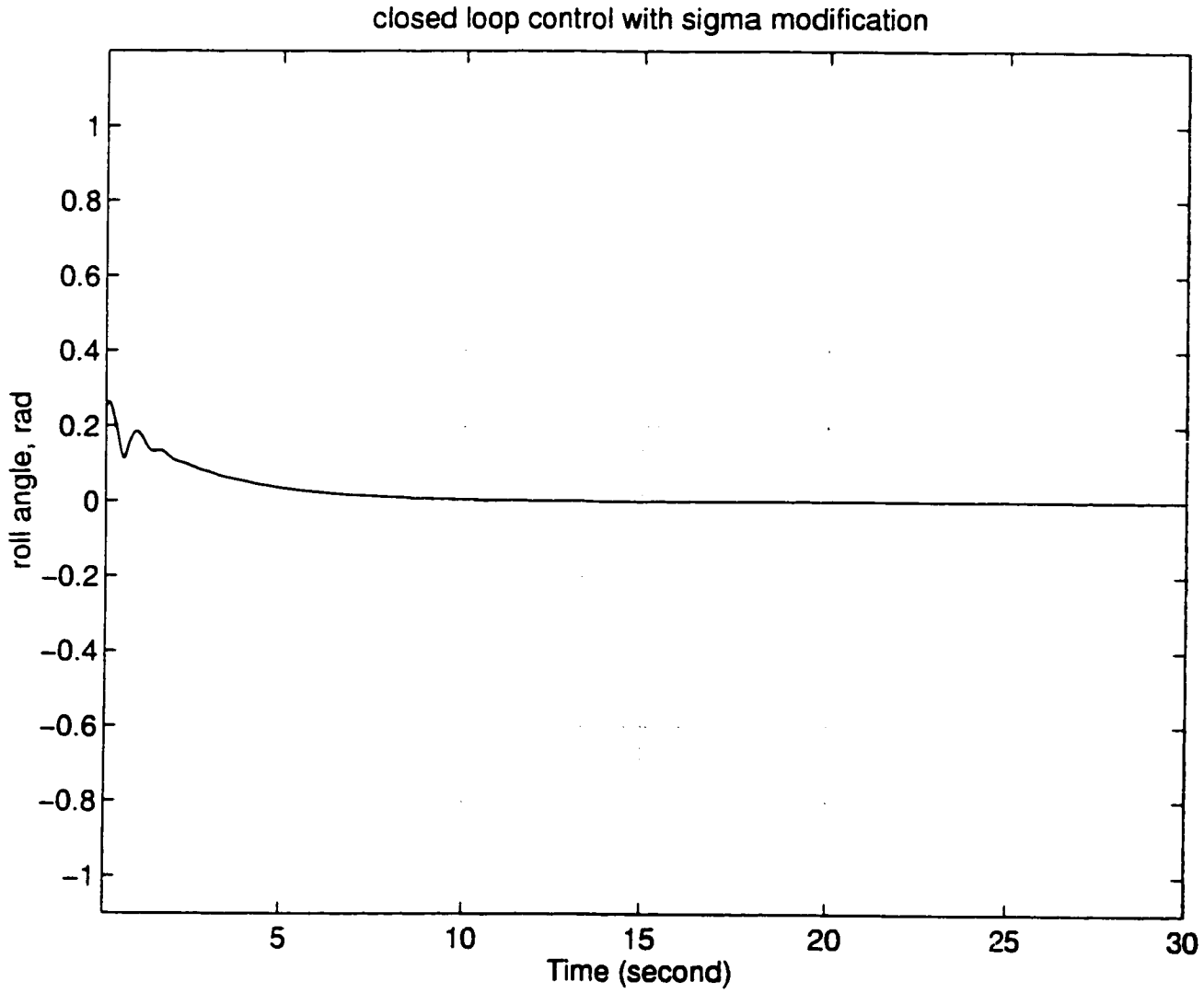

Figure 2.26: Suppression in roll angle (σ modification)

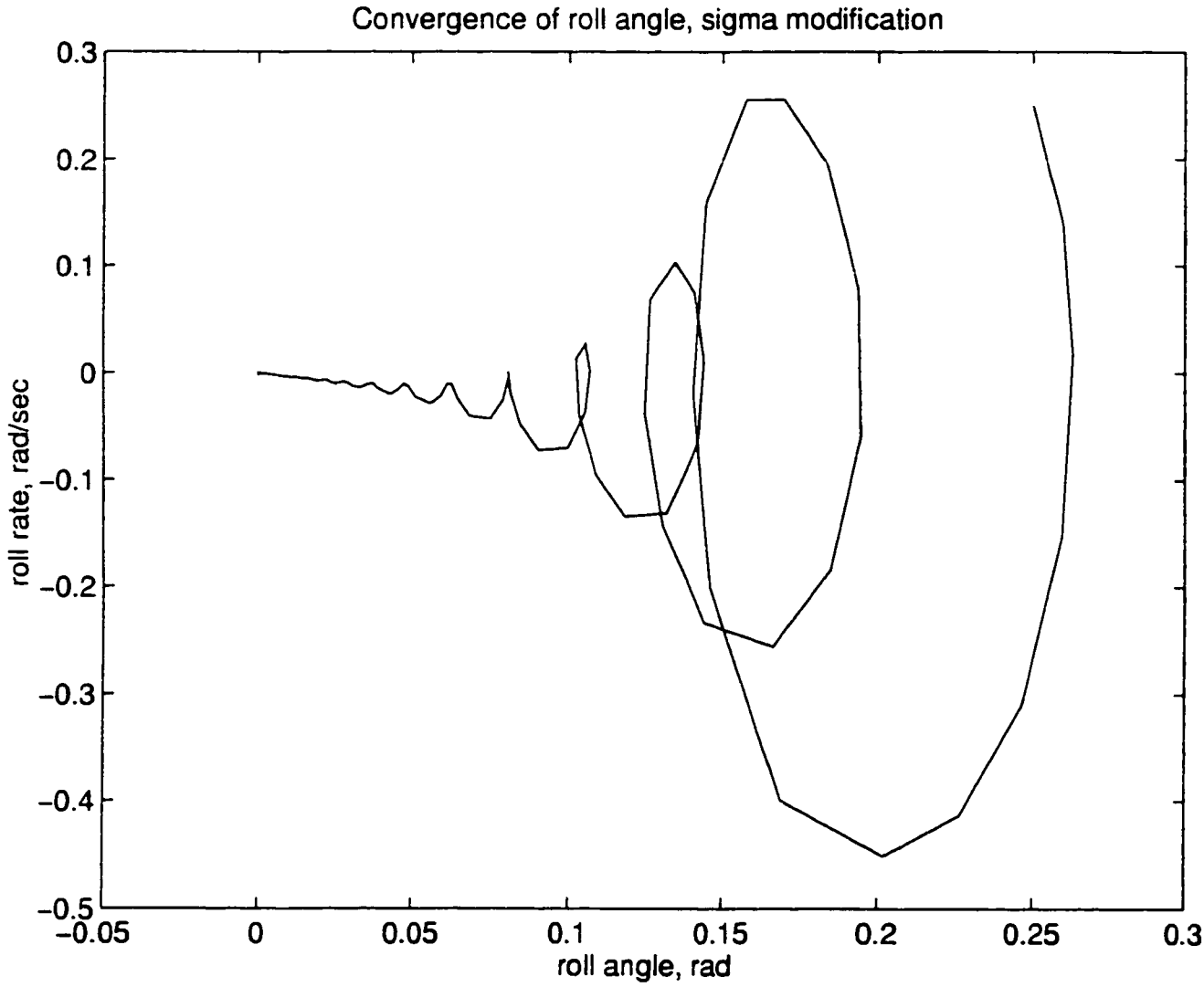

Figure 2.27: Convergence in roll angle (σ modification)

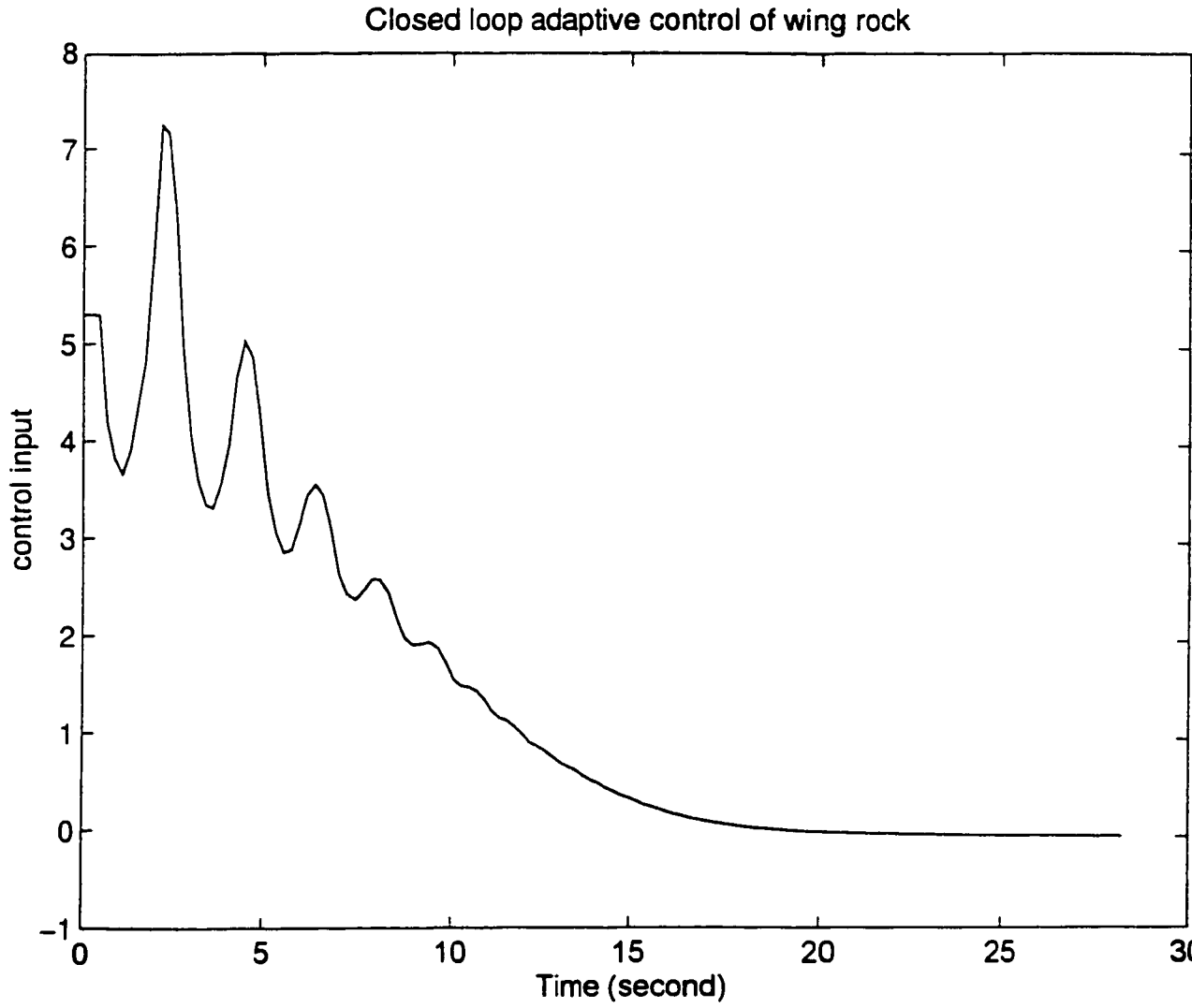

Figure 2.28: Closed loop control input (σ modification)

Chapter 3

Neural Networks Control Methodology

In recent years neural networks have been used successfully for controlling nonlinear systems. The research in this effort covers the control problems of regulation and tracking control with applications including robotic control, chemical process, medical and aerospace. The focus of the research in this thesis is the tracking control of wing rock in the aircraft for a given desired trajectory starting from any nonzero initial condition and it tends to zero as the time goes to infinity. The motivation of using a neural networks in such application is that the nonlinearity and the dynamics of the unknown system is poorly known and understood.

3.1 Neural Networks Structure

Neural networks are modelled by the process of *associative memory* which is capable to retrieve an output when the networks is presented with input pairs. The basis neural network architecture has the ability to perform function approximation by carrying out nonlinear mapping between the input-output pairs. The approximated

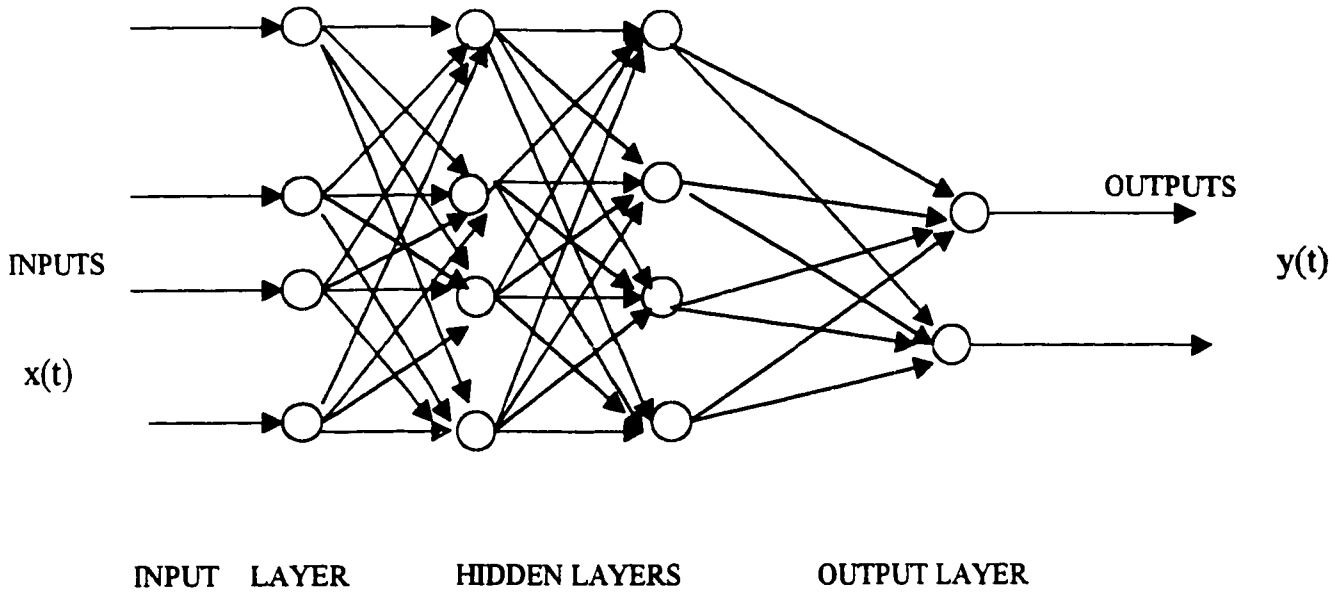

Figure 3.1: Multilayer Perceptron (MLP) with two hidden layers

function can be used for control purposes. In performing function approximation, the process of adjusting the neural network parameters takes place at the same time. This process is called *learning* in neural networks terminology. Learning process can be performed off-line or on line with a parameter adaptation scheme, such as in non linear process control. The neural network architectures employed for function approximation are normally feedforward networks and feedback propagation networks. Feedforward neural networks with feedback loop are considered in this research, and the following two commonly employed feedforward networks will be discussed. A good source of reference in neural networks can be found in Haykin [48].

3.1.1 Multilayer Perceptron

A Multilayer Perceptron (MLP) consists of an input layer, two hidden layers and an output layer is shown in Figure 3.1.

In a typical MLP network, the number of input units K defines the dimensionality

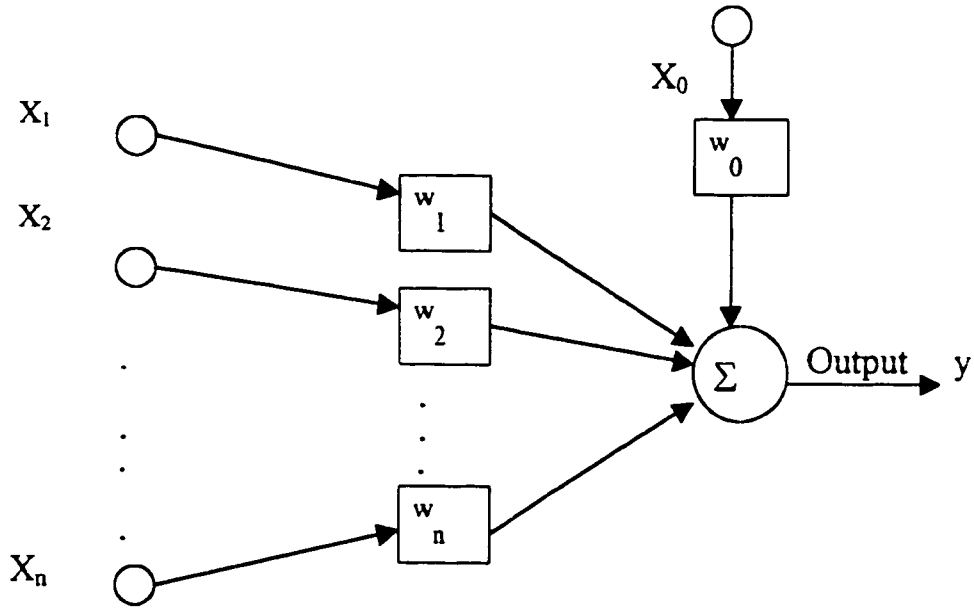

Figure 3.2: Adaptive Linear Combiner

of the input space denoted by $\mathbf{x}$ where $\mathbf{x} \in \Re^K$ and likewise the output units L defines the dimensionality of the output space denoted by $\mathbf{y}$ where $\mathbf{y} \in \Re^L$. The multilayer preceptron maps the inputs to the output patterns as $R : \mathbf{x} \rightarrow \mathbf{y}$ or the mapping of input space to output space by $R : \Re^K \rightarrow \Re^L$. In the networks the input signal is propagated through the processing layers before output is computed. Each processing layer consists of number of *nodes* (hidden units) and each *node* is composed of adaptive linear combiner which simply forms a weighted sum of the inputs to give an output. The transformation process in the input-output mapping depends on the connections in the mapping and the *activation function* in the *nodes* or hidden units. A typical adaptive linear combiner is shown in Figure 3.2.

Letting the n-dimensional input vector be denoted by $\mathbf{x}$ and the weight vector denoted by $\mathbf{w}$, the adaptive linear combiner's output $\hat{y}$ is given, with w_o as a bias, as

$$\bar{y} = \sum_{i=1}^{n} x_i w_i + w_o = \mathbf{x}^T \mathbf{w} + w_o \tag{3.1}$$

The above expression represents a hyperplane in the space of $\mathbf{x}$ and it has a form of linear discriminant function such as that employed in the application of pattern classification. There are different types of function can be used as activation function of which the most common is the *sigmoid function* given as below.

$$f(\bar{y}) = \frac{1}{1 + \exp(-\bar{y})} \qquad \in (0, 1) \tag{3.2}$$

where

$$\bar{y} = \mathbf{x}^T \mathbf{w} + w_o \tag{3.3}$$

The hidden unit with *sigmoid activation* function is also referred as *sigmoidal unit*. The thresholding is a firing operation of the neurons when its input exceeds certain limit of threshold value. In the case of pattern classification, the thresholding providing the discriminate function separates the $\mathbf{x}$ space in two regions. The *sigmoidal function*, a soft threshold, is a monotonic function which maps the input range $(-\infty, +\infty)$ to an output range $(0, 1)$. The output of the *sigmoidal function* in the hidden layer is constant along the $(n-1)$ dimensional hyperplanes given by $c = \mathbf{x}^T \mathbf{w} + w_o$ for some constant c. *Sigmoidal function* is termed *ridge function* because the output is constant along the hyperplanes in their input space.

The basic structure of MLP is flexible and can be employed for different applications such as modelling and control. It has been reported in Hornik [49], Brown and Harris [50] that any continuous nonlinear function can be approximated with three-layer MLP with sufficient number of hidden units. The MLP network deals efficiently with input data which are redundant, and the nonlinear functions which have local

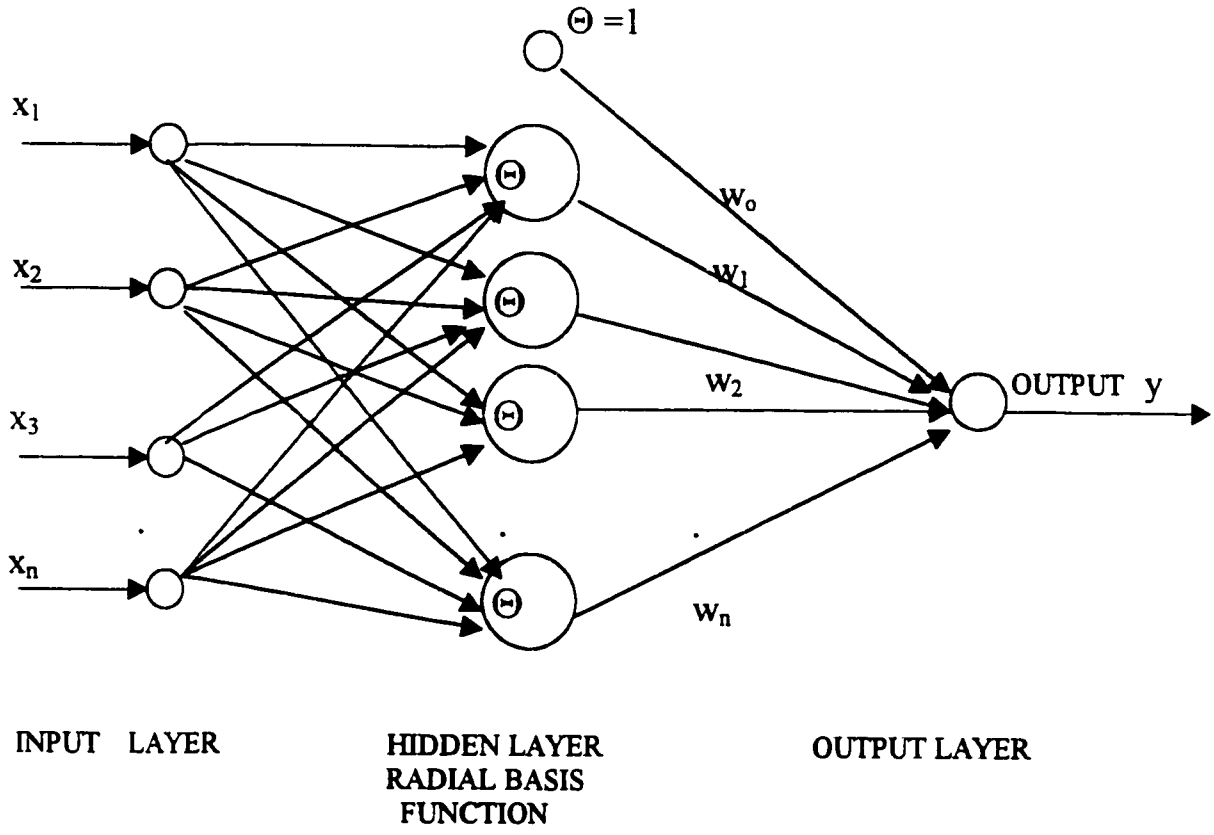

Figure 3.3: Radial Basis Function networks

variations.

3.1.2 Radial Basis Function Networks

Radial Basis Function (RBF) neural network uses standard three layer network architecture, namely input layer, hidden layer and the output layer where the output *nodes* are simply adaptive linear combiners. The hidden layer nodes may have specific structures. The typical RBF network architecture is shown in Figure 3.3.

The output of the general RBF network is represented by the following.

$$y = \sum_{i=1}^{n} w_i \phi(\|\mathbf{x} - \mu_i\|), \quad 1 \leq i \leq n \tag{3.4}$$

where w_i and μ_i are weight and centre of the i^{th} hidden layer node and $\|.\|$ is the

standard Euclidean norm, a distance measure between vector of basis function centres u_i and $\mathbf{x}$ the input space. The univariate nonlinear functions $\phi(.)$ used are generally (i) quadratic $\phi(r) = \sqrt{r^2 + c^2}$, (ii) thin plate splines $\phi(r) = r^2 \ln r$ and (iii) Gaussian $\phi(r) = \exp(-\frac{r^2}{\sigma^2})$. For a given problem in this research, Gaussian Radial Basis Function will be used in the design of control system where the basis function is given as $\Theta_i(x) = \phi\left(\frac{\|x-\mu_i\|}{\sigma_i}\right)$ for i^{th} hidden node, σ_i is the width of the Gaussian function. The question of localization in the internal network representation is an important consideration in the design of the network architecture. Gaussian RBF network with local representation and Gaussian receptive fields are suitable for learning for nonlinear evolving dynamical system such as flight dynamics.

3.1.3 Recurrent Neural Networks

A recurrent neural networks has at least one feedback loop [48] and the networks can take many different forms and configurations. The common feature of the recurrent network is its capability of capturing temporal behavior and provides multi-step ahead predictions.

In general, recurrent neural networks can be classified according to the three architectures [51], *globally recurrent networks*, *locally recurrent networks* and *NARX recurrent neural networks*.

In globally recurrent networks shown in Figure 3.4, the feedback connections come from the state vector of the hidden layer. Figure 3.5 shows the locally recurrent network representations where each neuron has a delay feedback loop around itself. The NARX recurrent networks [52] is shown in Figure 3.6 where output of the networks is feedbacked to the networks through time delay unit and this architecture is an popular research area. The networks can have a higher order of embedded memory consisting of the tapped delayed values. In this research, the recurrent network used is defined as feedback through single time delay unit with output memory of order

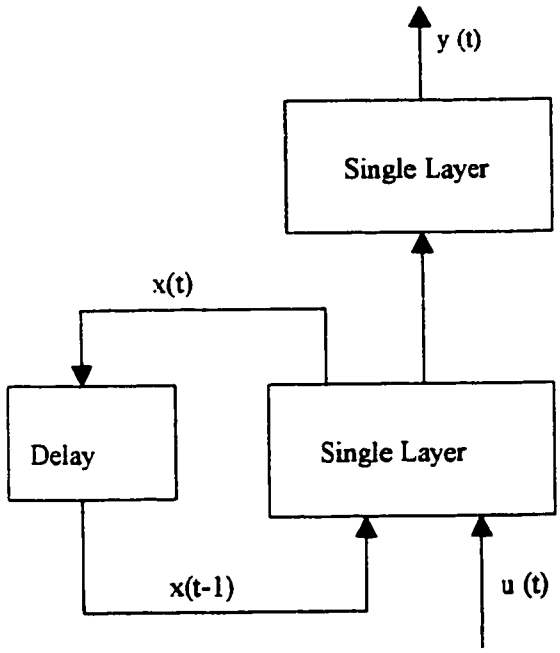

Figure 3.4: Globally Recurrent Networks

one.

The RBF network is powerful in performing function approximation, however it does not provide a way for determining the number of hidden units in the given architecture to achieve the approximation for a given required accuracy. In most of the control problem involving the use of the RBF networks, the fixed network design is employed where the number of radial basis functions are predetermined and they are placed on the regular grid. The research effort of this thesis is to propose a methodology for designing self adjusting dynamic recurrent RBF networks to solve the wing rock problem.

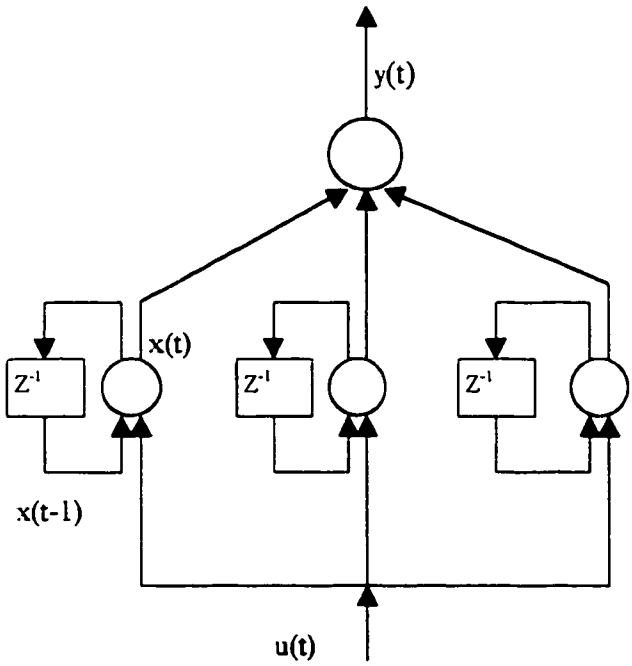

Figure 3.5: Locally Recurrent Networks

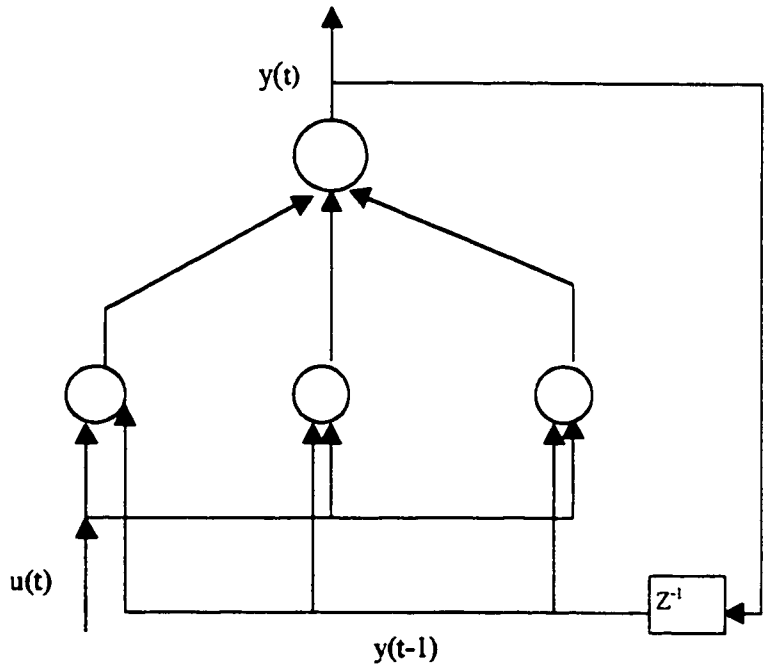

Figure 3.6: NARX Recurrent Networks (Output memory of order one)

3.2 Neural Control Methodology

Adaptive control methodology developed earlier is only applicable if the structure of the nonlinearities responsible to produce wing rock is known as " a priori ". However, in the aircraft the structure or the source of the wing rock is not known. To overcome this problem, the RBF neural network is used for identifying the nonlinear dynamics of the wing rock and the adaptive control methodology is employed to complete the control system design.

Multi-layer neural networks have been used by many researchers for various application such as the identification for the complex nonlinear process, pattern recognition, function approximation and control application etc. Neural networks can be combined with the conventional control methodology for controlling complex and nonlinear process. Neural networks had been proposed as a replacement for adaptive control for regulating wood chip refiner [53]. More direct application of neural networks to the flight control are reported in Steck et al. [54].

In the adaptive control scheme, the dynamic neural networks proposed will be used to identify the unknown nonlinear plant. The dynamic data generated by the aircraft model will be used in the network design and the learning process. Due to the evolving dynamic nature of the system, neural networks with local representation such as RBF will be used in the investigation. The overview of neural control methodology will be outlined in this section.

3.2.1 Neural Control Law

Consider the system to be controlled is a continuous time single input-single output aircraft dynamics with control input $u : R^+ \rightarrow R$, an output $y : R^+ \rightarrow R$ and an order n be represented by the following non linear affine system given by Hancock [55]

$$\begin{aligned} \dot{x} &= a(x) + b(x)u \\ y &= h(x) \end{aligned} \tag{3.5}$$

where $x(t) : R^+ \rightarrow R^n$ is a state vector, $a(x) : R^n \rightarrow R^n$ and $b(x) : R^n \rightarrow R^n$ are state dependent vector functions and $h(x) : R^n \rightarrow R$, a state dependent output function. It is assumed that the nonlinearities of $a(x)$, $b(x)$ and $h(x)$ are sufficiently smooth functions of the states and their partial derivatives exist and continuous. The control of wing rock is considered a trajectory tracking problem. The error $e = y - y_d$ is defined as tracking error where y_d is the desired function. The control objective is that given a desired output in the reference model, the controller forces the tracking error to converge to a neighborhood of zero. If the system given in equation (3.5) is assumed to have a strong relative degree γ, and output differentiation is terminated after $\gamma \leq n$ steps then the system can be represented by the following input-output dynamics.

$$y^{(\gamma)} = f(x) + g(x)\, u \tag{3.6}$$

In this research, we consider a sampled data system and the controller is assumed to be a discrete time regulator with state variables feedback implemented as RBF neural networks. The output of the non-linear system is sampled at $t = kT_s$, $k \in Z^+$ with uniform sampling period $T_s > 0$. It is assumed that in the sampling process of continuous time system, an infinite number of bit is used and there is no finite escapes and the general structure given in system (3.6) is preserved in the discrete time system. The general control architecture is shown in Figure 3.7.

Consider the sampled data non linear single input-single output relative degree one system be represented by the following in Chen [56].

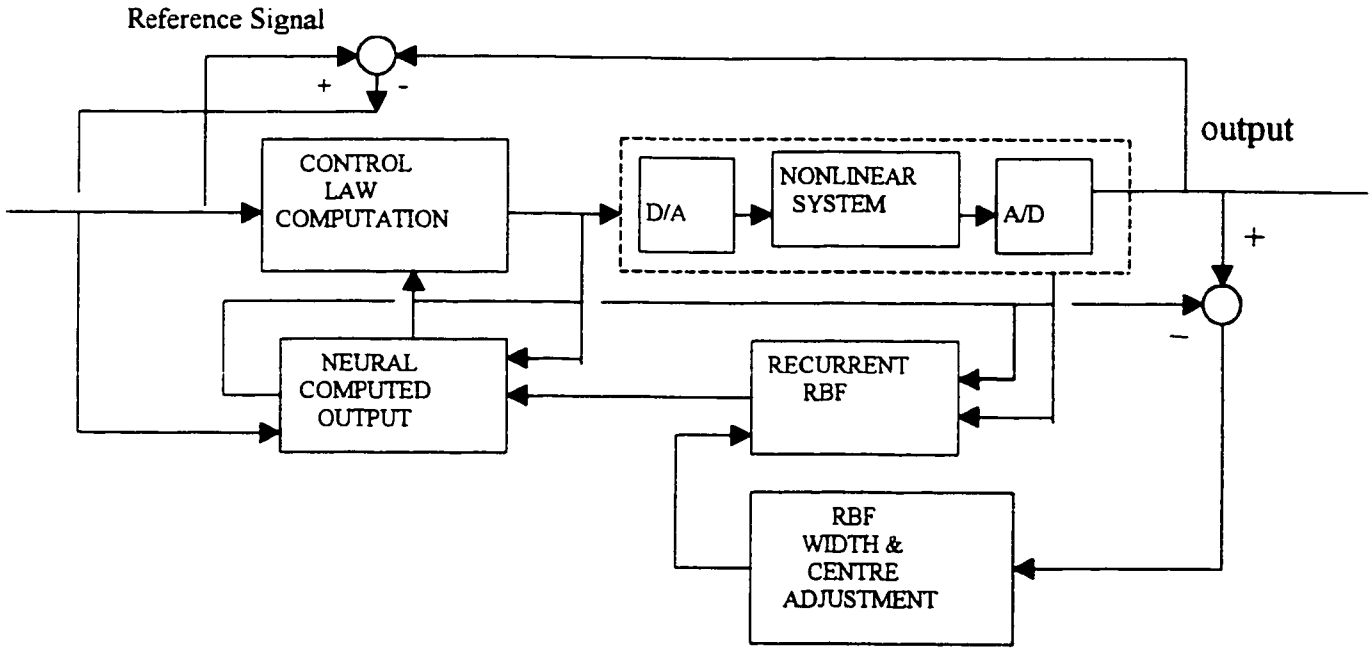

Figure 3.7: Dynamic Recurrent RBF Network Control Architecture

$$y_{k+1} = f(y_k, \ldots, y_{k-p+1}, u_{k-1}, \ldots, u_{k-m}) + g(y_k, \ldots, y_{k-p+1}, u_{k-1}, \ldots, u_{k-m})u_k \tag{3.7}$$

The non linear plant can be written in discrete time as below

$$y(k+1) = f(z(k)) + g(z(k))u(k) \tag{3.8}$$

The unknown nonlinear system to be modelled is represented by the following.

$$\hat{y}(k+1) = \hat{f}(z(k), w_f) + \hat{g}(z(k), w_g)u(k) \tag{3.9}$$

The following approximate feedback linearization control law is used in order to bring the tracking error to zero.

$$u(k) = \frac{-\hat{f}\,(z(k), w_f) + r(k)}{\hat{g}\,(z(k), w_g)} \tag{3.10}$$

where $z(k)$ is the input state variable, w_f and w_g are linear parameters of output layer of RBF networks and $r(k)$ is the reference command, the desired output. The estimates of $\hat{f}\,(z(k), w_f)$ and $\hat{g}\,(z(k), w_g)$ are constructed using a pair of RBF functions.

$$\hat{f}\,(z(k), w_f) = f_o(z(k)) + \sum_{i=1}^{K_f} w_{f_i} \Theta_{f_i}(z(k)) \tag{3.11}$$

$$\hat{g}\,(z(k), w_g) = g_o(z(k)) + \sum_{i=1}^{K_g} w_{g_i} \Theta_{g_i}(z(k)) \tag{3.12}$$

where K_f and K_g are the number of neurons in hidden layers for each separate BRF networks and $\Theta_{f_i}(z(k))$, $\Theta_{g_i}(z(k))$ are Gaussian functions in respective networks determined by the number of hidden neurons and neural parameters of centre and width, and $f_o(z(k))$ and $g_o(z(k))$ are assumed known prior knowledge of the functions $f(z(k))$ and $g(z(k))$ of the system. The neural parameters are updated by the Extended Kalman Filter. The task of neural control is to achieve stable output tracking for the nonlinear aircraft system represented by equation (3.6) where the nonlinearities of $f(x)$ and $g(x)$ are unknown. This implies that given the desired output y_d the tracking error $y - y_d$ is forced by the controller to converge to the neighborhood of zero while keeping the signals in the closed loop system bounded.

3.3 Learning in Neural Networks

It is well known that neural networks has the unique learning capability when the networks is presented with information of input-output pairs as in the case of approximating the unknown functions. The learning process is of the static type mapping

which involves the repeated presentation of input-output pairs of information until the networks connected weights converge. The optimization procedure such as least square error criterion is generally used in the learning algorithm. The most common learning algorithm is the *error back propagation* developed for multilayer feedforward networks in Rumelhart [57]. Other learning algorithm such as conjugate gradient descent is also utilized for neural network learning.

In the context of controlling wing rock in flight, learning in neural networks is required for the reason that the *prior* knowledge of the nonlinear wing rock structure is unavailable and unknown. Learning can be viewed as a two-phase process namely *structure identification phase* and *parameter optimization phase.* In this thesis we consider the neural networks mainly of the type RBF. Learning algorithm for *structure identification* is a non convex optimization problem whereby the data presented must take into account the complexity of target mapping, representational ability of local models and availability of data.

In most of the research of the RBF networks, a fixed number of radial basis functions was assumed based on the prior knowledge. In some cases the width is assumed constant as a thin plate function and the centres are optimized by clustering algorithm such as *self-organizing map* and *k-means clustering.* In this research *structure identification* determines the number of neurons in the hidden layer of RBF using the neurons addition/pruning criteria based on the Preisach hysteresis model concept. The whole scheme will be discussed in later chapter. Parameter optimization phase is carried out in two steps, firstly the centers and widths are adjusted using the Extended Kalman Filter for taking care of their nonlinear features. The linear outer weights are normally adjusted by least means square method or recursive least square. In this research the outer weights optimization is carried out by considering the stability analysis of the system.

3.4 Concluding Remarks

The review was carried out for the feedforward neural network structure namely multilayer perceptron and radial basis function related to the context in this research. Various different types of recurrent neural networks were discussed. Based on the radial basis function network, neural control methodology was outlined and formulated. The process of learning and adaptation in the proposed RBF networks are discussed.

Chapter 4

Application of the Preisach Model as a Neural Network

The concept and the properties of the Preisach hysteresis model are applied in the design and training of RBF neural networks. The obtained network is used in identifying the uncertain nonlinear system responsible for generating the wing rock. Based on the identification of the unknown nonlinear system, control law is formulated for controlling the of wing rock motion. The structure and memory mechanism in the Preisach model has a direct analogy to parallel connectivity and memory formation in the radial basis function network. Based on their similarities, the plausible reasonings will be given in the application of the Preisach model for the design of the dynamic recurrent RBF networks.

4.1 Overview of the Preisach Hysteresis Model

4.1.1 Hysteresis

Hysteresis means " *to lag behind* " defined as rate independent memory effect, a phenomenon in which the output depends on the evolution history of inputs. Several

physical phenomena exhibit hysteresis and they are found in chemistry, biology, ferromagnetism, ferroelectricity, superconductivity, porous media filter, granular motion and mechanical system. There are numerous classical models describing hysteresis using the concept of *hysteresis operator* such as Prandtl, Ishlinskiĭ, Preisach and Duhem [58].

The underlying idea of the Preisach model is illustrated by comparing the following figures. Figure 4.1 shows the relay without delay (top graph), a monotonic function which can be approximated by linear combination of a finite family of jump functions as shown in the bottom half of the graph. The input function is represented by u and the output function by w. Figure 4.2 shows the relay with delay (top graph) and their linear combination of the finite family of *delayed relays* yields the *hysteresis loop* shown in the bottom graph. The construction allows one to approximate a large class of continuous hysteresis laws and yields an operator which acts in the space of continuous time function.

In general, hysteresis can be classified as *continuous hysteresis* and *discontinuous hysteresis* (catastrophic hysteresis). Example of continuous hysteresis are friction controlled backlash also known as *play* and elasto-plasticity also known as *stop*. Discontinuous hysteresis deals with phase transition such as occurring in ferromagnetism whereby the transitions is characterized by discontinuity.

4.1.2 Classical Preisach Hysteresis Model

The classical Preisach hysteresis model was studied extensively by Mayergoyz [30] and is described as below.

$$f(t) = \hat{\Gamma}\, u(t) = \iint_{\alpha \geq \beta} \mu(\alpha, \beta)\ \hat{\gamma}_{\alpha\beta}\, u(t)\ d\alpha\ d\beta \tag{4.1}$$

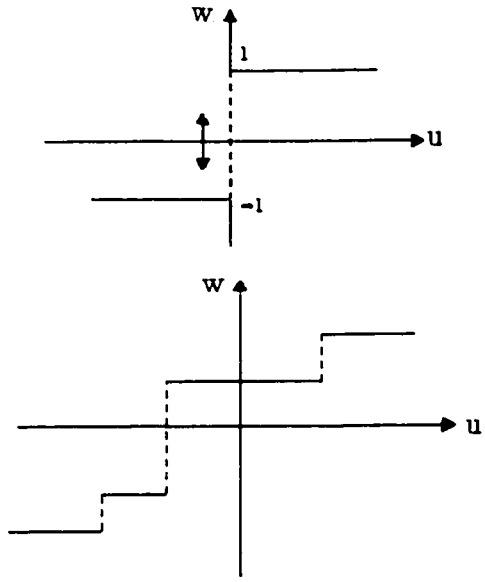

Figure 4.1: Relay without delay(top), and its approximation (bottom)[58]

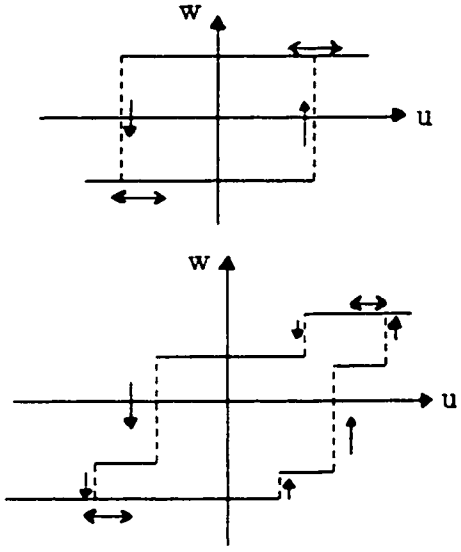

Figure 4.2: relay with delay(top) and its approximation(bottom)[58]

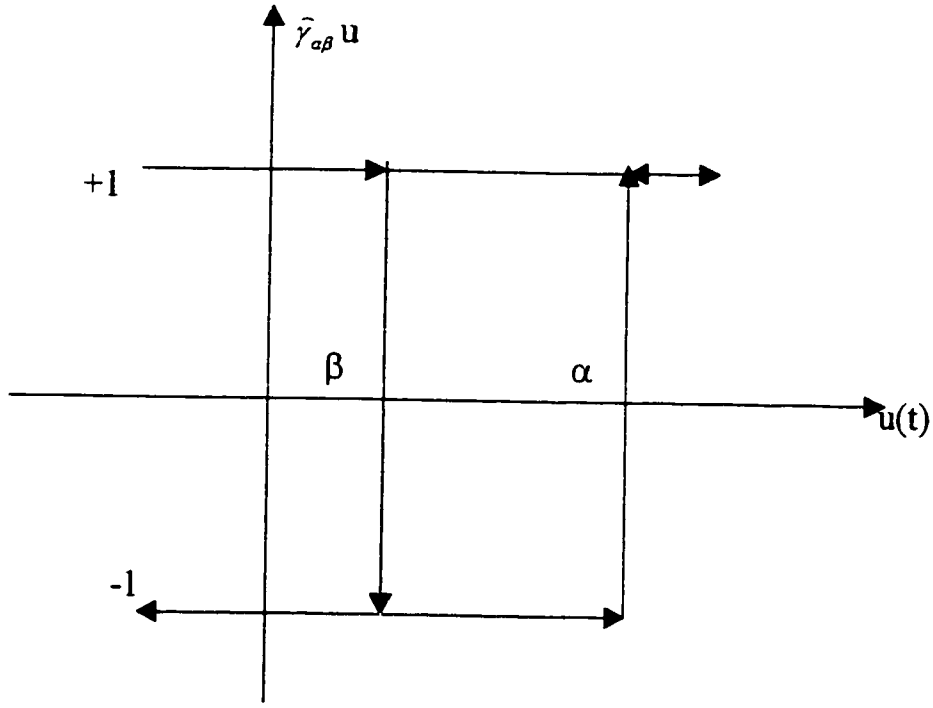

Figure 4.3: The Preisach Operator-representing input-output [30]

The model can be viewed as infinite set of simplest hysteresis operator $\hat{\gamma}_{\alpha\beta}$ represented by the notation $\hat{\Gamma}$ defined in equation (4.1), each of these operators can be represented by a rectangular loop of input $u(t)$ and output $f(t)$, and $\mu(\alpha, \beta)$ is the weight function where α and β represent up and down of the switching values of inputs where $\alpha \geq \beta$. The hysteresis operators can be interpreted as two-position relays with "up" and "down" positions corresponding to $\hat{\gamma}_{\alpha\beta}\ u(t) = +1$ and $\hat{\gamma}_{\alpha\beta}\ u(t) = -1$ respectively. The output of the hysteresis operator assumes two values of +1 or -1 as shown in Figure 4.3. Each of these operators has a local memory. In other words, the past exerts its influence upon the future through instantaneous values of output.

4.1.3 Geometric Interpretation of the Preisach Model

The Preisach operator is shown in Figure 4.3 and its geometric interpretation given in [30] is shown in Figure 4.4. There is a one to one corresponding between the operator $\hat{\gamma}_{\alpha\beta}$and the point (α, β) of the half plane $\alpha \geq \beta$. Each point of the half plane $\alpha \geq \beta$ can be identified with only one particular operator $\hat{\gamma}_{\alpha\beta}$ whose up and down switching values are respectively equal to α and β coordinates of the point. The operator $\hat{\gamma}_{\alpha\beta}$ and the half plane $\alpha \geq \beta$ are then uniquely defined by the point (α, β). The triangle T defined by points A, B and C as shown in Figure 4.4 is then subdivided into two sets $S^+(t)$ consisting of points (α, β) for which the operators $\hat{\gamma}_{\alpha\beta}\ u(t) = 1$ are in the up position and $S^-(t)$ consisting the points (α, β) such that the corresponding operators $\hat{\gamma}_{\alpha\beta}\ u(t) = -1$ are in the down position. The function $\hat{\gamma}_{\alpha\beta}\ u(t)$ is assumed zero outside the triangular T .

It is shown that the interface line $L(t)$ separating $S^+(t)$ and $S^-(t)$ is a staircase line whose vertices has α and β coordinates coinciding with local maxima and minima of input at previous instants of time. The final link of $L(t)$ is at the line $\alpha = \beta$ and moves when the input changes, and the link is a horizontal one and moves up when input increases and it is a vertical and moves right to left when input decreases. Using the geometric interpretation the model can be represented by the following equivalent form.

$$f(t) = \iint_{S+(t)} \mu(\alpha, \beta)\ \ d\alpha\ d\beta - \iint_{S-(t)} \mu(\alpha, \beta)\ \ d\alpha\ d\beta \tag{4.2}$$

From equation (4.2) the instantaneous value of output depends on the shape of the interface $L(t)$ which in turns is determined by the extremum value of input at previous instants of time.

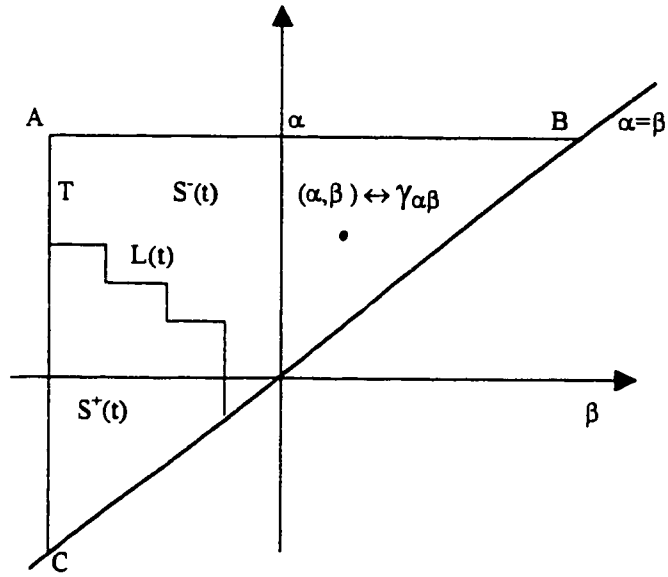

Figure 4.4: Geometric interpretation of the Preisach operator

4.1.4 Continuity Properties of the Preisach Model

The interpretation of the Preisach model and its properties in memory formation are used as criteria in the design of dynamic recurrent RBF. The objective of the RBF networks is to approximate the unknown nonlinear function of the physical system which generates the wing rock. The Preisach operator is purely phenomenological in nature, the issue of the operator being a continuous or discontinuous function depends on the underlying *Preisach measure*, the topic had been studied by many researchers and is beyond the scope of the present thesis. Depending on the interpretation and the particular application, the Presiach model can be considered an infinite summation of the operators (cells) $\hat{\gamma}_{\alpha\beta}$ (possibly discontinuous) to yield a continuous relationship. The Preisach operator exhibits continuity properties in several function spaces, this subject is thoroughly discussed in [58].

In the application where the Preisach is used directly to model piezoceramic ac-

tuator or shape memory alloy actuation, the problem of the Preisach operator being continuous or discontinuous becomes an important issue. The problem is resolved by using the smoothed Preisach operator and generalized hysteresis operators derived from the results obtained from Krasnoselskii and Pokrovskii [58].

4.2 Analogy of Preisach Hysteresis Model and RBF Networks

The Preisach hysteresis model is represented by block diagram as shown in Figure 4.5. The model can be interpreted as a spectral decomposition of the complicated hysteresis operator Γ into a single hysteresis operator $\hat{\gamma}_{\alpha\beta}$. From the mathematical point of view the Preisach model can be viewed as infinite summation of the hysteresis operator $\hat{\gamma}_{\alpha\beta}$.

Wing rock is the outcome of the hysteresis presents in the nonlinear aircraft system. Hysteresis is difficult to model or identify. The Preisach model has been defined without any reference to a particular physical origin of hysteresis. This shows the phenomenological nature of the Preisach model and its mathematical generality. As the result, researchers had interpreted its properties and applying in the control of nonlinear system exhibiting hysteresis in various field of applications, the most recent publications related to the use of the Preisach model are reported in [59], [60], [61], [62]-[64].

There is a striking similarly and parallel between the Preisach model and the RBF neural networks as shown in Figures 4.5 and 4.6. The RBF network has extra features in inter parallel connectivity at the input layer as compared to the Preisach model. The following are the common features found in the hysteresis model and the RBF networks.

(i) The hysteresis operator $\hat{\gamma}_{\alpha\beta}$ referred as *cell* in *the* Preisach model is analogous to

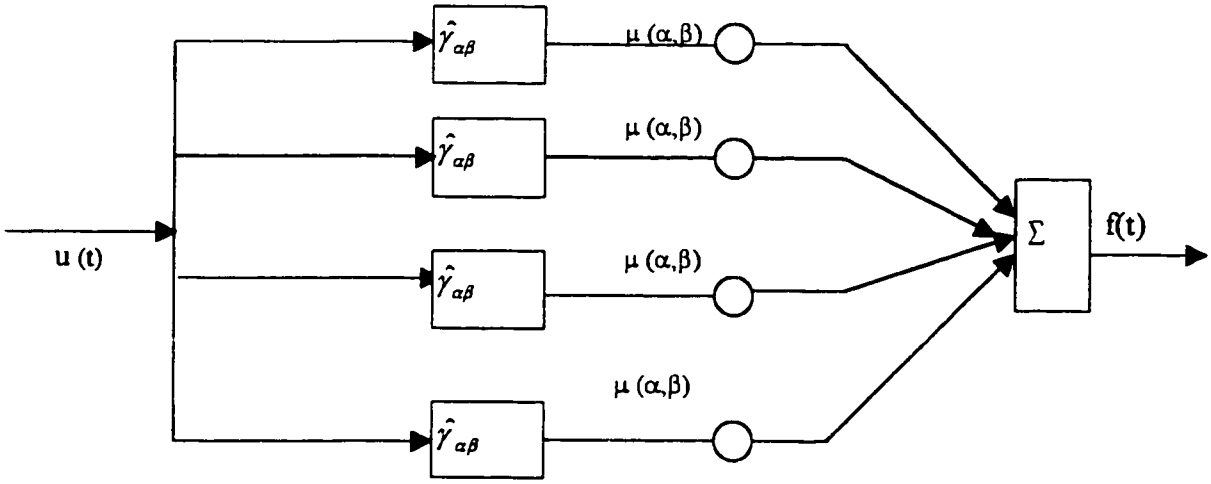

Figure 4.5: Representation of the Preisach Hysteresis Model [30]

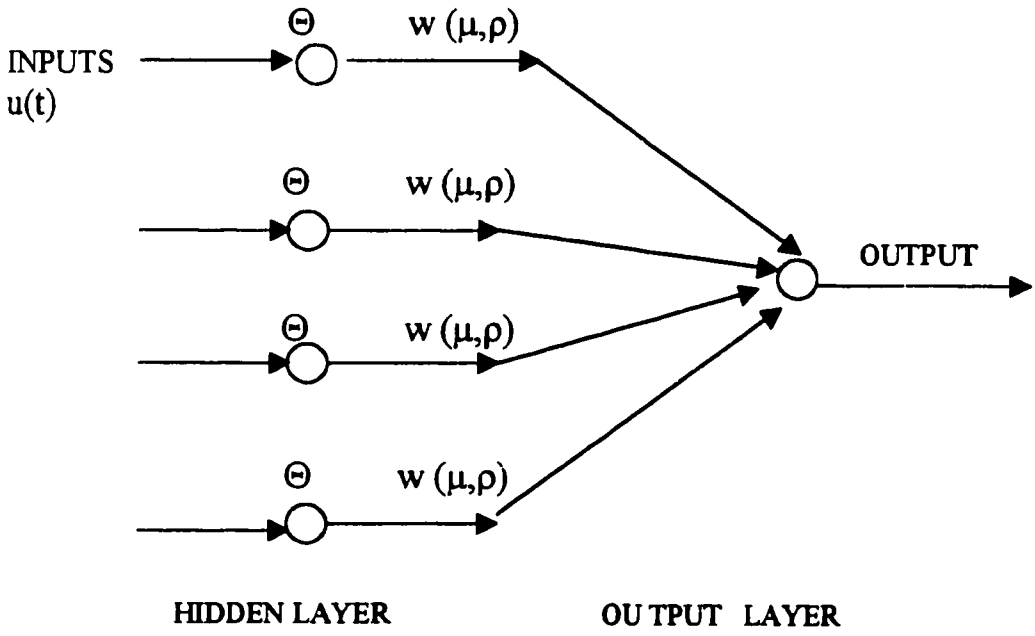

Figure 4.6: RBF Neural Networks

the Gaussian function. $\Theta_f(z)$. the *neuron* in the hidden layer of the RBF networks.

(ii) The mechanism of memory formation in the Preisach model results from the parallel connectivity of two position cells, $\hat{\gamma}_{\alpha\beta}$. The switching values α and β in the model play the same role as the centre μ and width σ of the Gaussian function as they are all affected by the input values to the function. The values μ and σ in the RBF correspond to α and β in the Preisach model in the sense that both these values can be adjusted. Gaussian function has a range between 0 and 1 whereas the Preisach operator has a switching values between -1 and $+1$. There are studies reported in [61] that the operator can be smoothed to a continuous function and the switching values can be modified to vary from 0 to 1 as reported in [59].

(iii) The weight $\mu(\alpha, \beta)$ of the model is analogous to the linear weights $w(\mu, \rho)$ at the output layer of the RBF networks. Determination of the weight $\mu(\alpha, \beta)$ in the model is corresponding to the supervised learning for the linear weights $w(\mu, \rho)$ determination in the RBF networks.

(iv) The function approximated by RBF is $\hat{f}_{RBF} = \sum \Theta \; w(\mu, \rho)$ which is analogous to the function output obtained from the Preisach model given by $\hat{f}_{model} = \sum \hat{\gamma}_{\alpha\beta} \; \mu(\alpha, \beta)$.

4.3 Application of the Preisach Model as Dynamic Recurrent RBF

Based on the above described analogies and their similarities in connectivity pattern, the RBF is an suitable network and excellent choice for such application of the Preisach model. The types and sources of the hysteresis are not crucial to the performance of the RBF networks employed in the approximation of the nonlinearities regardless as the aerodynamic or mechanical nature in the generation of wing rock. The encoding of knowledge source is realized by adaptive learning technique, namely

supervised learning in the networks. In order to capture the physical insights of the wing rock phenomena namely the noise disturbances generated from sensor readings, wind gust etc., a recurrent feature is included in the RBF networks as shown in Figure 4.7. The unknown functions $f(z(k))$ and $g(z(k))$ are estimated by the two separate recurrent RBF networks to give the approximated output of the unknown nonlinear system as $\hat{y}(k+1) = \hat{f}(z(k), w_f) + \hat{g}(z(k) w_g) u(k)$. The use of the recurrent feature will account for the dynamic nature of the nonlinearity.

The RBF networks is dynamic in the sense that the size of the networks is optimized constantly by adding or pruning the neurons based on the criteria of the growth of neurons. The Preisach hysteresis model is associated with memory and has the following properties.

(i) The mechanism of memory formation of the Preisach Model results from the superposition of parallel connection of the position cells $\hat{\gamma}_{\alpha\beta}$.

(ii) The information storage in the Preisach model is not localized in any particular cells as in the computer storage device, but some ensembles of all the cells $\hat{\gamma}_{\alpha\beta}$ participate in storage of each bit of information. This feature is used in the criteria for determining the addition/pruning of the neurons.

(iii) If some of the cells $\hat{\gamma}_{\alpha\beta}$ are destroyed, the stored information still might be preserved.

(iv) The Preisach model is bestowed with local memories. This means that if given the output values, $f(t_o)$ at some instant t_o, and the input values $u(t)$ will at all subsequent instants $t \geq t_o$ uniquely predetermine the value of output $f(t)$ for all $t \geq t_o$. In order to capture this feature we have considered the feedback of the output signal to give the recurrent RBF structure.

(v) The Preisach model has the *wiping out property* which states that subsequent events may erase the information previously stored in the memory. The erase of memory will occur if the new events have an impact characterized by larger input

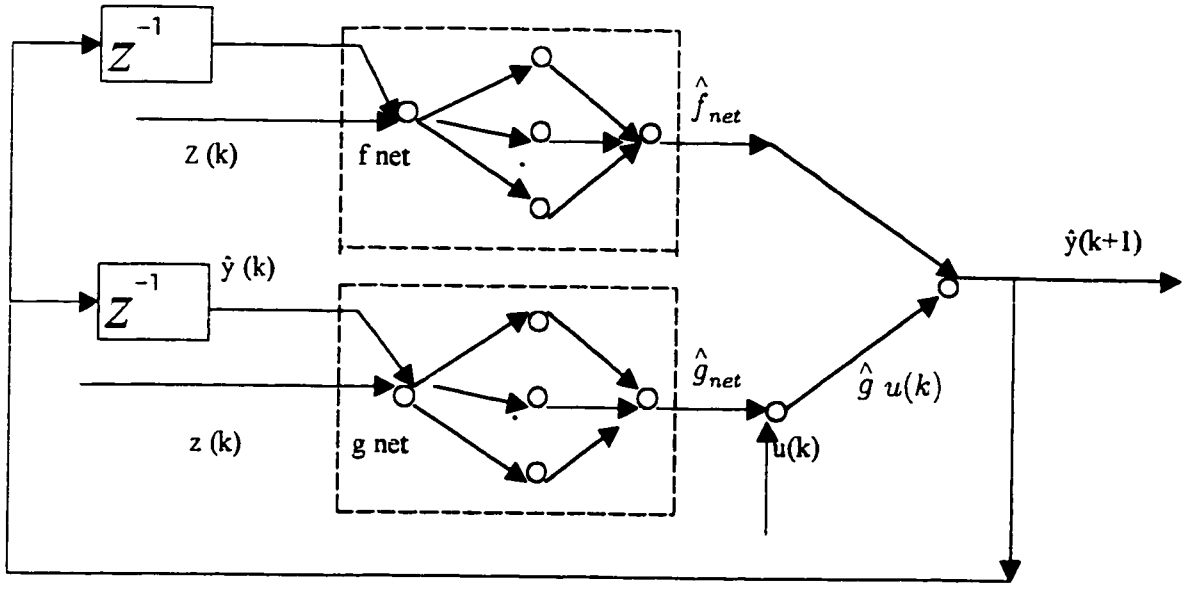

Figure 4.7: Recurrent RBF Model

extrema than previous one. If there is no impact on the input than the previous one, the output of the hidden units remains insignificant and unchanged after a specified consecutive observations. This property is used as a criterion for pruning the neurons in the networks training phase.

The influence of the RBF networks parameters on the estimation of $f(z(k))$ and $g(z(k))$ depends on factors such as network input and localization properties of the RBF networks. In the case where the height and centre of the RBF networks are kept constant, the greater the width the greater the space of the receptive field on the function estimation. The RBF network has a temporal localization in the parameter updating process. In the case of the design for the fixed size networks, on line learning requires the placing of a huge number of RBF functions on the regular grid for better approximation and very often the number of neurons increases with the increase of the input dimension, a feature referred to as the *curse of dimensionality.*

4.4 Concluding Remarks

The Preisach hysteresis model is introduced and its geometric interpretation and properties are discussed. The similarity between the Preisach hysteresis model and RBF networks as well as the reasonings of applying the Preisach model as RBF networks are given. The properties of memory formation of the Preisach model and the physical insights observed from wing rock phenomena are used in the design of dynamic RBF neural networks.

Chapter 5

Design of Dynamic Recurrent Neural Networks

In this chapter the concepts and the properties of the Preisach model will be used to design the dynamic RBF neural networks for controlling the wing rock motion. The RBF neural networks have been used widely for function approximation and applications such as pattern recognition, time series prediction by Poggio and Girosi [65] and adaptive control by Sanner and Slotine [66].

The original use of the RBF networks for function approximation was proposed by Powell [67]. The method is further refined by reducing the number of neurons by Broomhead and Lowe [68]. The RBF networks being considered in this research consist of input layer, hidden layer and one output layer. The RBF networks is normally trained by hybrid learning rule namely unsupervised learning in the hidden layer and supervised learning in the outer layer. The hidden layer could have a fixed centre or the centers trained by self organized map or supervised learning. The weights of linear outer layer are normally updated using delta learning rule. The issue of designing an optimal networks and the learning algorithm of the RBF networks have been studied by various researchers.

In [69] Moody and Darken proposed a hybrid algorithm where the number of hidden units are fixed and the centres are trained by k mean clustering while supervised learning using LMS (Least Mean Square) is employed for training the outer layer weights. Using the RBF networks to approximate non-linear function had also been studied by Chen et al. [70]-[72] where hybrid algorithm on learning is used for system identification.

Platt [73] proposed on-line sequential algorithm for Resource Allocating Networks (RAN) where hidden units are added based on the novelty of the new data and the weights in outer layer are updated using LMS. Novelty refers to *innovation* in adaptive filtering literatures and it is interpreted in this context that the input data is far away from the centres and the error between the system and estimated output is large. Kardirkamanathan et al. [74] and Kardirkamanathan [75] improved the RAN method by using the Extended Kalman Filter instead of LMS in outer layer network weights estimation. Their network is called RANEKF. Yingwei et al. [76] and [77] proposed a minimal radial basis function neural networks (RBFNN) with addition/pruning strategy to adjust neurons in the hidden layer and the Extended Kalman Filter is used for updating networks free parameters.

Karayiannis et al. [78] proposed a growing radial basis function (GRBF) networks in which the network grows by splitting one of the prototype at each growing cycle. A prototype constitutes a representation of feature space defined as if the response of RBF centered on these prototypes to the feature vectors from the same class are as similar as possible. Hybrid learning scheme is proposed whereby unsupervised learning algorithm is used for clustering. Learning vector quantization [48] employed in the algorithm is based on the fact that the weight vector is moved away from the input vector only when the current cluster of the winner in the competitive learning is incorrect. In the case of supervised learning, the scheme based on the minimization of class-conditional variance are used. The class-conditional variance measures the

similarity of the response of each RBF to feature vectors from the same class.

Based on the research carried out in [79] and the extension of the studies carried out by Platt [73], Yingwei [76]-[77] and Kardirkamanathan [74] and [75], the dynamic recurrent RBF controller (**DR-RBF**) is proposed. The proposed networks employ the ensemble average concept as the criteria in the network training and include the recurrent feature. The recurrent RBF networks employ two separate parameter adaptation schemes, the RBF parameters in centre and width are adjusted by the Extended Kalman Filter while the networks linear output parameters are adjusted based on the Lyapunov stability criteria. The adaptation of RBF parameters together with neurons addition/pruning strategy determine the optimum size of the networks while the outer layer adjusted weights are used in the control law computation

5.1 Sequential Neurons Growth

There are two separate RBF networks used in the design of DR-RBF. The response of one unit in the hidden layer where $\Theta_f(z)$, $\Theta_g(z)$ are p dimensional Gaussian function vectors whose ith elements are given below

$$\Theta_{f_i}(z(k)) = \exp(-\frac{1}{2\sigma_{fi}^2} \left\|\phi(k) - \mu_{f_i}(k)\right\|^2) \tag{5.1}$$

$$\Theta_{g_i}(z(k)) = \exp(-\frac{1}{2\sigma_{g_i}^2} \left\|\phi(k) - \mu_{g_i}(k)\right\|^2) \tag{5.2}$$

where μ_{f_i} and μ_{g_i} are p dimensional vectors representing centres of ith Gaussian function and $\sigma_{f_i}^2$, $\sigma_{g_i}^2$ are variances representing the spread or the width of the Gaussian functions and $\|.\|$ is a Euclidean norm. The input vector $\phi(k)$ of the recurrent networks is defined in terms of current input $z(k)$, the state variable and previous RBF networks prediction, $\hat{y}\ (k-1)$ as below

$$\phi(k) = \begin{bmatrix} z(k) \\ \hat{y}\,(k-1) \end{bmatrix} \tag{5.3}$$

The output layer of each pairs of the BRF networks is a linear combination of weighted individual outputs from the networks given below.

$$\hat{f}\,(z(k), w_f) = f_o(z) + \sum_{i=1}^{K_f} w_{f_i}\Theta_{f_i}(z(k)) \tag{5.4}$$

$$\hat{g}\,(z(k), w_g) = g_o(z) + \sum_{i=1}^{K_g} w_{g_i}\Theta_{g_i}(z(k)) \tag{5.5}$$

and the networks output is

$$\hat{y}\,(k+1) = \hat{f}\,(z(k), w_f) + \hat{g}\,(z(k), w_g)u(k) \tag{5.6}$$

where K_f and K_g are total number of hidden units in the respective RBF networks.

The mechanism of information storage in the Preisach model is not localized in any particular cell, but some ensembles of the cells $\hat{\gamma}_{\alpha\beta}$ participating in the storage of the information. As a results, if some of the cells are destroyed, the stored information is still present. The idea applies to the cell replenishment without affecting the currently stored information. This concept is incorporated in the adjusting of the neurons in hidden layers by adding or pruning the neurons according to the specified criteria. The strategy is used to compute the distance between the input vector and all the centre values in the hidden units to form an ensemble average of the centres.

The network starts with zero hidden units initialized as $w_o = y_o$, as input-output observation data are received, the networks grow and information are stored in the memory and some of the stored information will be used when a new neurons are added. The decision to add a new neuron to the networks depends on the following two criteria.

(i)The first criterion is given as

$$\left\|\phi(k) - \mu_{fa}\right\| > \epsilon_n \tag{5.7}$$

$$\left\|\phi(k) - \mu_{ga}\right\| > \epsilon_n \tag{5.8}$$

where ϵ_n is a threshold value to be selected appropriately, $\phi(k)$ input vector and μ_{fa}, μ_{ga} are ensemble values for the f and g networks respectively.

(ii)The second criterion is given as

$$er(k) = \hat{y}(k) - y(k) > e_{\min} \tag{5.9}$$

where $er(k)$ is the error between the network output $\hat{y}(k)$ and the system output $y(k)$, $e_{\min}$ is a threshold value to be selected.

The first criterion states that the input values must be far away from the ensemble average of the centres or the distance between input and ensemble average must exceeds certain threshold, ϵ_n. The second criterion states that the error $er(k)$ between the network output $\hat{y}(k)$ and the system output $y(k)$ must be significant or the error must exceeds the threshold value, $e_{\min}$. If the two criteria are satisfied, a new neuron is added to the networks. The value $e_{\min}$ is chosen to represent the desired accuracy of the networks approximated output and the choice of $e_{\min}$ will affect the size of the networks.

The distance ϵ_n represents the scale of resolution in the input space that the network is able to approximate at time instant k. Platt's RAN begins the learning of the networks by setting $\epsilon_n = \epsilon_{\max}$ which is the largest scale of interest, typically for the entire input space of nonzero probability density. The distance ϵ_n is let to shrink exponentially until it reaches the lower limit , $\epsilon_{\min}$ according to the following

$$\epsilon_n = \max\{\epsilon_{\max} \ \gamma^n \ \epsilon_{\min}\} \tag{5.10}$$

where $0 < \gamma < 1$ is a decay constant and n is the number of samples or observations.. At the beginning, the system performs a coarse approximation with large width then refines the approximation with the smaller widths. The growth pattern depends on γ which influences the growth of the networks, and the values $e_{\min}$ and $\epsilon_{\min}$ determine the final size of the networks.

The variables μ_{fa}, μ_{ga} are ensemble averages of the centres of the hidden units based on the concept that all the neurons participate in the information storage. Ensembles averages of the centres are defined as below

$$\mu_{fa}(k) = \frac{1}{n}\sum_{i}(\phi(k) - \mu_f\ (k, \zeta_i)) \tag{5.11}$$

$$\mu_{ga}(k) = \frac{1}{n}\sum_{i}(\phi(k) - \mu_g\ (k, \zeta_i)) \tag{5.12}$$

where $\mu_f\ (k, \zeta_i)$ and $\mu_g\ (k, \zeta_i)$ are samples of respective centres, ζ_i is the element of the sample set. The assumption is made that if the stochastic process of $\mu_f\ (k, \zeta_i)$ and $\mu_g\ (k, \zeta_i)$ are ergodic, the ensemble averages are approximated by time averages.

If the conditions given in equations (5.7), (5.8) and (5.9) are met, new hidden neurons are added in respective networks according to the following assignments and their values are set to the stored information for which the two conditions has been met.

$$w_f\ (K_f + 1) = er(k) \tag{5.13}$$

$$w_g\ (K_g + 1) = er(k) \tag{5.14}$$

$$\mu_f\ (K_f + 1) = \phi(k) \tag{5.15}$$

$$\mu_g\ (K_g + 1) = \phi(k) \tag{5.16}$$

$$\sigma_f(K_f+1) = \kappa \left\| \phi(k) - \mu_{fa} \right\| \quad (5.17)$$

$$\sigma_g(K_g+1) = \kappa \left\| \phi(k) - \mu_{ga} \right\| \quad (5.18)$$

where $w_f(K_f+1)$ and $w_g(K_g+1)$ are the newly assigned outer layer weights of the respective networks, $\mu_f(K_f+1)$ and $\mu_g(K_g+1)$ are the newly assigned centres, K_f and K_g are the optimal number of neurons in the respective networks. The constant κ is an overlap factor which determines the overlap of the responses of the hidden units in the input space. Its selection depends on the networks size and desired accuracy and as κ increases, the responses of the unit overlap more and more. The variances, $\sigma_f(K_f+1)$, $\sigma_g(K_g+1)$ are set equal to the widths corresponding to the distance between the ensemble average of the centres in hidden units and the nth input vector.

5.1.1 Ensemble Learning

The networks RAN [73] and RBFNN [76] employ the nearest centre of the RBF's neurons to compute its distance between the input data and uses as one of the conditions for adding the new hidden unit. The μ_{nr} is a nearest centre of a hidden unit whose distance from the input data is the nearest among those of the all other hidden units. The disadvantage of employing such a scheme is given as the following :

. *All the weighting are placed on the single neuron of nearest centre, if there is an error made on the computation, the result does not reflect the rest of non participating neurons.*

The property of the ensemble memory storage described in the Preisach model has motivated the use of ensemble average of the distance to enhance the scheme of RAN and RBFNN. The nearest distance is replaced by the ensemble average distance from the input data to all the centres of the participating neurons. The effective ensemble should consist of a set of centres (data or networks) that are not only highly correct, but ones that make their errors on the different parts of the input space as well [80].

The concept of ensemble approach to neural networks learning and generalization is the current research topic and the most recent reference can be found in [81]

5.2 Training of Recurrent RBF Networks

The performance of the RBF networks depend on the number of factors such as the number of hidden units, shape and method of training. In control application, the learning strategy for the RBF functions can be classified as below.

(i) Fixed centres placed in regular grid and the number of neurons are predetermined and the outer weights are updated by LMS (Least Mean Square) or RLS (Recursive Least Square) algorithms. The learning is carried out in the supervised manner based on the target, a set point. The number of neurons is normally determined based on the prior knowledge. In general, the larger the number of neurons chosen the larger the span is over the input space.

(ii) Fixed number of neurons with centers adjusted by k means clustering in unsupervised learning scheme. The k means clustering algorithm provides a simple mechanism for minimizing the sum of squared errors with k clusters, with each cluster consisting of a set of N samples x_1, x_2, ...x_N that are similar to each other.

5.2.1 Supervised Training of the RBF Networks

When the neurons growth criteria as described earlier are not met, the centres and widths of the hidden neurons of the respective BBF networks are adjusted according to the Extended Kalman Filter (EKF) algorithm as proposed in [74]. Extended Kalman Filter is preferred for estimation of the nonlinear terms in the networks parameters and the method had been employed by researchers Willaims [82], Elanayar [83] and Behera [84]. The EKF estimates the hidden neuron parameters for each separate pairs of the respective RBF networks. For the updating of RBF's centers and width,

the following modified updating law in the Extended Kalman Filter is proposed for parameters ϖ_f , and ϖ_g.

$$\begin{bmatrix} \varpi_f(k) \\ \varpi_g(k) \end{bmatrix} = \begin{bmatrix} \varpi_f(k-1) \\ \varpi_g(k-1) \end{bmatrix} + k_a(k) \begin{bmatrix} er(k) \\ u(k)er(k) \end{bmatrix} \tag{5.19}$$

$$er(k) = \hat{y}(k) - y(k) \tag{5.20}$$

$$k_a(k) = \frac{P(k-1)\, a(k)}{R(k) + a^T(k)\, P(k-1)\, a(k)} \tag{5.21}$$

$$P(k) = [I - k_a(k)a^T(k)]\, P(k-1) + Q_o I \tag{5.22}$$

where the parameter vectors of $\varpi_f(k)$ and $\varpi_g(k)$ are defined for $f(z(k))$ and $g(z(k))$ as below

$$\varpi_f(k) = [\mu_f^T(1), \sigma_f(1), ... \mu_f^T(K_f), \sigma_f(K_f)] \tag{5.23}$$

$$\varpi_g(k) = [\mu_g^T(1), \sigma_g(1), ..., \mu_g^T(K_g), \sigma_g(K_g)] \tag{5.24}$$

The vector $a(k) = \nabla_{\varpi} f(z(k))$ is the gradient of the functions $f(z(k))$ and $g(z(k))$ with respect to the parameters vectors ϖ_f and ϖ_g evaluated at $\varpi_f(k-1)$ and $\varpi_g(k-1)$. Hence,

$$a(k) = \nabla_{\varpi} f(z(k)) = [a_f(k)\ ,\ a_g(k)] \tag{5.25}$$

$$\begin{aligned} a_f(k) = {} & [1, \Theta_{f1}\phi(k), ...\Theta_{fK_f}\phi(k), \\ & \Theta_{f1}\phi(k)\frac{2w_{f1}}{\sigma_{f1}^2}(\phi(k) - \mu_{f1})^T, ... \\ & \Theta_{fK_f}\phi(k)\frac{2w_{fK_f}}{\sigma_{fK_f}^2}(\phi(k) - \mu_{fK_f})^T]^T \end{aligned} \tag{5.26}$$

$$a_g(k) = [1, \Theta_{g1}\phi(k), ...\Theta_{gK_g}\phi(k),$$

$$\Theta_{g1}\phi(k)\frac{2w_{g1}}{\sigma_{g1}^2}(\phi(k)-\mu_{g1})^T,....$$
$$\Theta_{gK_g}\phi(k)\frac{2w_{gK_g}}{\sigma_{gK_g}^2}(\phi(k)-\mu_{gK_g})^T]^T \tag{5.27}$$

The adjustment of parameter vectors in terms of centres and widths of the RBF functions are given in equation (5.19). The EKF algorithm obtains the posterior estimates of $\varpi_f(k)$ and $\varpi_g(k)$ from the prior estimates of $\varpi_f(k-1)$ and $\varpi_g(k-1)$ and their prior covariance estimate $P(k-1)$ where $k_a(k)$ is the Kalman gain vector, $er(k)$ is the error between the RBF networks and plant outputs, $P(k)$ is a error covariance matrix, I is a identity matrix and $R(k)$ is a variance of the measurement noise. The parameter Q_o is a scalar determining the random walk in the direction of gradient vector. The $P(k)$ matrix is a $N \times N$ positive definite matrix as given below where N is the total number of parameters to be adjusted.

$$P(k) = \begin{bmatrix} P(k-1) & 0 \\ 0 & P_oI \end{bmatrix} \tag{5.28}$$

When new hidden unit is added the dimensionality of $P(k)$ increases and new rows and columns are initialized. P_o is an estimate of the uncertainty in the initial values assigned to the parameters which in this algorithm is also the variance of the input and output of the networks. The dimension of the identity matrix I is equal to the number of new parameters introduced by adding a new hidden unit.

The updating of non linear parameters, the respective RBF's widths σ_f^2 and σ_g^2 as well as RBF's centres μ_f and μ_g is carried out during the approximation of the nonlinear function. The objective function is to minimize the error between neural computed output and system output in order to yield the optimal networks size. The

linear parameters are updated according to the following updating law.

$$\theta(k+1) = \theta(k) - \frac{\eta}{r_k} e(k+1) J(k) \tag{5.29}$$

where $\theta(k)$ is the linear parameter vector of the outer layer, η is the learning rate chosen as "a *priori* "and the performance of the networks in terms of convergence depends on its selection, $e(k+1)$ is the error between estimated plant output and measured plant output. $J(k)$ is Jacobian matrix of $\frac{\partial \hat{f}}{w_f}$ and $\frac{\partial \hat{g}}{w_g}$ and $r_k = 1 + J(k)'J(k)$.

5.2.2 Pruning of Neurons

The criteria of pruning the superfluous hidden unit is based on the *wiping out property* of the Preisach model which states that some subsequent events may erase the information previously stored in the memory. This erasing of memory occurs if only new input data makes a strong impact in terms of the significant increase of distance from the RBF's centre, characterized by larger input extremum than previous ones. On the contrary if no impact was made on the input signal, the change in output of the hidden unit remains insignificant. Unlike the dynamic networks method used in Kadirkamanathan [74] whenever the neuron is added there is no scheme to remove any redundant neuron, the dynamic recurrent network proposed in this research employs the similar strategy [76] for pruning the redundant neuron. The outputs of the respective hidden neurons are given in the following equations (5.30) and (5.31).

$$\Theta_f(z(k)) = \exp(-\frac{1}{2\sigma_f^2} \left\| \phi(k) - \mu_f \right\|^2) \tag{5.30}$$

$$\Theta_g(z(k)) = \exp(-\frac{1}{2\sigma_g^2} \left\| \phi(k) - \mu_g \right\|^2) \tag{5.31}$$

$$\left\| \Theta_f(z(k)) - \Theta_f(z(k-1)) \right\| < \varepsilon \tag{5.32}$$

$$\left\| \Theta_g(z(k)) - \Theta_g(z(k-1)) \right\| < \varepsilon \tag{5.33}$$

where ε is a threshold value. If the output of the ith hidden neuron between the kth and $(k-1)$th instants given in equations (5.32) and (5.33) is less than a threshold value for a consecutive observations M which represents the latest number of observations for calculating the root mean square values of the approximated error defined as

$$e_{rms} = \sqrt{\frac{\sum_{i=n-(M-1)}^{n} (er(i))^2}{M}} \tag{5.34}$$

then the pruning of the ith hidden neurons begins and the dimensionality of $P(k)$ matrix in the EKF algorithm is then reduced. The threshold value ε is selected less than e_{rms} to have a maximal consecutive observations

In practice, hysteresis encountered in wing rock motion is not absolutely static in nature. The classical Preisach model does not account for dynamic properties of hysteresis nonlinearities such as fast input variation and changes in aerodynamic parameters under certain flight conditions. The hysteresis model predicts that the stored information is slowly and gradually erased in the presence of perturbation in terms of rapid input and output variations. To enhance the performance of the RBF networks and to overcome the limitation of the static hysteresis model, a recurrent feature is introduced in the networks to account for the temporal loss of information. By introducing feedback of the output signal through a time delay, the recurrent networks is given a memory and improve its performance by taking into consideration of the dynamic characteristics of the hysteresis model.

5.3 Summary of Dynamic Recurrent Neural Networks

The dynamic recurrent RBF network is described mathematically as follows :

. Initialize $w_o = y_o$, $\epsilon_n = \epsilon_{\max}$

. Compute the input vector $\phi(k)$ in terms of current input $z(k)$ and previous RBF network prediction $\hat{y}\ (k-1)$.

. Computer the distance between the input vector and the ensemble average of the centres in the hidden units $\|\phi(k) - \mu_{fa}\|$ and $\|\phi(k) - \mu_{ga}\|$

Verify if the following conditions are met :

$$\begin{aligned} \|\phi(k) - \mu_{fa}\| &> \epsilon_n \\ \|\phi(k) - \mu_{ga}\| &> \epsilon_n \\ er(k) &= \hat{y}\ (k) - y(k) > e_{\min} \end{aligned}$$

. Allocate new neuron according to equations (5.13)-(5.18).

. If the conditions in equations (5.7), (5.8) and (5.9) are not met, the networks parameters (centres and widths) are updated according to the Extended Kalman Filter algorithm. The outer layer weights of the networks are updated by the stability analysis for control law computation according to equation (5.29).

. If the impact of input has no significant effect on the output of the hidden neuron as given by conditions in equations (5.32) and (5.33) for M consecutive observations, the dimensionality of $P(n)$ in equation (5.28) is reduced by one and pruning of the hidden neurons begins.

5.4 Bench Marking of Dynamic Recurrent RBF Networks

In this section the performance of the developed dynamic RBF networks will be evaluated and comparison of the results will be made by carrying out simulations of

the networks which includes various features considered on the networks design.

5.4.1 Simulation 1 - Platt's RAN

The purpose of this simulation is to demonstrate the performance of the developed dynamic RBF algorithm for function approximation and the results will be served for comparisons when features are added in the design of the algorithm. The following 2 input 2 output periodic functions are selected to verify the performance of the developed algorithm.

$$x_1(k) = \cos(0.2 * k) \tag{5.35}$$

$$x_2(k) = \sin(0.1 * \pi * k) \tag{5.36}$$

$$y_1(k) = (3 * \cos(x_1(k)) + 2 * \sin(x_2(k)))/5 \tag{5.37}$$

$$y_2(k) = (5 * \sin(x_1(k)) + \cos(x_2(k)))/6 \tag{5.38}$$

For comparison purpose simulation is carried out based on the following criteria for adding neuron in the hidden layer using the criteria given by Platt [73].

$$\|x(k) - \mu_{nr}\| > \epsilon_n$$

$$er(k) = \hat{y}(k) - y(k) > e_{\min}$$

where $\|x(k) - \mu_{nr}\|$ is a Euclidean distance between the input vector $x(k)$ and the centre of the hidden unit (μ_{nr}) whose distance from $x(k)$ is the nearest among those of the hidden units, ϵ_n and $e_{\min}$ are threshold values and $er(k)$ is a error between the

given function output, $y(k)$ and neural computed output, $\hat{y}(k)$.

Figure 5.1 shows the inputs and outputs of the periodic functions. Constant disturbance is included in the system and based on some initial simulation runs, the parameters required in the simulation are chosen as below.

$\epsilon_{\max} = 0.4$, $e_{\min} = 0.02$, $\epsilon_n = 0.2$, $e_{rms} = 0.2$, $\kappa = 0.85$, $R_n = 1.0$, $Q = 0.002$, $P_o = 1.0$,

The algorithm employes the Extended Kalman Filter for adjusting the RBF networks parameters. When applying the given inputs to the dynamic RBF networks the neural computed outputs are shown in Figure 5.2. The results indicate that for output y_1, error between the given system output and neural computed output is less than the case of output y_2. In this simulation 31 neurons in the hidden unit are required to perform the function approximation for a given number of samples. The evolution of the growth of RBF hidden unit (neurons) is shown in Figure 5.3 while the distribution of centres and widths of the hidden units are shown in Figure 5.4.

5.4.2 Simulation 2 - Ensemble Average Learning

The goal of simulation 2 is to demonstrate the improvement of performance over simulation 1 by including the concept from the Preisach hysteresis model that ensembles of the cells $\hat{\gamma}_{\alpha\beta}$ participate in the storage of information. In this simulation, instead of using the distance between the nearest centre from the input vector, the distance between the input vector and the ensemble average of the distance is computed. The following criteria is employed for determining the addition of neurons during the identification phase.

$$\begin{aligned} \|x(k) - \mu_a\| &> \epsilon_n \\ er(k) &= \hat{y}(k) - y(k) > e_{\min} \end{aligned}$$

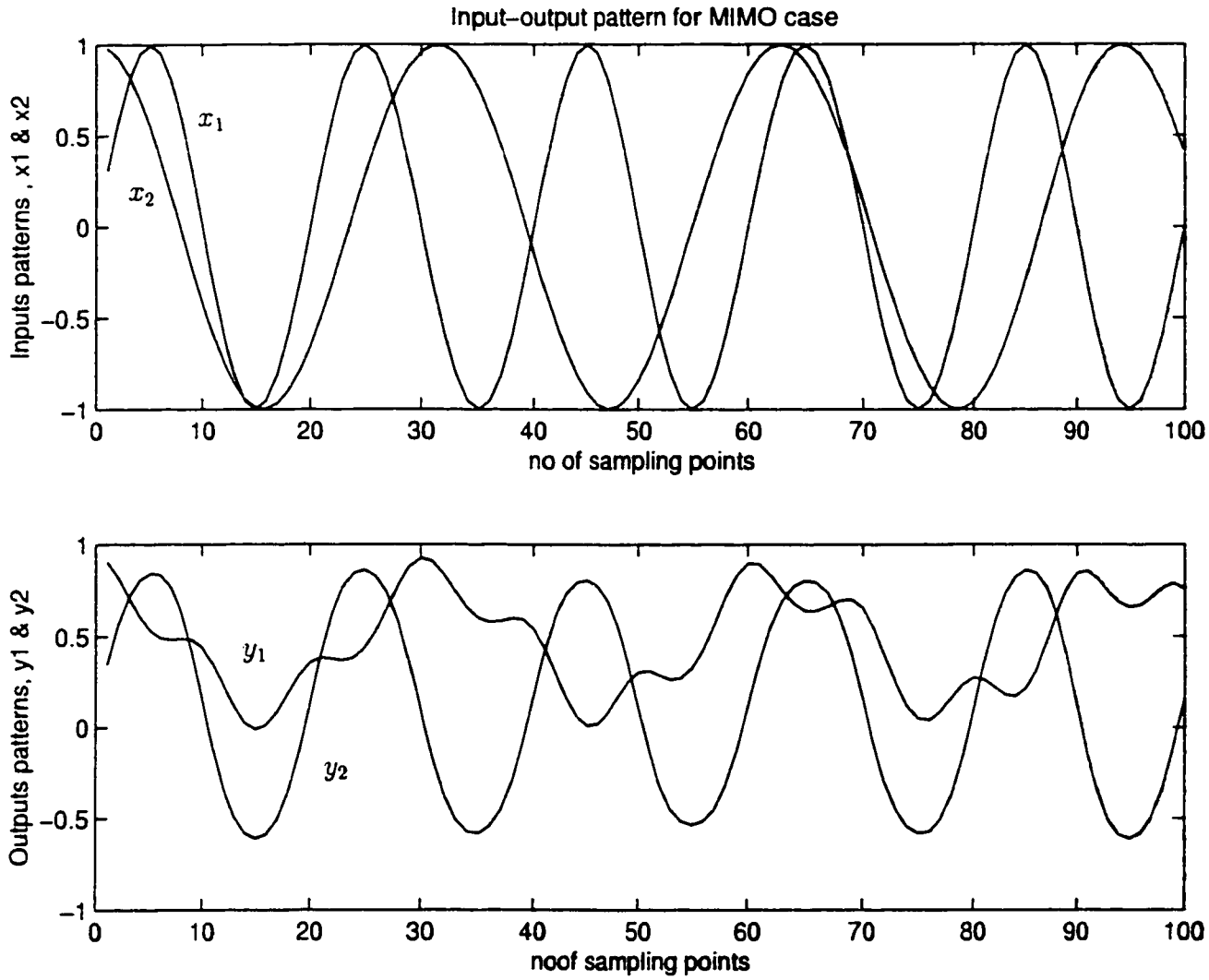

Figure 5.1: Reference system input and outputs

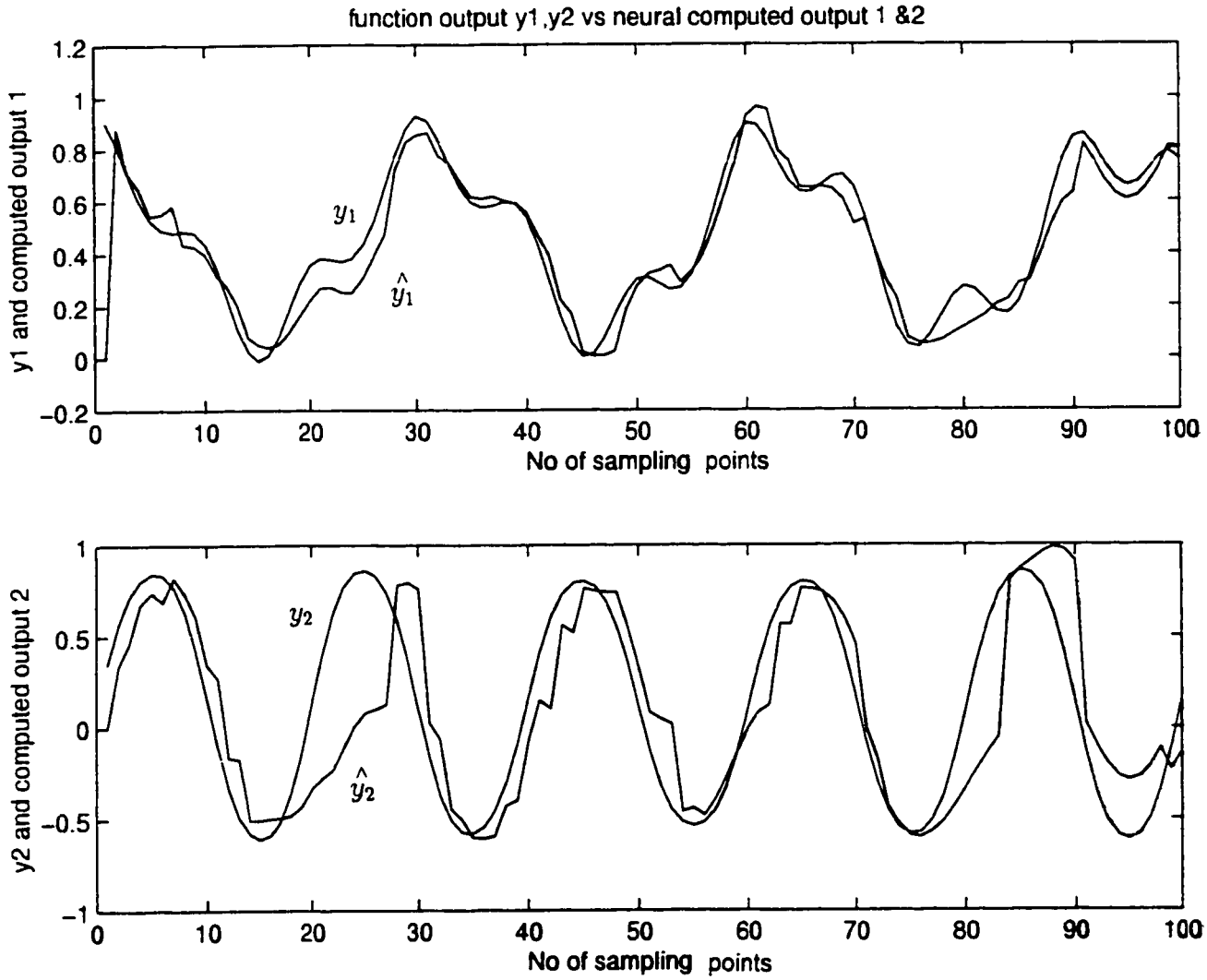

Figure 5.2: Comparison of System and neural computed outputs

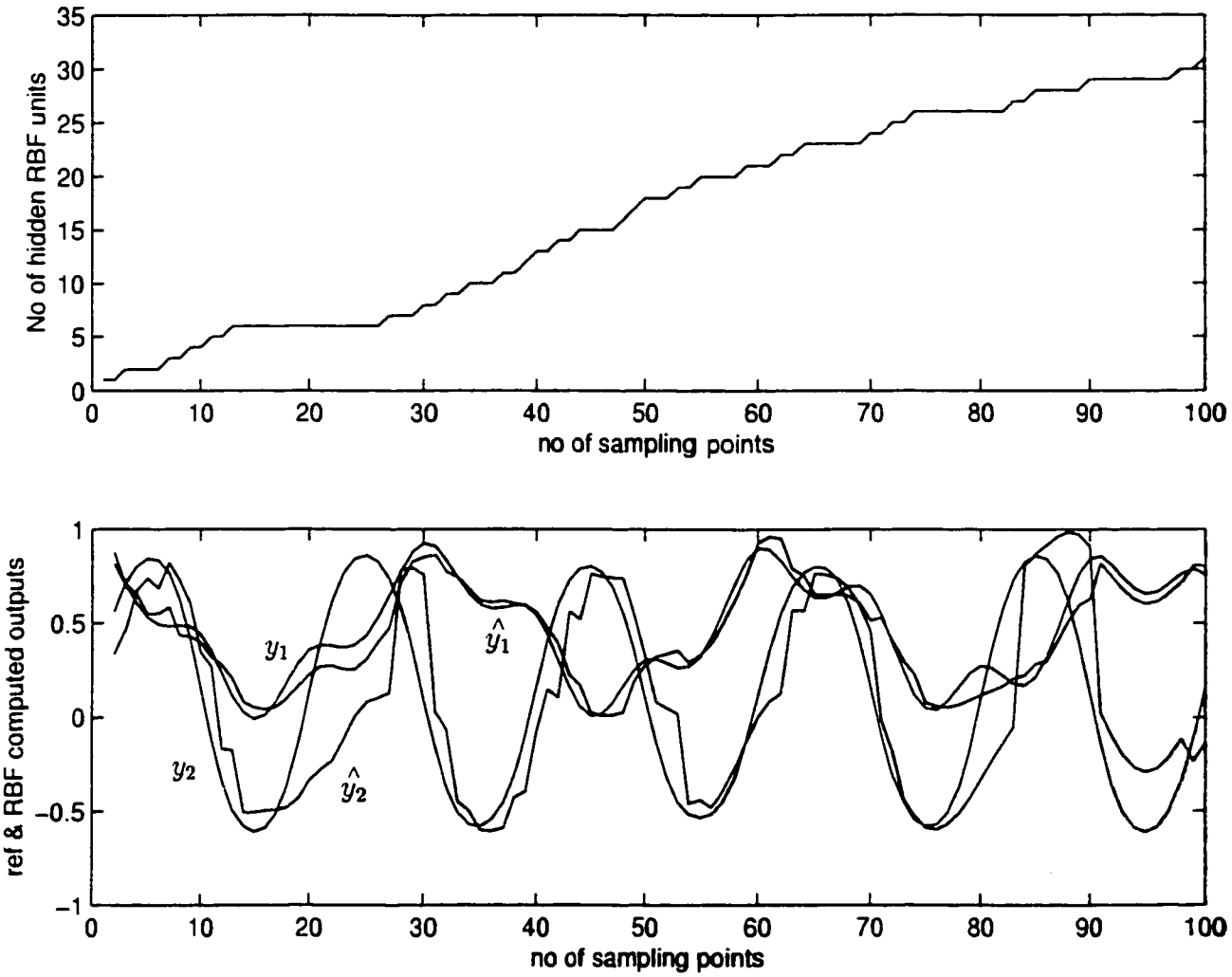

Figure 5.3: Evolution of hidden units & ref and neural computed output

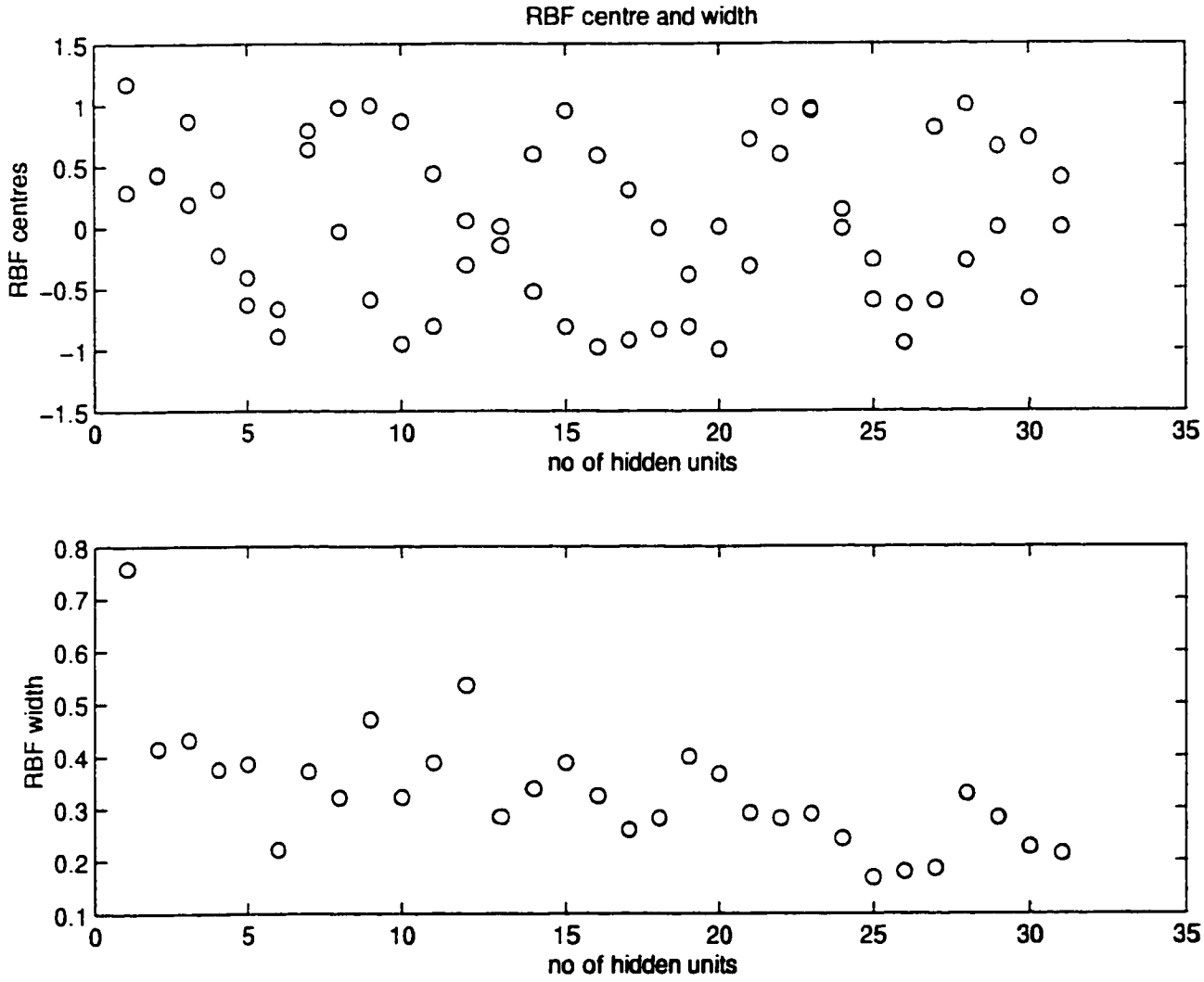

Figure 5.4: Distributoion of RBF centres and widths

$$\mu_a = \frac{1}{n}\sum_i (x(k) - \mu(k, \xi_i))$$

where μ_a is the ensemble average of the distance between the input vector and the centres, n is the total number of samples, $\mu(k, \xi_i)$ are samples of respective centres. Constant disturbance is included in the system for comparison purpose and the parameters required in the simulation are chosen as below.

$e_{\min} = 0.02$, $\epsilon_n = 0.2$, $\epsilon_{\max} = 0.4$, $e_{rms} = 0.2$, $\kappa = 0.85$, $R_n = 1.0$, $Q = 0.002$, $P_o = 1.0$.

Figure 5.5 shows the results of the outputs from the given system and the neural computed outputs based on the concept that the ensemble average of the distance between the input vector and respective centres is used in the algorithm. The Extended Kalman Filter (EKF) is employed for adjusting the RBF parameters. The results indicates an improvement over the previous of simulation shown in Figure 5.2 without using the concept of ensemble average of neurons participation. The number of hidden units required has increased to 55 as shown in Figure 5.6 as compared to 31 in the previous simulation. The distribution of centres and widths are given in Figure 5.7 and the ensemble average of the distance between input vector and the centres of the neurons as well as RBF function outputs are shown in Figure 5.8

The algorithm is sensitive to the selection of proper parameters values, the threshold values of $\epsilon_{\max}$, ϵ_n, $e_{\min}$ and e_{rms} will influence the growth rate of neuron, the number of final RBF units and the approximation error. The simulation for comparing RAN and ensemble average strategy are repeated with the following selected parameters.

$\epsilon_{\max} = 0.3$, $e_{\min} = 0.02$, $\epsilon_n = 0.2$, $e_{rms} = 0.2$, $\kappa = 0.85$, $R_n = 1.0$, $Q = 0.002$, $P_o = 1.0$

The results given in Figure 5.9 for the case of ensemble average show an improvement over the results given in Figure 5.5 and the algorithm selects 65 hidden units.

For the case of RAN, the results given in Figure 5.10 show little improvement over the previous simulation given in Figure 5.2 and 50 neurons are selected. The evolution of neuron growth for RAN and ensemble average strategy is shown in Figure 5.11.

Figures 5.5 and 5.10 compare the performance of RAN and ensemble networks for the same order of magnitude of neurons in the networks, around 50, the result in Figure 5.5 shows that ensemble average has a better performance over RAN given in Figure 5.10.

5.4.3 Simulation 3 - Recurrent Networks

In this simulation, the purpose is to verify the performance of the algorithm by introducing the recurrent signal from the neural computed output and comparing the performance over the two previous simulations.

$$\begin{aligned} x_1(k) &= \cos(0.2 * k) \\ x_2(k) &= \sin(0.1 * \pi * k) \end{aligned}$$

$$x_3(k) = \hat{y}\ (k-1) \tag{5.39}$$

where $\hat{y}\ (k-1)$ is the feedback from neural computed output. The input vector is defined as below

$$\phi(k) = \begin{bmatrix} x_1(k) \\ x_2(k) \\ x_3(k) \end{bmatrix}$$

and the neuron adding criteria and ensemble average of the distance between the input vector and the centres are given below.

$$\|\phi(k) - \mu_a\|$$

$$\mu_a = \frac{1}{n}\sum_i (\phi(k) - \mu(k, \xi_i))$$

The parameters used in the simulation are :

$\epsilon_{\max} = 0.4$, $e_{\min} = 0.02$, $\epsilon_n = 0.2$, $e_{rms} = 0.2$, $\kappa = 0.85$, $R_n = 1.0$, $Q = 0.002$, $P_o = 1.0$

Figure 5.12 shows the results of the neural computed outputs versus given system outputs. Comparing to the results in Figure 5.5 without the recurrent feature, the improvement over y_2, is more noticeable than y_1. The number of hidden units require is increased towards 70 as shown in Figures 5.13. Simulation is repeated with 250 sampling points, the results indicate the required number of neurons level off at 72 as shown in Figure 5.14.

5.4.4 Simulation 4 - Recurrent with Noise

The objective of this simulation is to demonstrate that the recurrent feature of the RBF networks is capable of giving good performance in function approximation in the presence of disturbance. The conditions of this simulation are the same as in Simulation 3 with the exception that Gaussian white noise is included in the given functions. Figure 5.15 shows the a satisfactory approximation results between the outputs y_1 and y_2 versus the respective networks approximated outputs. However, the number of neurons required increases threefold. The simulation results shows that the recurrent feature as interpreted from the Preisach model is capable of handling of the dynamic characteristics of the model. The concept of the ensemble average used in computing the distance between the RBF centres and input vector will better represent the information storage. Figure 5.16 shows the distribution of distances to

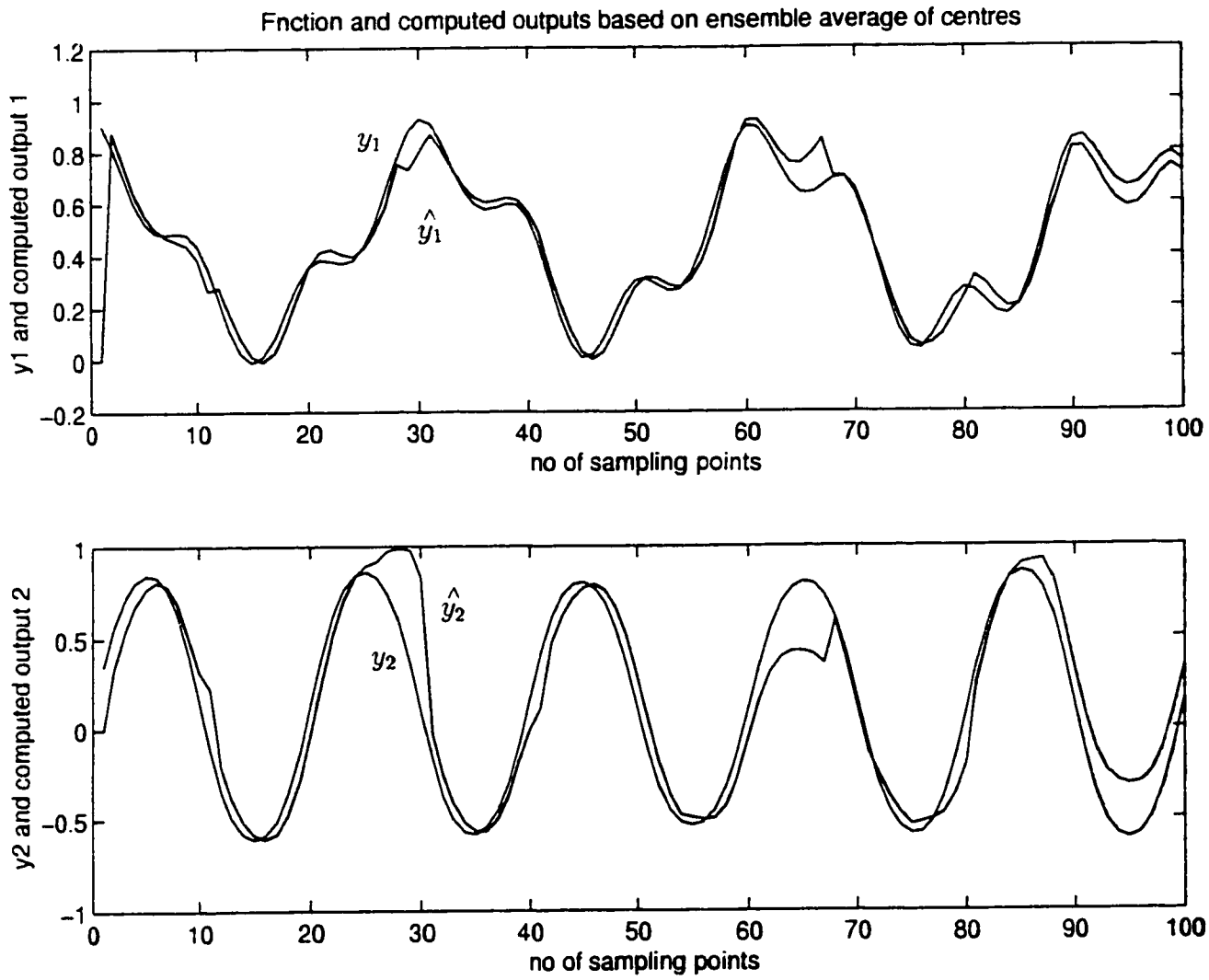

Figure 5.5: Function and computed outputs based on ensemble average

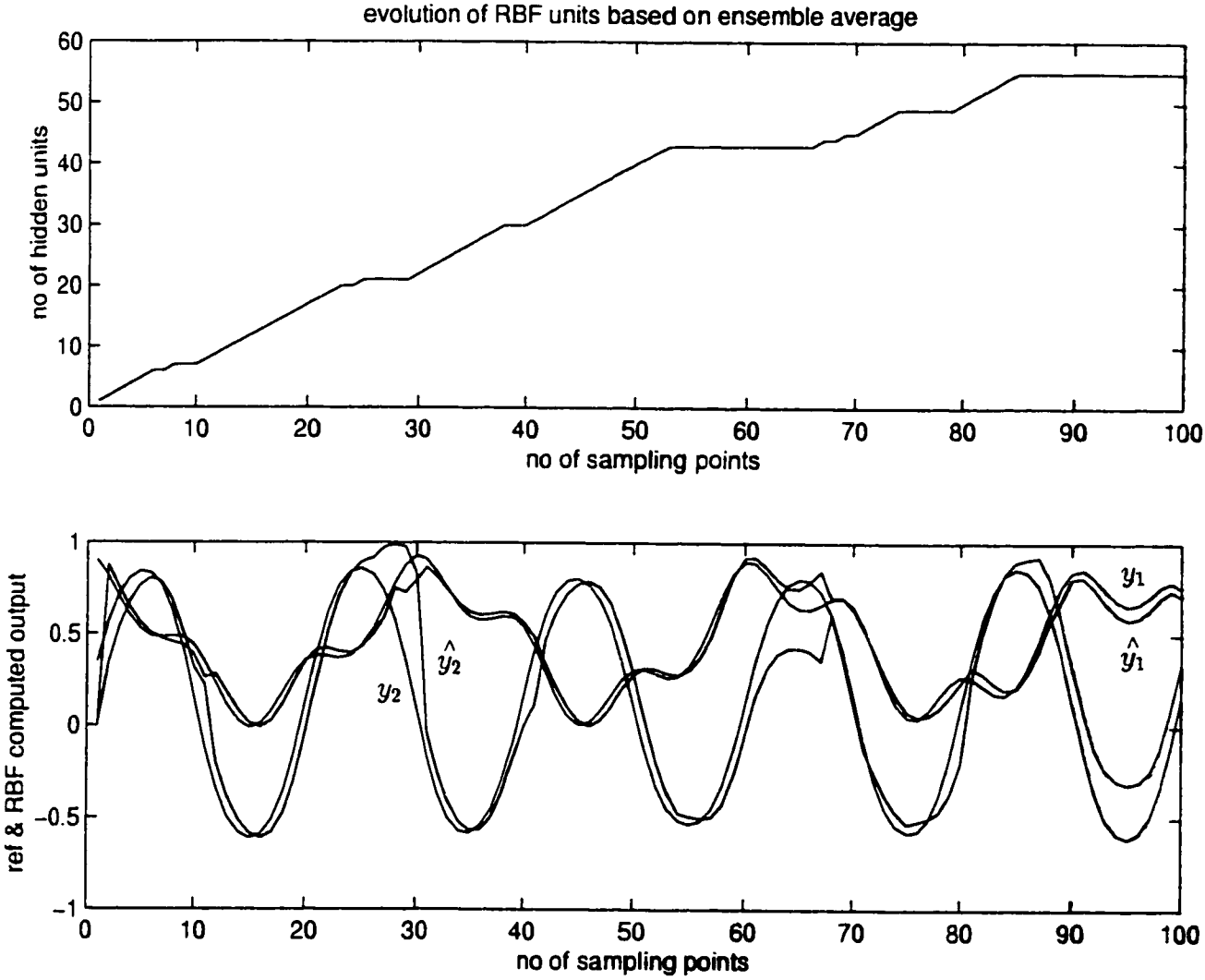

Figure 5.6: Evolution of RBF based on ensemble average

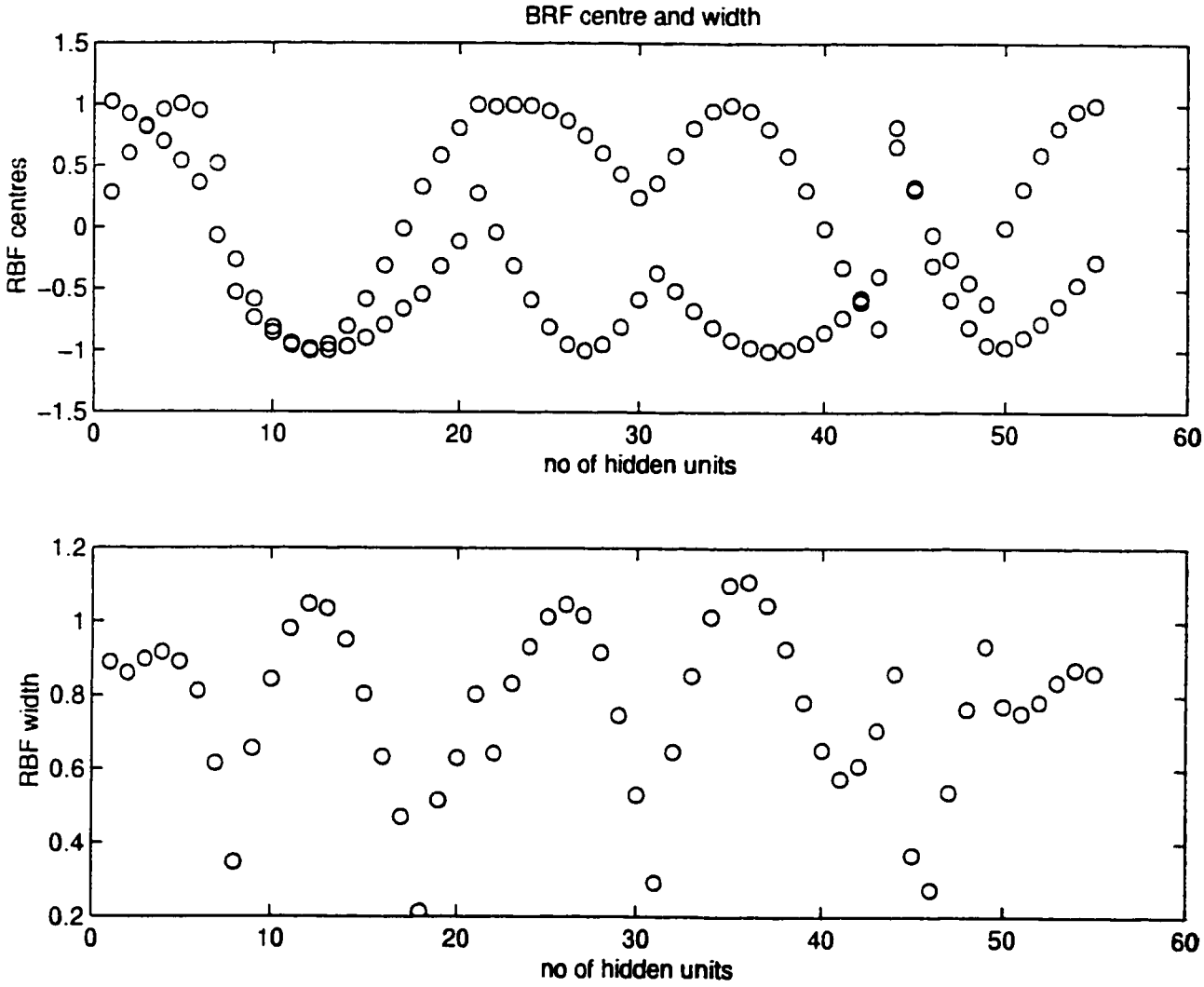

Figure 5.7: Distribution of RBF centres and widths

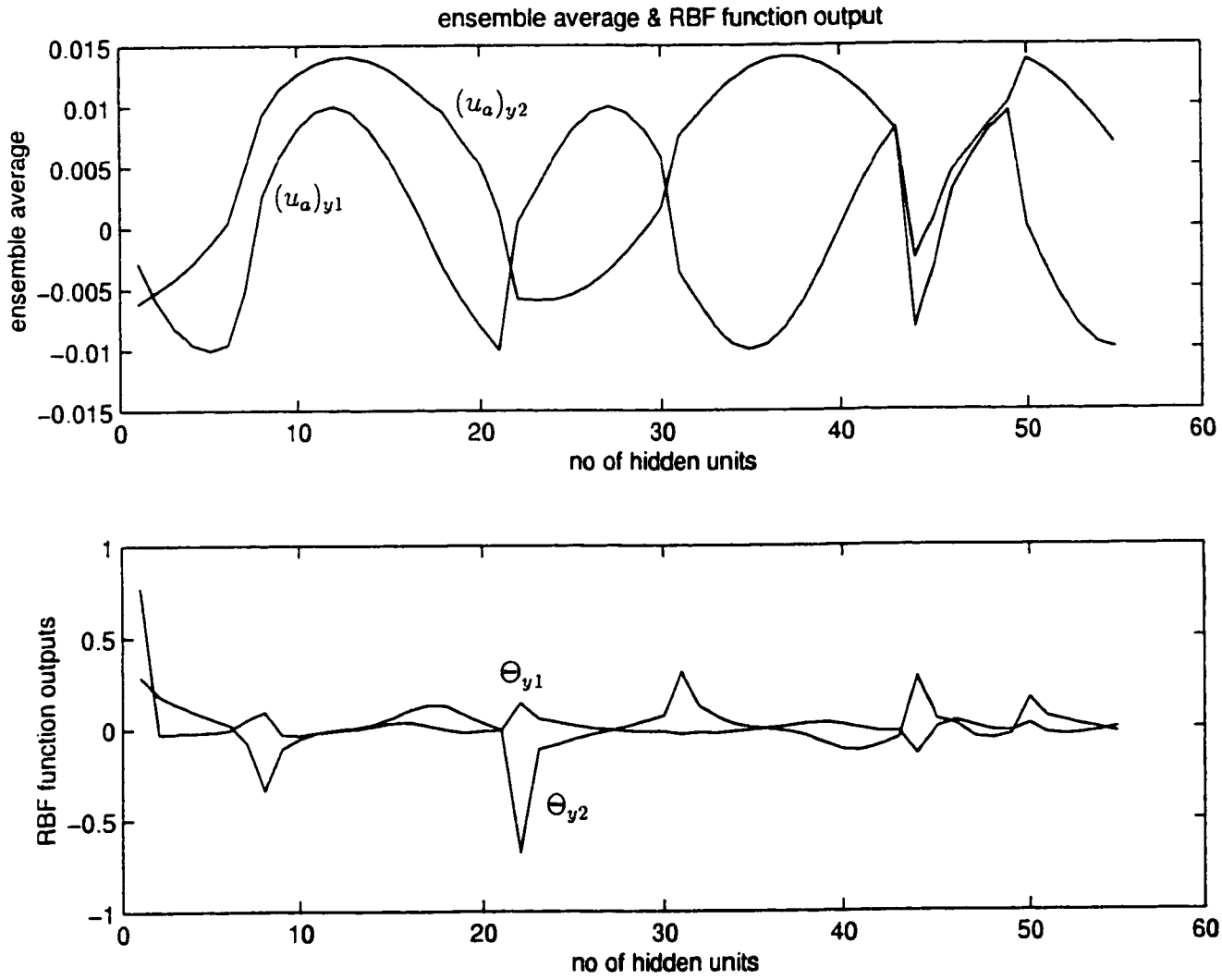

Figure 5.8: RBF function output and ensemble average

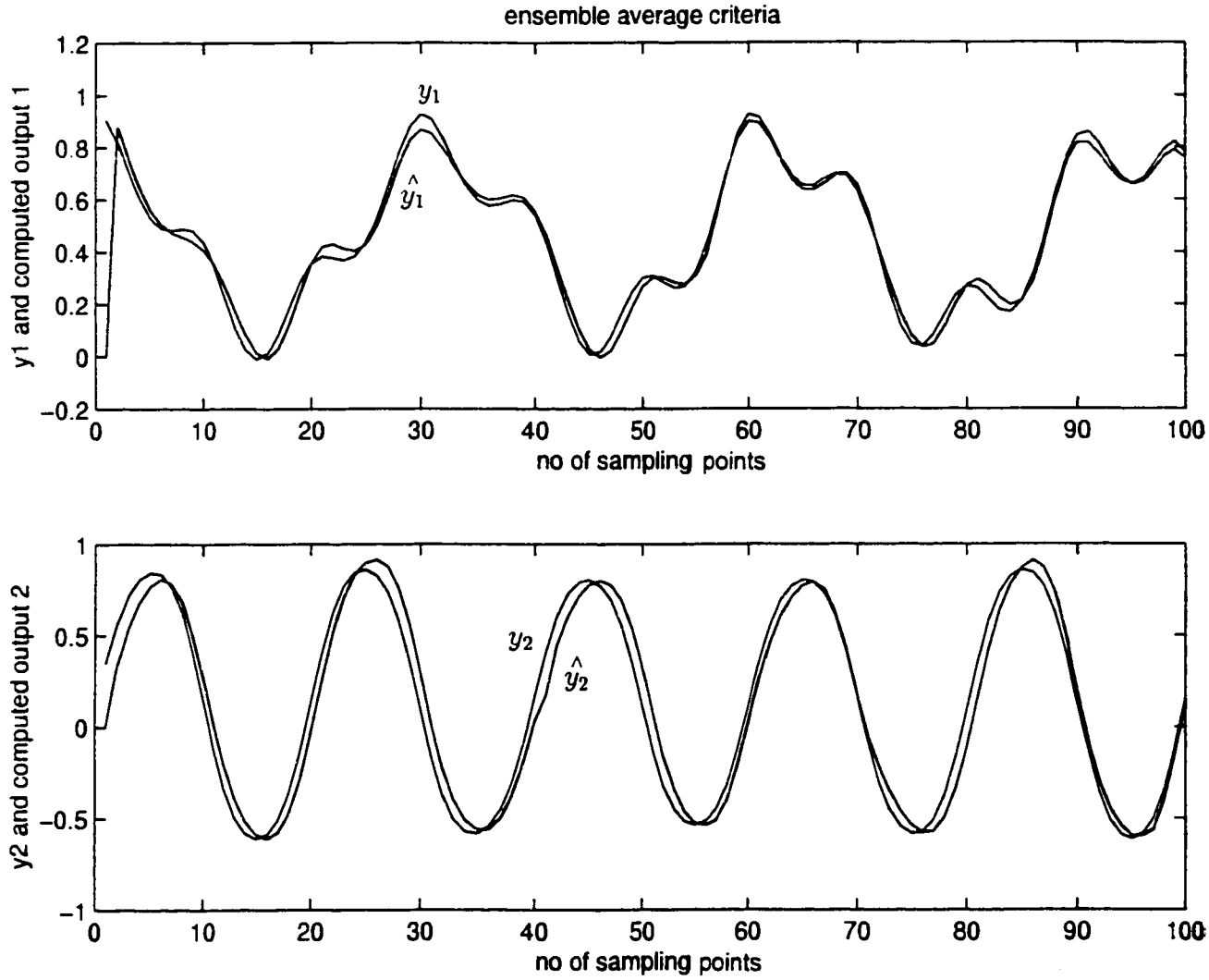

Figure 5.9: Output y1 and y2 with improved ensemble average

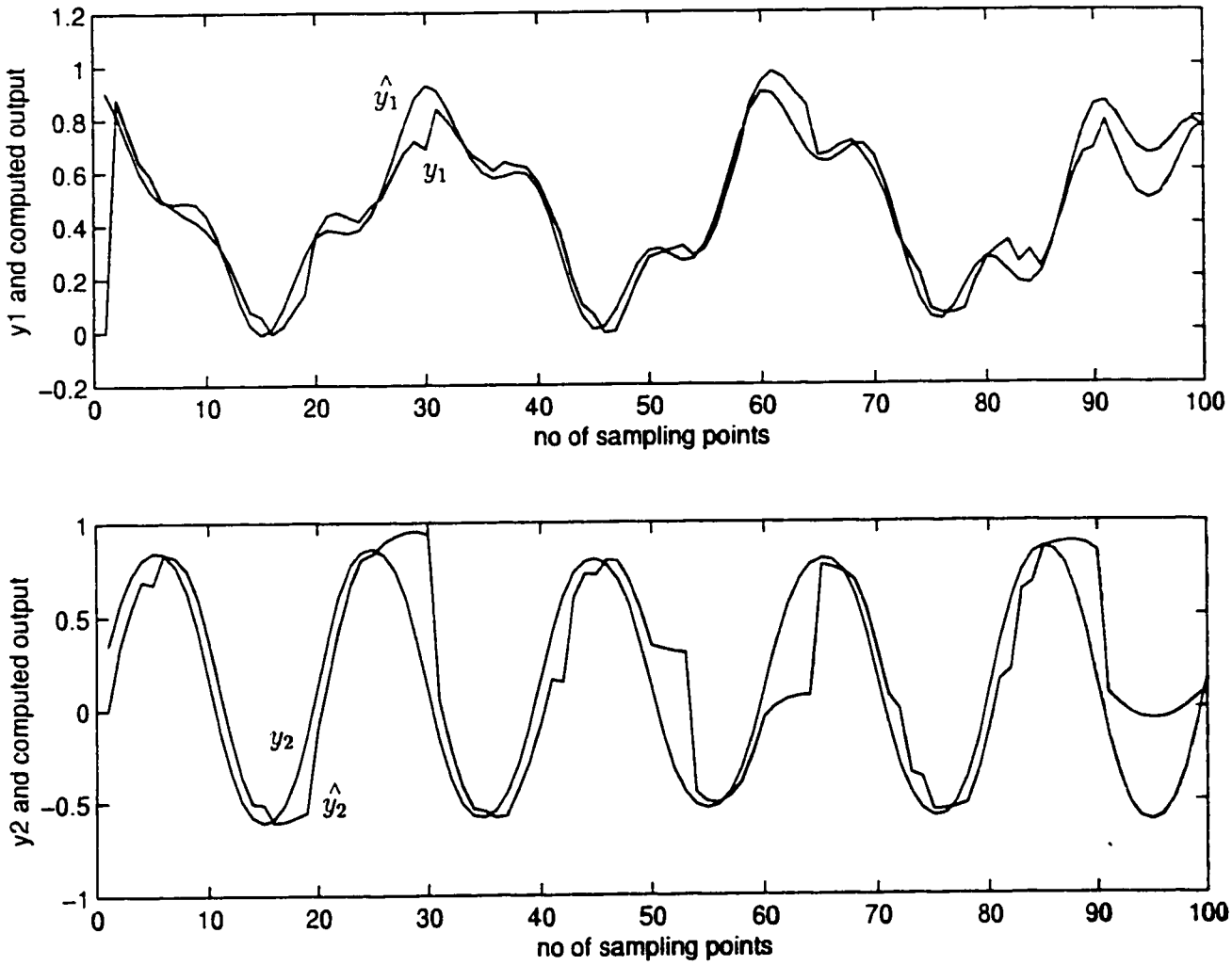

Figure 5.10: Outputs in y1 and y2 in Platt's RAN

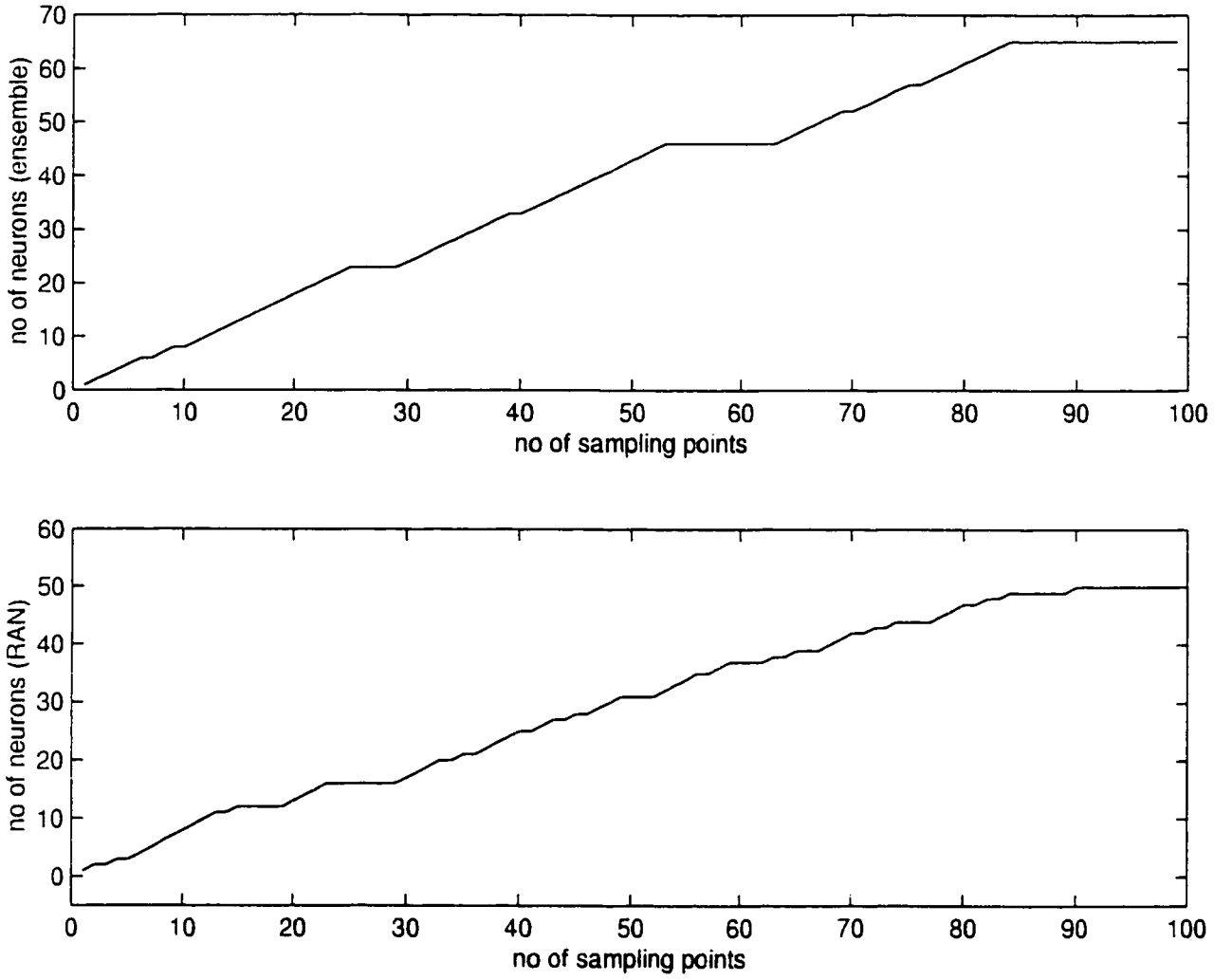

Figure 5.11: RBF unit of RAN and Ensemble

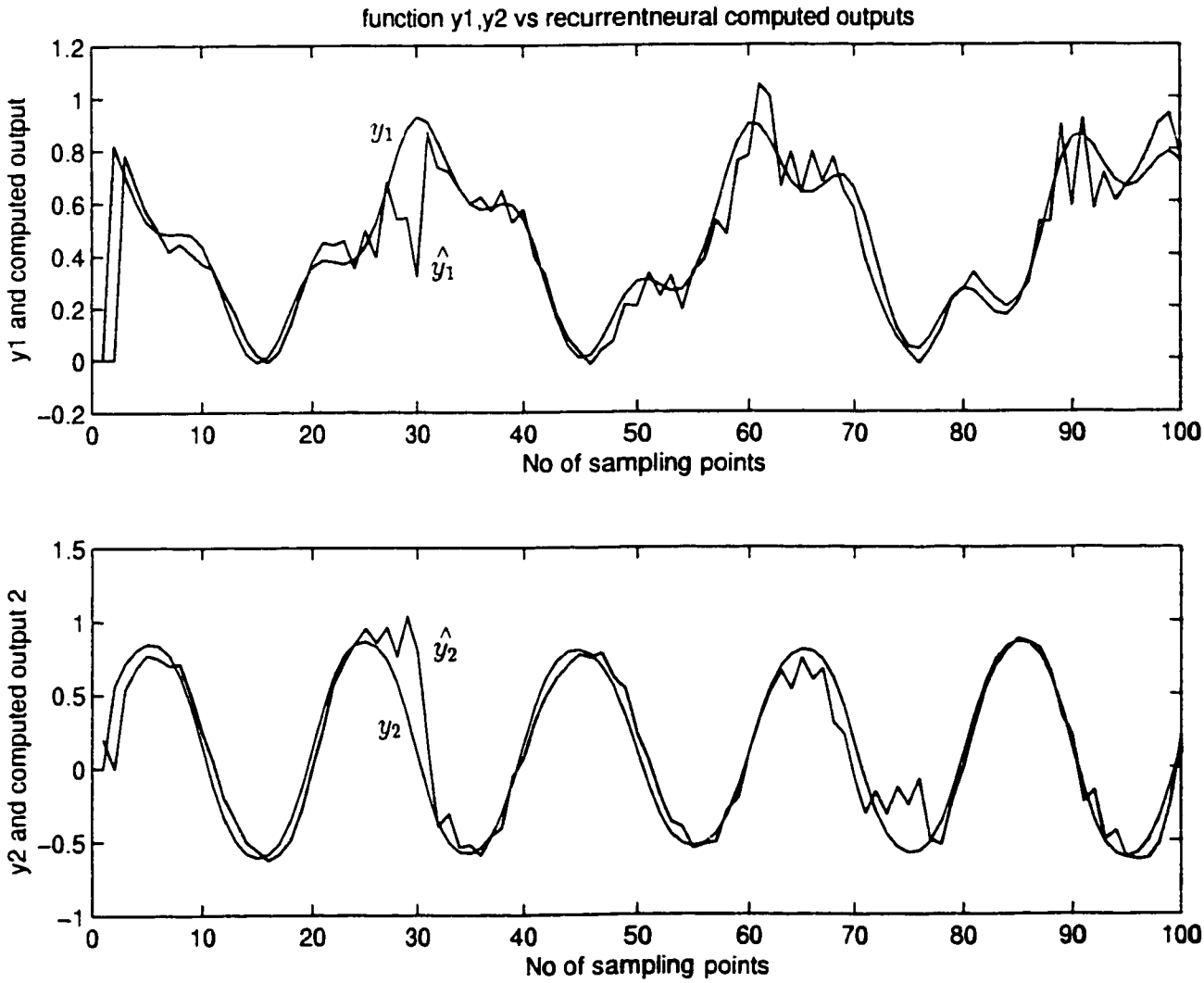

Figure 5.12: Functions Approximation by Recurrent RBF Networks

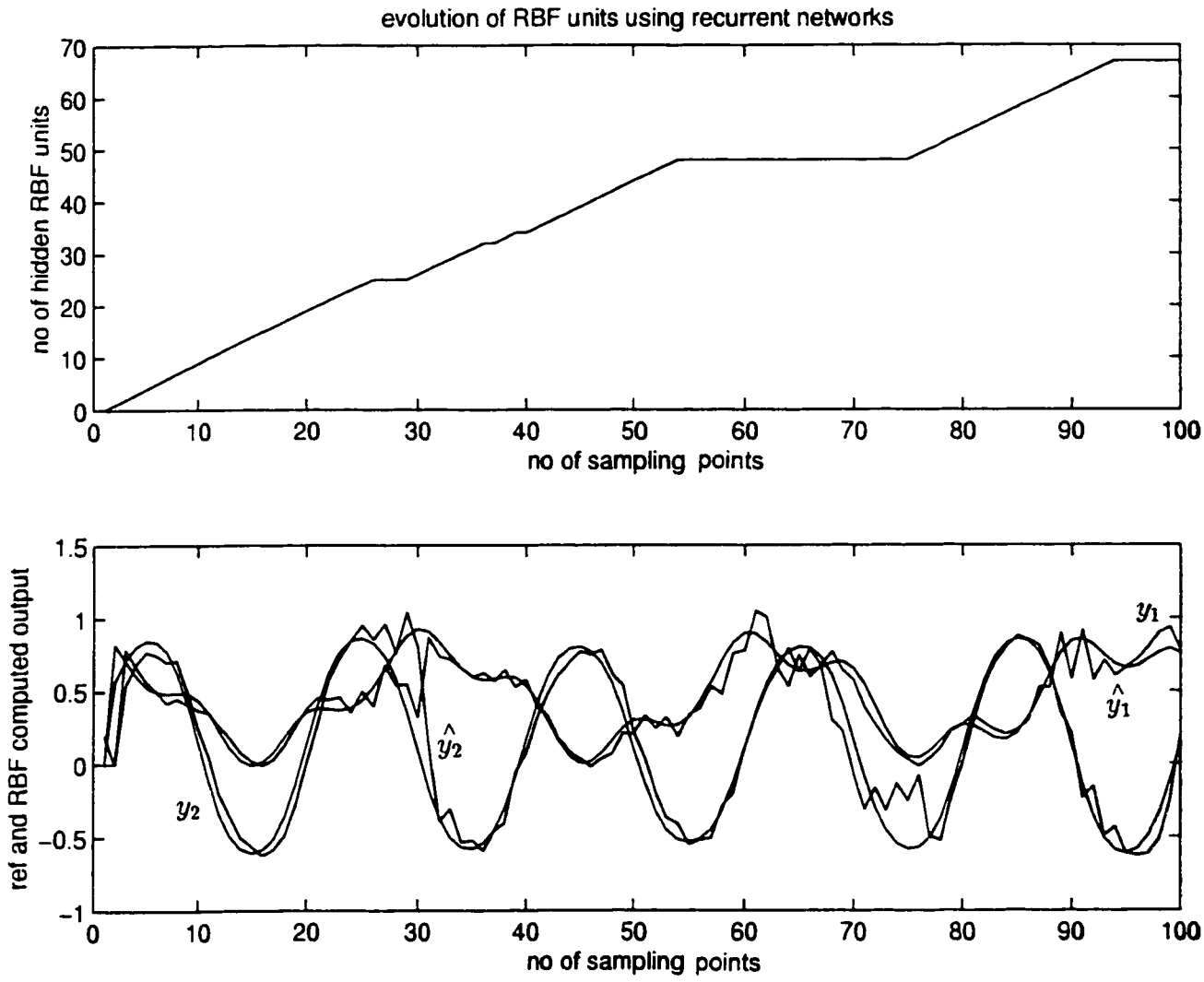

Figure 5.13: Evolution of RBF units using recurrent networks

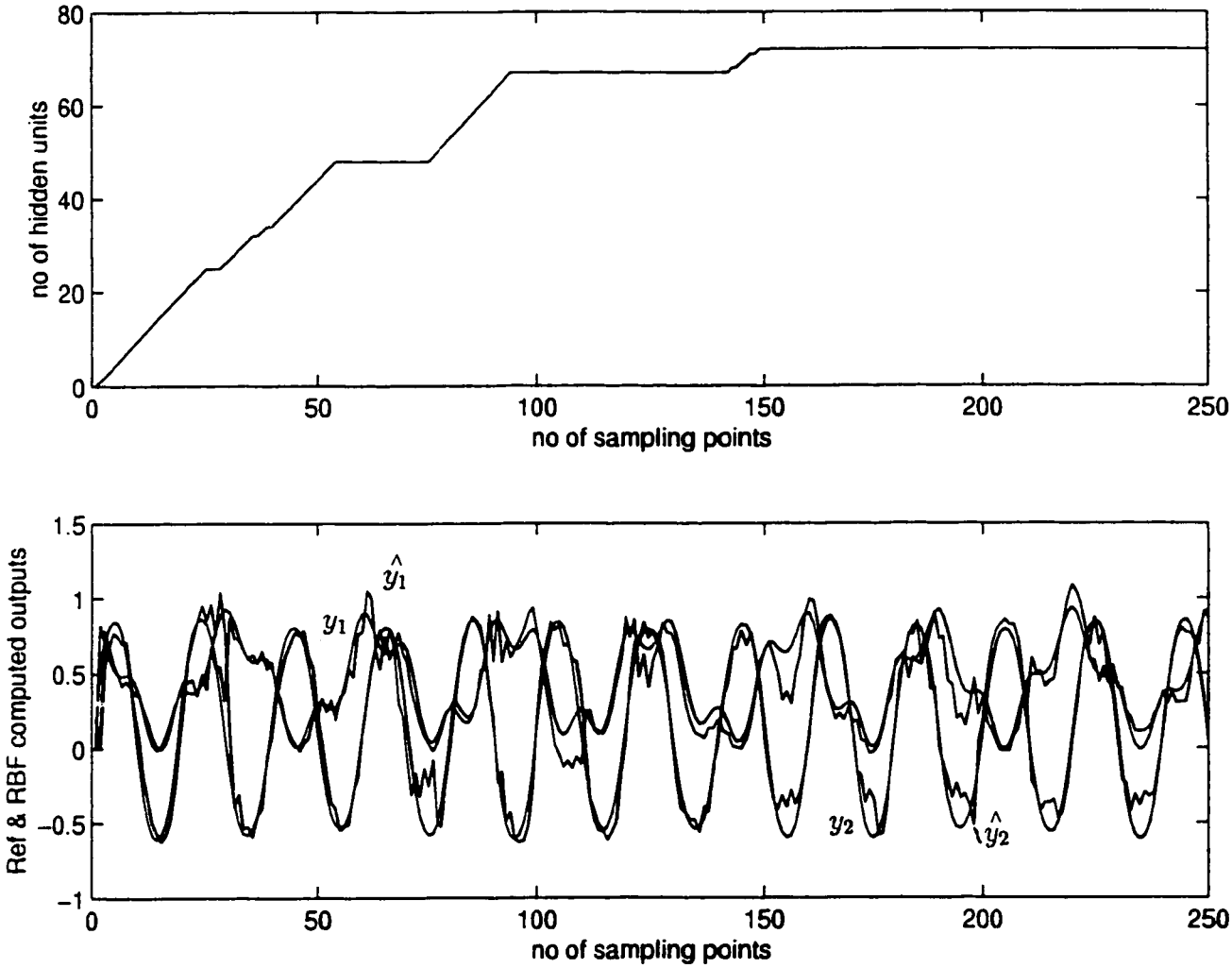

Figure 5.14: Evolution of RBF units based on ensemble average

RBF centres tends to be clustered between the range of $\pm$ 1 of minimum values. The RBF's widths distribution is shown in Figure 5.17.

5.5 Concluding Remarks

The application of the Preisach model as dynamic recurrent RBF networks was demonstrated through simulations. The memory formation properties in the hysteresis model is employed for the design of the RBF networks. Supervised training of the RBF's centres and widths are carried out using the Extended Kalman Filter while outer linear weights are adjusted based on the Lyapunov stability analysis. Bench marking of the developed networks were carried out for function approximation to compare the performance of various features included in the networks design. Networks with ensemble average shows a better performance than the RAN networks. With the presence of disturbance, the recurrent networks is capable of handling the dynamic natures of the disturbances.

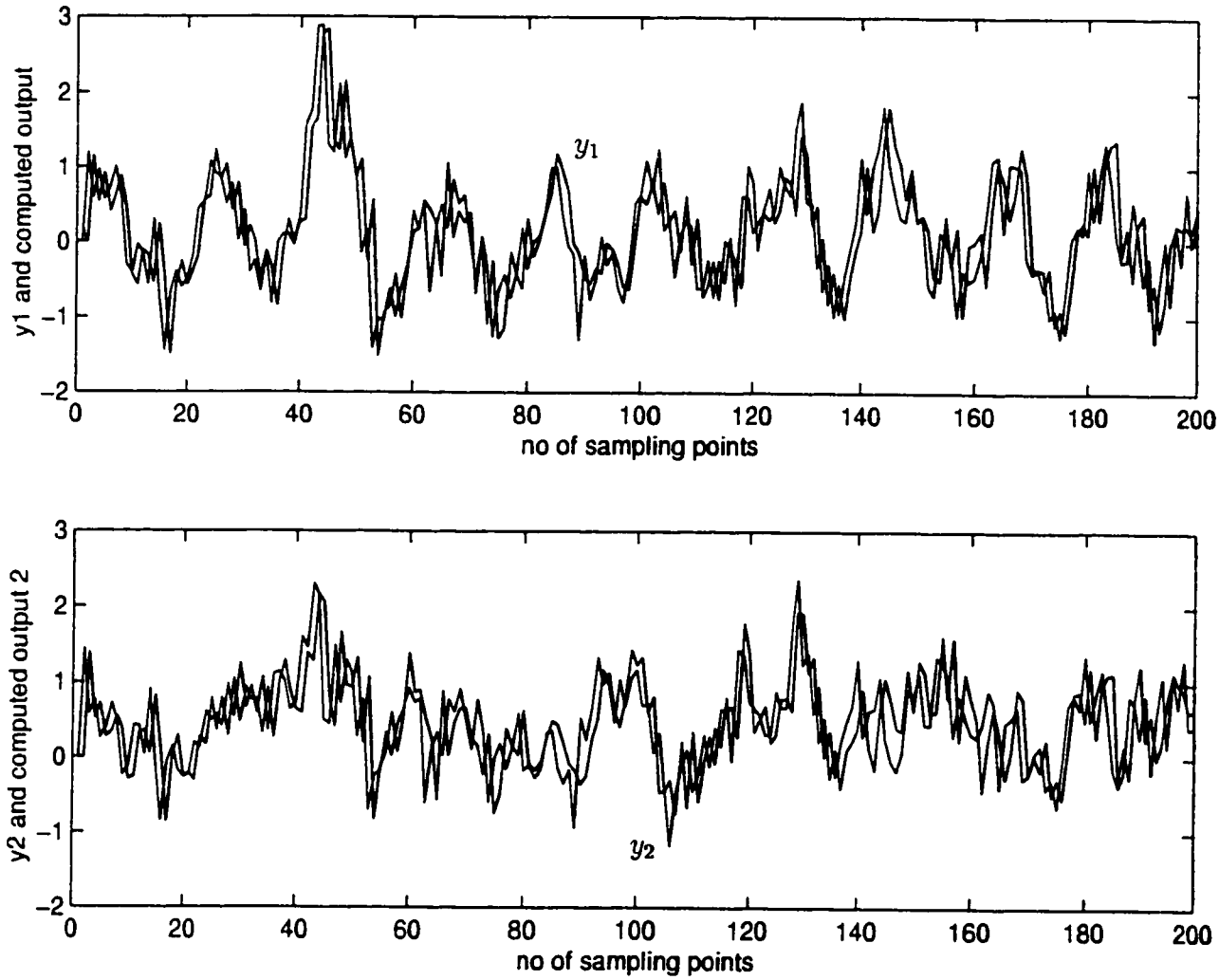

Figure 5.15: Function Approx. by Recurrent RBF with noise

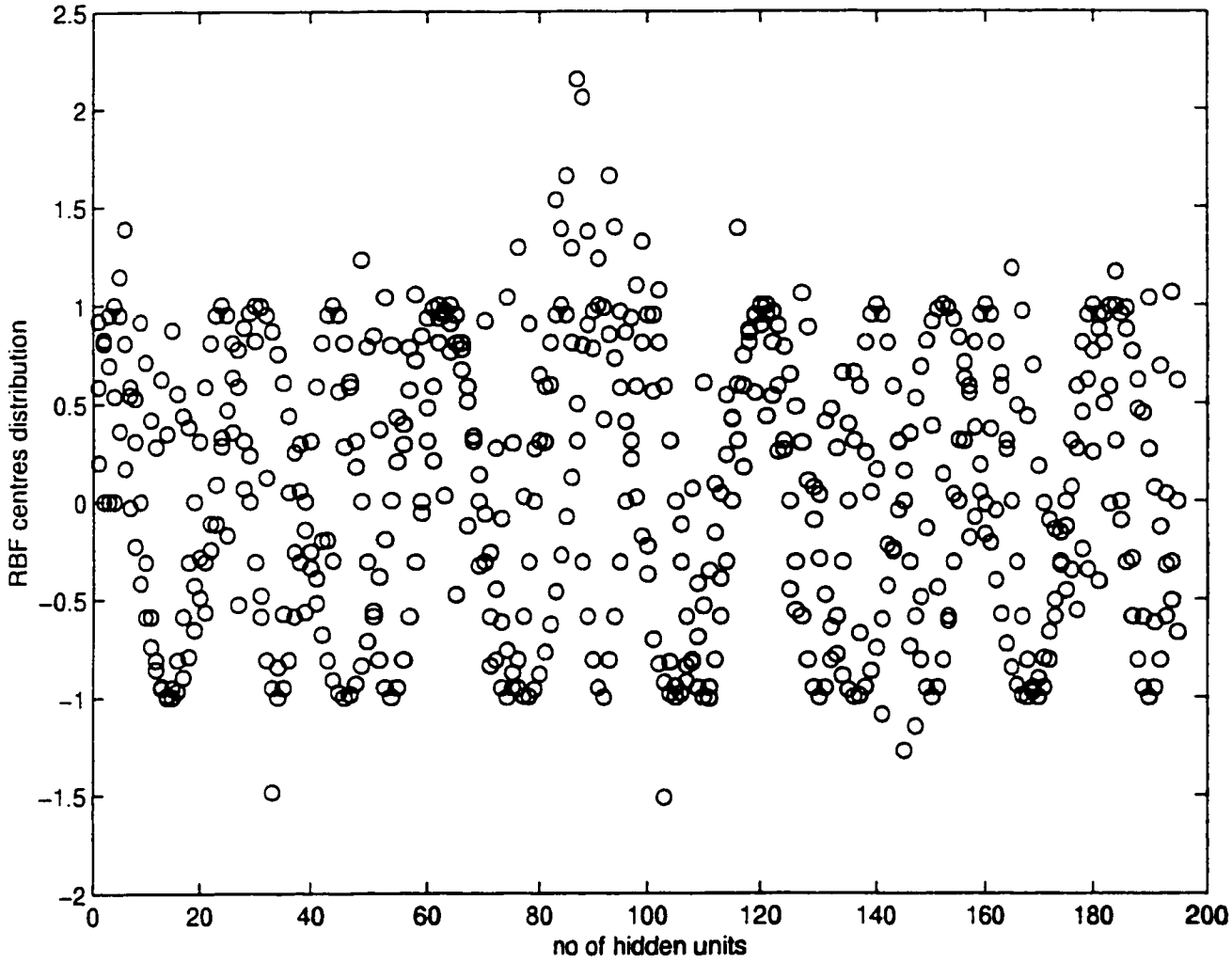

Figure 5.16: RBF centres distribution

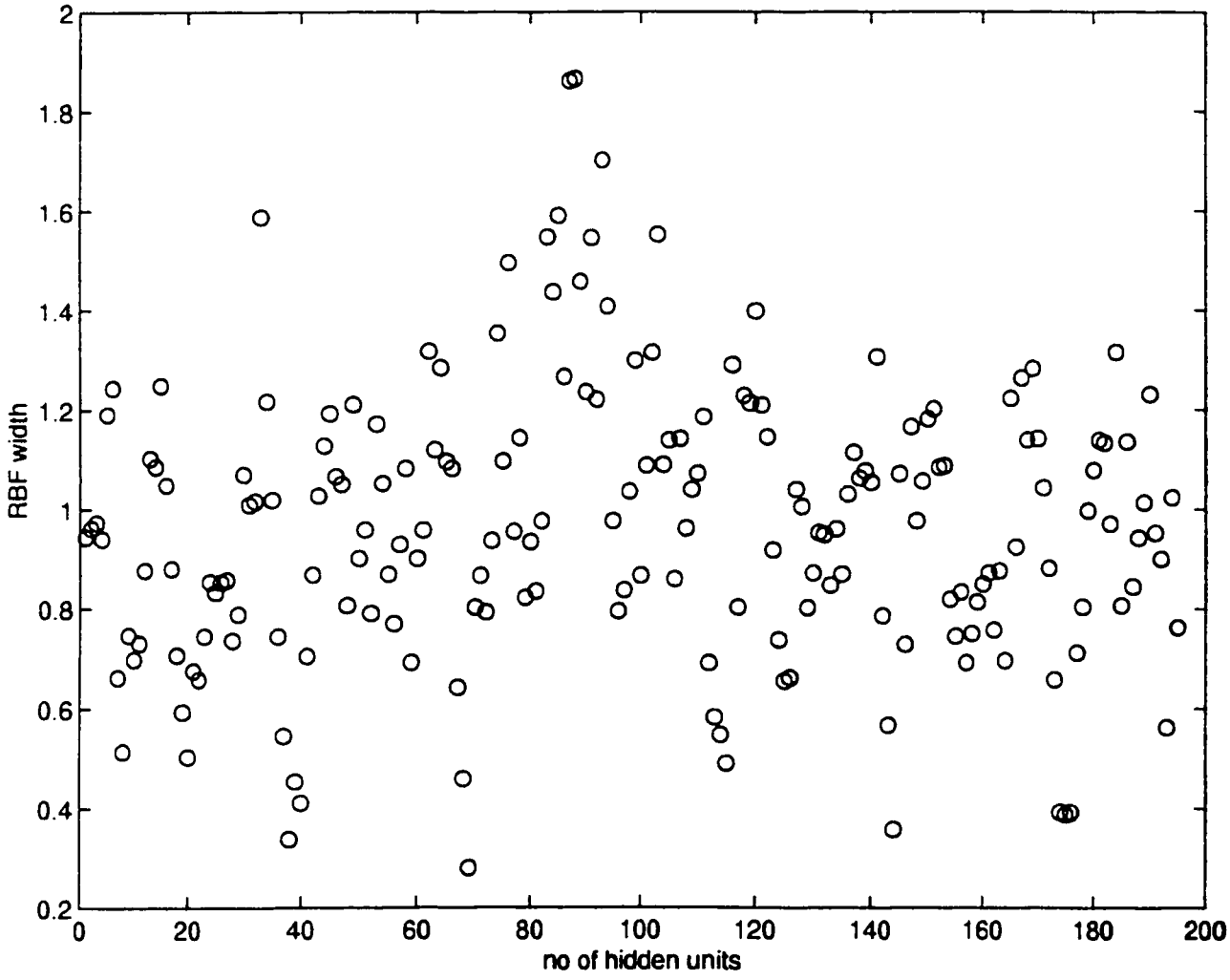

Figure 5.17: Distribution of RBF widths

Chapter 6

Dynamic Neural Networks Controller Design

In this chapter, the developed dynamic recurrent RBF networks will be demonstrated for the adaptive control of wing rock motion. To derive the linearizing feedback control, a sampled data system is considered in the design of the recurrent RBF networks. It is assumed that the system is a minimum phase that is the zero dynamics are asymptotically stable. The unknown nonlinear function of the physical system which generates the wing rock is modelled by recurrent dynamic RBF networks based on the concept of the Preisach hysteresis model. The resulting optimal RBF network is obtained through supervised learning. The linearizing feedback control law is obtained by using the model approximated by the RBF networks. The error between the approximated plant output and the nonlinear uncertain system output is used in the formulation of Lyapunov stability criteria to adjust the outer weights of the RBF networks for control law computation.

6.1 Feedback Linearization

In this section a general review of the concept of feedback linearization based on the continuous system will be given. The definitions and the various notions of *relative degree, normal form and internal dynamics* will be presented and these notions will serve as the basis for the analysis of the controller design to be described in the remaining chapters. The derivation of nonlinear control theory can be found in [32], [85] and [86]. The main results are summarized in the following for the purpose of this thesis.

Definition 6 ***Diffeomorphism*** *:A vector field in R^n, a vector function $f : R^n \rightarrow R^n$ defined in region Ω is called a diffeomorphism if it is smooth, and if its inverse f^{-1}exists and is smooth. A set $M \subset R^n$is a smooth manifold of dimension k if it is locally diffeomorphic to R^k. If U and V are open subsets of R^n and R^m,respectively with $m \geq n$, it is said $x \in U$ is a regular point of f, if the rank of the Jacobian of f at x is equal to n.*

A diffeomorphism is used to transform a nonlinear system into another nonlinear system in terms of new set of states.

Definition 7 ***Lie Derivative:*** *The Lie derivative of a smooth scalar function $h(x) : R^n \rightarrow R$ with respect to a smooth vector field $f(x) : R^n \rightarrow R^n$ is denoted by $L_f h(x) = \frac{\partial h}{\partial x} f(x)$.The Lie derivative $L_f h$ is a directional derivative of h along the vector f.The Lie bracket of two vector fields f an g denoted by $[f, g]$ or $ad_f g$ is a vector field defined by $[f, g] = \frac{\partial h}{\partial x} f(x) - \frac{\partial h}{\partial x} g(x)$.*

The Lie derivative and Lie bracket can be defined recursively

$$
\begin{aligned}
L_f^o h &= h \\
L_f^i h(x) &= L_f(L_f^{i-1} h) = \frac{\partial (L_f^{i-1} h)}{\partial x} f(x)
\end{aligned}
$$

$$
\begin{aligned}
ad_f^o g &= g \\
ad_f^k g &= [f, ad_f^{k-1} g], \ k > 0
\end{aligned} \tag{6.1}
$$

6.1.1 Relative Degree

Consider a SISO nonlinear system represented by

$$
\begin{aligned}
\dot{x} &= f(x) + g(x)u \\
y &= h(x)
\end{aligned} \tag{6.2}
$$

where $x \in R^n$ denotes the state vector, $u \in R^m$ is the input vector and the function $f(x)$ and $g(x)$ are smooth vector fields and $h(x)$ is a nonlinear function. Differentiate the y with respect to time we obtain the following.

$$
\dot{y} = \frac{\partial h}{\partial x} f(x) + \frac{\partial h}{\partial x} g(x)u = L_f h(x) + L_g h(x)u \tag{6.3}
$$

where $L_f h(x) : R^n \rightarrow R$ and $L_g h(x) :\rightarrow R^n \rightarrow R$ are Lie derivatives of $h(x)$ with respect to $f$and g respectively. If $L_g h(x)$ is non-singular for all $x \in R^n$, then the following feedback law

$$
u = \frac{1}{L_g h(x)} [-L_f h(x) + v] \tag{6.4}
$$

yields the output linear equation from v to y. Substitute u into equation (6.3) we obtain

$$
\dot{y} = v \tag{6.5}
$$

where v becomes the input that is chosen to make the closed loop system linear in input-output form.

If $L_g h(x) = 0$ for all x,we differentiate $\dot{y}$ to obtain the following

$$\ddot{y} = L_f^2 h(x) + L_g L_f h(x) u \tag{6.6}$$

where $L_f^2 h(x) = L_f(L_f h(x))$ and $L_g L_f h(x) = L_g(L_f h)(x)$. If $L_g L_f h(x)$ is nonzero for all $x \in R^n$, the input-output control law is given below.

$$u = \frac{1}{L_g L_f h(x)}[-L_f^2 h(x) + v] \tag{6.7}$$

and the input-output system becomes

$$\ddot{y} = v \tag{6.8}$$

If $L_f L_g h(x) = 0$ and the process is repeated the feedback control law becomes

$$u = \frac{1}{L_g L_f^{\gamma-1} h(x)}[-L_f^{\gamma} h(x) + v] \tag{6.9}$$

and the output equation becomes

$$y^{(\gamma)} = v \tag{6.10}$$

The number γ differentiation required for the input u to appear is called the *relative degree* of the system. For the smallest integer γ such that

$$\begin{aligned} L_g L_f^i h(x) &= 0 \; i = 0,.....\gamma - 2 \\ L_g L_f^{\gamma-1} h(x) &\neq 0 \; for \; all \; x \in R^n \end{aligned} \tag{6.11}$$

is called the relative degree of the nonlinear system. If such γ exists, the nonlinear system has a well defined *relative degree*. If x_o is assumed an operating point, and coefficient of u is nonzero at x_o equation (6.11) implies that the system has a *relative degree* γ at the point x_o. Contrarily, if the coefficient $L_g L_f^{\gamma-1} h(x)$ is zero at x_o and nonzero at some point arbitrarily close to x_o, the *relative degree* of the nonlinear system is said to be undefined at x_o [32].

6.1.2 Normal Form

Whenever the relative degree $\gamma \leq n$ is well defined the nonlinear system can be transformed from the states equations involving x to a new states equations involving the output y, its derivatives and $n-\gamma$ additional equations [85]. To show the nonlinear transformation exists, the following diffeomorphism exists $\Phi(x)$ where

$$\Phi(x) = \begin{bmatrix} \Phi_1(x) \\ ..... \\ \Phi_\gamma(x) \\ \eta_1(x) \\ ... \\ \eta_{n-\gamma}(x) \end{bmatrix} = \begin{bmatrix} y \\ ..... \\ y^{(\gamma-1)} \\ \eta_1(x) \\ ... \\ \eta_{n-\gamma}(x) \end{bmatrix} \tag{6.12}$$

where $y^{(i)}$ denotes ith order of the derivatives of the system output y and η_j denotes n-γ additional equations which render the coordinate transformation valid.

Lemma 8 *If the relative degree of the system γ is well defined in $\Omega \subset R^n$ the differentials $d\Phi_1(x)$,.....$d\Phi_\gamma(x)$ are linearly independent in Ω where $\Phi_1(x) = h(x)$,.....$\Phi_\gamma(x) = L_f^{\gamma-1} h(x)$ [85]*

Lemma 9 *If the system has well defined relative degree γ in Ω and if γ is less than n, there exists $n-\gamma$ functions η_1,.....$\eta_{n-\gamma}$ such that the mapping has non singular*

Jacobian in Ω.[85]

$$\Phi(x) = \begin{bmatrix} h(x) \\ L_f h(x) \\ .... \\ L_f^{\gamma-1} h(x) \\ \eta_1(x). \\ ... \\ \eta_{n-\gamma}(x) \end{bmatrix} \tag{6.13}$$

Lemma 10 *Define coordinates* (ξ, η) *where*

$$\begin{bmatrix} \xi \\ \eta \end{bmatrix} = \begin{bmatrix} \xi_1 \\ ... \\ \xi_\gamma \\ \eta_1 \\ ... \\ \eta_{n-\gamma} \end{bmatrix} = \begin{bmatrix} \phi_1(x) \\ ... \\ \phi_\gamma \\ \eta_1(x) \\ ... \\ \eta_{n-\gamma} \end{bmatrix} = \Phi(x) \tag{6.14}$$

where $\xi = (\xi_1, ...\xi_\gamma)^T$ *and* $\eta = (\eta_1, ...\eta_{n-\gamma})^T$. *In the new coordinates* (ξ, η) *the nonlinear system (6.2) is represented as below*

$$\begin{aligned} \dot{\xi}_1 &= \xi_2 \\ \dot{\xi}_2 &= \xi_3 \\ &..... \\ \dot{\xi}_\gamma &= L_f^\gamma h(x) + L_g L_f^{\gamma-1} h(x) u \\ \dot{\eta} &= q(\xi, \eta) \\ y &= \xi_1 \end{aligned} \tag{6.15}$$

The system obtained from the nonlinear transformation in equation (6.14) is called local normal form of the system (6.2). If the relative degree γ is well defined then the system (6.2) can be transformed into the normal form of (6.15).

6.1.3 Internal Dynamics

The input-output linearization of the dynamics of a nonlinear system can be decomposed into *external* (input-output) part and the *internal* (unobservable) part. The external part consists of linear relation between y and v, the input can be designed to have the desired output.

The input-output linearizing control of equation (6.9) in normal form of the system (6.2) results in the following closed loop system

$$\begin{aligned}
\dot{\xi}_1 &= \xi_2 \\
\dot{\xi}_2 &= \xi_3 \\
&\cdots\cdots \\
\dot{\xi}_\gamma &= v \\
\dot{\eta} &= q(\xi, \eta) \\
y &= \xi_1
\end{aligned} \tag{6.16}$$

The variables η are unobservable states and they do not appear in the output y. The closed loop dynamics (6.16) can be separated into output dynamics involving ξ_1,.....ξ_γ and the internal dynamics involving ξ and η. The $\dot{\eta}= q(\xi, \eta)$ is called internal dynamics because q dynamics are unobservable and internal to the closed loop system. By definition the special form of internal dynamics, $q(0, \eta)$ is called zero dynamics. By setting the output and its higher derivatives to zero, and zero dynamics

is obtained.

$$\begin{aligned} \dot{\xi} &= 0 \\ \dot{\eta} &= q(\xi, \eta) \end{aligned} \tag{6.17}$$

For a linear system, the zeros of the original system is the same as the poles of the zero dynamics.

6.2 Neural Networks Controller Design

Geometric nonlinear control theory has provided a tool for the design of nonlinear feedback system. For nonlinear tracking control, feedback linearization and input-output linearization technique had been used to solve nonlinear control problems and flight control in [86]-[95]. In this section a single layer RBF networks will be used to model the unknown physical system and to generate the feedback law. If the affine nonlinear system of equation (6.2) has a relative degree γ the output differentiation is terminated after $\gamma \leq n$ steps, then the system can be represented by the following input-output representation [55] and [96].

$$y^{(\gamma)} = f(x) + g(x)u \tag{6.18}$$

where control input $u : R_+ \rightarrow R$, output, $y : R_+ \rightarrow R$, γ is relative degree. The following assumptions are made regarding the nonlinear system.

(1)The nonlinear system has a strong relative degree γ.

(2)The system is assumed to be a minimum phase.

(3)The system is feedback linerizable and the zero dynamics are stable.

(4)The system is controllable and the state vector is available for measurement.

6.2.1 Sampled Data Nonlinear System

The control scheme employed in this research is generally known as *hybrid adaptive control scheme.* The hybrid control scheme uses the sampled continuous time system output to discretely carry out the estimate of networks or system parameters and redesign adaptive law for the continuous time feedback control of the system. The issue of stability of the hybrid adaptive control is thoroughly discussed in the paper by Zhang and Middleton [97]. The overall system stability can be established under the conditions that the sampling period is chosen to be sufficiently small and the presence of persistent excitation. In the recent paper by Fuchun Sun et al. [98] a neural network based adaptive control for sampled data nonlinear system was developed and variable structure control was considered.

In this research, sampled data system is considered in the design of recurrent RBF networks and the controller. The objective and interest is to convert the system given in equation (6.18) into a discrete time input-output representation needed for the purpose of identification and control.

According to Narendra [99] that the given discrete time dynamical system can be represented by the state equation.

$$\begin{aligned} x(k+1) &= f[x(k), u(k)] \\ y(k) &= h[x(k)] \end{aligned} \tag{6.19}$$

If the system (6.19) has relative degree d and well defined, it implies that the input at instant k affects the output only d units of time later. Consequently it also represents the delay of the system (6.19) from input u to output y. When the system has relative degree d, it can be shown that the input-output representation of the system is given by the following general form.

$$y(k+d) = F\,[y(k), y(k-1), ...y(k-n+1), u(k), u(k-1), ..u(k-n+1)] \quad (6.20)$$

To overcome the computational complexity occurred in equation (6.20), Narendra had proposed the following NARMA-L2 Model (Non-linear ARMA)

$$\begin{aligned} y(k+d) &= f_o[y(k), ...y(k-n+1), u(k-1), ..u(k-n+1)] \\ & \quad g_o[y(k), ...y(k-n+1), u(k-1), ..u(k-n+1)]u(k) \end{aligned} \quad (6.21)$$

The main feature of this model is that the control input $u(k)$ at time k occurs linearly in the equation relating the input and the output. In equation (6.21) f_o and g_o are functions of $[y(k), ...y(k-n+1), u(k-1), ..u(k-n+1)]$. This is the model that is required for the purpose of identification and control and it will be used in the controller design.

Following the same procedures given in Guillaume [100], a sampled data system is designed with digital control of non-linear continuous time system of equation (6.18) implemented using sampling of output and zero order hold control action as shown in Figure (6.1).

The output $x(t)$ of the non-linear system and the control $u(t)$ are supposed to be sampled at the same rate, $t = kT_s$ with uniform sampling period $T_s > 0$.

$$t_k = kT_s, \quad k \in Z^+ \quad (6.22)$$

the sampled output at sampling instant is given by

$$x(k) \triangleq x(t = kT_s) \quad (6.23)$$

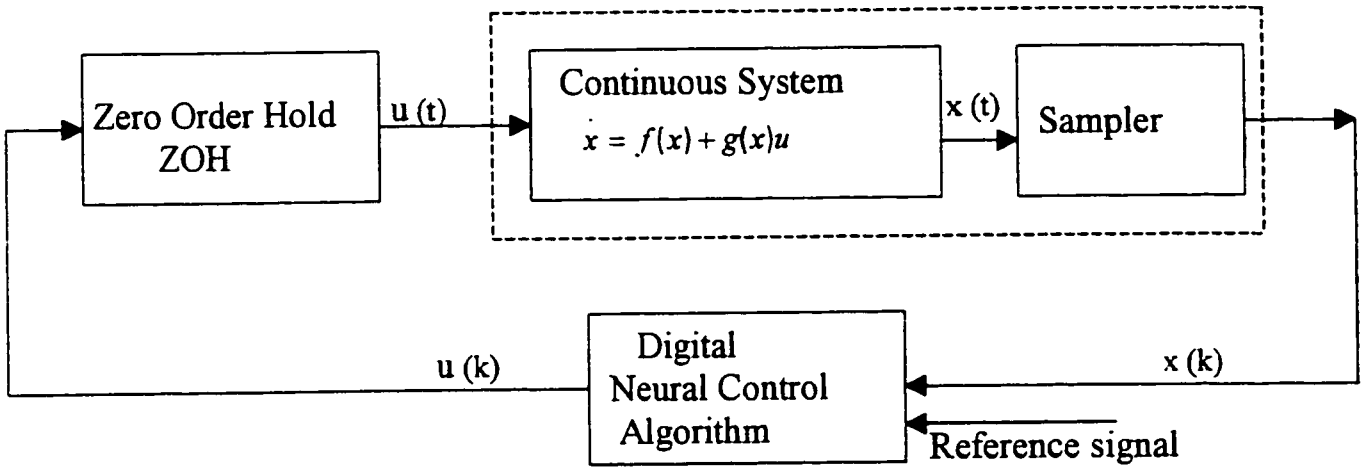

Figure 6.1: Closed Loop Sampled Data System

The ZOH control action is given as

$$u(t) = u(kT_s) \triangleq u(k), \quad \forall t : kT_s < t < (k+1)T_s \tag{6.24}$$

It is assumed that in the sampling process of continuous time system a infinite number of bit is used and there is no finite escapes and the general structure in system (6.18) is preserved in the discrete time system. Monaco and Normand Cyrot [101] had shown that the sampled data version of the following continuous time non linear system

$$\dot{x} = f(x,\theta) + G(x,\theta)u \tag{6.25}$$

can be written as follow .

$$Dx(k) = \sum_{j=1}^{\infty} \frac{\delta^{j-1}}{j!}[L_f + \sum_{l=1}^{m} u_l(k)L_{gl}]^j(x(k)) \tag{6.26}$$

where $Dx(k) \triangleq \frac{x(k+1)-x(k)}{T_s}$, θ is unknown constant parameter vector, T_s is a sampling period. $u_l(k)$ is control input and L_{gl} is lie derivative along the vector field g. The limitations of the above sampled data system occur in the transposition from continuous time to discrete time case for example :

. The exact discrete model is valid only if the right hand side (RHS) of equation (6.26) does converge. The concern is regarding the appearance of finite time escape through the sampling process.

. The RHS of equation (6.26) is an infinite series with respect to sampling period and the discrete model is not tractable for control design.

. There is no guarantee of state feedback linear stabilizability because the model given in equation (6.26) is not linear in the control input.

The treatment of these issues is beyond the scope of the present thesis. The issues and difficulties in the above limitations had been discussed and the solutions to get around these problems had been proposed by Guillaume [100].

6.2.2 Dynamic Recurrent RBF Control Strategy

The concept of zero dynamics and minimum phase properties introduced earlier for non linear continuous system were extended to discrete time case by Monaca and Cyrot [102].

The sampled data nonlinear single input-single output relative degree one system can be represented by the following [56].

$$\begin{aligned} x(k+1) &= f(x(k), u(k)) \\ y(k) &= h[x(k)] \end{aligned} \tag{6.27}$$

It was shown that if certain conditions are satisfied, there exists a feedback control

$$u = \gamma(x, r) \tag{6.28}$$

By performing change of coordinates $z = T(x)$ the closed loop system is given as below.

$$\begin{aligned} z_1(k+1) &= Az_1(k) + Br(k) \\ z_2(k+1) &= F(z_1(k), z_2(k), r(k)) \\ y(k) &= Cz_1(k) \end{aligned} \tag{6.29}$$

where (A, B, C) are controllable observable triple. If the system (6.27) starts at $z_1(0) = 0$, $r = 0$, then $z_1 = 0$, then the plant output stays at zero. The dynamics of the system is determined by z_2, the zero dynamics which is defined by

$$z_2(k+1) = F(0, z_2(k), 0) \tag{6.30}$$

and the system is a minimum phase if zero dynamics have a asymptotically stable equilibrium at the origin

The overall dynamic recurrent RBF networks control strategy is shown in Figure (6.2). Consider the sampled data nonlinear input-output relative degree one system be represented by the following representation in Chen [56]. The same model had been proposed by Narendra given in equation (6.21).

$$\begin{aligned} y_{k+1} &= f(y_k, \ldots, y_{k-p+1}, u_{k-1}, \ldots, u_{k-m}) + \\ & \quad g(y_k, \ldots y_{k-p+1}, u_{k-1}, \ldots, u_{k-m})u_k \end{aligned} \tag{6.31}$$

Choosing the following state variables as

$$
\begin{aligned}
z_{11}(k) &= y_{k-p+1} \\
&\vdots \\
z_{1p}(k) &= y_k \\
z_{21}(k) &= u_{k-m} \\
&\vdots \\
z_{2m}(k) &= u_{k-1}
\end{aligned}
$$

The state space model can be obtained as

$$
\begin{aligned}
z_{11}(k+1) &= z_{12}(k) \\
&\vdots \\
z_{1p}(k+1) &= f\{z(k)\} + g\{z(k)\}u(k) \\
z_{21}(k+1) &= z_{22}(k) \\
&\vdots
\end{aligned}
\tag{6.32}
$$

$$z_{2m}(k+1) = u_k$$
$$y(k) = z_{1p}(k)$$

The non linear plant can be written in discrete time as below

$$y(k+1) = f(z(k)) + g(z(k))u(k) \tag{6.33}$$

The plant is modelled by the RBF networks as below

$$\hat{y}(k+1) = \hat{f}(z(k), w_f) + \hat{g}(z(k), w_g)u(k) \tag{6.34}$$

The estimated plant output is given as below where $w_f(k)$ and $w_g(k)$ are estimate of w_f and w_g at time instant k.

$$y^*(k+1) = \hat{f}(z(k), w_f(k)) + \hat{g}(z(k), w_g(k))u(k) \tag{6.35}$$

At each time step the following control action is chosen in order to bring the tracking error to zero.

$$u(k) = \frac{-\hat{f}(z(k), w_f(k)) + r(k)}{\hat{g}(z(k), w_g(k))} \tag{6.36}$$

where $w_f(k)$ and $w_g(k)$ are linear parameters of output layer of the RBF networks and $r(k)$ is the reference command, the desired output. The model output from the RBF networks is given by.

$$\hat{f}(z(k), w_f) = f_o(z) + \sum_{i=1}^{K_f} w_{f_i}\Theta_{f_i}(z(k)) \tag{6.37}$$

$$\hat{g}\,(z(k).\,w_g) = g_o(z) + \sum_{i=1}^{K_g} w_{g_i}\Theta_{g_i}(z(k)) \tag{6.38}$$

where K_f. K_g are the number of neurons in the hidden layer for each separate RBF networks and $\Theta_{f_i}(z(k))$, $\Theta_{g_i}(z(k))$ are Gaussian functions in respective networks determined by the number of hidden neurons and neural parameters of centre and width, $z(k)$ is the input state variable and $f_o(z)$ and $g_o(z)$ are prior knowledge of nonlinearities of the system. The neural parameters are updated by the Extended Kalman Filter.

6.2.3 Neural Networks Control Law Derivation

Assumption 1 : The discrete time nonlinear plant is given as below

$$y(k+1) = f\,(z) + g(z)u(k) \tag{6.39}$$

and the RBF networks model output is

$$\hat{y}\,(k+1) = \hat{f}\,(z(k), w_f) + \hat{g}\,(z(k), w_g)u(k) \tag{6.40}$$

$f(z)$ is unknown and assumed to be a smooth function and differentiable a sufficient number of times and vanishes at the origin and $g(z)$ is unknown and assumed smooth and bounded away from zero over the compact set S

Assumption 2 : The system is minimum phase which implies the following zero dynamics has an globally exponentially stable equilibrium at the origin.

$$z_{21}(k+1) = z_{22}(k)$$

.

.

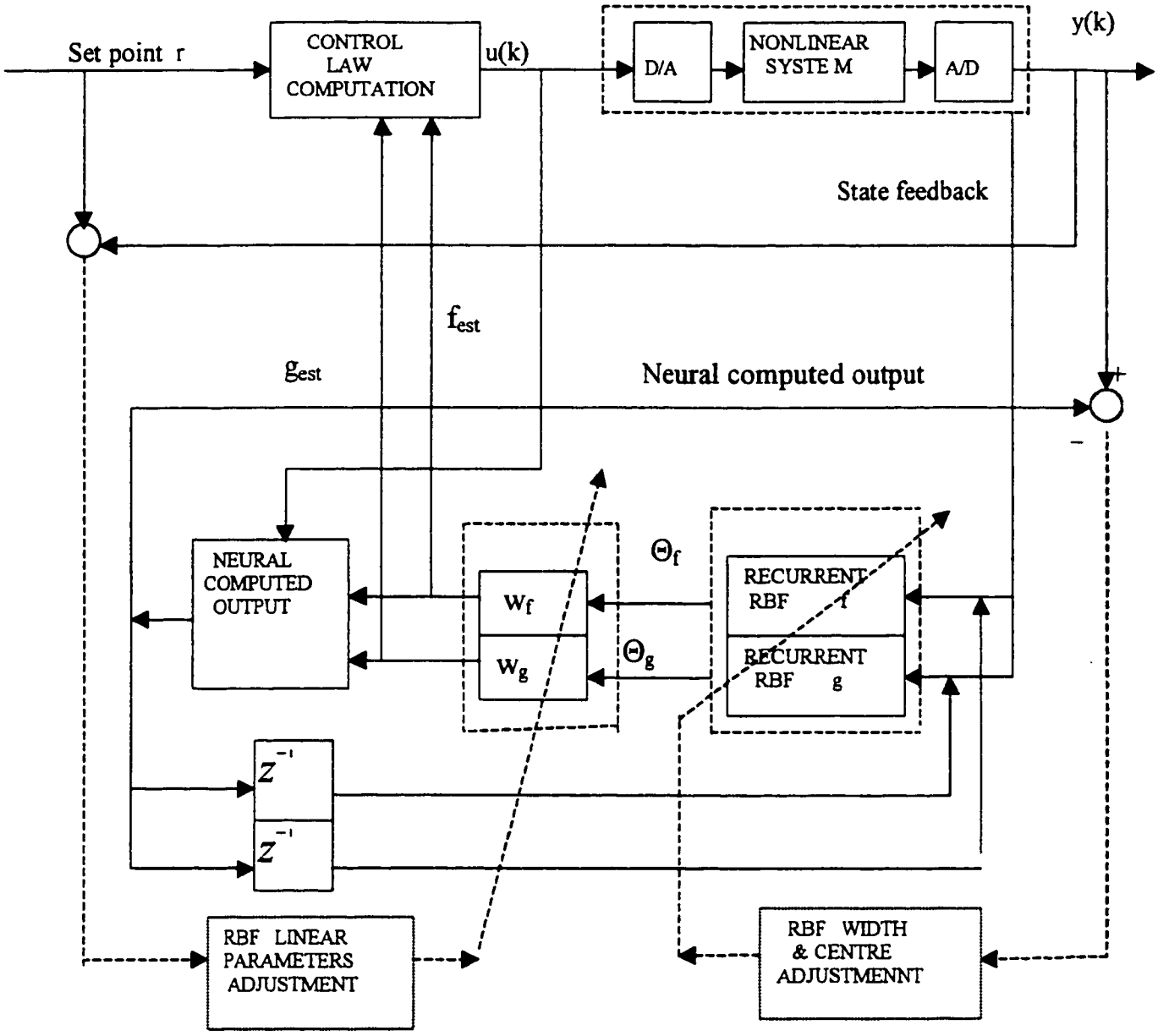

Figure 6.2: Dynamic Recurrent RBF Control Strategy

$$z_{2m}(k) = \frac{-f(z(k))}{g(z(k))} \mid z_{1i=0} \tag{6.41}$$

From the above assumption, the converse Lyapunov theorem [103] suggests that the following Lyapunov function $V_2(z_2(k))$ exists such that

$$c_1 |z_2(k)|^2 \leq V_2(z_2(k)) \leq c_2 |z_2(k)|^2 \tag{6.42}$$

$$V_2(z_2(k+1)) - V_2(z_2(k)) \leq -\alpha |z_2(k)|^2 \tag{6.43}$$

$$\left|\frac{\partial V_2(z)}{\partial z}\right| \leq L |z| \tag{6.44}$$

in some ball $B_{\rho 2} \subset R^m$, where c_1, c_2, α and L are positive constants.

Proof : See Chen [56].

Assumption 3 : For a given positive constant ϵ and a compact set $S \in R$, there exists a coefficient w_f and w_g such that $\hat{f}\,(z(k), w_f)$ and $\hat{g}\,(z(k), w_g)$ approximate the unknown nonlinear functions $f(z(k))$ and $g(z(k))$ in z domain.

$$|\Delta_f| = \left|\hat{f}\,(z(k), w_f) - f(z(k))\right| \leq \epsilon \tag{6.45}$$

$$|\Delta_g| = \left|\hat{g}\,(z(k), w_g) - g(z(k))\right| \leq \epsilon \tag{6.46}$$

In the expression $\hat{f}\,(z(k), w_f) = f(z(k), w_f^*, K_f)$ and $\hat{g}\,(z(k), w_g) = g(z(k), w_g^*, K_g)$, where K_f and K_g are the optimal numbers of respective RBF units in functions $f(z)$ and $g(z)$ obtained from the dynamic network design. The parameter vectors w_f^* and w_g^* are optimal parameters obtained to ensure for the minimum error during the estimation. The control under this scheme is given as below.

$$u(k) = \frac{-\hat{f}\,(z(k), w_f(k)) + r(k)}{\hat{g}\,(z(k), w_g(k))} \tag{6.47}$$

where $r(k)$ is the command reference and the parameters, $w_f(k)$ and $w_g(k)$ are updated at each time step.

6.2.4 Adaptation Law

The following parameter updating law is adopted from [56] by adding an extra term η, the learning rate.

$$\theta(k+1) = \theta(k) - \frac{\eta}{r_k} e(k+1) J(k) \tag{6.48}$$

where θ is the linear parameters, $e(k+1)$ is the error between the estimated plant output and the measured actual plant output as given as follow :

$$e(k+1) = y^*(k+1) - y(k+1) \tag{6.49}$$

$$\eta = \begin{bmatrix} \eta_f \\ \eta_g \end{bmatrix} \tag{6.50}$$

$$\theta = \begin{bmatrix} w_f \\ w_g \end{bmatrix}$$

The Jacobian matrix of $\frac{\partial \hat{f}}{\partial w_f}$ and $\frac{\partial \hat{g}}{\partial w_g}$ and r_k are defined as follow :

$$J(k) = \left[\frac{\partial y^*(k+1)}{\partial \theta} \right]^T_{\theta(k)} \tag{6.51}$$

$$= \begin{bmatrix} \left(\frac{\partial \hat{f}(z(k), w_f)}{\partial w_f} \right)^T_{w_f(k)} \\ \left(\frac{\partial \hat{g}(z(k), w_g)}{\partial w_g} \, |_{wg(k)} \right)^T u(k) \end{bmatrix}$$

$$r_k = 1 + J^T(k) J(k) \tag{6.52}$$

The parameter error is defined as below.

$$\widetilde{\theta}\ (k) = \theta(k) - \theta^* \tag{6.53}$$

The linear parameter w_f and w_g are updated using Lyapunov stability analysis to ensure closed loop system is stable.

6.2.5 Stability Analysis

Theorem 1 : If assumptions 1, 2 and 3 are satisfied and $|r(k)| \leq \rho$, $\forall\ k \geq 0$ and $\left|\widetilde{\theta}\ (k)\right| \leq \delta < \delta^*$, where ρ, δ and δ^* are positive constants, then

(1) $\left|\widetilde{\theta}\ (k)\right|$ will be monotonically nonincreasing and $|\theta(k+1) - \theta(k)|$ will converge to zero.

(2) The tracking error between the plant output and the reference command will converge to zero.

Proof : The stability analysis of the dynamic recurrent RBF controller are established by following the steps outlined in Chen [104].

Step 1 : Plant Output Equation

From equations (6.33), (6.45) and (6.46) express the plant output as the following

$$y(k+1) = \hat{f}\ \{z(k), w_f\} - \epsilon + \{\hat{g}\ (z(k), w_g) - \epsilon\}u(k)$$

$$y(k+1) = \hat{f}\ (z(k), w_f) + \hat{g}\ (z(k), w_g)u(k) + O(\epsilon) \tag{6.54}$$

where $O(\epsilon) = \{-\epsilon - \epsilon\ u(k)\}$

Step 2 : Error Equation

The error between the estimated plant output and measured plant output is expressed as below.

$$
\begin{aligned}
e(k+1) &= y^*(k+1) - y(k+1) \qquad (6.55)\\
&= \hat{f}\,(z(k), w_f(k)) - \hat{f}\,(z(k), w_f) + \\
&\quad \{\hat{g}\,(z(k), w_g(k)) - \hat{g}\,(z(k), w_g\}u(k) \\
&\quad + O(\epsilon) \\
&= \tilde{\theta}\,(k)^T \left[\begin{array}{c} \left(\frac{\partial \hat{f}(z(k), w_f)}{\partial w_f} \right)^T_{w_f(k)} \\ \left(\frac{\partial \hat{g}(z(k), w_g)}{\partial w_g} \mid_{wg(k)} \right)^T u(k) \end{array} \right] \\
&\quad + O\{\left|\tilde{\theta}\,(k)\right|^2\} + O(\epsilon) \\
&= \tilde{\theta}\,(k)^T J(k) + \beta(k)
\end{aligned}
$$

Step 3: Parameters Updating Law

Rewrite $e(k+1) = \tilde{\theta}\,(k)^T J(k) + \beta(k)$ and for a bounded $z(k)$,there exist c_1 and c_2 such that

$$
|\beta(k)| < c_1 \left|\tilde{\theta}\,(k)\right|^2 + c_2\epsilon \qquad (6.56)
$$

and assume ϵ is small enough such that

$$
|\beta(k)| \leq M < d_o \qquad (6.57)
$$

where d_o is assumed a ball of radius at the origin, the following three cases are analyzed.

$$(i) \text{ If the error } e(k+1) > d_o \Longrightarrow \tilde{\theta}(k)^T J(k) + \beta(k) > d_o \tag{6.58}$$

$$\text{then } \tilde{\theta}(k)^T J(k) > 0 \quad \text{since} \quad |\beta(k)| < d_o \tag{6.59}$$

$$(ii) \text{ If the error } e(k+1) < -d_o \Longrightarrow \tilde{\theta}(k)^T J(k) + \beta(k) < -d_o \tag{6.60}$$

$$\text{then } \tilde{\theta}(k)^T J(k) < 0 \quad \text{since} \quad |\beta(k)| < d_o \tag{6.61}$$

$$(iii) \text{ If the error } e(k+1) < d_o \Longrightarrow \tilde{\theta}(k)^T J(k) + \beta(k) < d_o \tag{6.62}$$

$$\text{then } \tilde{\theta}(k)^T J(k) \geq 0 \quad \text{since} \quad |\beta(k)| < d_o \tag{6.63}$$

In general $e(k+1)$ can be written by the following

$$e(k+1) = \alpha(k)\, \tilde{\theta}(k)^T J(k) \tag{6.64}$$

where $0 \leq \alpha(k) < 1$. The parameter updating law (6.48) is written as

$$\theta(k+1) = \theta(k) - \eta \frac{\alpha(k)[\tilde{\theta}(k)^T J(k)] J(k)}{1 + J(k)^T J(k)} \tag{6.65}$$

For the RBF function, the Jacobian matrix $J(k)$ can be evaluated by taking partial derivative of $\hat{f}(z(k), w_f)$ in equation (6.37) with respect to w_f and partial derivative

of $\hat{g}\,(z(k), w_g)$ in equation (6.38) with respect to w_g, the following is obtained.

$$J(k) = \begin{bmatrix} \Theta_f(z(k)) \\ \Theta_g(z(k))\ u(k) \end{bmatrix}^T \tag{6.66}$$

Step 4 :Select the following nonnegative Lyapunov function

$$V(k) = \tilde{\theta}\,(k)^T\,\tilde{\theta}\,(k) \tag{6.67}$$

Assume that the initial summed square parameter error $V(0)$ is finite if $\Delta V(k) = V(k) - V(k-1)$ is non positive for all k. It concludes that nonpositive $\Delta V(k) \to 0$, as $k \to \infty$ which implies $\Delta V(k) \leq 0$, $V(k) \geq 0$ and $V(0) < \infty$.

$$\begin{aligned}
\Delta V(k) &= \tilde{\theta}\,(k+1)^T\,\tilde{\theta}\,(k+1) - \tilde{\theta}\,(k)^T\,\tilde{\theta}\,(k) \\
&= \left[\tilde{\theta}\,(k) - \eta\frac{\alpha(k)[\tilde{\theta}\,(k)^T J(k)]J(k)}{1 + J(k)^T J(k)}\right]^T \\
&\quad \left[\tilde{\theta}\,(k) - \eta\frac{\alpha(k)[\tilde{\theta}\,(k)^T J(k)]J(k)}{1 + J(k)^T J(k)}\right] \\
&\quad - \tilde{\theta}\,(k)^T\,\tilde{\theta}\,(k) \\
&= \tilde{\theta}\,(k)^T\,\tilde{\theta}\,(k) - 2\eta\alpha(k)\frac{[\tilde{\theta}\,(k)^T J(k)]^2}{1 + J(k)^T J(k)} \\
&\quad + \eta^2\alpha^2(k)\frac{[\tilde{\theta}\,(k)^T J(k)]^2 J(k)^T J(k)}{(1 + J(k)^T J(k))^2} \\
&\quad - \tilde{\theta}\,(k)^T\,\tilde{\theta}\,(k)
\end{aligned}$$

$$\leq \quad -2\eta\alpha(k)\frac{[\tilde{\theta}\ (k)^T J(k)]^2}{1+J(k)^T J(k)}$$

$$+\eta^2\alpha^2(k)\frac{[\tilde{\theta}\ (k)^T J(k)]^2}{1+J(k)^T J(k)}$$

$$\leq \quad -\eta^2\alpha^2(k)\frac{[\tilde{\theta}\ (k)^T J(k)]^2}{1+J(k)^T J(k)}$$

$$-[2\eta\alpha(k)-2\eta^2\alpha^2(k)]\frac{[\tilde{\theta}\ (k)^T J(k)]^2}{1+J^T(k)J(k)} \tag{6.68}$$

$$\leq -\eta^2\alpha^2(k)\frac{[\tilde{\theta}\ (k)^T J(k)]^2}{1+J(k)^T J(k)} \leq 0 \tag{6.69}$$

provided the second term in equation (6.68) given below is positive

$$[2\eta\alpha(k)-2\eta^2\alpha^2(k)]\frac{[\tilde{\theta}\ (k)^T J(k)]^2}{1+J(k)^T J(k)} > 0 \tag{6.70}$$

then the condition that $0 < \eta < \frac{1}{\alpha(k)}$ must be satisfied. Hence $|\theta(k+1)-\theta(k)|$ or $\Delta V(k)$ converges to zero as $k \rightarrow \infty$ and it implies that $u(k)$ is bounded.

Step 5 : Convergence Analysis

Since equation (6.69) is valid for all $k \geq 0$ and the condition that $\tilde{\theta}\ (k)^T\theta(k)$ is monotonically non-increasing which implies that

$$\eta^2\alpha^2(k)\frac{[\tilde{\theta}\ (k)^T J(k)]^2}{1+J(k)^T J(k)} = \eta\alpha(k)\frac{[\tilde{\theta}\ (k)^T J(k)]}{\sqrt{1+J(k)^T J(k)}} = 0, \quad \text{as} \quad k \rightarrow \infty \tag{6.71}$$

$$\alpha(\tilde{k})\theta\ (k)^T J(k) \longrightarrow 0, \quad \text{as } k \longrightarrow \infty \tag{6.72}$$

It follows from equation (6.64), the following is obtained.

$$|e(k+1)| = |y^*(k+1) - y(k+1)| = 0 \tag{6.73}$$

Recalling from equation (6.35) and substitute $u(k)$ from equation (6.36) into (6.35) hence, $y^*(k+1) = r(k)$ and the tracking error $|r(k) - y(k+1)| = 0$.□

6.3 Concluding Remarks

The concept of geometric nonlinear control theory was reviewed in this chapter. Various concepts such as relative degree, normal forms, internal dynamics and feedback linearization are also reviewed, these notions will provide an understanding in the discussion of the remaining chapters. The concept of zero dynamics given in continuous time is applied to the case of discrete time control. The control design is carried out using the hybrid system whereby the digital control of nonlinear continuous system is implemented by sampling the output signal and zero order hold control action. Based on the sampled data model the adaptation law for neural networks controller is derived and the proof of the stability of the closed loop system is given.

Chapter 7

Application to Wing Rock Control in Aircraft

Wing rock model in slender delta wing has been used as a benchmark by many researchers to demonstrate the adaptive and neural control strategy to suppress the wing rock motion. Various adaptive control methods have been successfully used to control the wing rock motion as reported in [21], [23] and [28] and neural control method in [28] and [29]. The limitation of various adaptive control methods employed to control the wing rock is based on the assumption that the structure of the nonlinear model in wing rock is known as "a priori ".

In the neural control method reported, a radial basis function network or single layer network was normally employed which requires a predetermined number of neurons in the hidden layer [98], [104] and [105]. The network has a fixed architecture and the number of neurons required are arbitrarily chosen. The centres of the Gaussian function in RBF networks were uniformly placed on the regular grid and the widths of the kernel units were set to one. In theory, as the number of neurons is increased the larger the spread will be to cover the input space. The method often results in excessive redundant of neurons in the networks and computationally intensive. Not all

the neurons introduced will contribute to the computation and the designed networks is not optimum. Although the method used in [29] requires a single neuron combined with fuzzy logic to suppress the wing rock, the method is based on the known model of wing rock in slender delta wing and the rule based control constraints were established through experience as "a priori".

The idea of structural adaptation in the design of neural networks refers to the on-line structure identification during the neural network design. The scheme is provided to add or prune the neurons through a learning algorithm based on the given problems on hand. Dynamic RBF networks had been reported in Yingwei [76] and [77] for function approximation through the neuron addition and pruning scheme for adjusting the number of neurons required in the networks. Sanner & Slotine [106] proposes using structurally dynamic wavelet networks for the adaptive control of uncertain robotic system. An algorithm has been developed which dynamically varies the actual structure of the networks which is used for controlling the robotic system. In the area of the RBF neural networks, the idea of incorporating the dynamic neural network design in the sense of adding/pruning neurons and with the recurrent feature has not been applied to the control problems. The use of the ensemble concept to train the networks and applying to the control problem is new. In the paper given by Fabri et al. [107] dynamic neural networks were applied to control problem. Radial basis function is used in the networks, neurons are added to the networks according to the growth criteria, however once the neuron is added there is no scheme to prune the networks if the neuron does not contribute to the performance.

The developed dynamic RBF networks controller can be applied to control the hysteresis phenomena experienced in general physical system and the wing rock in particular. It was reported in P.Ge [59] that the hysteresis nonlinearities in piezoceramic actuator had been modelled using the Preisach model and closed loop tracking control had been implemented using PID feedback loop. It was also reported by

Hayward [60] that the Preisach hysteresis model is interpreted in terms of phase shift which leads to simple linear compensator design for control of the actuator with non linear characteristics. The Preisach hysteresis model has also been applied in modelling and control of magnetostrictive material and smart actuator. There are numerous reports in this area, a good reference is given in Bank [64]. In chapter 5, simulation studies had demonstrated that the dynamic RBF networks based on properties of the Preisach model is capable to approximate the general hysteresis like cyclic function.

Recurrent neural networks had been used in recent years for the identification and function approximation [108]-[113] and for adaptive control [114]-[117]. Most of the works were based on the back-propagation networks and the feature of recurrent is the feedback from the individual neuron output. In this thesis the recurrent signal is taken from the networks output which represents the approximated nonlinear function output. In the recurrent network the input vector is defined as current input $z(k)$ and the previous RBF network prediction $\hat{y}\ (k-1)$, such a scheme has been used by Billing [113] for noise cancellation in signal processing application.

In this chapter, the dynamic recurrent RBF networks will be demonstrated to control the wing rock in delta wing model and comparing the results obtained using the fixed neural networks design. The developed dynamic recurrent RBF control strategy was effectively demonstrated by suppressing the wing rock in AFTI/F-16 testbed aircraft having similar delta wings configuration. The robustness analysis and the issues of performance and the practicality of potential application were addressed.

7.1 Control of Wing Rock in Slender Delta Wings

In this section the developed dynamic RBF networks will be demonstrated to control the wing rock in slender delta wing and comparisons between the dynamic and fixed

neural control will be given.

7.1.1 Control of Wing Rock using Dynamic RBF Networks

In the design of dynamic RBF networks, the memory formation properties of the Preisach model is included by using the ensemble average of the cells participating in the information storage. As the non-linear function in the wing rock in slender delta wing to be approximated is known as "a *priori* ", no recurrent feature is included in the design of the RBF networks. The idea is to illustrate the proposed control strategy over the current neural control method. The wing rock model for slender delta wing is given below [12].

$$\ddot{\phi} = L_o \ + \sin\ \alpha_s L_\beta \phi \ + L_{po}\ \phi + \sin\alpha_s\ L_{p\beta}\ |\phi|\ \dot{\phi} + L_{pp}\left|\dot{\phi}\right|\ \dot{\phi} \ + a_o\ u \qquad (7.1)$$

Let $\phi = x_1$ *and* $\dot{\phi} = x_2$ the model can be written in state space equations as below

$$\begin{aligned} \dot{x}_1 &= \dot{\phi} \\ \dot{x}_2 &= \ddot{\phi} = f(x) + a_o u + \nu \\ where\ f(x) &= c_o + c_1 x_1 + c_2 x_2 + c_3\,|x_1|\,x_2 + c_4\,|x_2|\,x_2 \end{aligned} \qquad (7.2)$$

and $c_o = L_o$, $c_1 = \sin\alpha_s\ L_\beta$, $c_2 = L_{po}$, $c_3 = \sin\alpha\ L_{p\beta}$, $c_4 = L_{pp}$, the c_i s are expressed in terms of aerodynamic parameters

In the neural control method the nonlinear function $f(x)$ is assumed unknown. The term $a_o\,u$ is added to the original model where a_o is the estimate of control effectiveness relating to input signal, a_o is generally unknown and estimate from prior

knowledge, in this example a_o is assumed known, $a_o = 1$. The neural control method approximates $f(x)$ using radial basis function networks. Assuming the state x_1 and the output x_2 , are measurable. Following the analysis of the sampled data system outlined in section 6.2.1, the signal from the system is sampled using A/D converter. The output of radial basis function $\hat{f}\ (x(k))$ approximates the nonlinear function $f(x(k))$ in discrete form such that

$$f(x(k)) = \hat{f}\ (x(k)) + er(k) \tag{7.3}$$

where $er(k)$ is the error between the networks output and the nonlinear function $\hat{f}\ (x(k))$ which is given as below

$$\hat{f}\ (x(k)) = f_o(x(k)) + \sum_{i=1}^{K_f} w_i(k)\Theta_i(x(k)) \tag{7.4}$$

$w_i(k)$ is the weight vector, K_f is the optimal number of neurons and $\Theta_i(x(k))$ is a Gaussian function given as below

$$\Theta_i(x(k)) = \exp(-\frac{1}{2\sigma^2}\|x_1 - \mu_a\|^2) \tag{7.5}$$

where x_1 is the input, the state variable and μ_a is the ensembles average of centres value in the hidden layer. By choosing the control law of the following form

$$u = -\frac{1}{a_o} w(k)\ \Theta(x(k)) \tag{7.6}$$

and the weight is updated using the following updating law

$$w(k+1) = w(k) - \frac{\eta}{r_k} e(k+1) J(k) \tag{7.7}$$

where $r_k = 1 + J(k)' J(k)$, and $J(k)$ is given as below

$$J(k) = \frac{\partial \hat{f}\,(x(k))}{\partial w} = \Theta(k) \tag{7.8}$$

7.1.2 Simulation

The purpose of this simulation to demonstrate that using the developed dynamic RBF control strategy the wing rock in slender delta wing can be suppressed without the prior knowledge of the nonlinearity structure. In this simulation example constant disturbance is included in the system and the following parameters are chosen.

$e_{\min} = 0.02$, $\epsilon_{\max} = 0.4$, $\epsilon_n = 0.2$, $e_{rms} = 0.2$, $\kappa = 0.85$, $P_o = 1.0$, $Q_o = 0.002$, $f_o = 0.5$, the learning rate $\eta = 0.85$, T_s, the sampling period is set to 0.05 sec. The following criteria are used for neurons addition

$$\|x - \mu_a\| > \epsilon_n \tag{7.9}$$

$$er(k) = \hat{f}\,(x(k)) - f(x(k)) \tag{7.10}$$

The ensemble average μ_a is used in the calculation of the centre distance between the input vector and the centres as given below.

$$\mu_a = \frac{1}{n}\sum_i (x - \mu(k, \xi_i)) \tag{7.11}$$

Figures 7.1 and 7.2 show the wing rock in roll angle and roll rate of slender delta wings. Figure 7.3 shows the suppression of wing rock and only 32 neurons in the RBF hidden layer are used as compared to 441 neurons needed using the fixed RBF architecture [28]. The ensemble average plot shows the response stabilizes in a relative short time. The roll angle and phase plot are shown in Figure 7.4.

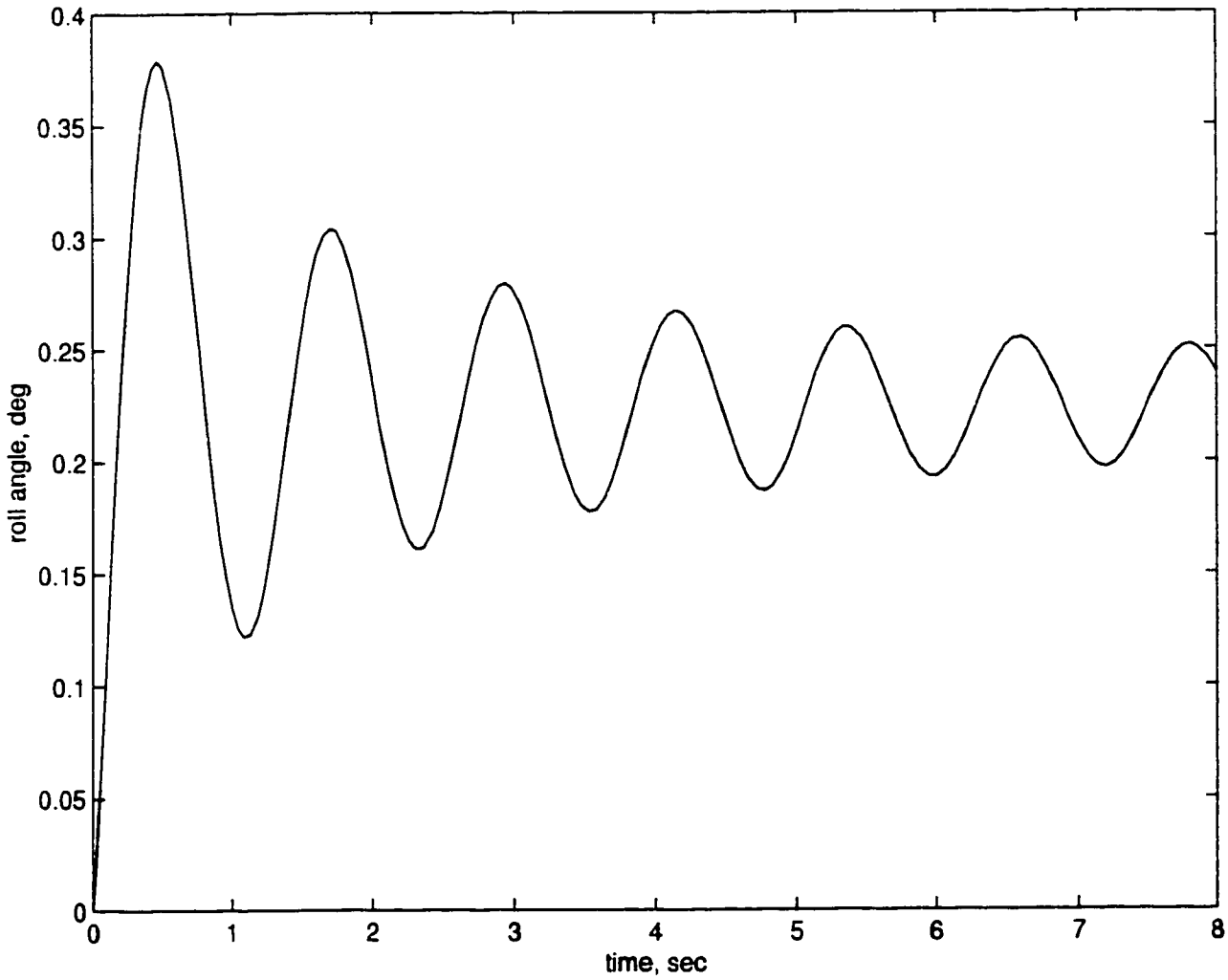

Figure 7.1: Wing rock in roll angle

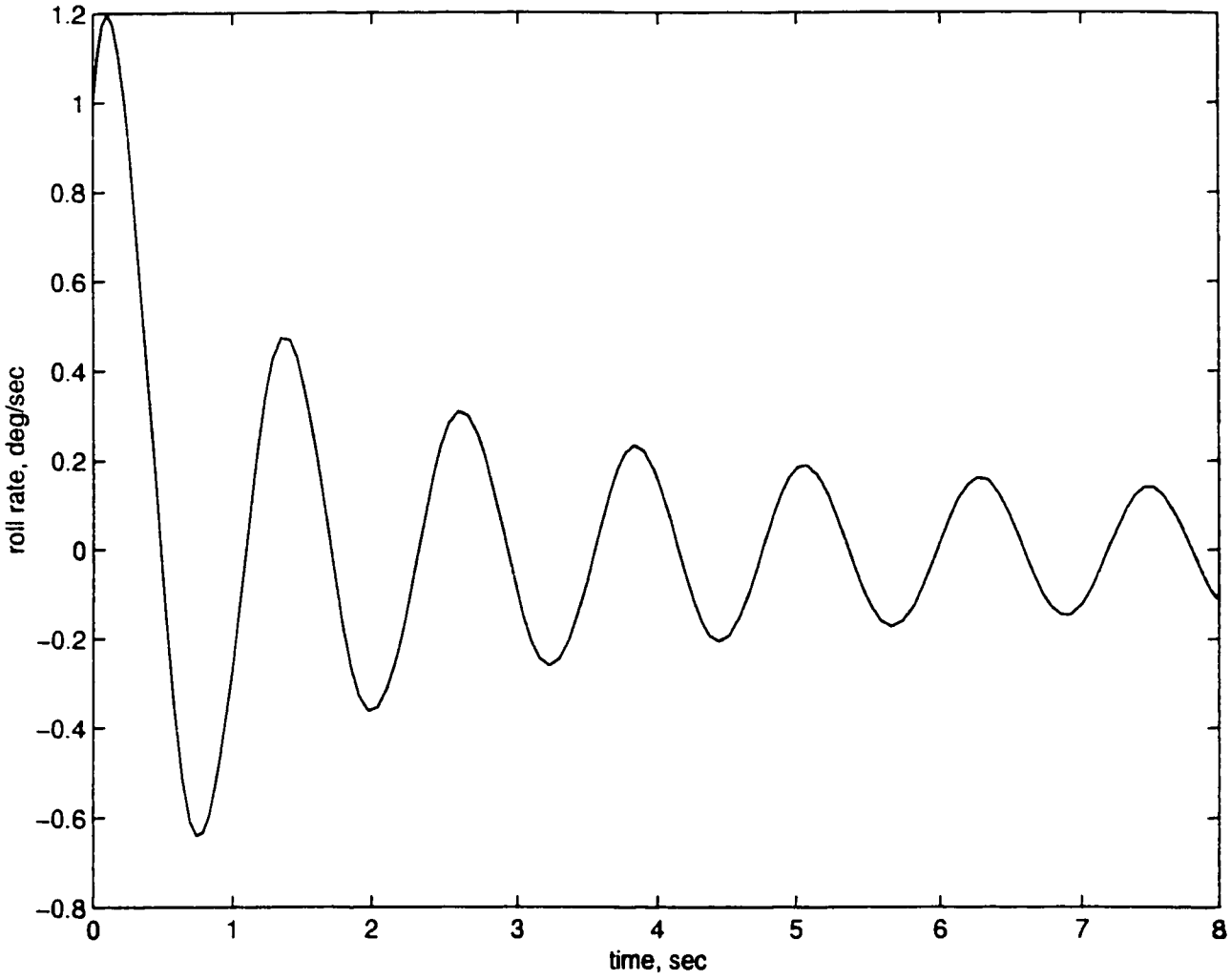

Figure 7.2: Wing rock in roll rate

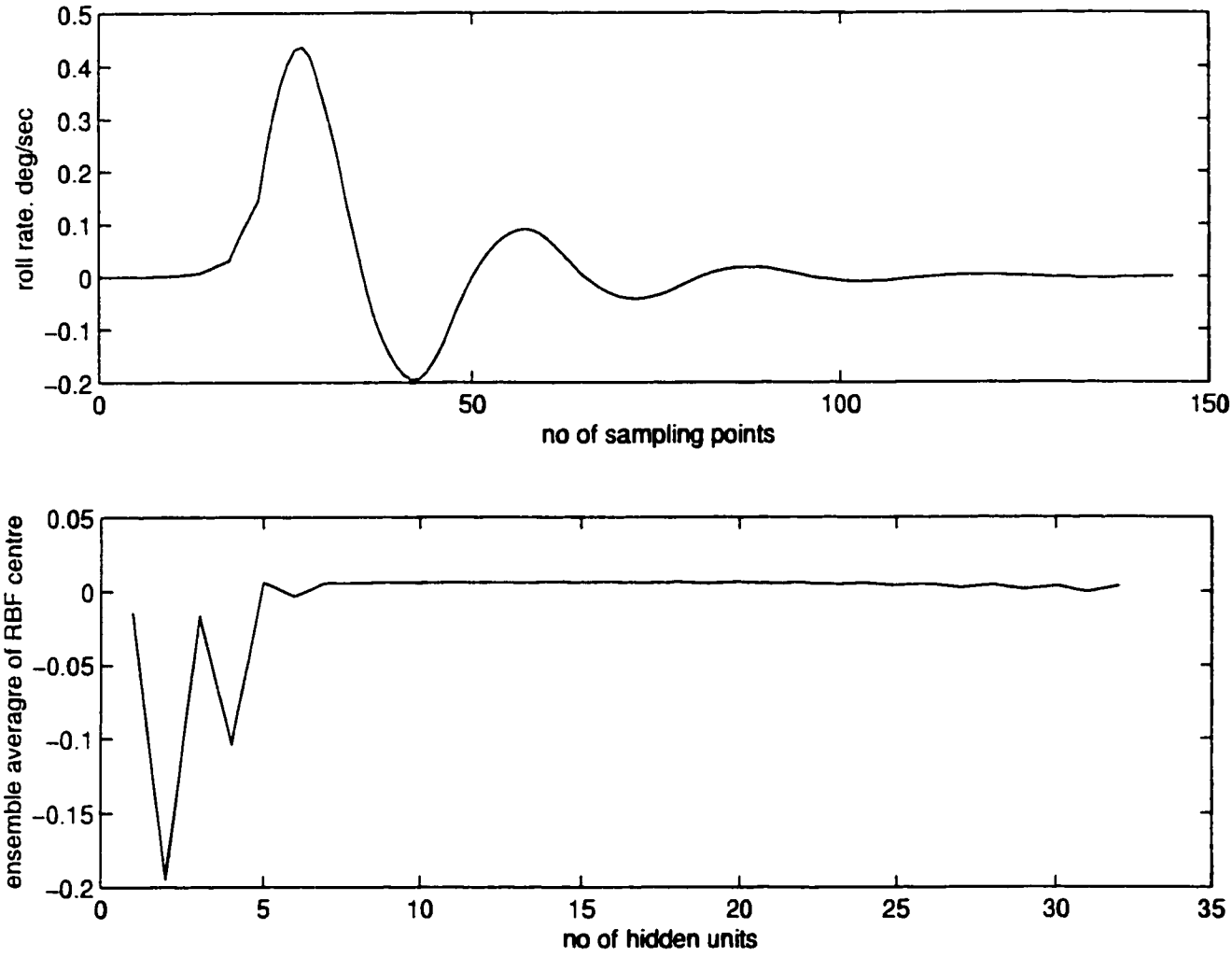

Figure 7.3: Supression of Wing rock and Ensemble Average of RBF Centre

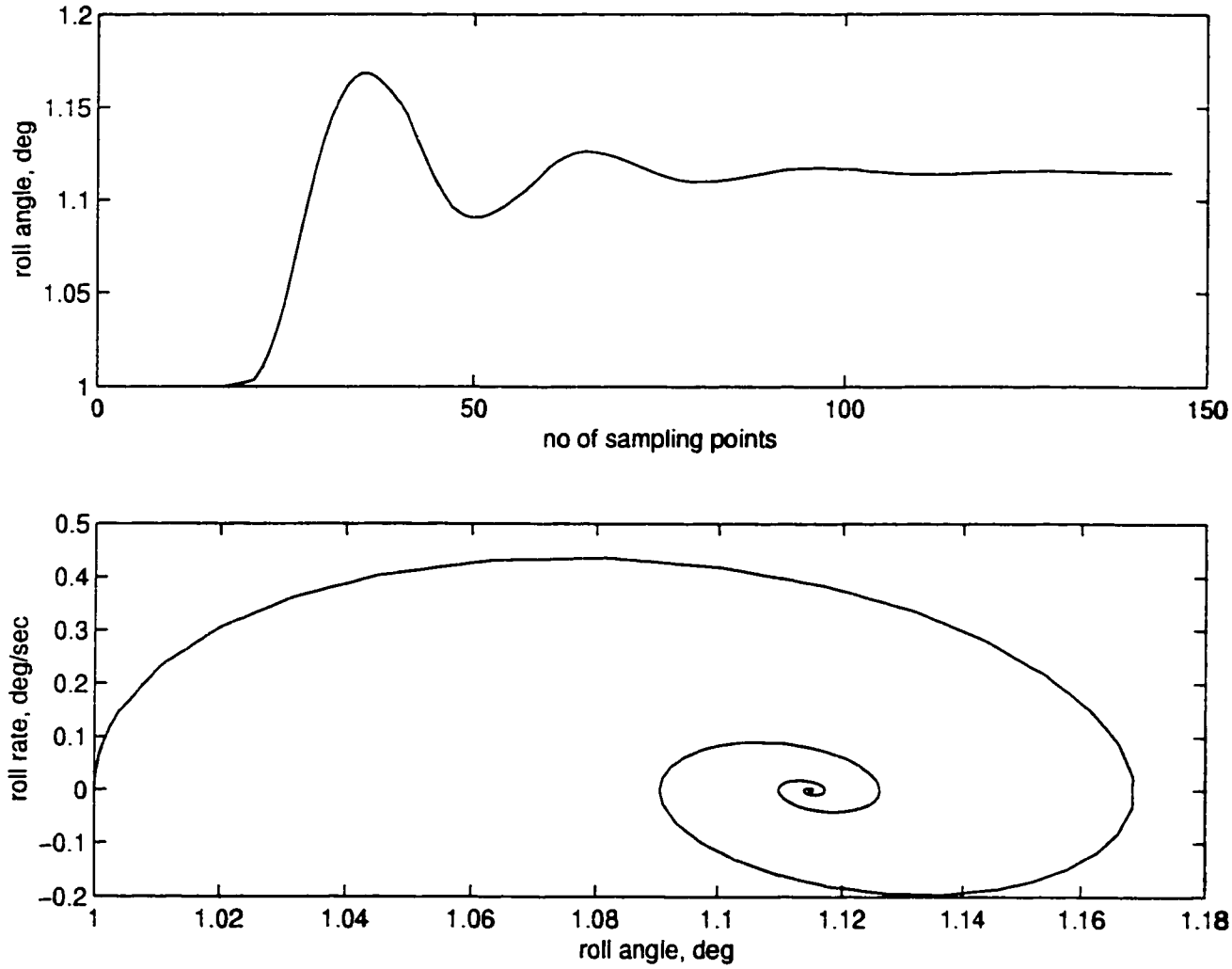

Figure 7.4: Wing rock suppression using dynamic RBF

7.1.3 Control of Wing Rock using Fixed RBF Networks

Based on the same wing rock model in slender delta wing in the previous section, suppression of wing rock is carried out using fixed number of neurons in the RBF networks. The purpose is to compare the results of using fixed networks and dynamic RBF networks based on the same control methodology.

7.1.4 Simulation

A RBF networks consists of 445 neurons in the hidden layer was used to control the wing rock in slender delta wing. The centres of the Gaussian function is chosen to be uniformly spaced according to the following choice.

$$u_i = j\triangle \tag{7.12}$$

where $\triangle = 0.009$, and $j \in \{-2, -1, ...1, 2\}$. The width of the Gaussian function is chosen to be one. The simulation was carried out with the sampling period $T_s = 0.05$. The following function is to be approximated by the RBF networks and the control law is chosen as before.

$$\hat{f}\ (x(k)) = f_o(x(k)) + \sum_{i=1}^{445} w_i(k)\Theta_i(x(k)) \tag{7.13}$$

where $\Theta_i(x(k))$ is given below.

$$\Theta_i(x(k)) = \exp(-\frac{1}{2}\left\|x_1 - u_i\right\|^2) \tag{7.14}$$

The control law is chosen as below

$$u = -\frac{1}{a_o} w(k)\ \Theta(x(k)) \tag{7.15}$$

The weight $w(k)$ is updated according to the following adaptation law

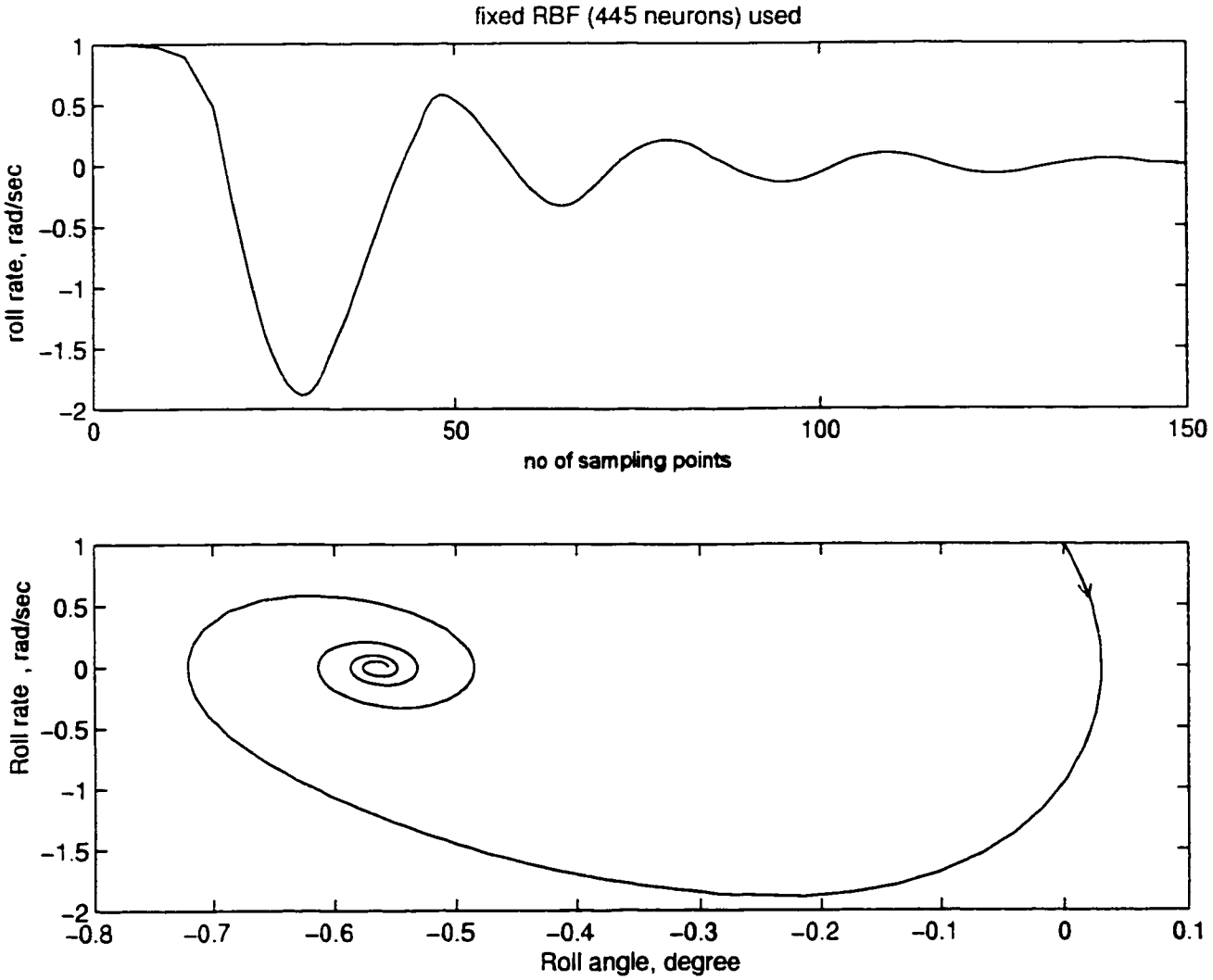

Figure 7.5: Closed loop response of wing rock (fixed RBF)

$$w(k+1) = w(k) - \frac{\eta}{r_k} e(k+1) J(k) \tag{7.16}$$

Figure 7.5 shows the suppression of wing rock in slender delta wing using the fixed number of neurons. It is noted that the response is more oscillatory. The phase plot shows that the roll rate converges to zero

7.1.5 Comparison of Dynamic and Fixed RBF Networks Performance

The simulations show that in the control design for dynamic RBF networks only the nonlinear function $f(x(k))$ needs to be approximated by the RBF networks. The feature that all the cells participate in the memory storage based on ensemble average of the centres is used as criterion for adding new neurons. For dynamic RBF, 32 neurons are required in the hidden layer as compared to the case of fixed RBF networks where 445 neurons are needed. In the static design of the RBF networks the centres are placed in the regular grids and often results in the huge number of neurons required to cover the input space. Moreover, in the dynamic RBF design, neurons are added as required and pruned if it becomes redundant. The mechanism for adjusting the centres and widths are provided by using the Extended Kalman Filter algorithm. The linear weights are separately estimated in both fixed and RBF networks using Lyapunov stability criteria for ensuring closed loop stability. The simulation results indicate that the wing rock was suppressed using both methods. Wing rock is suppressed in lesser time by using dynamic RBF design as shown in Figure 7.3 as compared to the case of fixed RBF design as shown in Figure 7.5 and the response is more oscillatory.

7.2 Control of Wing Rock in AFTI/F-16 Aircraft

In this section the developed dynamic recurrent RBF networks control methodology will be demonstrated to control the wing rock generated from AFTI/F-16 testbed aircraft having the similar delta wings configuration. Wing rock model development, design specification and simulation results will be discussed.

7.2.1 Wing Rock Model for AFTI/F-16

The AFTI/F-16 is the modified F-16A testbed aircraft for Air Force Systems Command's Advanced Fighter Technology Integration (AFTI) program. The testbed aircraft has a slender delta wing configuration, and the wing rock in delta wing has been tested by NASA Langley Research Centre [118] using the experimental wind tunnel model. Based on the experimental data the mathematical model was developed by Hsu & Lan [5]. Monahemi and Kristic [21] added additional factor characterizing the actuator control surface dynamics to the wing rock model.

The physical scale model of 80 deg sweep delta wing was mounted on apparatus that allows to rotate freely about the body fixed roll axis with no angular limitation. For a one degree of freedom system, the following model is obtained for $\alpha = 30$ deg.

Letting

$$\dot{\phi} = p \tag{7.17}$$

$$\dot{p} = (qSb / I_{xx}) [C_{lp\beta}(\alpha)\ \beta \sin\alpha + C_{lpp}(\alpha, \beta)\ (pb / 2V_{\infty})] \tag{7.18}$$

where :

α : angle of attack, deg

ϕ : roll angle in radian

p : roll rate in, rad/sec

q : dynamic pressure, lb/ft^2

S : wing surface area, ft^2

b : wing span, ft

I_{xx} : roll moment of inertia, $slug - ft^2$

V_{∞} : free stream air speed, $ft/\sec$

$C_{lp\beta}$: roll damping derivative due to sideslip β

C_{lpp} : roll damping derivative due to roll rate p

The following parameters are defined

$$\theta_2 = (qSb\,/\,I_{xx})\ (\sin\alpha)\ C_{lp\beta} \tag{7.19}$$

$$\theta_3 = (qSb\,/\,I_{xx})\ \ (b/2V_\infty)\ C_{lp\beta} \tag{7.20}$$

$$\theta_4 = (qSb\,/\,I_{xx})\ \ (b/2V_\infty)(-3.82) \tag{7.21}$$

where $\phi = 2\beta$. Monahemi and Krstic [21] added additional parameter θ_6 to account for the influence of aerodynamic control surface namely the rolling moment derivative because of the aileron coefficient $C_{l\delta_A}$ as defined as below

$$\theta_6 = (qSb\,/\,I_{xx})\ C_{l\delta_A}(\alpha,\beta) \tag{7.22}$$

For a high performance vehicle the $C_{l\delta A}$ must be large to accommodate large and rapid movement. The higher the value of $C_{l\delta_A}$ the better the suppression of wing rock. The control surface angle δ_A is included with aerodynamic coefficient. It is assumed that by including the aerodynamic control surface the coupling with other variables is not significant for the range the wing rock occurred. The aileron control surface is modelled as first order actuator dynamics as below

$$\dot{\delta_A} = -(1/\tau)\delta_A + (1/\tau)\delta_{ACOM} \tag{7.23}$$

where τ is a time constant and δ_{ACOM} is a control input u, a command aileron deflection in deg. With the added terms equation (7.18) is transformed into the following equation.

$$\dot{p} = \theta_1 + \theta_2\phi + \theta_3 p + \theta_4\,|\phi|\,p + \theta_5\left|\dot{\phi}\right|\dot{\phi} + \theta_6\delta_A \tag{7.24}$$

Let $\phi = x_1$, $\dot{\phi} = x_2$, $\delta_A = x_3$ and $\delta_{ACOM} = u$, the dynamics governing the wing rock

are given as below.

$$\begin{aligned} \dot{x} &= x_2 \\ \dot{x_2} &= \theta_1 + \theta_2 x_1 + \theta_3 x_2 + \theta_4 |x_1| x_2 + \theta_5 |x_2| x_2 + \theta_6 \delta_A \\ \dot{x_3} &= -(\frac{1}{\tau})x_3 + (\frac{1}{\tau})\delta_{ACOM} \end{aligned} \tag{7.25}$$

7.2.2 Dynamic Characteristics of Wing Rock

The aircraft under study is the Advanced Fighter Technology Integrated (AFTI) F-16 testbed aircraft. The aircraft has a slender delta wing that its wing rock dynamics is described by equations (7.17), (7.23) and (7.24). The following aerodynamic parameters are given in [21].

Mach number :0.6

Flight altitude : $39,000 ft$

Dynamic Pressure $(q) = 158.81, lb/ft^2$

Wing reference area $(S) = 300.0\ ft^2$

Wing mean aerodynamic cord $(c) = 11.32 ft$

Wing span $(b) = 30.0\ ft$

Trim velocity $(V_T) = 569.91\, ft/\sec$

Weight $(W) = 21,018.0\, lb$

Moment of Inertia $(I_{xx}) = 100033.4\ slug/ft^2$

Aileron deflection coefficient, $C_{l\delta_A} = -0.003489\,(1/\deg)$

Time constant $(\tau) = 0.0496 \sec$

The resulting parameters obtained by substituting the above aerodynamics constants are $\theta_2 = -32.748, \theta_3 = 1.436, \theta_4 = -5.481$ with $\theta_1 = 4$, $\theta_5 = 0.1$ and $\theta_6 = -0.49$.

Using the above parameters the dynamic characteristics of wing rock in roll angle

without control is shown in Figure 7.6 and the wing rock in roll rate is given in Figure 7.7. The phase plot and nonlinear damping are shown in Figures 7.8 and 7.9 respectively. The shape of Figure 7.9 is different from Figure 2.7 that the two loops are not symmetrical. At the small roll angle, ϕ the linear negative damping, $\dot{\phi}$ is still larger than nonlinear damping $\dot{\phi}\,|\phi|$, however at positive roll angles the linear negative damping values are much larger that nonlinear damping compared to the case for the negative roll angles. As the roll amplitude becomes larger, the nonlinear damping increases while the roll rate decreases. At $\phi \approx +0.8\ rad$ and $\phi \approx -0.6$ *rad* the net damping changes from negative to positive and restoring rolling moment drives the roll angle to the zero point. Figure 7.10 shows the rolling moment diagram indicating that there is a centre clockwise unstable hysteresis balanced by the two counterclockwise unstable loops. The net result is that the exchange of energy is balanced.

7.2.3 Controller Design Considerations

The dynamics of wing rock for AFTI/F-16 testbed aircraft from equation (7.25) can be written as below

$$\begin{aligned} \dot{x}_1 &= x_2 \\ \dot{x}_2 &= f(x_1, x_2, x_3) \\ \dot{x}_3 &= -(\frac{1}{0.0496})x_3 + (\frac{1}{0.0496})u \\ y &= x_1 \end{aligned} \tag{7.26}$$

where

$x_1 = \phi,\ \ x_2 = \dot{\phi},\ \ x_3 = \delta_A$ and $u = \delta_{ACOM}$

$f(x_1, x_2, x_3) = 4 - 32.748x_1 + 1.436x_2 - 5.481\,|x_1|\,x_2 + 0.1\,|x_2|\,x_2 - 0.49x_3$

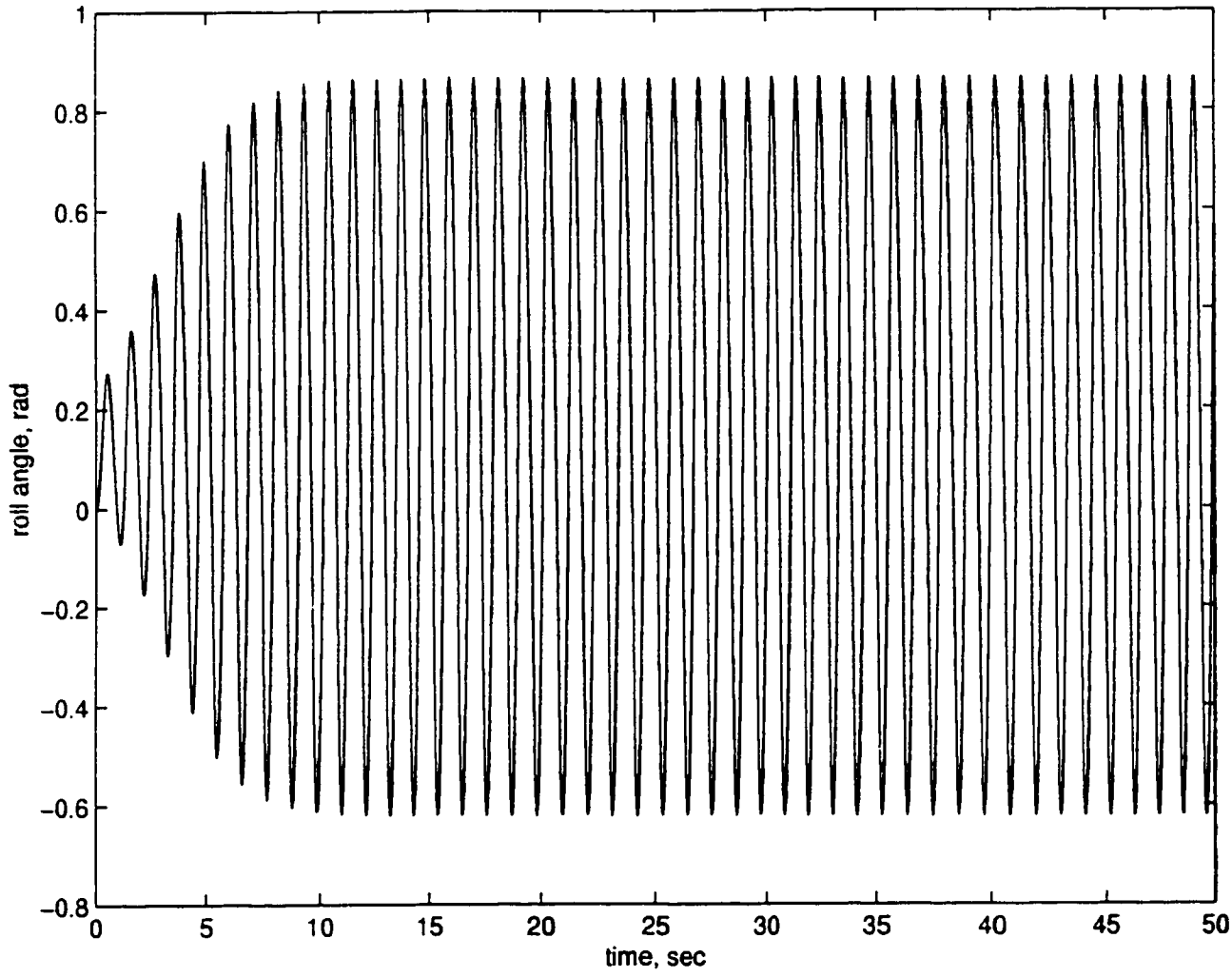

Figure 7.6: Wing Rock in AFTI/F-16 Roll angle

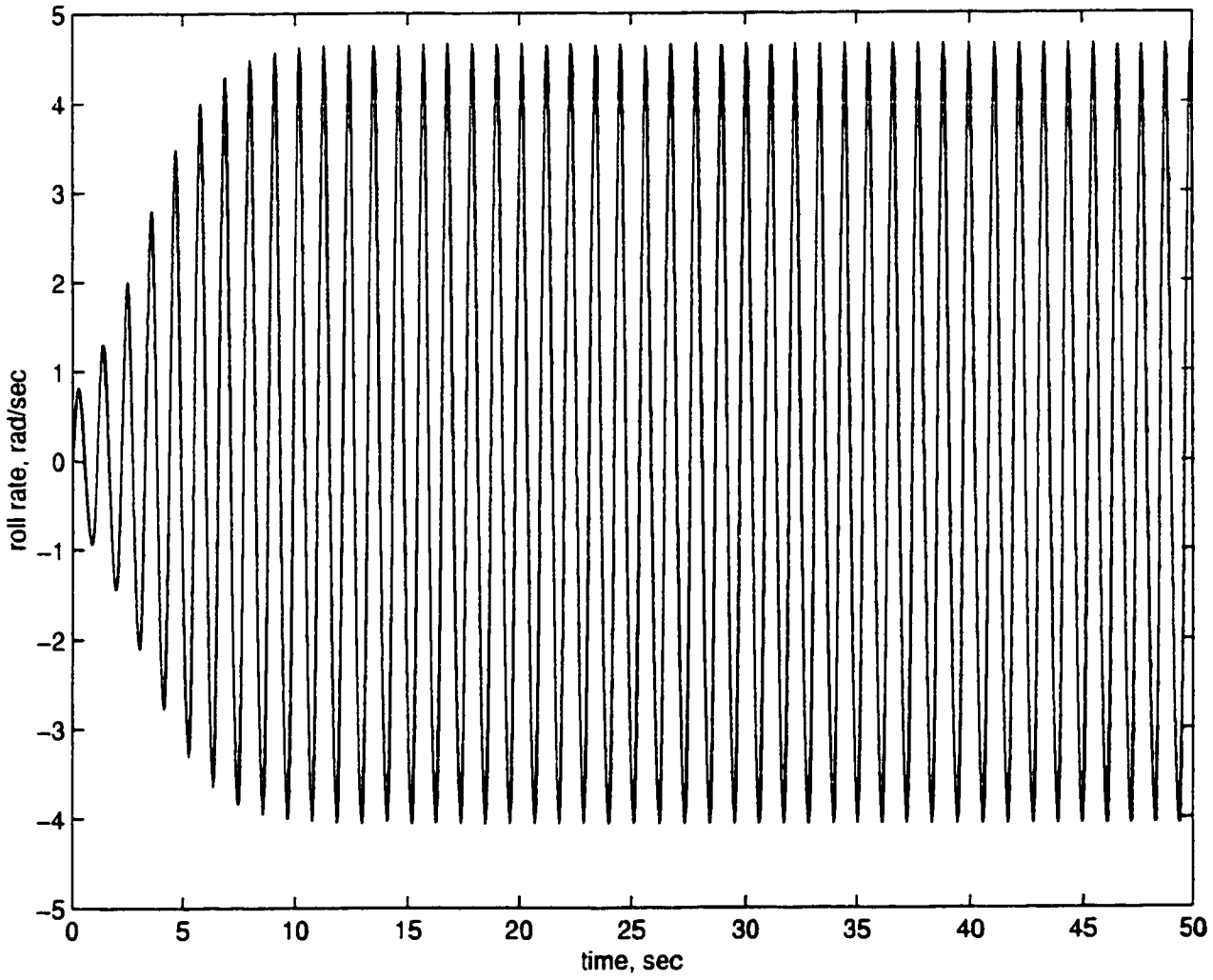

Figure 7.7: Wing Rock in AFTI/F-16 Roll Rate

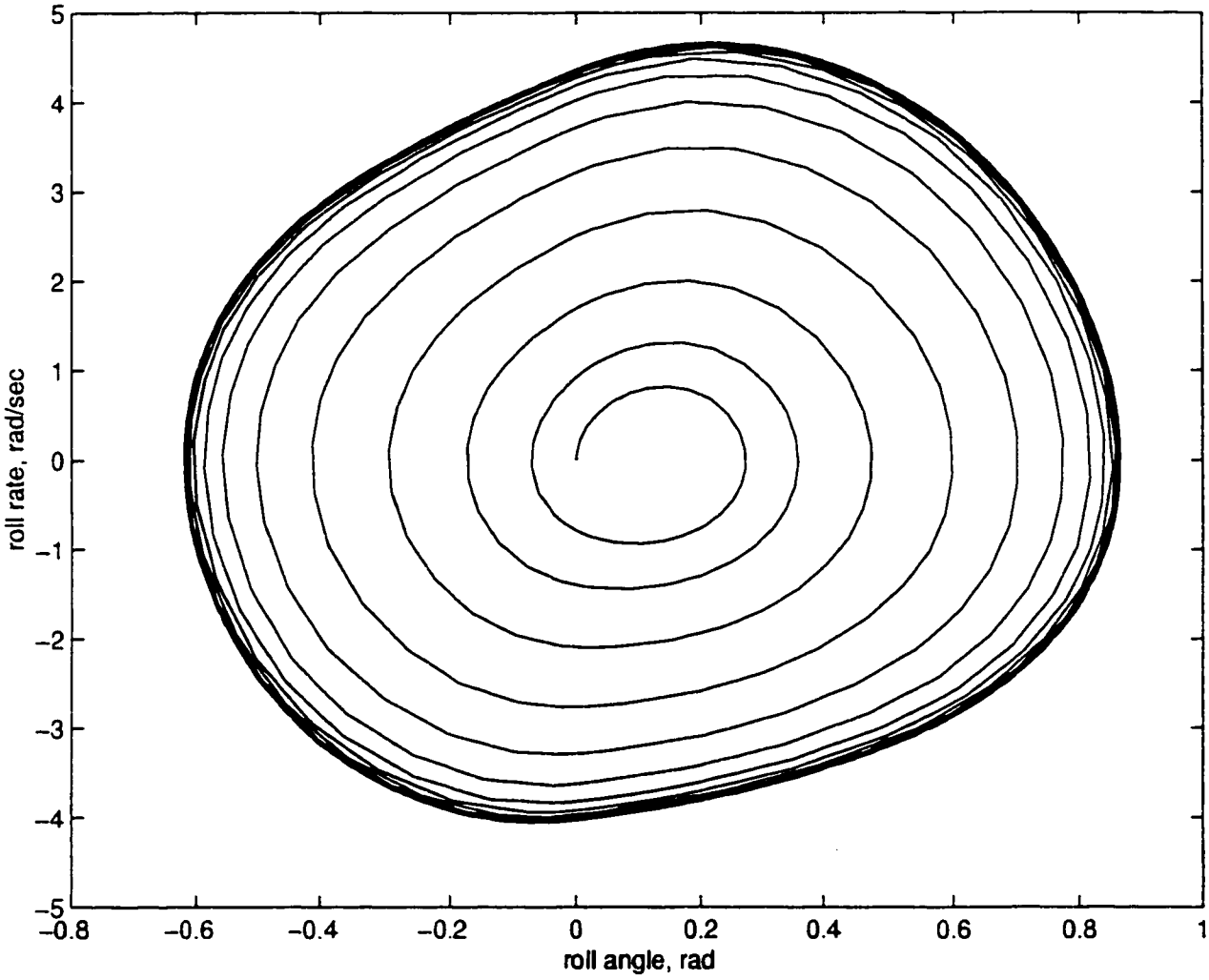

Figure 7.8: Phase Plot of Wing Rock in AFTI/F-16

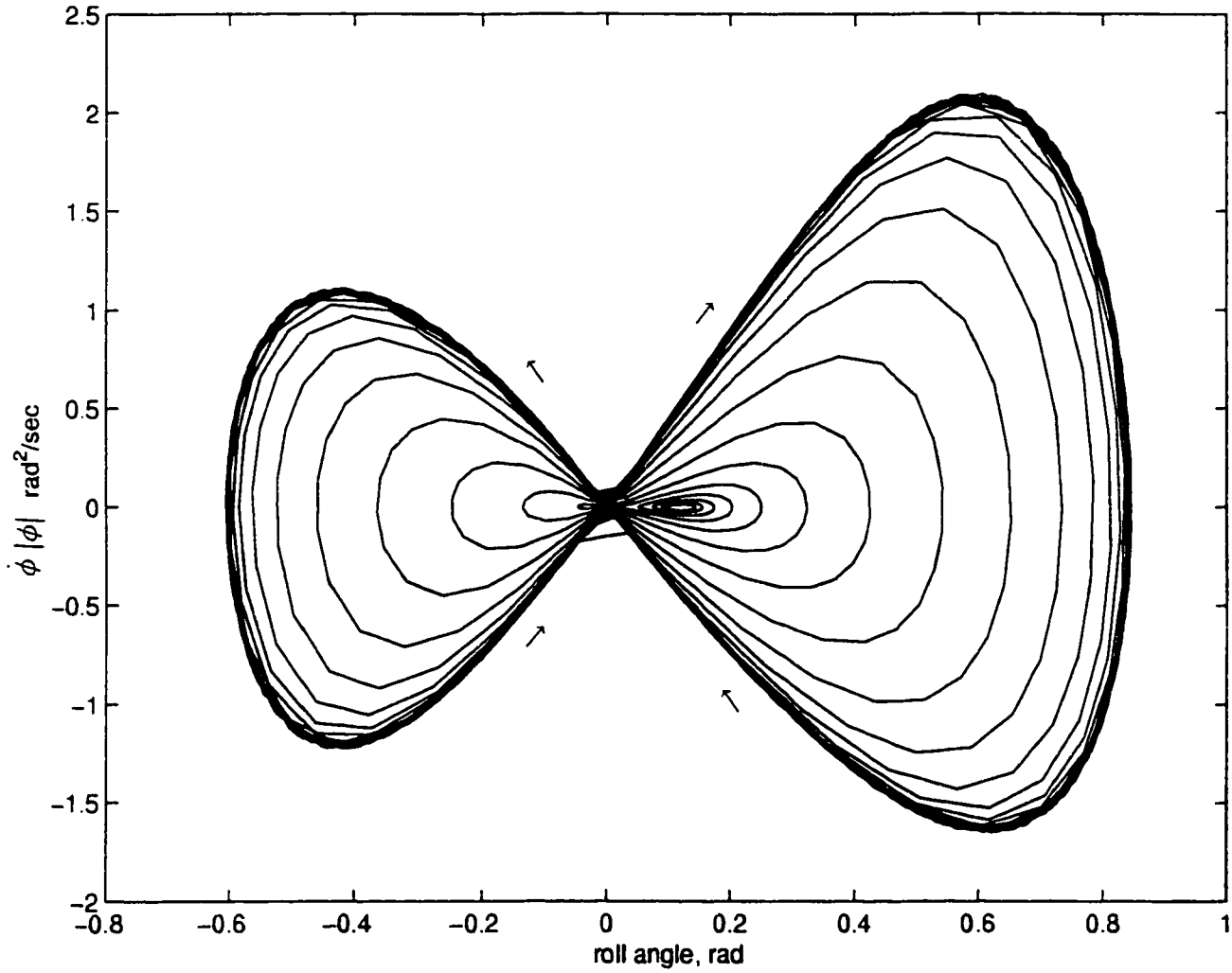

Figure 7.9: Nonlinear damping versus roll angle (AFTI/F-16 testbed aircraft)

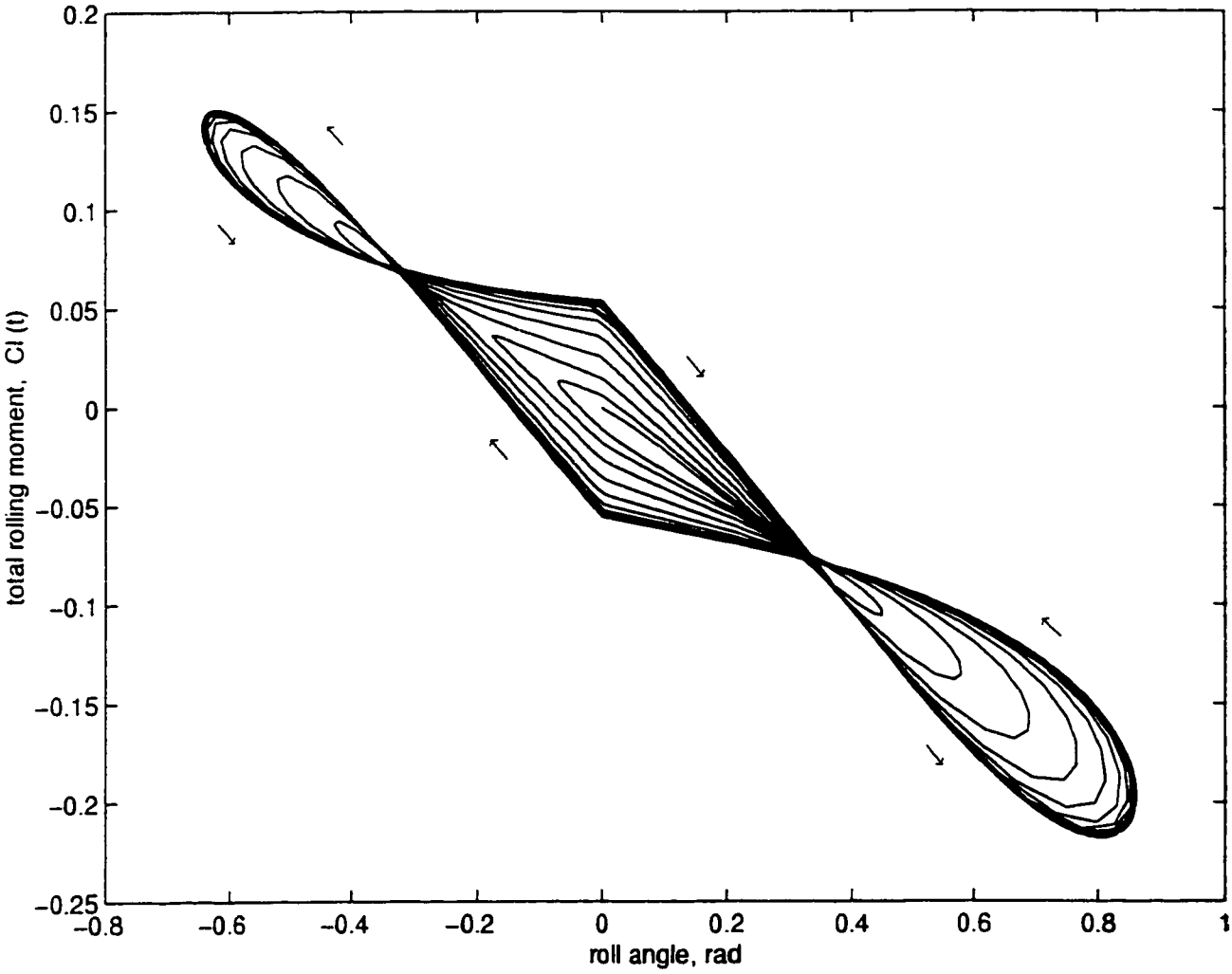

Figure 7.10: Rolling Moment diagram for AFTI/F-16 testbed aircraft

The system (7.26) can be written in compact form as below

$$\dot{x} = f(x,\theta) + g(x,\theta)u \tag{7.27}$$

where :

$$x = [x_1, x_2, x_3]^T \tag{7.28}$$

$$f(x,\theta) = \begin{bmatrix} x_2 \\ f(x_1,x_2,x_3) \\ -(\frac{1}{0.0496})x_3 \end{bmatrix} \tag{7.29}$$

$$g(x,\theta) = \begin{bmatrix} 0 & 0 & \frac{1}{0.0496} \end{bmatrix}^T \tag{7.30}$$

$$y = x_1 \tag{7.31}$$

Single input-single output system is considered and the transformation of the system (7.27) into sampled data input-output representation is carried out. Following the procedures as outlined in Section 6.2.1 in this thesis, with sampling rate of T_s = 0.05 sec and ZOH, the system (7.27) is transformed into a sampled data discrete time domain. The original system given in equation (7.26) has a strong relative degree $\gamma = 3$, hence, according to Narendra [99] the transformed discrete time system can be represented by the following input-output form.

$$y_{k+1} = f_o(.) + g_o(.)u_k \tag{7.32}$$

where $f_o(.)$ and $g_o(.)$ are differentiable functions defined as

$$f_o(.) = f(y_k, ..., y_{k-n+1}, u_{k-1}, ..., u_{k-n+1}) \tag{7.33}$$

$$g_o(.) \quad = \quad g(y_k, ..., y_{k-n+1}, u_{k-1}, ..., u_{k-n+1}) \tag{7.34}$$

In practice the non-linear functions $f_o(.)$ and $g_o(.)$ of the system is completely unknown and they are estimated by a pair of RBF networks based on the input-output signals from the physical system. The physical system is modelled by RBF networks given by.

$$\hat{y}\ (k+1) = \hat{f}\ (z(k), w_f) + \hat{g}\ (z(k), w_g)u(k) \tag{7.35}$$

where the unknown nonlinear functions $f_o(.)$ and $g_o(.)$ are estimated by two separate RBF networks $\Theta_f(z)$ and $\Theta_g(z)$ given by

$$\hat{f}\ (z(k), w_f) = f_o(z) + \sum_{i=1}^{K_f} w_{f_i}\Theta_{f_i}(z(k)) \tag{7.36}$$

$$\hat{g}\ (z(k), w_g) = g_o(z) + \sum_{i=1}^{K_g} w_{g_i}\Theta_{g_i}(z(k)) \tag{7.37}$$

The input vector is defined as state variable, roll rate $z(k)$ and the previous RBF networks prediction of the system output, the roll angle $\hat{y}\ (k-1)$ as a recurrent signal. The optimal size of the respective networks are namely K_f and K_g to be determined by the neurons growth during the training phase. The RBF networks free parameters μ_f, μ_g and σ_f, σ_g are adjusted by the Extended Kalman Filter according to equations (5.19), (5.20), (5.21) and (5.22).

At each time step the following control action is chosen in order to bring the tracking error to zero.

$$u(k) = \frac{-\hat{f}\ (z(k), w_f(k)) + r(k)}{\hat{g}\ (z(k), w_g(k))} \tag{7.38}$$

The reference command $r(k)$ starts from non zero initial condition and tends toward

zero as $t \rightarrow \infty$ and $w_f(k)$ and $w_g(k)$ are parameters of the recurrent networks used to approximate the function $f(z(k))$ and $g(z(k))$ and are updated using Lyapunov stability criteria for closed loop control according to equation (6.48).

The prior estimates of the functions are set at $f_o = 0.1$ and $g_o = 0.2$, the learning rate of the two Gaussian networks during the training phase are chosen as $\eta_f = 0.8$ and $\eta_g = 0.8$. The threshold values employed are $\epsilon_{\max} = 0.4$, $e_{\min} = 0.012, e_{rms} = 0.012$, $\epsilon_n = 0.2$. The various constants used in the Extended Kalman Filter are $\kappa = 0.85$, $R_n = 1.0$, $Q_f = 0.002$, $Q_g = 0.002$, $P_f = 1.0$, $P_g = 1.0$

7.2.4 Simulation Results

Figure 7.11 shows the closed loop response of roll angle and roll rate based on the dynamic RBF control methodology. The transients in both roll angle and roll rate stabilizes in 2 sec to steady zero value. The phase diagram given in Figure 7.12 shows the roll angle and roll rate converge to the neighborhood of zero and the control input is given in Figure 7.13

Figure 7.14 shows the evolution of neurons growth in f and g nets. The f networks selects 10 neurons while the g networks gives 32 neurons. Both f and g-networks have a same input signals consist of roll rate and recurrent signal from the whole RBF network output. Each separate networks are trained independently and their growth rate are different as shown in Figures 7.14. The term $u(k)$ is included for the g-networks in the parameter updating equation (5.19). The neurons addition/pruning strategy are governed by the criteria given in equations (5.7), (5.8), (5.9) as well as (5.32), (5.33) and (5.34).

Figure 7.15 shows the error between the estimated output and the physical system output converges to zero. Figures 7.16 shows the estimated RBF outputs for f-net and g-net respectively. Figures 7.17 and 7.18 show the distribution of the distance between input vector and the centres for f net and g net respectively. The distribution

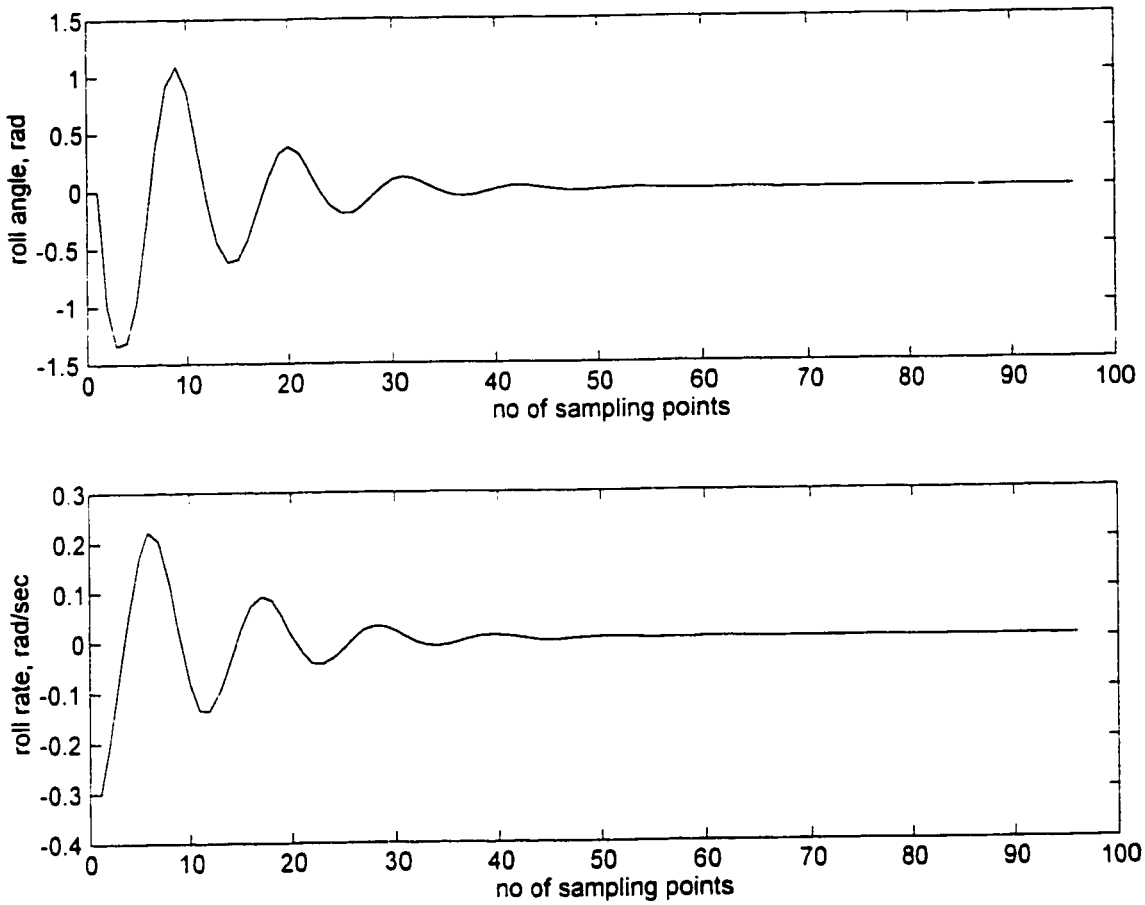

Figure 7.11: Closed loop control based on dynamic RBF control strategy

of RBF widths for f and g networks are shown in Figure 7.19.

7.3 Robustness Analysis

In this section the robustness analysis of the closed loop dynamic recurrent networks will be given and guidelines regarding the potential application will be provided. Figure 7.20 shows the structure of feedback control in the presence of unmodeled dynamics and disturbances. In general, system uncertainties may result from unmodeled dynamics, nonlinearities, time variances and external disturbances or measurement

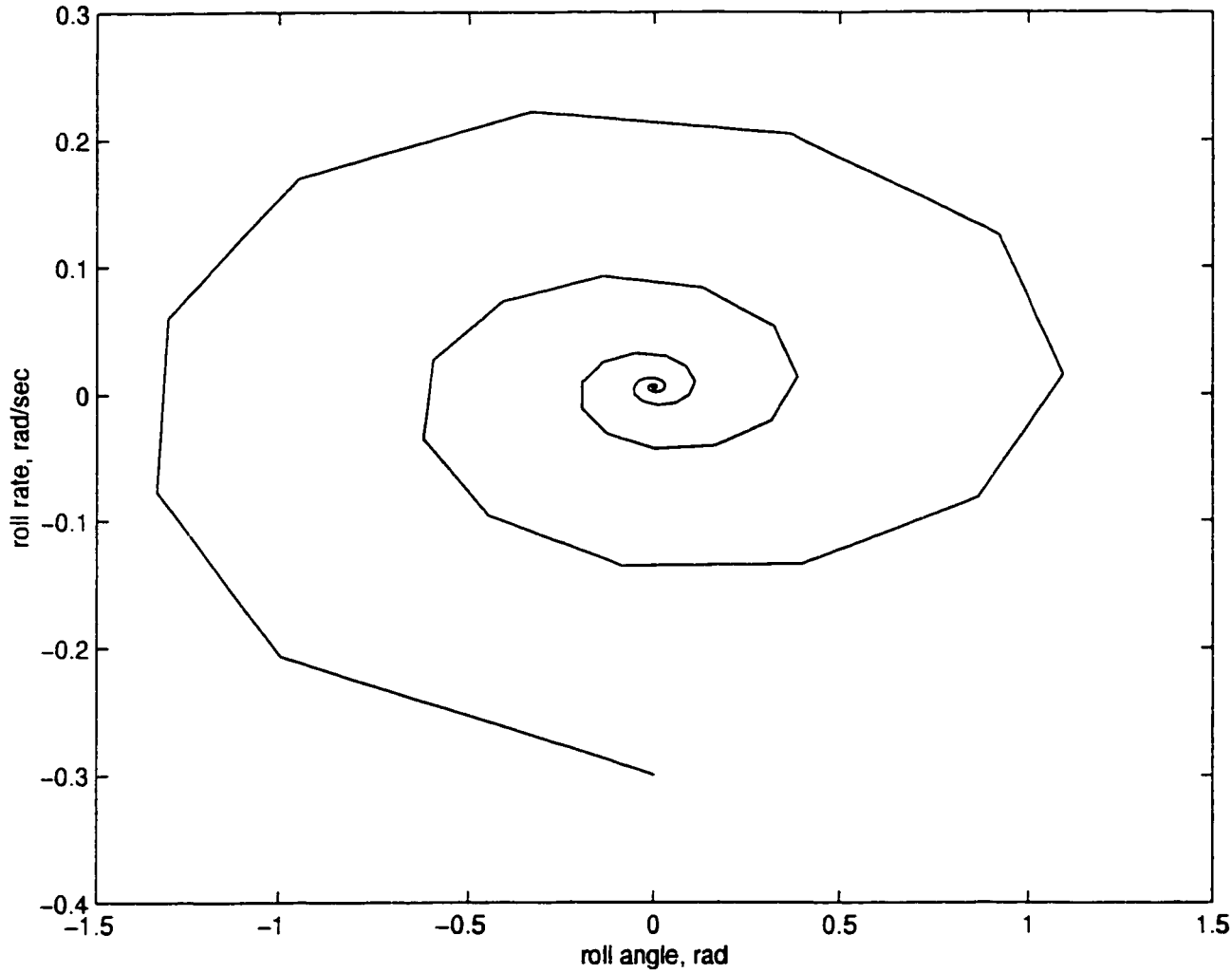

Figure 7.12: Phase plot of roll angle and roll rate

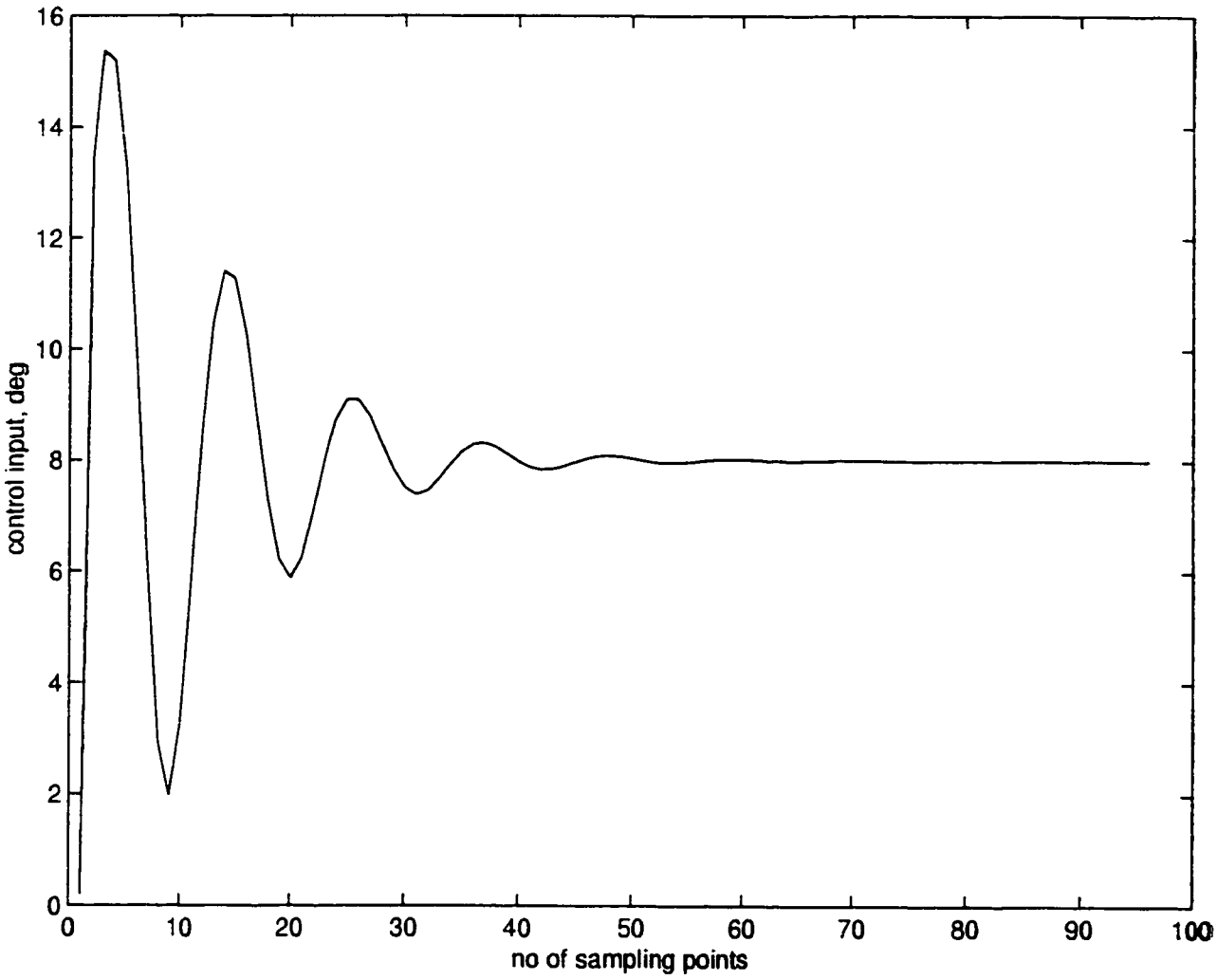

Figure 7.13: Control input for dynamic RBF control strategy

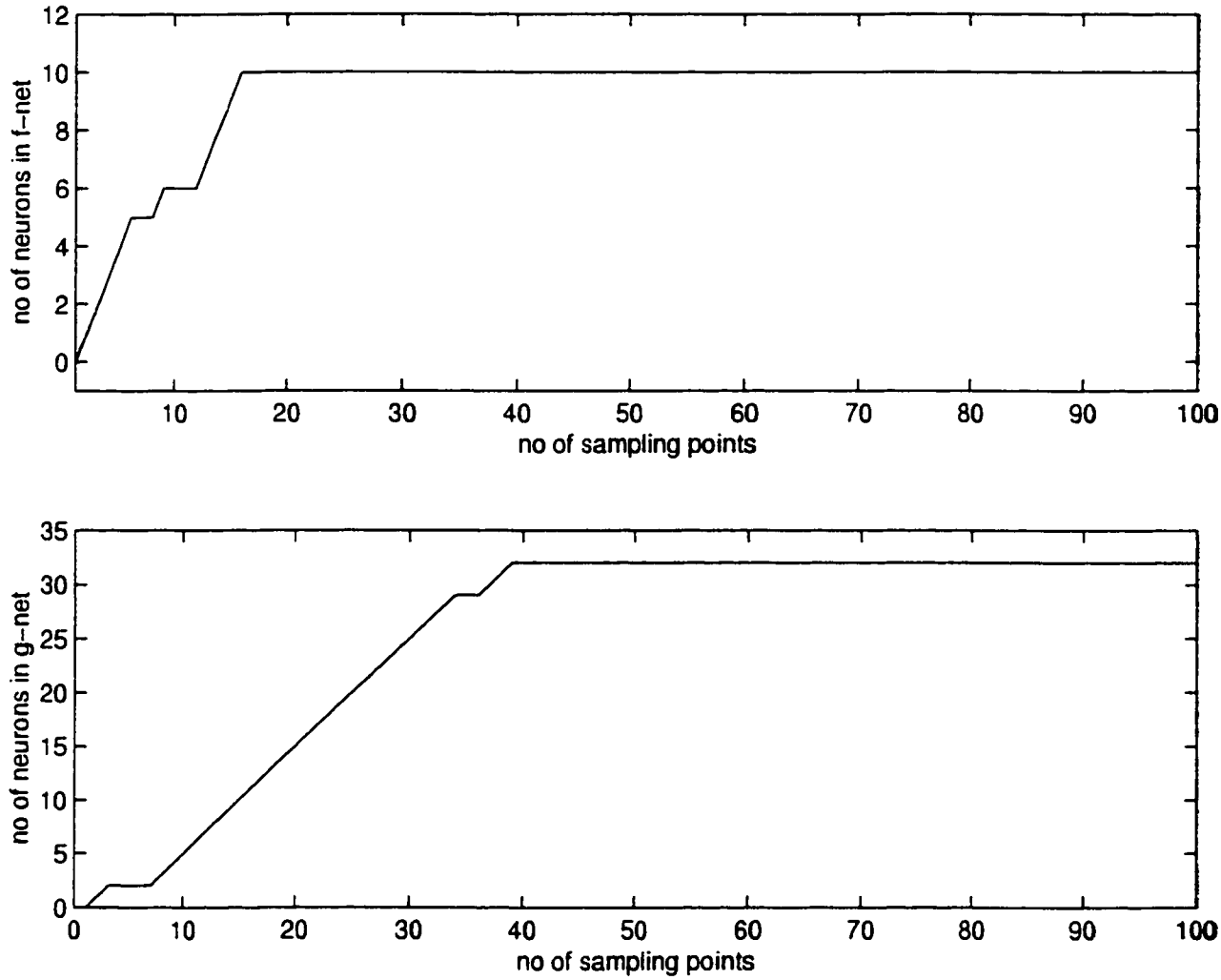

Figure 7.14: Evolution of neurons growth in f and g nets

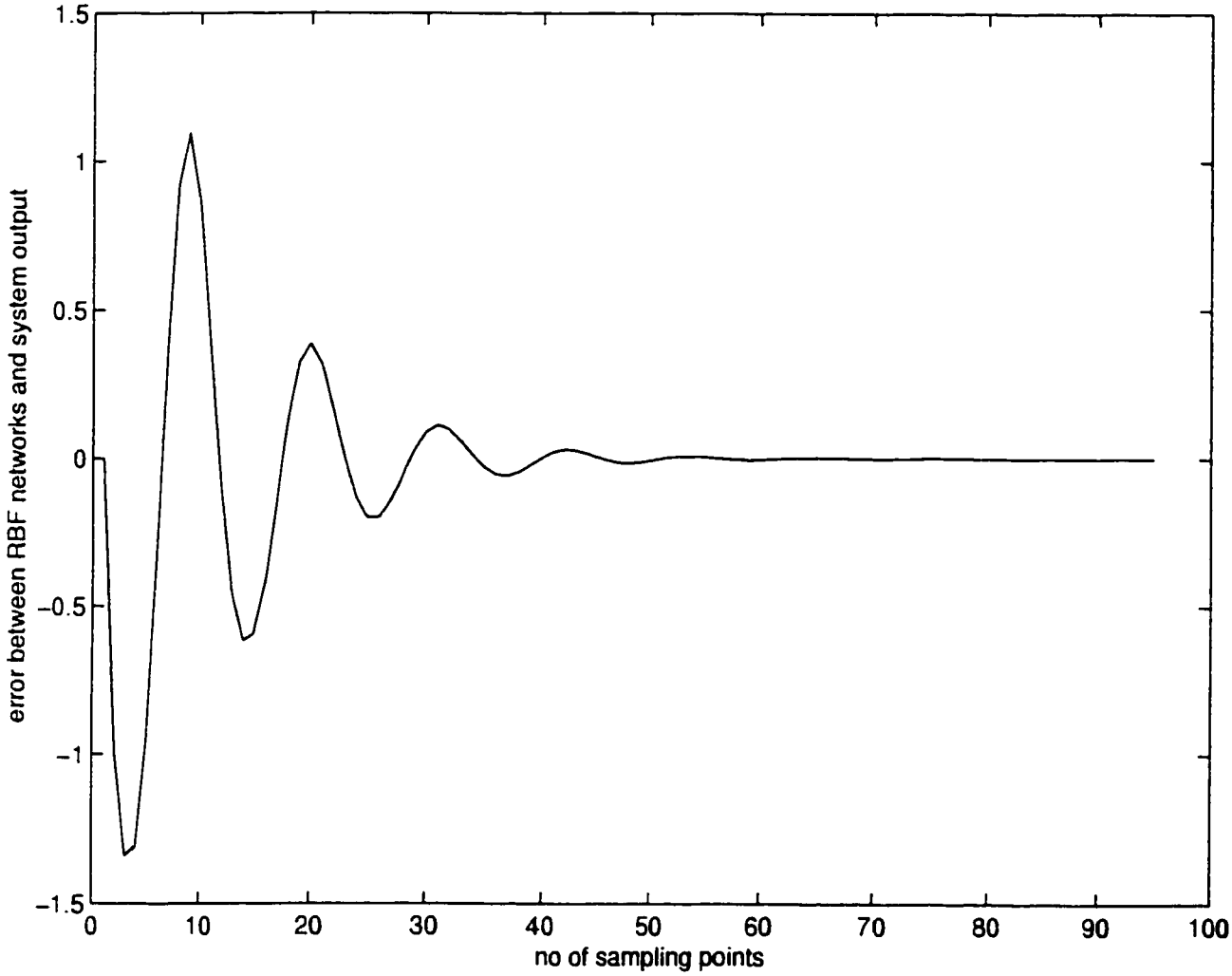

Figure 7.15: Error between RBF networks output and system output

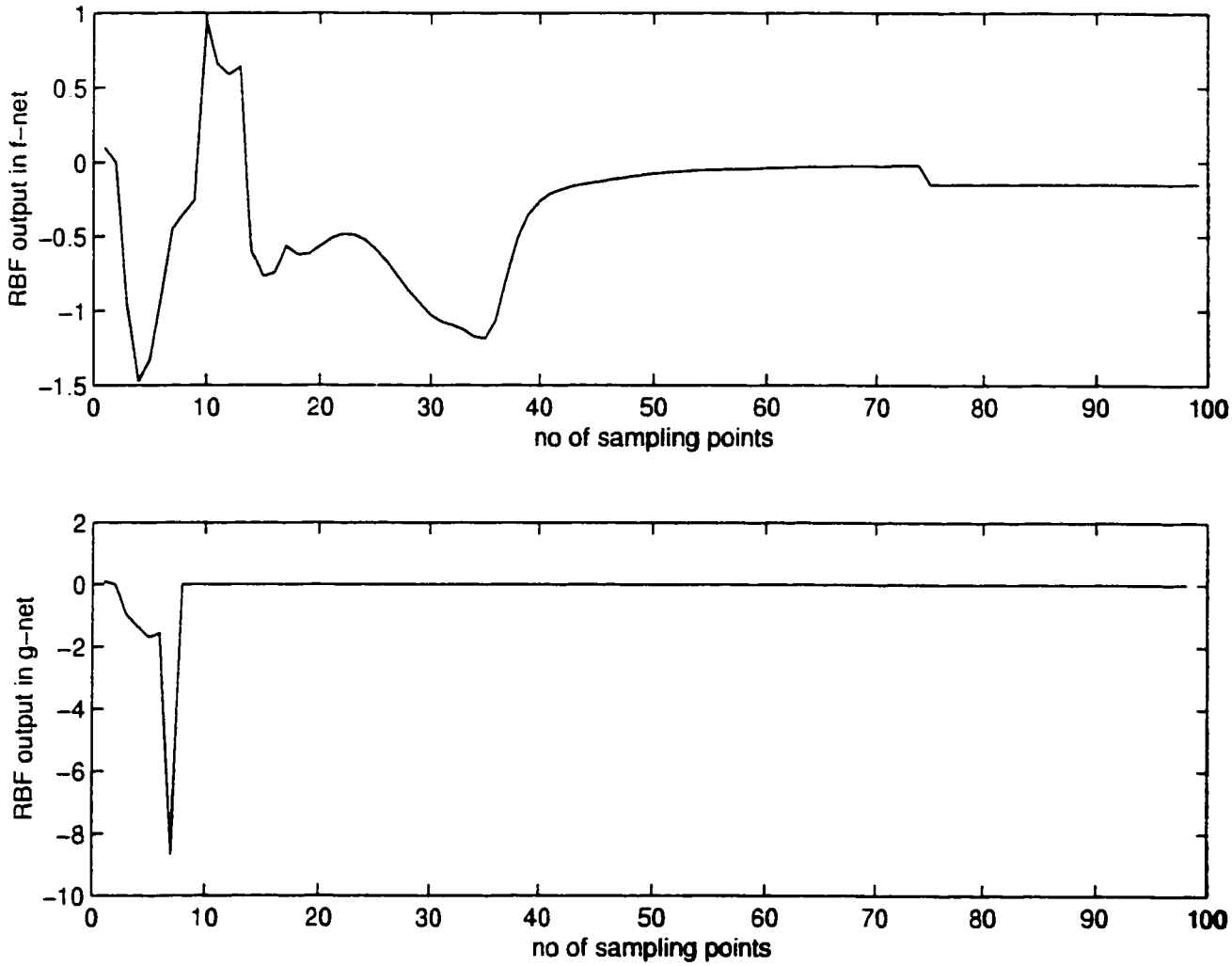

Figure 7.16: RBF estimated outputs in f-net and g-net

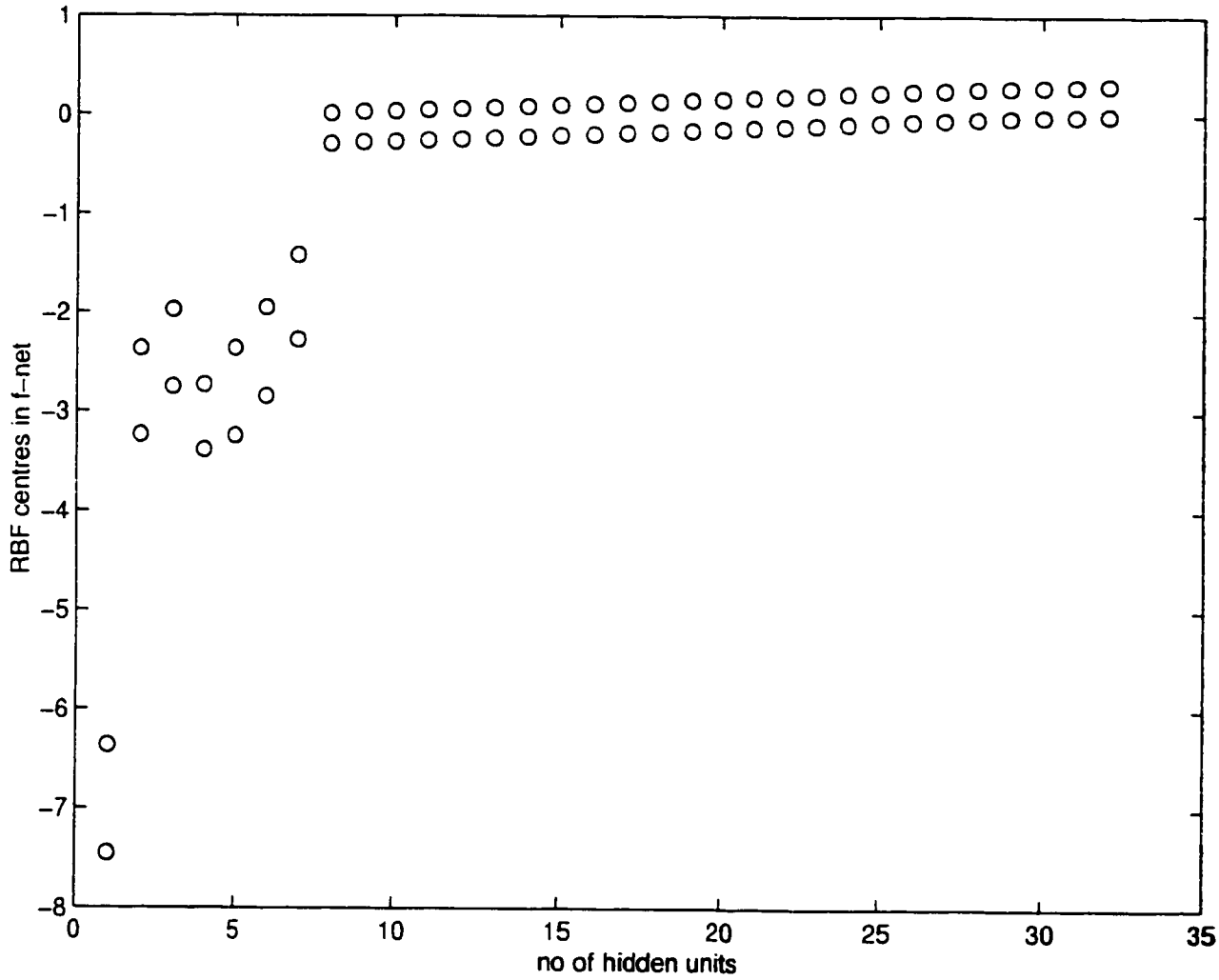

Figure 7.17: Distribution of Distance between input vector and centre values (f-net)

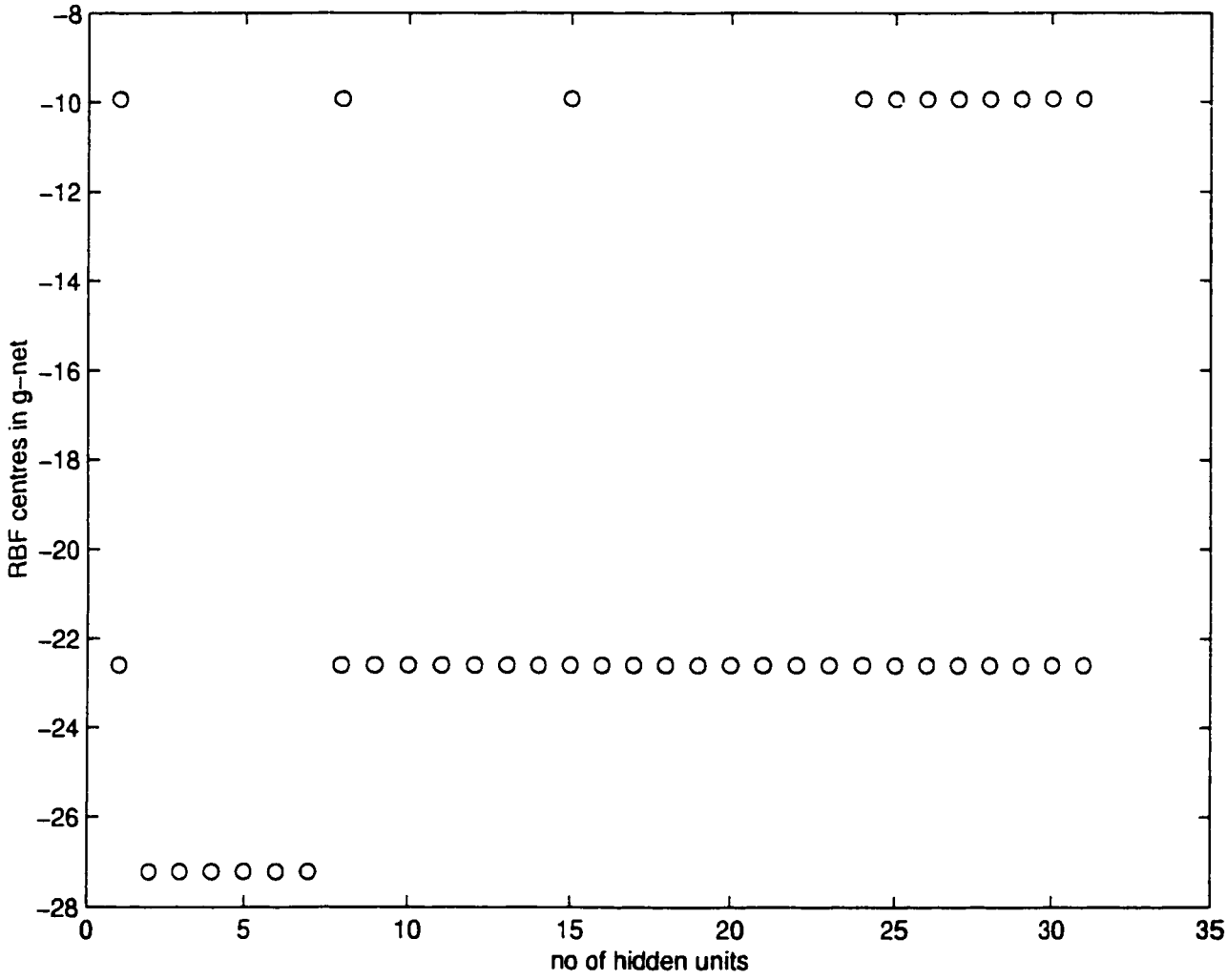

Figure 7.18: Distribution of distance input vector and centre value (g-net)

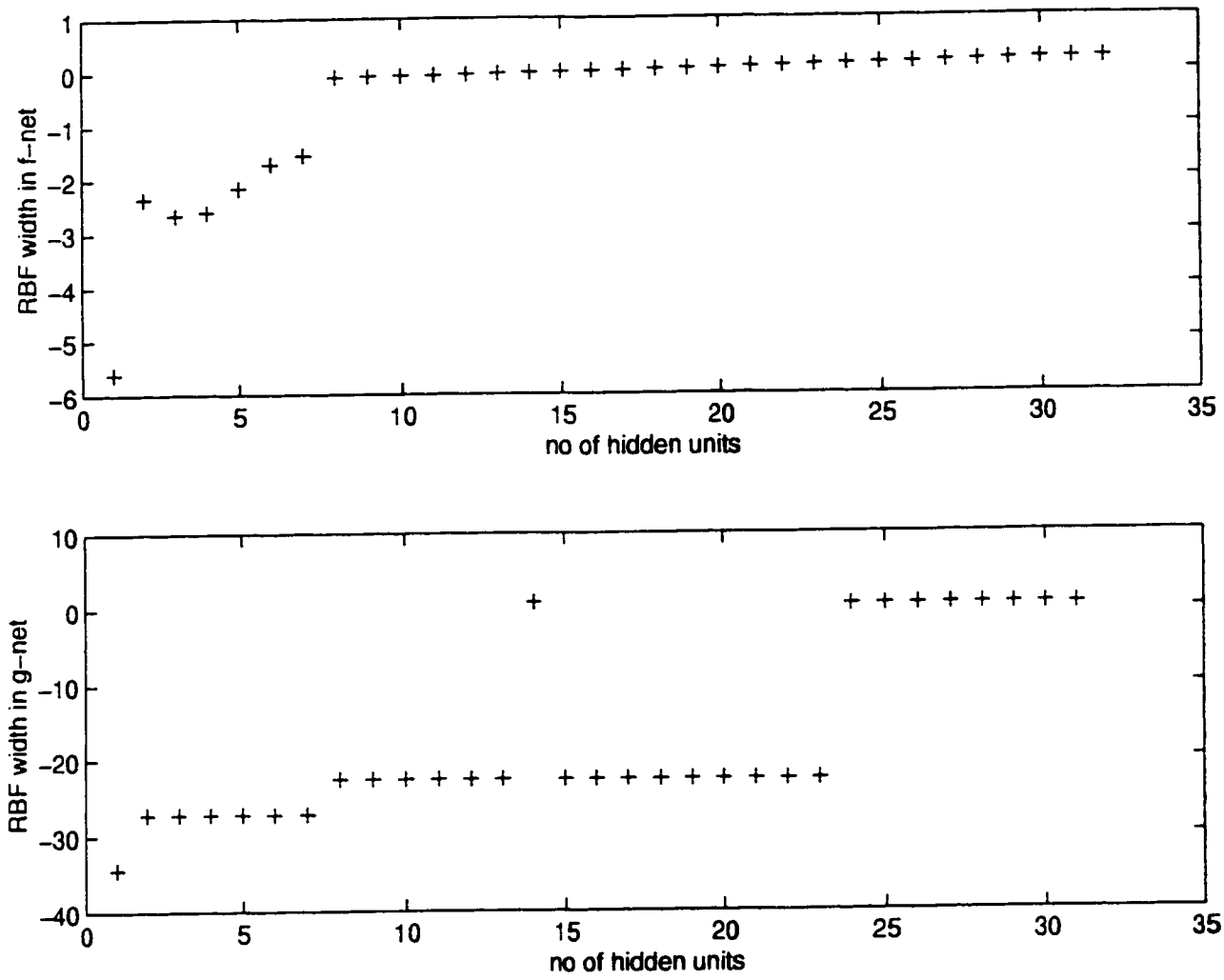

Figure 7.19: Distribution of widths in RBF f -net and g-net

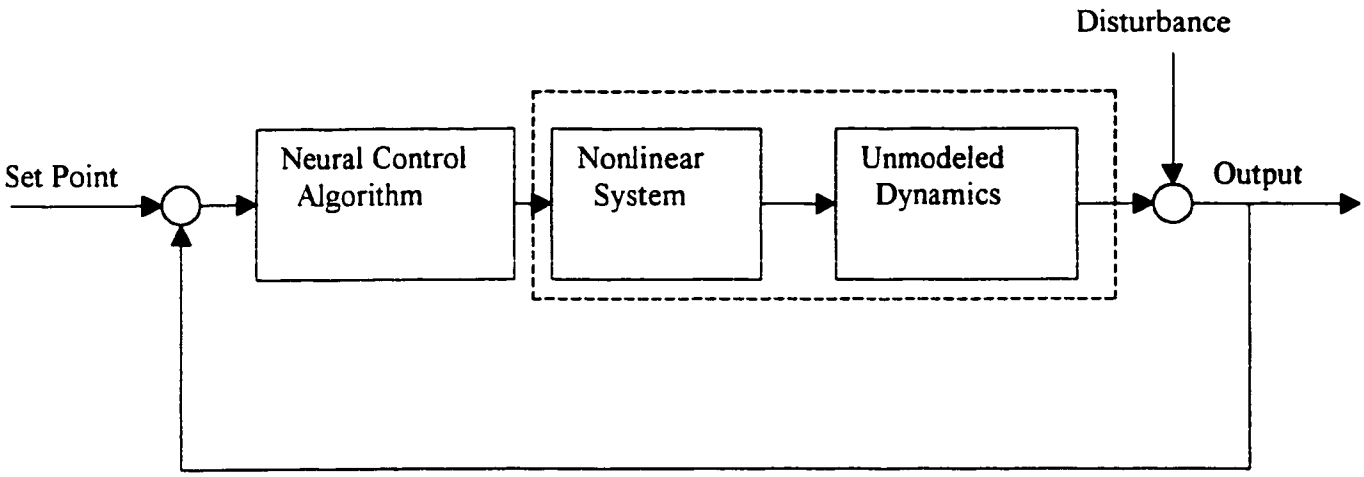

Figure 7.20: Unmodeled Dynamics and Measurement Noise

noise. In the design of the dynamic recurrent RBF controller, the essential concept of the Preisach model and physical insights of the wing rock generated from the aircraft were incorporated. The analysis of the tolerance of the performance of the recurrent dynamic RBF controller under different system perturbations will be given. Finally the guidelines for design considerations to deal with the system uncertainties will be outlined and issue of the potential practical application will be addressed.

7.3.1 Robustness to Disturbances

The disturbances under study are unmodeled excitations of the aircraft caused by external disturbances such as wind gust or measurement noises of various sensors. The effect of these disturbances are collected and represented at the system output as shown in Figure 7.20. In the dynamic recurrent RBF controller, the introduction of the recurrent feedback signal is mainly motivated by the concern of the incompleteness of the knowledge of the system which generates the wing rock and to account the effect of the dynamic characteristics of the disturbances.

7.3.2 Simulation 1

In this simulation the study is carried out to examine the robustness of the recurrent RBF controller in the presence of disturbances. Random disturbance is introduced to the system and the conditions for various parameters used in the simulation are as below.

$\epsilon_{\max} = 0.4$, $e_{\min} = 0.012$, $\epsilon_n = 0.2$, $e_{rms} = 0.012$, $\kappa = 0.85$, $R_n = 1.0$, $Q = 0.002$, $P_o = 1.0$, $f_o = 0.1$, $g_o = 0.2$, $T_s = 0.05\,\text{sec}$

The same aircraft model AFTI/F-16 employed in section 7.2.4 is used to generate the wing rock. Figure 7.21 shows the response of the closed loop control of roll angle in the presence of disturbance. The roll rate and control input are shown in Figure 7.22. The result indicates the controller is capable to suppress the wing rock and shows robustness in the presence of disturbances. Figure 7.23 shows the evolution of neurons growth in f and g nets, it was noted that the growth pattern of neurons in g-net increases to 65 and then decreases to 37. Figure 7.24 shows the distribution of the distance between the inputs and RBF centres and the distance stabilizes near the minimum value of zero. The corresponding distribution of widths of the RBF units is shown in Figure 7.25. The RBF parameters in respective f and g networks shown in Figure 7.26 both stabilize towards minimum zero.

The growth pattern of f and g nets are influenced by the randomness of the disturbance signal included in the system. The threshold values used in $e_{\min}$, ϵ_n and e_{rms} are in the same magnitude as the change of random signal. The final number selected by the networks are considered sufficient to bring the suppression of the wing rock to a satisfactory level as shown by the response in roll angle and roll rate. The RBF centres and width are clustered towards minimum zero.

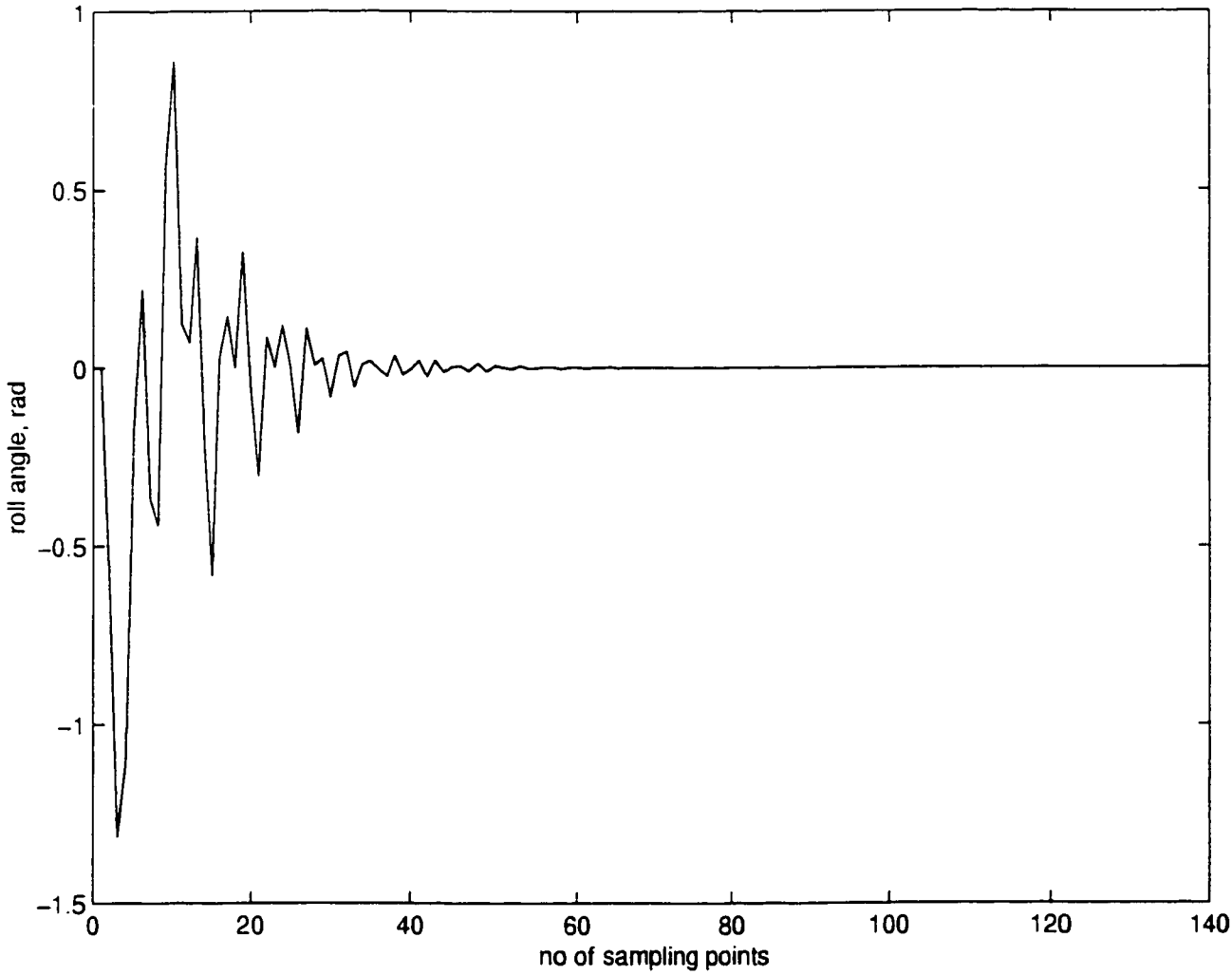

Figure 7.21:Closed loop response of Roll angle

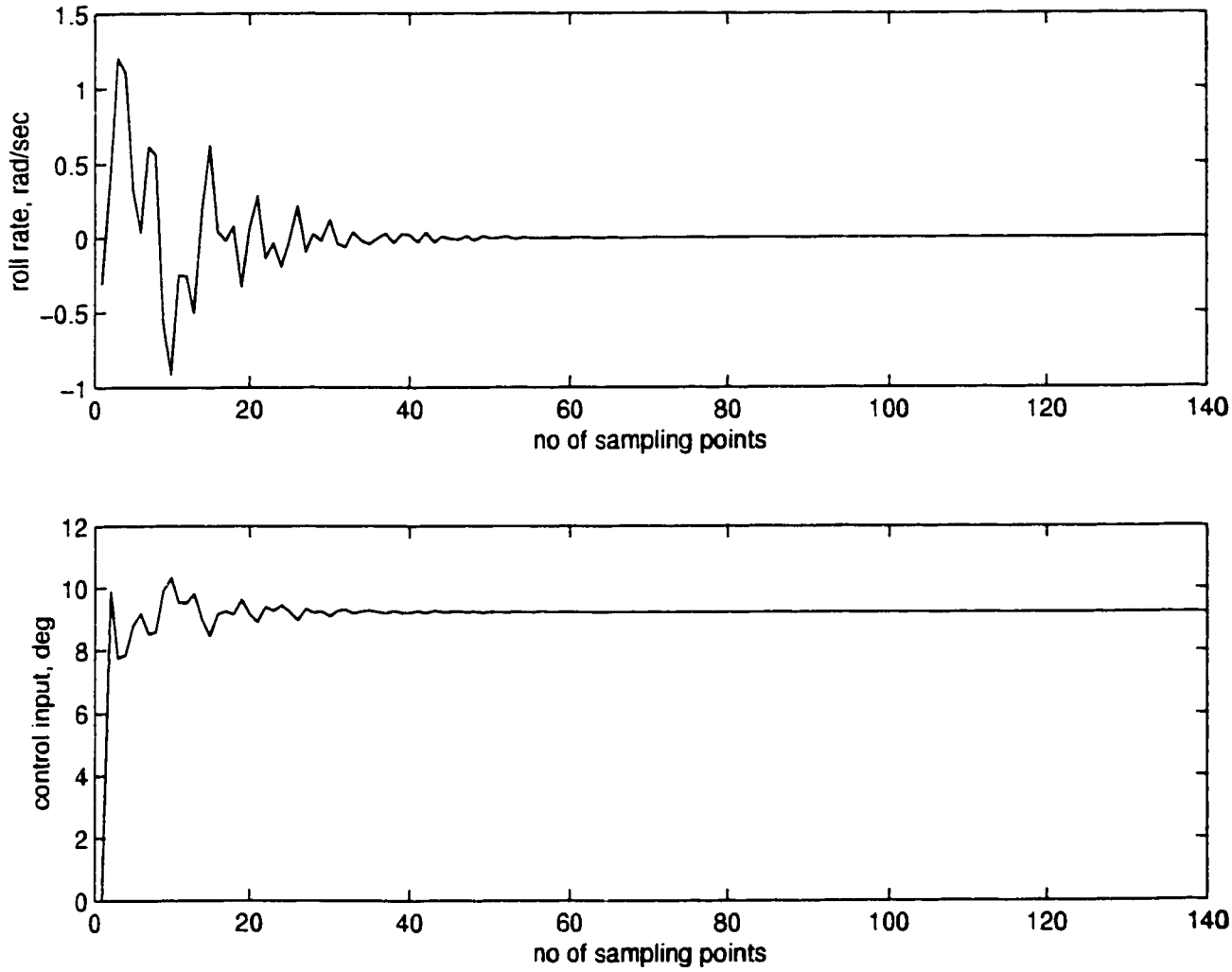

Figure 7.22: Closed loop roll rate and control input

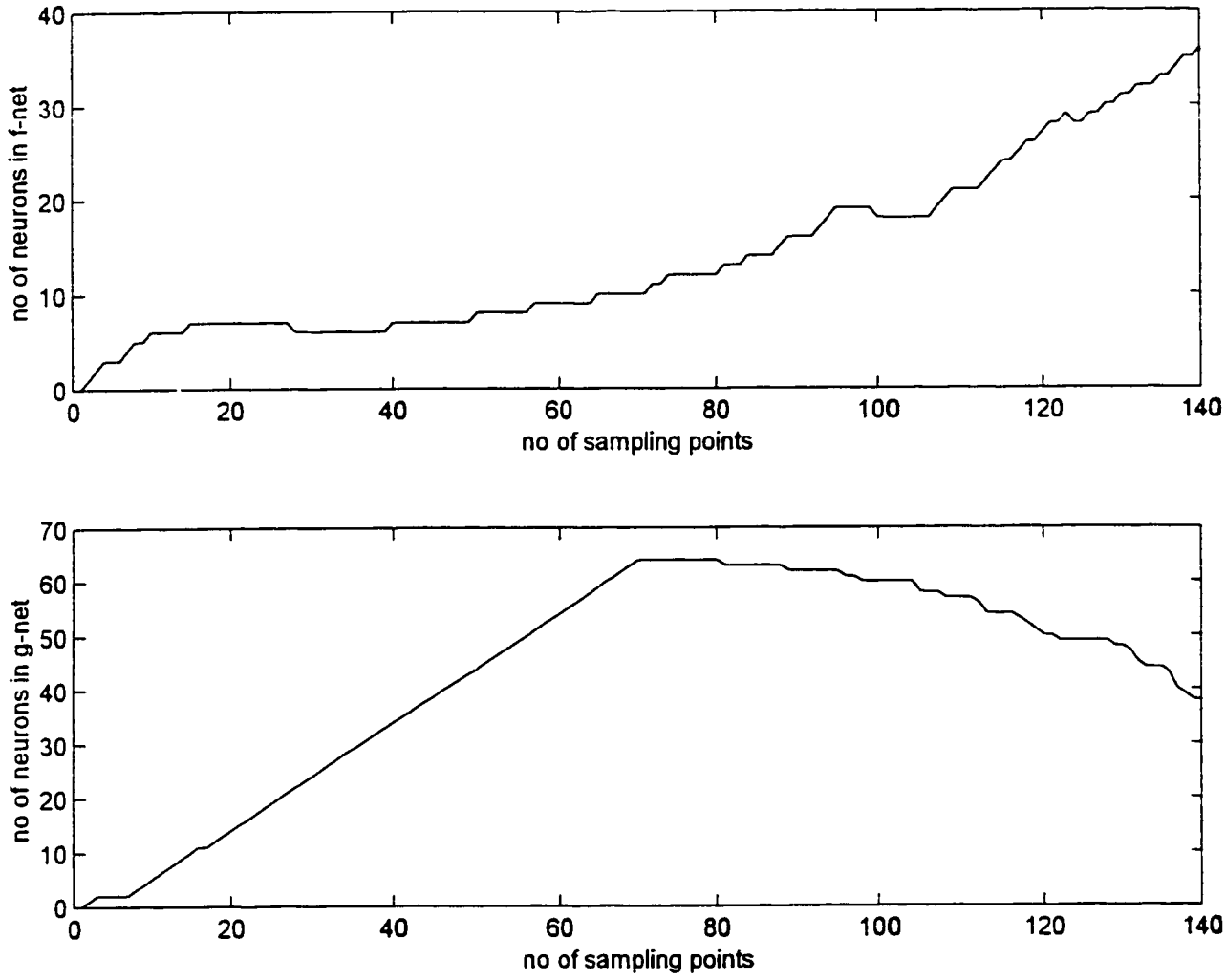

Figure 7.23: Evolution of neurons growth in f.-g nets (with disturbance)

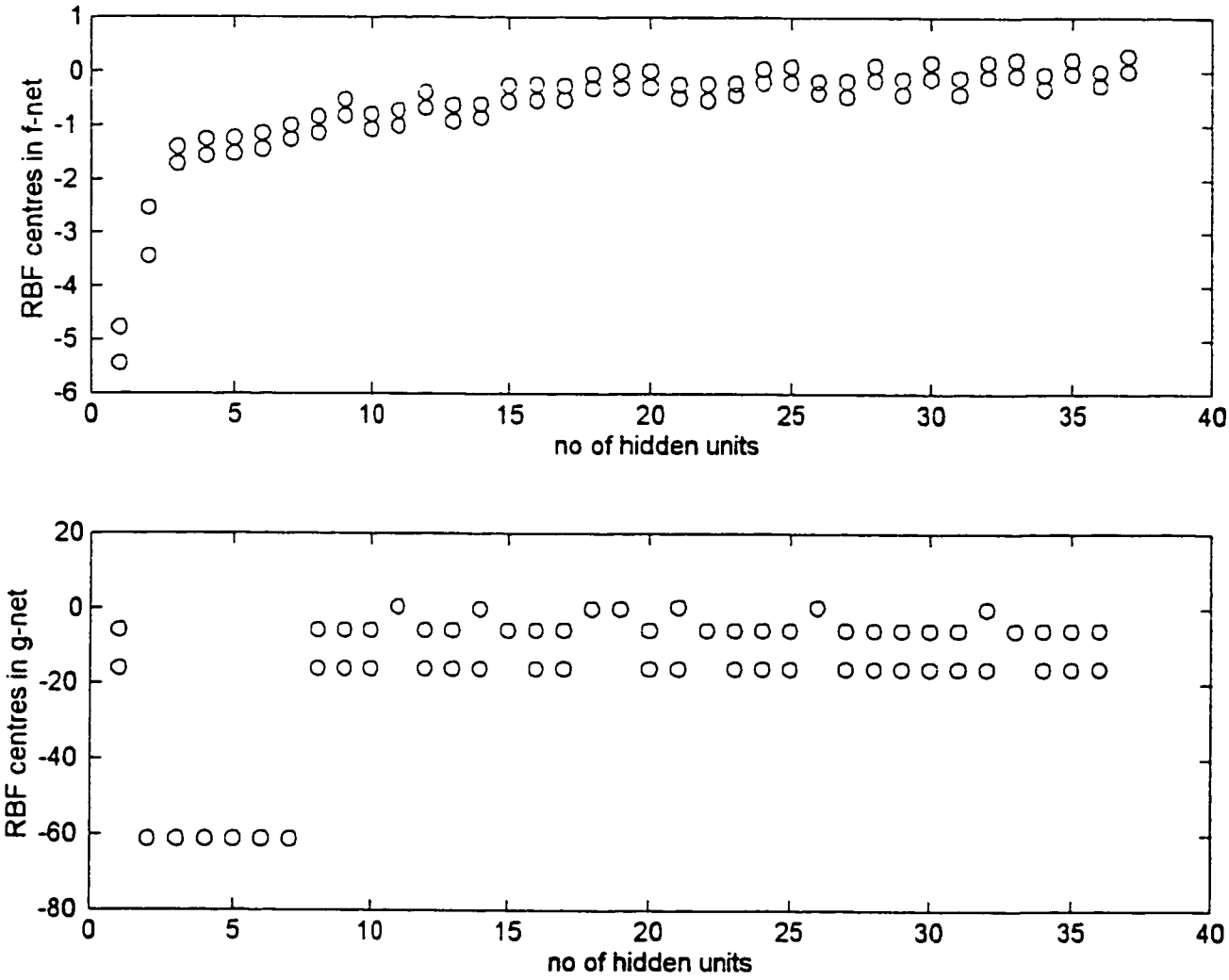

Figure 7.24: Distribution of distance to RBF centres in f-g nets

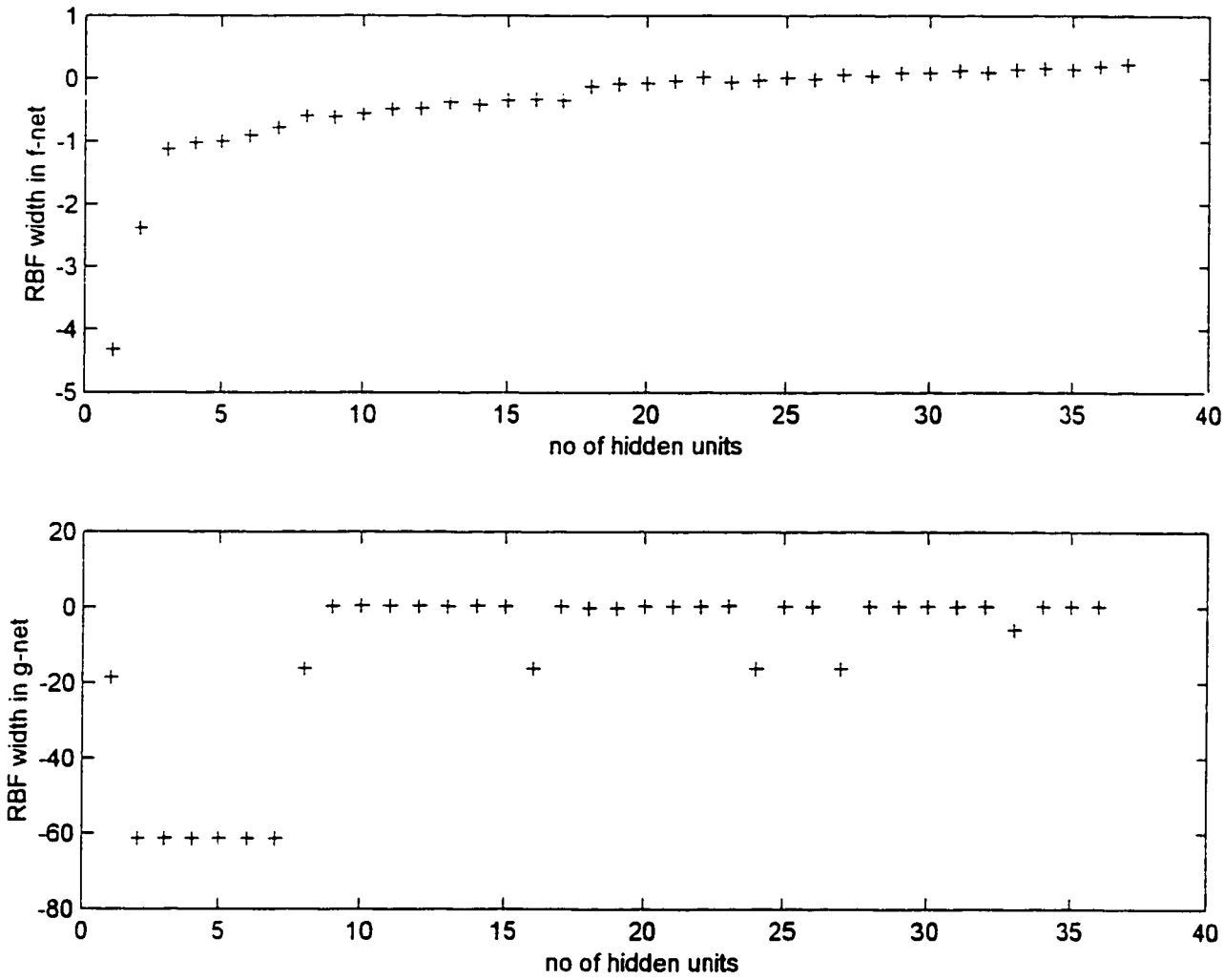

Figure 7.25: Distrubution of RBF widths

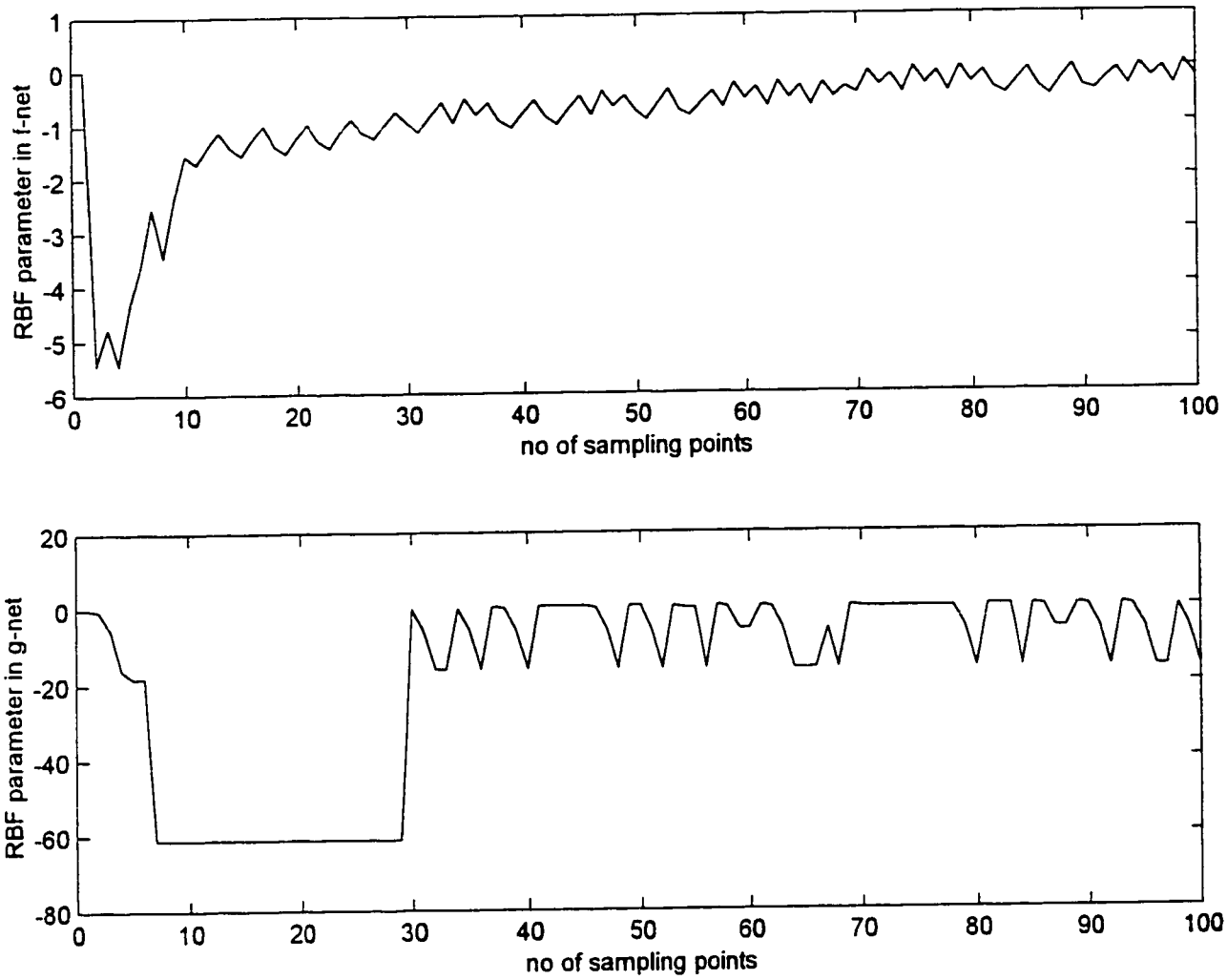

Figure 7.26: RBF parameters in f-g nets

7.3.3 Robustness to Unmodeled Dynamics

In the following simulations the robustness feature of the recurrent RBF controller will be examined with respect to model uncertainties. Model uncertainties can be caused by *parametric uncertainties* and *structural uncertainties*. The *parametric uncertainties* relates to the deviations, nonlinearities and time variances of parameters while *structural uncertainties* are due to imperfect structure of the model. The developed recurrent RBF networks was based on properties of the Preisach model which deals with the general hysteresis system exhibiting limit cycle phenomena. Through simulations, the developed recurrent RBF controller will be tested for robustness under various aspects of model uncertainties. For simulating the *structure uncertainties* we had introduced the dynamics of Coulomb friction, transport delay and second order dynamics in the model.

7.3.4 Simulation 2

The generation of wing rock depends very much on factors such as angle of attack, flight conditions, flight envelops, aerodynamic parameters, types and configurations of the aircraft etc. The existence and generation of the wing rock is sensitive to the variations of these parameters and depends very much on the prevalence of the right conditions. In this study, simulation is carried out to examine the generation of wing rock with respect to the variations of parameters used in AFTI/F-16 testbed aircraft model. The following parameter is selected for the study.

$$\theta_2 = (\bar{q}\, Sb / I_x)\, (\sin\alpha)\, C_{l\beta} \tag{7.39}$$

By decreasing the angle of attack α from 30 deg in θ_2 to 8.7 which corresponds to the change of θ_2 from 1.436 to 0.436, the wing rock motion disappears as shown in Figure 7.27. When the angle of attack was increased from 30 deg upwards the wing

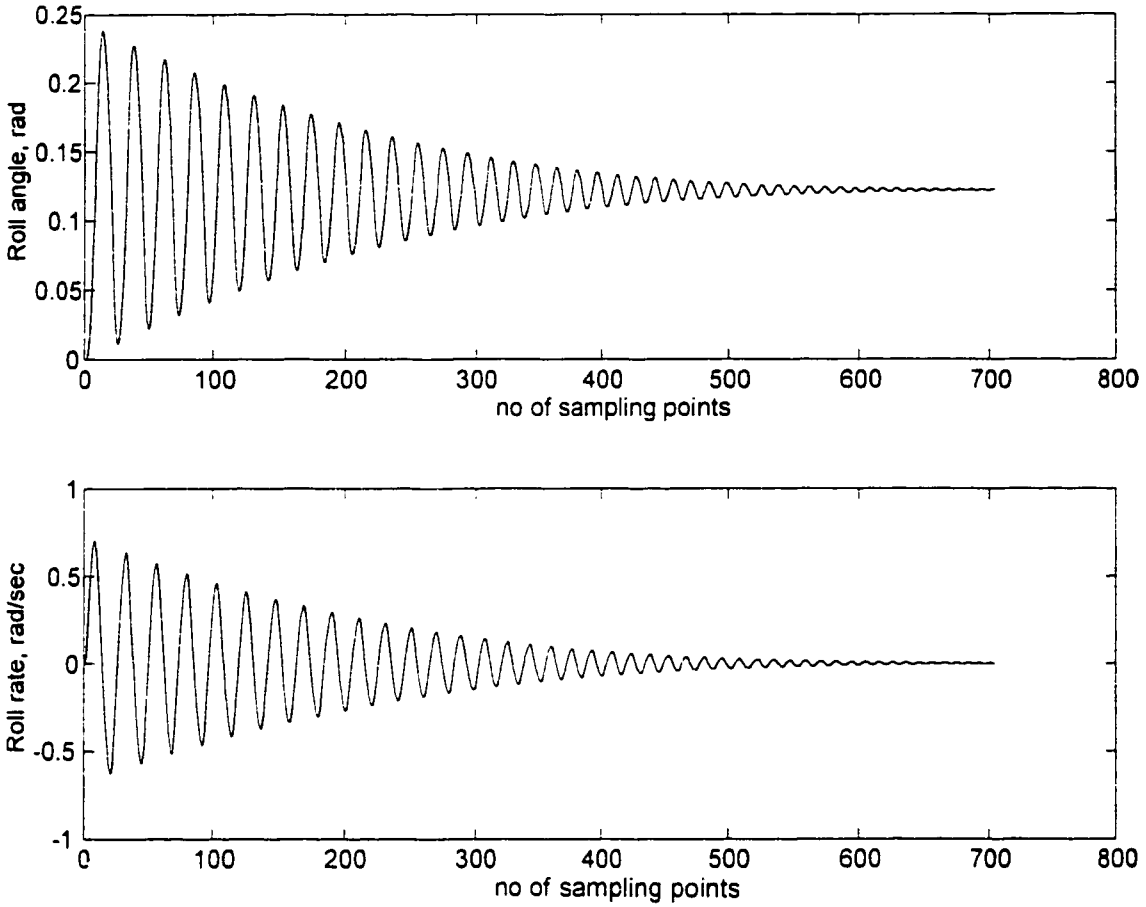

Figure 7.27: Open loop response of wing rock model with change in θ_2

rock motion prevails.

When the aerodynamic parameter θ_1 is increased from 4 to 40, without control the wing rock motion has disappeared as shown in Figure 7.28. The simulation studies conclude that the existence of wing rock is sensitive to the change and time variances of the parameter.

7.3.5 Simulation 3

Structural uncertainties result from the imperfection of the model due to presence of unmodeled dynamics. In this simulation, the same AFTI/F-16 model is used to

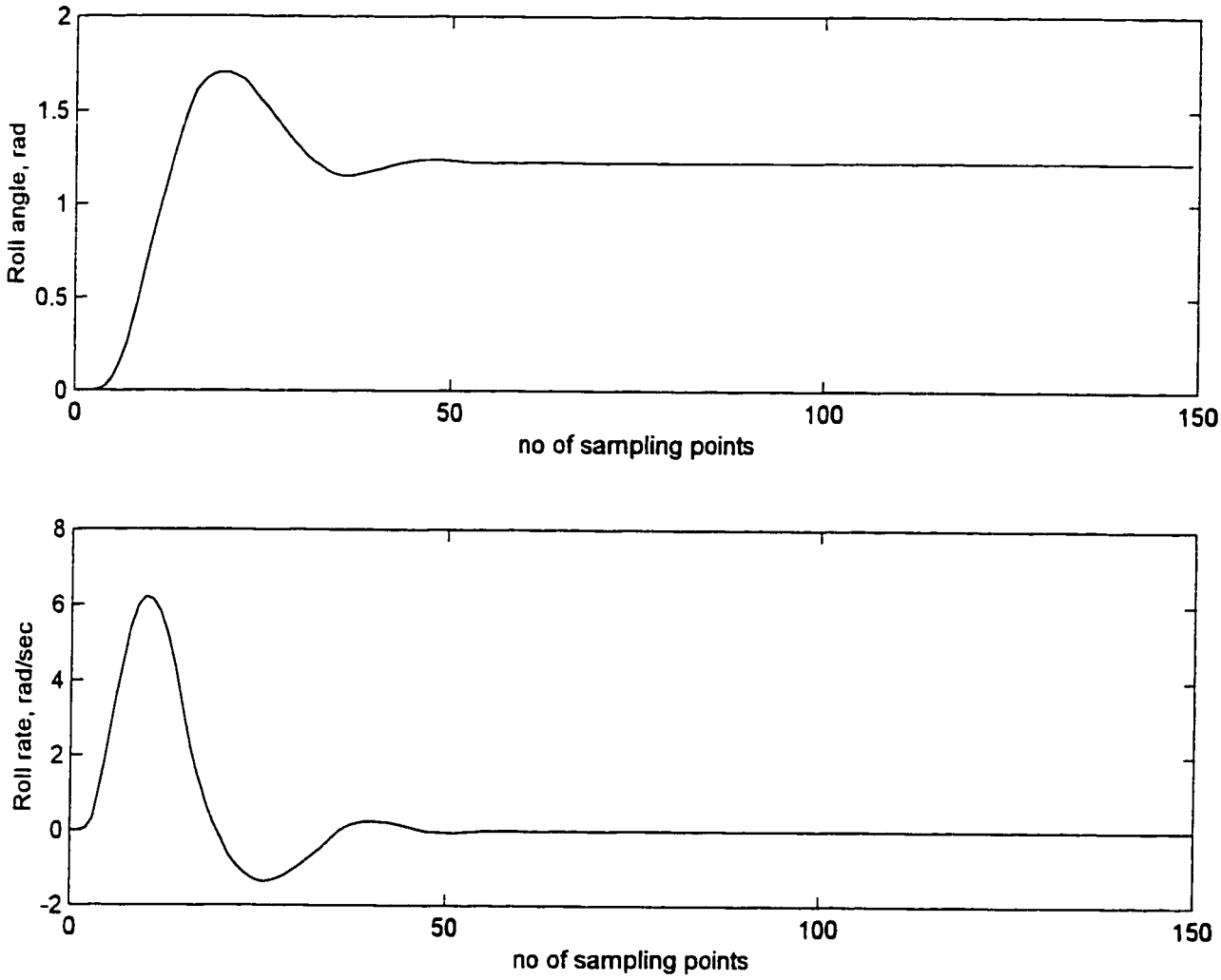

Figure 7.28: Open loop response in wing rock in change in θ_1

verify the robustness feature of the recurrent RBF controller in the presence of both low frequency unmodeled dynamics namely Coulomb friction and disturbances. The conditions used in this study are :

$\epsilon_{\max} = 0.4$, $e_{\min} = 0.012$, $\epsilon_n = 0.2$, $e_{rms} = 0.2$, $\kappa = 0.85$, $R_n = 1.0$, $Q = 0.002$, $P_o = 1.0$, $f_o = 0.1$, $g_o = 0.2$, $T_s = 0.05\,\text{sec}$

The closed loop response is given in Figure 7.29, the roll angle is oscillating at 0.6 rad and the roll rate is varying at zero rad. The control input and the root mean square error are given in Figure 7.30. The simulation concludes that in the presence of Coulomb friction and the disturbance, the controller is not capable to stabilize the wing rock motion.

7.3.6 Simulation 4

The simulation was carried out to include the transport delay in the absence of disturbance to verify the performance of the recurrent RBF controller. The conditions used in the simulation are the same as in Simulation 3.

Figure 7.31 shows that the wing rock in roll angle and roll rate were suppressed after the first 40 sampling points. The evolution of neurons in f and g nets are shown in Figure 7.32. Based on the above parameters the networks select 25 neurons in g net and 2 neurons in the final evolution in f net. The number of selected neurons is sufficient to suppress the wing rock as indicated by the results in Figure 7.31. The simulation study concludes that the performance of recurrent RBF controller is robust in the presence of low frequency unmodeled dynamics.

7.3.7 Simulation 5

The procedures given in [32] is followed to examine the robustness of the recurrent RBF controller by including the following 2nd order unmodeled dynamics in the system.

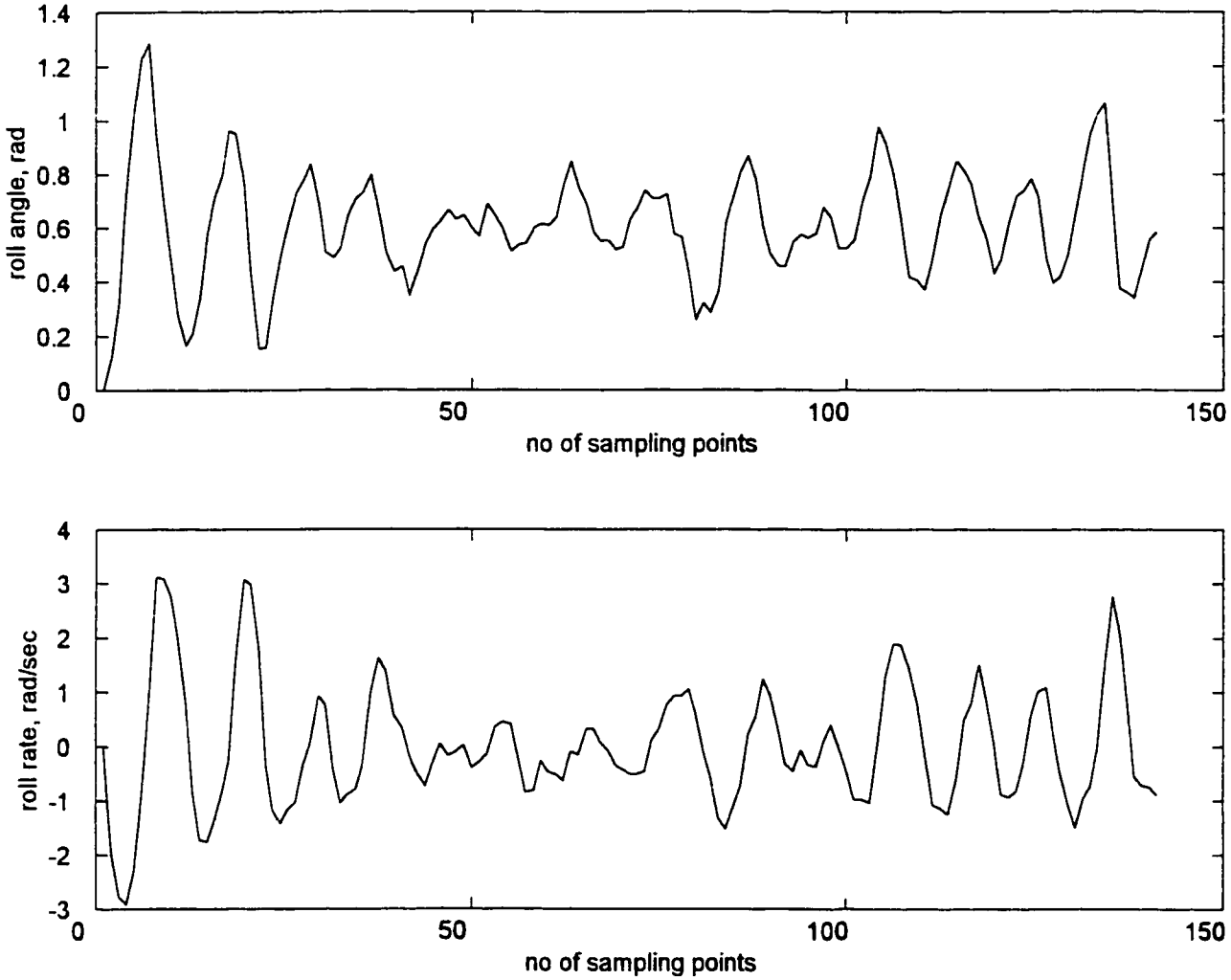

Figure 7.29: Closed loop response in the presence of noise and Coulomb friction

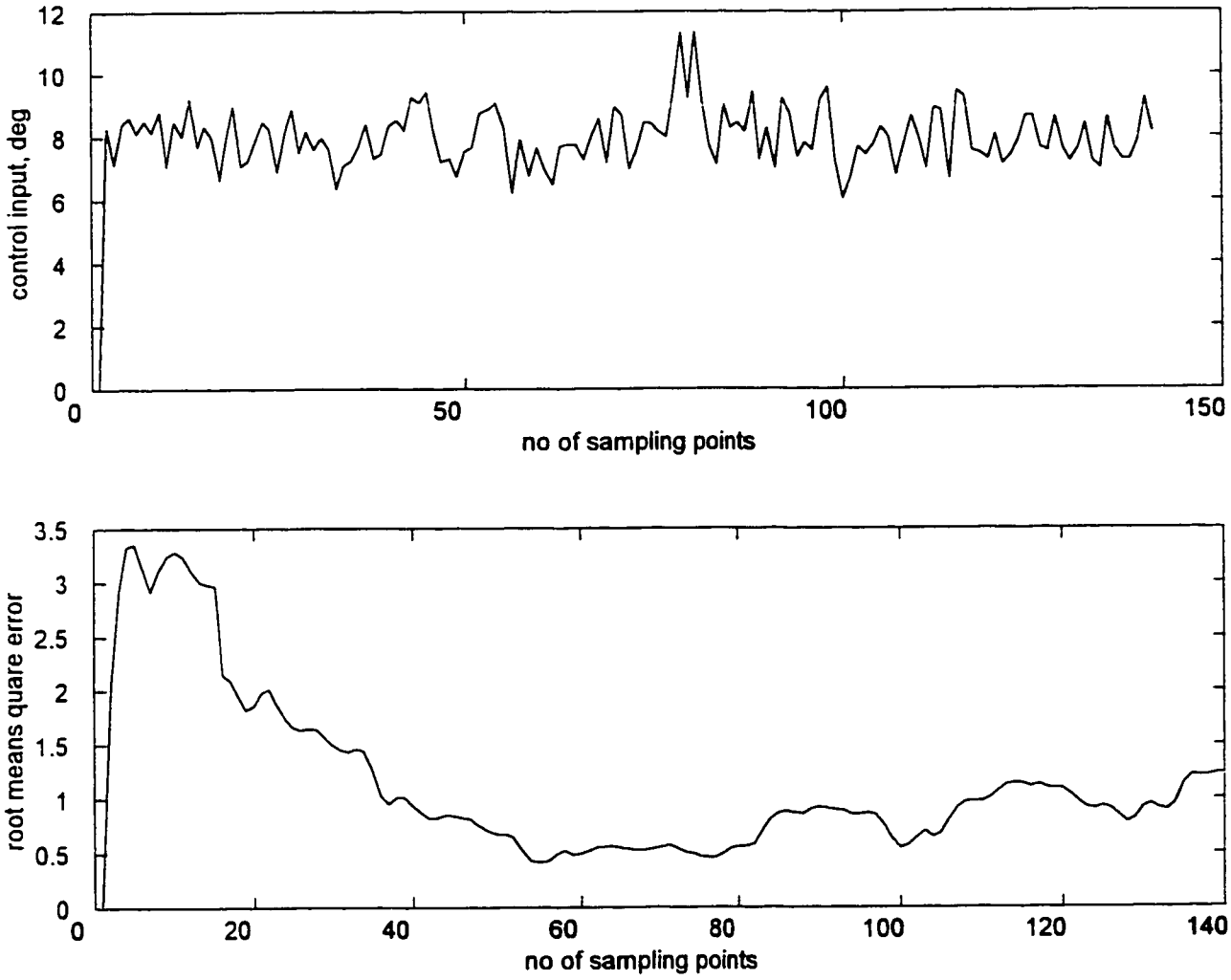

Figure 7.30: Control input and root mean square error

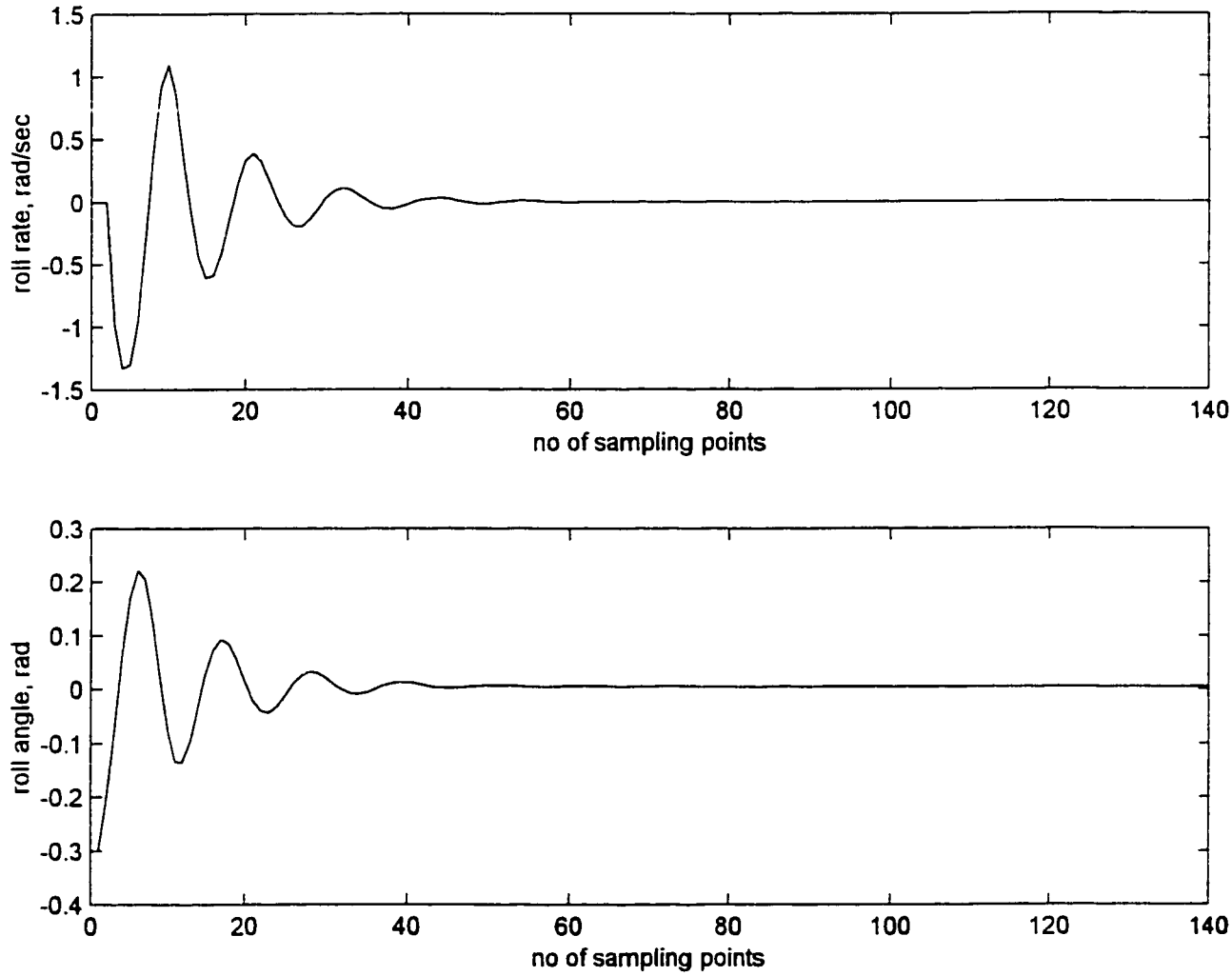

Figure 7.31: Closed loop response with transport delay as unmodeled dynamics

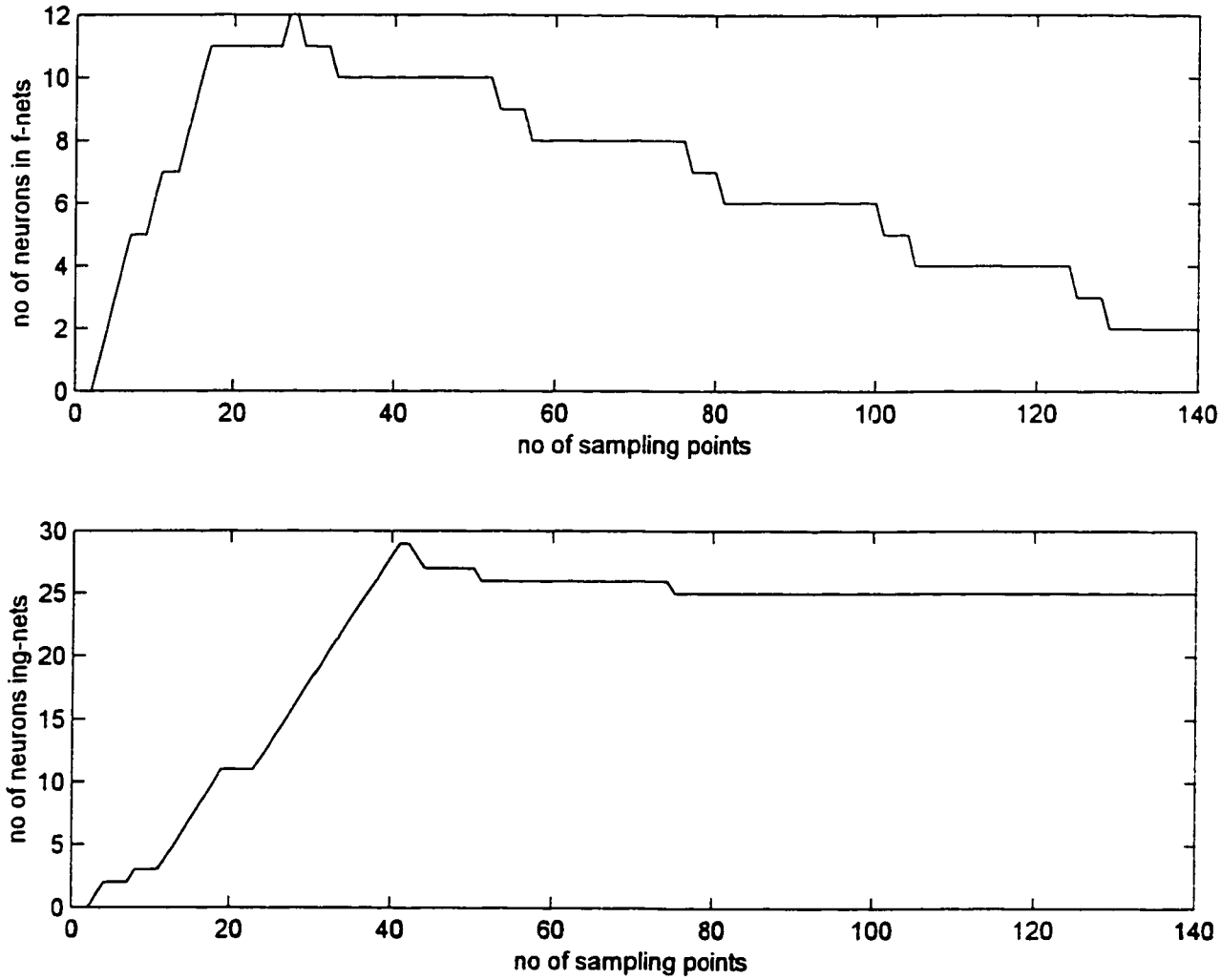

Figure 7.32: Evolution of neurons in f-g nets (transport delay)

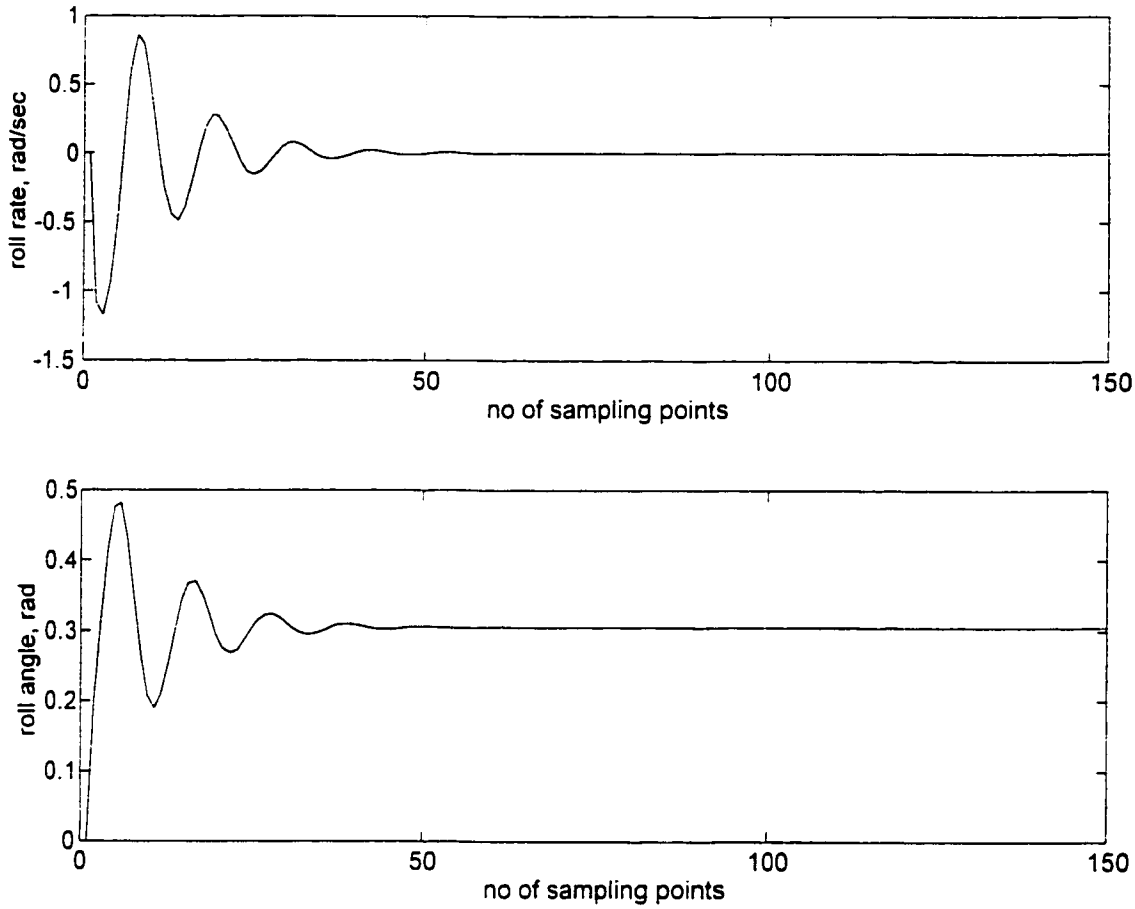

Figure 7.33: Closed loop response with 2 nd order unmodeled dynamics

$$\frac{229}{s^2 + 30s + 229} \tag{7.40}$$

Simulation is carried out using the following conditions :

$\epsilon_{\max} = 0.4$, $e_{\min} = 0.012$, $\epsilon_n = 0.2$, $e_{rms} = 0.012$, $\kappa = 0.85$, $R_n = 1.0$, $Q = 0.002$, $P_o = 1.0$, $f_o = 0.1$, $g_o = 0.2$, $n_f = 0.8$, $n_g = 0.8$, $T_s = 0.05\,\text{sec}$

The closed loop response of the simulation is given in Figure 7.33, it is noted that wing rock in roll angle and roll rate are suppressed. The study concludes the controller is capable of suppressing the wing rock in the presence of 2nd order unmodeled dynamics.

7.3.8 Guidelines for Design Considerations

The above simulation studies indicate that the recurrent RBF controller has robustness feature and performance tolerances in the presence of disturbances or low frequency unmodeled dynamics. The performance of the controller deteriorates in the presence of both unmodeled dynamics and disturbances. In dealing with dynamic and time varying nature of the parameters, the existence of the wing rock is sensitive to the changes in parameters.

The robustness concerns with the performance of the closed loop system. There are various methods available in the design of robust controller such as use of dead zone, sensitivity method, sliding mode control, root locus and high stability margin etc. Further references on robust control can be found in [119] where the whole issue is devoted to the discussion on this subject.

The difficulties and guidelines in applying the developed recurrent RBF control strategy in real aircraft will be discussed with respect to the following points.

(i)Modelling of Uncertain Control System

The dynamic recurrent RBF model was developed to represent the system dynamics responsible for generating the wing rock. In practice, the developed model can be readily used to control the wing rock based on the information available in the real aircraft. However, the main problem of using neural network in direct flight control is the difficulty to obtain the certification from regulatory agency for safety considerations. The concern is that there is no guarantee of what the output of the networks will be and this could lead to unsafe conditions. Owing to the uncertain perturbations exist in the aircraft, extensive verifications of the developed control strategy has to be carried out using engineering full scale flight simulator. The precautionary safety measures should be considered in order to implement the control strategy in the practical situation.

(ii)Analysis of Uncertain Control System

The performance index of the controller has be to defined and the question of *robustness requirement* has to be specified. Through simulation studies it is learned that the performance of the developed control strategy depends on the variations of the parameters. The relationship between the questions of sensitivity and robustness has to be examined. In applying the robust control method for the particular type of aircraft the questions of which parameters are uncertain and their ranges of possible values have to be answered. The specification of the performance index and *robustness requirement* will provide guidelines of the closed loop system performance which lies in the acceptable range for all the possible parameter values. The method of sensitivity can be employed to specify the bounds of the uncertainties. Defining the uncertain system as G and some characteristic measure of the wing rock $q(G)$ the *sensitivity function* $\check{S}$ given in equation 7.41 can be defined to indicate how strongly this characteristic depends on the parameters a, in the aircraft system responsible for wing rock generation.

$$\check{S} = \frac{dq}{da} \mid_{a=\hat{a}} \tag{7.41}$$

$\check{S}$ is a measure of sensitivity, if $\check{S} = 0$ the property $q(G)$ is insensitive to a at $a = \hat{a}$ where $\hat{a}$ is a parameter values where there is no occurrence of wing rock.

(iii) Design of Robust Controller for Uncertain Nonlinear System

The developed control strategy, to a certain extend should take care of variations in parameters of the uncertain system as well as unmodeled dynamics. In practice the system uncertainties of the aircraft that generates the wing rock is not completely unknown. Although the system or mechanism responsible for the generation of the wing rock is unknown, the bounds of these uncertainties are known. For example the bounds for parametric uncertainties are known, such as the range of angle of attack, aerodynamic constants, flight conditions where wing rock is likely to occur. The

bounds and conditions under which the closed loop system is stable can be specified beforehand. The method of using *element-by-element bounds* of the uncertainties can be employed in the design for robust controller for each different types of aircraft under study. The detailed analysis and design of robust controller is beyond the scope of the present thesis.

7.4 Concluding Remarks

In this chapter the effectiveness of the developed dynamic recurrent RBF control methodology was demonstrated to suppress the wing rock of AFTI/F-16 testbed aircraft having the delta wings configuration. The simulation results show that the unknown nonlinear functions in the physical system responsible for wing rock generation were estimated by the two separate f and g networks. The optimal networks size were determined by training based on memory properties of the Preisach model. The results confirm that the developed control strategy provide a satisfactory control of wing rock experienced in AFTI/F-16 aircraft. The robustness analysis is carried out by examining the performance of the closed loop control in the presence of parametric uncertainties as well as unmodeled dynamics. Finally the difficulties and guidelines in applying the control strategy in real aircraft were given.

Chapter 8

Conclusions

The aim of this study is to develop a dynamic recurrent RBF control methodology for potential application in the suppression of wing rock in the aircraft having delta wing configuration. This control strategy can be extended to control the wing rock in other types and wing configurations of the aircraft. In developing the control methodology the concept and properties of the Preisach hysteresis model is interpreted in design of dynamic RBF networks. The developed RBF networks combined with Lyapunov stability analysis allows the design of stable closed loop control for the suppression of wing rock. The developed dynamic RBF control strategy had been benchmarked to control the wing rock in slender delta wing. The effectiveness of the dynamic recurrent RBF control methodology had been demonstrated to suppress the wing rock of AFTI/F-16 testbed aircraft having the delta wings configuration.

8.1 Summary and Conclusions

The sources of wing rock in aircraft were identified as mechanical and aerodynamic hysteresis and the review of different methods for the control of wing rock were given. In the adaptive control method the limitation is that the structure of the nonlinear

function in wing rock has to be known as "*a priori* ". Although the knowledge of the nonlinear structure is not required in the neural control design, the issue of robustness such as model uncertainty and unmodeled dynamics are normally addressed by including the sliding mode control. In the adaptive control method the σ modified adaptive law is applied to handle uncertainty and disturbances. Simulation results indicate there is an improvement in performance with the inclusion of σ modified adaptive law in the controller design.

Application of the Preisach Model as a Neural Network

Preisach model had been studied extensively to model hysteresis of physical system in the area of ferromagnetism [30] and other application areas. In most applications, the Preisach model is used to model the hysteresis phenomena occurred at the source of the physical system, the examples of using the Preisach model in piezocreamic can be found in [58], [59] and [61]. The properties of phase shift in the Preisach model is used in [60] to design the controller for quenching the limit cycle of the actuator. The application of the Preisach model as RBF networks is novel and is proposed the first time for identifying the wing rock generated from the uncertain nonlinear system in the aircraft.

Dynamic Networks

In using the RBF networks for either function approximation or controlling the nonlinear system including wing rock motion, researchers [28], [32], [55], [65]-[72] employ the strategy where the centres of the basis functions are placed in the regular grid, for example a square mesh covering the region where the state is known as a " *a priori* " and the number of basis functions used is predetermined based on prior knowledge. The distance between the centres affect the number of basis function required and the accuracy of the approximation. Owing to the basis functions having localized receptive field, most of the functions outside this field are not used in function approximation [66], [55]. Dynamic basis function where RBF networks is grown are

proposed for function approximation in [73]. [74]-[78] and dynamic basis function for controlling nonlinear system was proposed in [107]. In [76] and [77] the dynamic basis function has feature for neuron growth and pruning, however it is used in function approximation. In [107] the dynamic RBF can only grow, however once the neuron is added there is no provision to prune the redundant neurons. The dynamic recurrent RBF controller described in this thesis is novel and it is the first time being proposed to control the nonlinear uncertain system and the aircraft in particular responsible for generating wing rock motion. The dynamic RBF controller has the following features.

Ensemble average

By incorporating the property of ensembles of the cells participating in information storage, the idea of ensemble averages of the centres of basis functions is used as a criteria for training the dynamic recurrent networks. The use of ensemble average concept in training has resulted in better approximation as compared to the studies in [76], [77] where the distance of the nearest centre of RBF units and input vector is used as criteria for training.

Recurrent Networks

The novel feature of the proposed RBF network over the networks in [76] , [77] is the introduction of recurrent signal to the input vector of the networks. The inclusion of recurrent signal is motivated by the concern of incompleteness of the RBF model in order to take care of dynamic characteristics of the uncertain system. Simulation studied earlier concludes that recurrent feature renders robustness in closed loop performance in the presence of disturbances. Using fixed RBF without the recurrent feature in the function approximation, the approximation error will sometime give rise to disturbance signal [55], [66] and may eventually leading to parametric drifts.

Another novel feature of the dynamic recurrent RBF network is that the recurrent signal with memory order of one is taken from the combined networks output (f and g nets) as compared to most of the reported literatures in [108], [110]-[117]

where the recurrent signal is taken from individual neurons output. The activation functions used in these studies are either sigmoid or *tanh* functions other than basis functions. Recurrent RBF had been used in system identification for signal processing application in [113], but it has never been used as dynamic recurrent RBF network for control application as proposed in this thesis.

Hybrid Adaptive Control

The choice was made to employ the *hybrid adaptive control* which involves continuous time control of the physical system and discrete time identification of the RBF networks. In this thesis the sampled data system was employed where the continuous signals of output of the system are sampled and zero order hold control action is used. The choice of hybrid system is preferred for the reason that if the whole control strategy is carried out in continuous time domain, the analog hardware will become too complicated to carry out the computation. Similar study using sampled data system had been reported in [98] where fixed RBF structure is used and sliding mode control is employed to control nonlinear system as compared to the novelty of the work carried out in this thesis. It is concluded that the proposed hybrid control scheme is feasible for potential application giving the fact that aircraft dynamics is a continuous system and the control strategy can be implemented by digital control.

Training of f and g Nets by the EKF

In the proposed recurrent RBF networks, training is carried out in two separate adaptation schemes. The Extended Kalman Filter is used for training the networks during the identification phase for determining the optimal networks size while outer networks weights are updated by modified delta rule based on Lyapunov stability analysis. The Extended Kalman Filter had been proposed for training the centres and widths of the RBF units in function approximation [74]-[76] involving one RBF networks. In this thesis the EKF [120] is used to separately train the centres and widths of the RBF units for the respective f and g nets required for the estimation

of two unknown nonlinear functions of $f(z)$ and $g(z)$. In updating the parameter in the g- net. a term $u(k)$ is proposed and included in equation (5.19) for the estimation of weights associated to function $g(z)$.

8.2 Future Work

The idea and control methodology presented in this thesis suggests the possibility of potential application in real life situation. There are two main directions that the future work can be carried out namely, additional research and analysis on the developed methodology and experimentation / implementation.

8.2.1 Research and Analysis on the Control Methodology

(i) The delay of the estimated network output was introduced together with the input vector to the RBF network. The networks becomes recurrent in nature in order to better represent the properties of the Presiach model. Published literatures indicates a lot of research have been carried out in this area of using recurrent neural networks for control applications. Most of the studies are limited to multilayer back propagation networks . In this research single layer radial basis function networks are used in the design carried out in the discrete time domain. There is no published paper giving a comprehensive analysis of stability and convergence in discrete time domain dealing with the similar case in this research. Also further research effort should be directed towards analysis of approximation capability of recurrent networks and improvement by reducing the modelling error.

(ii) More research is required with respect to the refinement of approximation carried out by recurrent RBF networks. The issue of optimality in the selection of number of neurons and its impact influenced by the threshold parameters has to be further investigated.

(iii) The property of robustness is important in the design and performance of the control system. To investigate further the issue of robustness, various methods such as sensitivity analysis, sliding mode control and dead zone should be examined in the control law design.

(iv) The design of the RBF networks and control algorithm formulation are carried out in discrete time. In the sampling process of continuous time plant the assumption was made that a very fast sampling rate is used and also the general structure of the form in the system is preserved in the sampled data system. Stability analysis for the hybrid adaptive control require a separate treatment and it would be a investigating topics for future work.

(v) The dynamic recurrent RBF control methodology developed can be extended to control of wing rock of aircraft having different configurations than delta wings and having the source of wing rock originated from mechanical hysteresis such as, backlash of the control valve, motor saturation etc.

8.2.2 Implementation

Further research is needed to study the practical aspects of the potential implementation of the developed control methodology in the aircraft. The control strategy can be prototyped using the engineering flight simulator before implementing in the aircraft. Investigation can be carried out through either using software or hardware implementation. Chips for neural computation is available and the feasibility for hardware implementation could be a viable option.

Bibliography

[1] L.E.Ericson, *Various Sources of Wing Rock*, Journal of Aircraft, Vol. 27, No.6, June 1990. pp 488-494.

[2] L.V.Schmidt, *Wing Rock due to Aerodynamic Hysteresis*, Journal of Guidance, Control and Dynamics, Vol. 16, No.3, pp. 129-133, 1979.

[3] B.S.Liebst and R.C.Nolan, *Method of Prediction of the Onset of Wing Rock*, Journal of Aircraft, Vol.31, No. 6, pp. 1419-1421, 1994.

[4] N.Ananthkrishnan and K.Sudhakar, *Characterization of Periodic Motions in Aircraft Lateral Dynamics*, Journal of Guidance, Control and Dynamics, Vol. 19, No.3, pp. 680-685, 1996.

[5] C.Hsu and E.Lan, *Theory of Wing Rock*, Journal of Aircraft, Vol. 22, No.10, pp. 920-924, 1985.

[6] J.M.Elzeba, A.H.Nayfeh and D.T.Mook, *Development of an Analytical Model of Wing Rock for Slender Delta Wings*, Journal of Aircraft, Vol. 26, No.8, pp. 737-743, 1989.

[7] L.E.Ericsson, *The Fluid Mechanics of Slender Wing Rock*, Journal of Aircraft, Vol. 21, No.5, pp. 322-328, 1984.

[8] J.M.Elzeba, D.T.Mook and A.H.Nayfeh, *Influence of Pitching Motion on Subsonic Wing Rock of Slender Delta Wings*, Journal of Aircraft, Vol. 26, No.6, pp. 503-508, 1989.

[9] A.J.Ross, *Investigation of Nonlinear Motion Experienced on a Slender Wing Research Aircraft*, Journal of Aircraft, Vol. 9, No.9, pp. 625-631, 1972.

[10] D.Levin and J.Katz, *Dynamic Load Measurement with Delta Wings Undergoing Self Induced Roll Oscillation*, Journal of Aircraft, Vol. 21, No.1, pp. 30-36, 1984.

[11] P.Konstadinopoulos, D.T.Mook and A.H.Nayfeh, *Subsonic Wing Rock of Slender Delta Wings*, Journal of Aircraft, Vol.22, No.3, pp. 223-228, 1985.

[12] J.Luo and C.E.Lan, *Control of Wing Rock Motion of Slender Delta Wings*, Journal of Guidance, Control and Dynamics, Vol. 16, No.2, pp. 225-231, 1993.

[13] G.S.Wong, S.M.Rock, N.J.Wood and L.Roberts, *Active Control of Wing Rock Using Tangential Leading Edge Blowing*, Journal of Aircraft, Vol. 31, No.3, pp.659-665, 1994.

[14] S.P.Shue, M.E.Sawan and K.Rokhsaz, *Optimal Feedback Control of a Nonlinear System Wing Rock*. Example, Journal of Guidance,Control and Dynamics,Vol. 19, No.1, pp.166-171, 1996.

[15] A.Gelb, *The Analysis and Design of Limit Cycling Adaptive Automatic Control System*, Ph.D Dissertation, Massachusetts Institute of Technology, Aug 1961.

[16] I. Horowitz, J.Samy and A.Shapiro, *A sysnthesis Theory for Self Oscillating Adaptive System (SOAS)*, Automatica, Vol. 10, pp. 381-392, 1974.

[17] I.Horowitz, *Comparison of Linear Feedback System with Self-Oscillating Adaptive System*, IEEE Transaction on Automatic Control, AC(9), pp. 386-392, 1964.

[18] G.Tao and P.Kokotovic, *Adaptive Control of Systems with Backlash*, Automatica, Vol. 29, No.2, pp.323-335, 1993.

[19] G.Tao and P.Kokotovic, *Adaptive Control of Plants with Unknown Hystereses*, IEEE Transaction on Automatic Control, Vol. 40, No. 2, pp. 200-212, 1995.

[20] G.Tao and P.Kokotovic, *Adaptive Control of Systems with Unknown Output Backlash*, IEEE Transaction on Automatic Control, Vol. 40, No.2, pp.326-330, 1995.

[21] M.M.Monahemi and Miroslav Krstic, *Control of Wing Rock Motion Using Adaptive Feedback Linearization*, Journal of Guidance, Control and Dynamics, Vol. 19, No.4, pp.905-912, 1996.

[22] R.M.Rogers, *Parameter Optimal Control of Wing-Rock*, Journal of Guidance, Control and Dynamics, Vol. 17, No.5, pp.1131-1133, 1994.

[23] A.D.Araujo and S.N.Singh, *Variable Structure Adaptive Control of Wing Rock Motion of Slender Delta Wing*, Journal of Guidance, Control and Dynamics, Vol. 21, No. 2, pp. 251-256, 1998.

[24] D.J.Linse and R.F.Stengel, *Identification of Aerodynamic Coefficient Using Computational Neural Networks*, Journal of Guidance, Control and Dynamics, Vol. 16, No.6, Nov-Dec. 1993.

[25] B.S.Kim and A.J.Calise, *Nonlinear Flight Control Using Neural Networks*, Journal of Guidance, Control and Dynamics, Vol. 20, No.1, Jan-Feb. 1997.

[26] M.B.McFarland and A.J.Calise, *Robustness Analysis for a Neural Network Based Adaptive Control Scheme*, Proceeding of the American Control Conference, Seattle, Washington, June 1995.

[27] C.M.Ha, *Neural Network Approach to AIAA Aircraft Control Design Challenge*, Journal of Guidance, Control and Dynamics, Vol. 18, No. 4, July-August, 1995.

[28] S.N.Singh, W.Yim and W.R.Wells, *Direct Adaptive and Neural Control of Wing Rock Motion of Slender Delta Wings*, Journal of Guidance, Control and Dynamics, Vol. 18, No.1, January-February 1995.

[29] S.V.Joshi, A.G.Sreenatha and J.Chandrasekhar, *Suppression of Wing Rock of Slender Delta Wings Using a Single Neuron Controller*, IEEE Transaction on Control System Technology, Vol. 6, No. 5, Sept 1998.

[30] I.D.Mayergoyz, *Mathematical Models of Hysteresis*, 1991, Springer Verlag, New York Inc.

[31] K.S.Narendra and A.M.Annaswamy, *Stable Adaptive Systems*, Prentice Hall, Englewood Cliffs, New Jersey, 1989.

[32] J.J.E.Slotine and W.Li, *Applied Nonlinear Control*, Prentice Hall, Englewood Cliffs, New Jersey, 1991.

[33] A.S.Arena.Jr, *An Experimental and Computational Investigation of Slender Wings Undergoing Wing Rock*, Ph.D Dissertation, University of Notre Dame, Notre Dame, IN. April 1992.

[34] C. H. Hsu, *Theory of Wing Rock*, Ph.D Dissertation, Department of Aerospace Engineering, University of Kansas, Feb. 1984

[35] R. C. Nelson, *Flight Stability and Automatic Control*, McGraw Hill Book Company, 1989

[36] J.D.Anderson, *Fundamental of Aerodynamics*, McGraw Hill, Inc 1991.

[37] Szu-Ying Tan, *Identification of Aerodynamic Models in Limit Cycle Oscillations*, Ph.D Dissertation, Department of Aerospace Engineering, University of Kansas, May 1996.

[38] J.Katz and D.Levin, *Static Measurement of Slender Delta Wing Rolling Moment Hysteresis*, Journal of Aircraft, Vol. 28, No.4, Engineering Notes, April 1991.

[39] C.Edward Lan, *Private Communication Ref: Wing Rock Model Developed by Hsu and Lan*, Dec. 1998.

[40] S.B.L.Kooi, *Feedback Stabilization of Non Linear End Milling Process*, IFAC Conference on Nonlinear Control System Design (NOLCOS ' 95), Lake Tahoe, CA. U.S.A, June 1995, pp. 196-201.

[41] D.G.Taylor, P.Kokotovic, R.Marino and I.Kanellakopoulos, *Adaptive Regulation of Nonlinear System with Unmodeled Dynamics*, IEEE Transaction on Automatic Control, 34(4), pp. 405-412, 1989

[42] S.Sastry and A.Isidori, *Adaptive Control of Linearizable System*, IEEE Transaction on Automatic Control, 34(11), pp.1123-112, 1989.

[43] I.D.Landau and B.Courtiol, *Adaptive Model Following Systems for Flight Control and Simulation*, Journal of Aircraft, Vol. 9, No.9, pp. 668-674, 1972.

[44] K.Narendra and S.Tripathi, *Identification and Optimization of Aircraft Dynamics*, Journal of Aircraft, Vol. 10, No.4, pp.193-199, 1973.

[45] S.B.L.Kooi, *Adaptive Inferential Control of Wood Chip Refiner*, Second IEEE Conference on Control Applications, Sept 13-16, 1993, Vancouver, B.C. pp. 445-450 . & in Tappi Journal, vol. 77, No.11, November 1994, pp. 185-194.

[46] P.A Ioannou and P.V. Kokotovic, *Adaptive System with Reduced Models*, New York Springer Verlag, 1983.

[47] S.B.L.Kooi, *Robust Adaptive Control for Nonlinear End Milling Process*, Proceedings of the American Control Conference, Seattle, Washington, June, 1995 pp.2995-2999.

[48] Haykin Simon, *Neural Networks -A Comprehensive Foundation*, Macmillan College Publishing Company, 1994.

[49] K.Hornik, M.Stinchcombe and H.White, *Multilayer Feedforward Networks are Universal Approximations*, Neural Networks, Vol.2, pp.551-560, 1989.

[50] M.Brown & C.Harris, *Neurofuzzy Adaptive Modelling and Control*, Prentice Hall International, 1994.

[51] L. Tsungnan, Bill G. Horne and C.Lee Giles, *How Embedded Memory in Recurrent Neural Network Architectures Helps Learning Long-term Temporal Dependencies*, Computer Science Technical Report CS-TR-3626 and UMIACS, University of Maryland, College Park, MD 20742, 1996.

[52] K.S.Narendra and K.Parthasarathy, *Identification and Control of Dynamical System using Neural Networks*, IEEE Transaction on Neural Networks, 1(1) : pp. 4-27, 1990

[53] S.B.L.Kooi and K.Khorasani, *Control of Wood Chip Refiner Using Neural Network*, Proceedings of Artificial Neural Network in Engineering, ANNIE 1991, St.Louis, Missouri November 1991, pp. 567-572. & in Tappi Journal, Vol. 75, No. 6, June 1992, pp. 156-162.

[54] J.E.Steck, K.Rokhsaz and S.P.Shue, *Linear and Neural Network Feedback for Flight Control Decoupling*, IEEE Control System Magazine, August 1996.

[55] E.Tzirkel-Hancock. *Stable Control of Nonlinear System Using Neural Network*, Ph.D. Dissertation. Cambridge Univ. Eng. Dept.. Cambridge. U.K., June 1992

[56] F.C.Chen and H.K.Khalil, *Adaptive Control of Nonlinear Systems using Neural Networks*, International Journal of Control, 1992, Vol . 6, pp.1299-1317.

[57] D.E.Rumelhart and J.L.McCelland Eds, *Parallel Distributed Processing Explorations in the Microstructure of Cognition*, Vol. 1 ; Foundation Bradord Books MIT Press Cambridge, MA, 1986.

[58] A.Visintin, *Differential Models of Hysteresis*, Springer Verlag, 1991.

[59] Ge Ping and M.Jouaneh, *Tracking Control of a Piezoceramic Actuator*, IEEE Transaction on Control System Technology, Vol. 4, No. 3, pp. 209-216, May 1996.

[60] Hayward et al, *On the Control of Actuator with Non Linear Characteristics*, Centre of Intelligent Machines, McGill University, Montreal, Canada, 1997.

[61] H.T.Bank, A.J.Kurdila and G.Webb, *Identification of Hysteretic Control Influence Operators Representing Smart Actuator Part I : Formulation* , North Carolina State University, CRSC-TR96-14 Report, April 1996.

[62] G. Webb, *Adaptive Identification and Compensation for a Class of Hysteresis Operators*, Ph.D Thesis, Texas A&M University, College Station TX, May 1998.

[63] Gorbey R. Benjamin, *Control of Hysteresis System with Preisach Representation*, Ph.D Thesis, University of Waterloo, Department of Mechanical Engineering, 1996.

[64] H.T.Bank, Smith.R.C., Yang.Y, Smart, *Material Structure- Modeling, Estimation and Control*, John Wiley & Sons, Masson, Paris, 1996.

[65] T.Poggio and F.Girosi, *Networks for Approximation and Learning*, Proc. IEEE, 1990, 78, pp. 1481-1497.

[66] R.M.Sanner and J.Slotine, *Gaussian Network for Direct Adaptive Control*, IEEE Transaction on Neural Networks, 1992, 3(6), pp.837-863.

[67] M.J.D.Powell, *Ridial Basis Function for Multivaiable Interpolation: A Review*, in Masson, J.C and Cox M.G Eds : Algorithm for Approximation (Clarendon Press Oxford, 1987), pp.143-168.

[68] D.S.Broomhead and D.Lowe, *Multivariable Functional Interpolation and Adaptive Networks*, Complex System, 1988, 2, pp.321-355.

[69] J.Moody and C.J.Darken, *Fast Learning in Network of Locally Tuned Processing Units*, Neural Comput, 1989, 1, pp.281-294.

[70] S.Chen, S.A.Billings, C.F.N.Cowan and P.M.Grant, *Practical Identification of NARMAX models Using Radial Basis Functions*, Int. Journal of Control, Vol.52, No.6, pp.1327-1350, 1990.

[71] S.Chen, S.A.Billing and P.M.Grant, *Recursive Hybrid Algorithm for Nonlinear System Identification Using Radial Basis Function Networks*, Int. Journal of Control, Vol.55, No.5, pp.1051-1070, 1992.

[72] C.L.Chen, W.Chen and F.Y Chang, *Hybrid Learning Algorithm for Gaussian Potential Function Networks*, IEE Proceeding -D, Vol. 140, No. 6, pp. 442-448, November 1993.

[73] J.C Platt, *A Resource Allocating Network for Function Interpolation*, Neural Comput, 1991,3, pp.213-225.

[74] V.Kadirkamanathan and M.Niranjan, *A Function Estimation Approach to Sequential Learning with Neural Network*, Neural Comput, 1993,5, pp.954-975.

[75] V.Kardirkamanathan, *Sequential Learning in Artificial Neural Networks*, Ph.D Dissertation, Cambridge Uni. Eng. Dept: Cambridge,U.K.,Sept 1991.

[76] L.Yingwei, N.Sundrararajan and P.Saratchandran, *Identification of Time Varying Nonlinear System using Minimal Radial Basis Function Neural Networks*, IEE Proc: Control Theory Appl. Vol. 144, No. 2, March 1997, pp.202-208.

[77] L.Yingwei, N.Sundrararajan and P.Saratchandran, *Performance Evaluation of a Sequential Minimal Radial Basis Function (RBF) Neural Learning Algorithm*, IEEE Transaction on Neural Network Vol (9) No.2 March 1998 pp. 308-318.

[78] Nicolaos B.Karayiannis and Glenn Weiqun M, *Growing Radial Basis Neural Network: Merging Supervised and Unsupervised Learning with Network Growth Technique*, IEEE Transaction on Neural Network, Vol. 8, No. 6, Nov 1997, pp. 1492-1506.

[79] S.B.L.Kooi and J.V.Svoboda, *Dynamic Recurrent Neural Networks for Stable Adaptive Control of Wing Rock Motion*, 14th IFAC Symposium on Automatic Control in Aerospace, August 24-28, 1998, Seoul, Korea, pp. 218-223.

[80] Optiz D.W. and Shavlik Jude.W, *Actively Searching for an Effective Neural Network Ensemble*, Conection Science, 8(3-4), 1996.

[81] B. Igelnik, Y.H. Pao, S.R.LeClair and C.Y. Shen, *The Ensemble Approach to Neural Network Learning and Generalization*, IEEE Transaction on Neural Networks Vol. 10, No. 1, January 1999, pp. 19-30.

[82] R Williams, *Training Recurrent Networks Using the Extended Kalman Filter*, Proceedings 1992, IEEE International Joint Conference Neural Network, Vol. IV, Baltimore, MD, pp. 241-246.

[83] V.T Elanayar and Yung C.Shin, *Radial Basis Function Neural Network for Approximation and Estimation of Nonlinear Stochastic Dynamic Systems*, IEEE Transaction on Neural Network, Vol. 5, No. 4, July 1994, pp. 594-683.

[84] L.Behera, M.Gopal and S.Chaudhury, *On Adaptive Trajectory Tracking of a Robot Manipulator Using Inversion of Its Neural Emulator*, IEEE Transaction on Neural Network, Vol. 7. No. 6, Nov 1996, pp. 1401-1414.

[85] A.Isidori, *Nonlinear Control Theory : An Introduction*, 2nd edition Springer Verlag, 1989.

[86] A.W.Lee, *Control of Nonlinear Systems Under Input Constraints with Applications to Flight Control*, Ph.D Dissertation, University of California at Berkeley, 1992.

[87] S.N.Singh and M.Steinberg, *Adaptive Control of Feedback Linearizable Nonlinear Systems with Application to Flight Control*, Journal of Guidance, Control and Dynamics, Vol. 19, No. 4, July-Aug 1996, pp. 871-877.

[88] A.Yesildrek and F.L.Lewis, *Feedback Linearization Using Neural Networks*, Automatica, 31, 11, Nov. 1995, pp. 1659-1664.

[89] A.W.Lee and J.K.Hedrick, *Application of Approximate I/O Linearization to Aircraft Flight Control*, Journal of Dynamic Systems, Measurement and Control, Sept. 1994, Vol. 116, pp. 429-436.

[90] S.N.Singh, M.Steinberg and R.D.DiGirolamo, *Nonlinear Predictive Control of Feedback Linearizable Systems and Flight Control System Design*, Journal of Guidance, Control and Dynamics, Vol. 18, No. 5, Sept-Oct 1995, pp. 1023-1028.

[91] B.Wigdorowitz, *Application of Linearization Analysis to Aircraft Dynamics*, Journal of Guidance, Control and Dynamics, Vol. 15, No. 3, May-June, 1992, pp. 746-750.

[92] Y.Ochi and K.Kanai, *Design of Reconstructible Flight Control Systems Using feedback Linearization*, Journal of Guidance, Control and Dynamics, Vol. 14, No. 5, Sept-Oct. 1991, pp. 903-911.

[93] M.Azam and S.N.Singh, *Invertibility and Trajectory Control for Nonlinear Maneuver of Aircraft*, Journal of Guidance, Control and Dynamics, Vol. 17, No.1, Jan-Feb. 1994, pp. 192-200.

[94] S.N.Singh, *Control of Nearly Singular Decoupling Systems and Nonlinear Aircraft maneuver*, IEEE Transaction on Aerospace and Electronic Systems, Vol. 24, No.6, November 1988, pp. 775-784.

[95] J.Romano and S.N.Singh, *I/O Map Inversion , Zero Dynamics and Flight Control*, IEEE Transaction on Aerospace and Electronic Systems, Vol. 26, No. 6, November 1990. pp. 1022-1029.

[96] E.T.Hancock and F.Fallside, *Stable Control of Nonlinear System using Neural Network*, International Journal of Robust and Nonlinear Control, Vol.2, 1992, pp.63-86.

[97] C.Zhang, R.Middleton and R.J.Evans, *Stable Hybrid Adaptive Control*, International Journal Control 1991, Vol. 53, No. 6, pp. 1377-1394.

[98] F.Sun, Z.Sun and P.Y.Woo, *Stable Neural Network Based Adaptive Control for Sampled Data Nonlinear Systems*, IEEE Transaction on Neural Networks, Vol 9, No. 5, September 1998, pp. 956-968.

[99] K.S.Narendra and S.Mukhopadhyay, *Adaptive Control Using Neural Networks and Approximate Models*, IEEE Transaction on Neural Networks, Vol. 8, No. 3, May 1997, pp. 475-485.

[100] A.M.Guillaume, G.Bastin and G.Campion, *Sampled Data Adaptive Control of a Class of Continuous Non-Linear System*, International Journal of Control, 1994, Vol. 60, No. 4, pp. 569-594.

[101] S.Monaca and Normand Cyrot, *On the Sampling of a Linear Analytic Control System*, 24th Conference on Decision and Control, Ft. Lauderdale, Florida, U.S.A. 1985, pp. 1457-1462.

[102] S.Monaca and Normand Cyrot; *Minimum Phase Non-Linear Discrete Time System and Feedback Stabilization*, Proceedings of the 1987 IEEE Conference on Decision and Control, 1987, pp. 979-986.

[103] H.K.Khalil, *Nonlinear System*, Macmillan Publishing Company, 1992.

[104] F.C.Chen and H.K.Khalil, *Adaptive Control of a Class of Nonlinear Discrete Time System Using Neural Networks*, IEEE Transaction of Automatic Control, Vol. 40, No. 5, pp. 791-801.

[105] T.L.Liao and C.M.Chiu, *Adaptive Output Tracking of Unknown MIMO Nonlinear Systems Using Radial Basis Function Neural Networks*, JSME International Journal Series C, Vol. 40, No. 1, 1997, pp. 52-59.

[106] R.M. Sanner and Slotine Jean-Jacques, *Structurally Dynamic Wavelet Networks for the Adaptive Control of Uncertain Robotic Systems*, Proceeding of the 34th IEEE Conference on Decision & Control, New Orleans, LA. Dec 1996 pp 2460-2467.

[107] S.Fabri and V.Kadirkamanathan, *Dynamic Structure Neural Networks for Stable Adaptive Control of Nonlinear System*, IEEE Transaction on Neural Network. Vol. 7, No. 6. Sept 1996. pp.1151-1167.

[108] D.Obradovic, *On-line Training of Recurrent Neural Networks with Continuous Topology, Adaptation* IEEE Transaction on Neural Networks, Vol.7, No.1, pp. 222-228, January 1996.

[109] M.M.Livstone, Jay Farrell and W.L.Baker, *A Computationally Efficient Algorithm for Training Recurrent Connectionist Networks*, American Control Conference (ACC), pp. 555-560, 1992

[110] R.J.Williams and D.Zipser, *A Learning Algorithm for Continuously Running Fully Recurrent* Neural Networks Neural Computation, 1, pp. 270-280, 1989

[111] M.K.Sundareshan and T.A.Condarcure, *Recurrent Neural Network Training by Learning Automation Approach for Trajectory Learning and Control System Design*, IEEE Transaction on Neural Networks. Vol. 9, No. 3, May 1998, pp. 354-368.

[112] Andrew J.Meade and R.Moreac, *Recurrent Neural Network Simulation of Chaotic System Without Training*, J. Guidance, Vol. 18, No. 6, 1995, pp.1463-1466.

[113] S.A.Billing and C.F.Fung, *Recurrent Radial Basis Function Networks for Adaptive Noise Cancellation*, Neural Networks, Vol. 8, No. 2, pp. 273-290, 1995.

[114] C.C.Ku and K.Y.Lee, *Diagonal Recurrent Neural Networks for Dynamic Systems Control*, IEEE Transaction on Neural Networks, Vol. 6, No. 1, pp. 144-156, January 1995.

[115] M.A.Brdys. G.J.Kulawski and J.Quevedo, *Recurrent for Nonlinear Adaptive Control*, IEE Proc. Control Theory Application, Vol. 145, No.2, pp. 177-188, March 1998.

[116] Jin Liang, P.N.Nikiforuk and M.M.Gupta, *Adaptive Control of Discrete time nonlinear System using Recurrent Neural Networks*, IEE Proc. Control Theory Applications. Vol. 141. No. 3. pp. 169-176, May 1994.

[117] P.S.Sastry, G.Santharam and K.P.Unnnikrishnan, *Memory Neuron Networks for Identification and Control of Dynamical System*, IEEE Transaction on Neural Networks. Vol. 5. No. 2. March 1994. pp. 306-319

[118] L.T.Ngunyen, D.Whipple and J.M.Brandon, *Recent Experiences of Unsteady Aerodynamic Effect on Aircraft Flight Dynamics at High Angle of Attack*, Unsteady Aerodynamic-Fundamentals and Applications to Aircraft Dynamics, Joint Symposium of the Fluid Dynamics and Flight Mechanics Panels (Gottigen, Germany),AGARDCP 386, May 1985 (Paper 28).

[119] H.Kwakernaak. Editor *Special Issue on Robust Control*, Automatica, Vol. 29, Number 1, January 1993.

[120] Haykin Simon, *Adaptive Filter Theory*, Prentice Hall Inc, 1996.